https://doi.org/10.35662/unine-thesis-3105

Université de Neuchâtel

Faculty of Science
Department of Chemistry

Greener perspectives in Conservation Science

Design, characterisation, and evaluation of bio-formulations for the cleaning of altered indoor historical metal heritage

Dissertation for the degree of
Doctorate in Sciences

Arianna Passaretti

Jury members:

Prof. Edith Joseph, thesis director, Université de Neuchâtel & Haute Ecole Arc, Switzerland
Prof. Stephan von Reuss, thesis co-director, Université de Neuchâtel, Switzerland
Prof. Giorgia Sciutto, thesis co-supervisor, Università di Bologna, Italy
Prof. Giuseppe Lazzara, Università di Palermo, Italy
Dr. David Thickett, English Heritage, United Kingdom

Defended on February 1, 2024

unine
Université de Neuchâtel
Faculté des sciences

Rue Emile-Argand 11
CH-2000 Neuchâtel
doctorat.sciences@unine.ch

IMPRIMATUR POUR THESE DE DOCTORAT

La Faculté des sciences de l'Université de Neuchâtel autorise l'impression de la présente thèse soutenue par

Madame Arianna PASSARETTI

Titre :

"Greener perspectives in Conservation Science: design, characterization, and evaluation of bioformulations for the cleaning of altered indoor metal heritage"

sur le rapport des membres du jury composé comme suit :

- **Prof. Edith Joseph,** directrice de thèse, Université de Neuchâtel / Haute Ecole Arc, Suisse
- **Prof. Stephan von Reuss,** co-directeur de thèse, Université de Neuchâtel, Suisse
- **Prof. Giorgia Sciutto**, Università degli Studi di Bologna, Italie
- **Prof. Giuseppe Lazzara,** Università degli Studi di Palermo, Italie
- **Dr David Thickett**, English Heritage, Royaume-Uni

Neuchâtel, le 9 avril 2024

Le Doyen, Prof. R. Bshary

"Eppure, vedi questi pazzi? Senza badare al fantasma che portano con sé, in se stessi, vanno correndo, pieni di curiosità, dietro il fantasma altrui! E credono che sia una cosa diversa."

Luigi Pirandello, *Così è, se vi pare*

Table of Contents

List of Figures

List of Tables

List of Abbreviations

ANOVA	Analysis of Variance
ATR	Attenuated Total Reflection
Brass ZL	Brass sheet (Cu 66%, Zn 34%) coated with Zaponlack
CH	Cultural Heritage
CR(s)	Conservator-restorer(s)
DFO	Deferoxamine B
EDDS	Ethylenediamine-N,N'-disuccinic acid
EDTA	Ethylenediamine-N,N,N',N'-tetraacetic acid
EDX	Energy-dispersive X-ray (spectroscopy)
EL	Ethyl lactate
Fe PB72	Mild steel sheet coated with Paraloid® B72 (10% in ethyl acetate)
FTIR	Fourier-transform infrared (spectroscopy)
ICP-MS	Inductively Coupled Plasma Mass Spectrometry
ICP-OES	Inductively Coupled Plasma Optical Emission Spectroscopy
LCA	Life Cycle Assessment
-min	Minutes
PB72	Paraloid® B72
PCA	Principal Component Analysis
PHA	Polyhydroxyalkanoates
PHB	Polyhydroxybutyrate
PLA	Polylactic acid
RT	Room temperature
SEM	Scanning Electron Microscopy
TGA	Thermogravimetric analysis
Tukey's HSD test	Tukey's Honest Significant Difference test
UV	Ultraviolet
XRD	X-Ray Diffraction
XRF	X-Ray Fluorescence (spectroscopy)
ZL	Zaponlack

Abstract

(English version)

The advent of the Green Chemistry principles is nowadays an unconditional driving force for the research carried out in the field of Conservation Science. Great attention is currently addressed in response to the potential risks derived from cleaning methods conventionally employed in art conservation, which are frequently relying on the use of petroleum-based and toxic substances, such as solvents and complexing agents. Within this scenario, the doctoral research here discussed was addressed to explore greener alternatives for the cleaning of altered historical metal collections.

The core issue for the preservation of metals lies in the spontaneous and irreversible process of corrosion towards which they naturally tend over time. Therefore, conservator-restorers (CRs) typically rely on the application of organic coatings to protect the metallic surface from atmospheric agents (e.g., water, gaseous sulphide species). However, also these materials tend to deteriorate through time due to several environmental factors (e.g., temperature, UV light), leading to a failure of these protective systems. Consequently, it is common that the appearance, functionality, or conservation conditions of metal artworks are jeopardised by the presence of altered organic coatings associated to corroded underlying metal substrates, leading to the necessary removal of both these degradation features by CRs.

Therefore, innovative greener gelled solutions were designed in order to tackle individually (i.e., selective action) or simultaneously (i.e., controlled double-action) corrosion and altered organic coatings possibly present on historical metal collections. Great attention was addressed to the selection of possibly renewable and bio-degradable gel "building-blocks". The research led to a first investigation of several bio-polymers, among which poly-3-hydroxybutyrate (PHB) was selected as suitable thickening agent to design double-action cleaning systems. Namely, two organogels were developed using a poly-3-hydroxybutyrate matrix, loaded with ethyl lactate and complexing agents for the removal of organic coatings and corrosion, respectively. Specifically, the potential of biodegradable complexing agents, such as deferoxamine B (DFO) and ethylenediamine-N,N'-disuccinic acid (EDDS), were explored. The cleaning targets were selected being the most representative of alloys and organic coatings present in indoor historical metal collections. Therefore, steel, brass, and sterling silver were chosen as metal substrates, whereas an acrylic resin (i.e., Paraloid® B72) and a nitrocellulose lacquer (i.e., Zaponlack) were the organic coatings of interest.

A multi-modal analytical protocol was performed on gelled formulations and metal samples before and after cleaning intervention in order to evaluate the efficiency and reliability of the innovative cleaning methods. In general terms, both cleaning systems provided an effective removal of the organic materials while yielding moderate cleaning on the corrosion layers. This outcome would ensure a versatile intervention, fine-tuning gel application time and reiteration, which is a sought feature for the controlled cleaning of historical metal collections.

From an audacious perspective, the results obtained within the doctoral research were shared with conservator-restorers and the scientific community aiming to promote the exploitation of the innovative methods and materials, while fostering the interest in researching for more sustainable approaches of production (e.g., EDDS manufactured without the use of ethylene bromide) at the industrial scale.

Keywords: Historical metals, biocleaning, organogels, Green Chemistry, organic coatings, corrosion.

Résumé

(Version en français)

L'avènement des principes de la "Chimie Verte" est désormais une force motrice inconditionnelle pour la recherche menée dans le domaine de la Science de la Conservation. L'attention portée aux risques potentiels liés aux méthodes de nettoyage conventionnellement employées dans la conservation des œuvres d'art, qui reposent souvent sur l'utilisation de substances toxiques à base de pétrole, telles que les solvants et les agents complexants, est particulièrement importante. Dans ce contexte, la recherche doctorale présentée ici visait à explorer des alternatives plus écologiques pour le nettoyage des collections historiques en métal altérées.

Le problème central de la préservation des métaux réside dans le processus spontané et irréversible de corrosion vers lequel ils tendent naturellement. C'est pourquoi les conservateurs-restaurateurs (CRs) s'appuient normalement sur l'application de revêtements organiques pour protéger la surface métallique des agents atmosphériques (par exemple, l'eau, les espèces de sulfure gazeux). Toutefois, ces matériaux ont également tendance à se détériorer avec le temps sous l'effet de plusieurs facteurs environnementaux (température, lumière UV, etc.), ce qui entraîne une défaillance de ces systèmes de protection. Par conséquence, il est commun que l'apparence, la fonctionnalité ou les conditions de conservation des œuvres d'art métalliques soient compromises par la présence de revêtements organiques altérés associés à des substrats métalliques sous-jacents corrodés, ce qui conduit à l'élimination nécessaire de ces deux caractéristiques de dégradation par les CRs.

Des solutions gélifiées vertes et innovantes ont donc été conçues pour traiter individuellement (action sélective) ou simultanément (double action contrôlée) la corrosion et les revêtements organiques altérés éventuellement présents sur les collections historiques en métal. Une grande attention a été accordée à la sélection des " composant-blocs " potentiellement renouvelables et biodégradables des gels. La recherche a conduit à une première étude de plusieurs bio-polymères, parmi lesquels le poly-3-hydroxybutyrate (PHB) a été sélectionné comme agent épaississant approprié pour concevoir des systèmes de nettoyage à double action. Deux organogels ont été développés à partir d'une matrice de poly-3-hydroxybutyrate, chargée de lactate d'éthyle et d'agents complexants pour l'élimination des revêtements organiques et de la corrosion, respectivement. Plus précisément, les potentialités des agents complexants biodégradables, tels que la déféroxamine B (DFO) et l'acide éthylènediamine-N,N'-disuccinique (EDDS), ont été explorées. Les cibles de nettoyage ont été sélectionnées comme étant les plus représentatives des alliages et revêtements organiques présents dans les collections historiques de métaux à l'intérieur. L'acier, le laiton et l'argent sterling ont donc été choisis comme substrats métalliques, tandis qu'une résine acrylique (Paraloid® B72) et une laque nitrocellulosique (Zaponlack) ont été les revêtements organiques étudiés.

Un protocole analytique multimodal a été réalisé sur les formulations gélifiées et les échantillons métalliques avant et après l'intervention de nettoyage afin d'évaluer l'efficacité et la fiabilité des méthodes de nettoyage. Globalement, les deux systèmes ont permis d'éliminer efficacement les matériaux organiques tout en assurant un nettoyage modéré de la corrosion. Ce résultat garantirait une intervention polyvalente, en ajustant le temps d'application des gels et la réitération, ce qui est une caractéristique recherchée pour le nettoyage contrôlé des collections historiques de métaux.

Dans une perspective audacieuse, les résultats obtenus ont été partagés avec les conservateurs-restaurateurs et la communauté scientifique afin de promouvoir l'exploitation des méthodes et matériaux innovants, tout en encourageant l'intérêt pour la recherche d'approches de production plus durables (par exemple, EDDS fabriqué sans utilisation de bromure d'éthylène) à l'échelle industrielle.

Mots-clés : Métaux historiques, bionettoyage, organogels, Chimie Verte, revêtements organiques, corrosion.

Riassunto

(Versione in italiano)

L'avvento dei principi della "Chimica Verde" è un input trainante per la ricerca condotta nel campo della Scienza della Conservazione al giorno d'oggi. Grande attenzione è rivolta in risposta ai potenziali rischi derivanti dai metodi di pulitura convenzionalmente impiegati nella conservazione delle opere d'arte, che spesso si basano sull'uso di sostanze tossiche e derivate dal petrolio, come solventi ed agenti complessanti. In questo scenario, la ricerca di dottorato qui discussa è orientata all'esplorazione di alternative più ecologiche per la pulitura di collezioni storiche in metallo.

Il problema centrale nella conservazione dei metalli risiede nel processo spontaneo ed irreversibile di corrosione a cui tendono naturalmente nel tempo. Pertanto, i conservatori-restauratori (CR) normalmente si affidano all'applicazione di rivestimenti organici per proteggere la superficie metallica dagli agenti atmosferici, quali ad esempio, umidità e gas contenti zolfo. Tuttavia, anche questi materiali tendono a deteriorarsi nel tempo a causa di diversi fattori ambientali (ad esempio, temperatura, raggi UV), portando al fallimento di questi sistemi protettivi. Di conseguenza, è frequente che l'aspetto, la funzionalità o le condizioni di conservazione delle opere d'arte in metallo siano compromesse dalla presenza di rivestimenti organici alterati associati a substrati metallici affetti da corrosione, con la conseguente necessità di rimuovere entrambe le forme di degrado mediante l'intervento di CRs.

Pertanto, il lavoro qui discusso è incentrato sullo sviluppo di soluzioni innovative tramite l'uso di gel "green" per lavorare singolarmente (azione selettiva) o simultaneamente (doppia azione controllata) su corrosione e rivestimenti organici alterati eventualmente presenti su collezioni storiche in metallo. Grande attenzione è stata rivolta alla selezione di "mattoncini" costituiti da materiali potenzialmente rinnovabili e biodegradabili per la formulazione dei gel. La ricerca ha condotto ad una prima indagine su diversi biopolimeri, tra i quali è stato selezionato il poli-3-idrossibutirrato (PHB) come agente addensante adatto alla formulazione di sistemi di pulitura a doppia azione. In particolare, sono stati sviluppati due organogel utilizzando una matrice gel di poli-3-idrossibutirrato, caricata con lattato di etile e agenti complessanti, rispettivamente per la rimozione di rivestimenti organici e della corrosione. Nello specifico, sono state esplorate le potenzialità di agenti complessanti biodegradabili, come la deferoxamina B (DFO) e l'acido etilendiammino-N,N'-disuccinico (EDDS). I target dell'azione di pulitura sono stati selezionati in quanto rappresentativi delle leghe e dei rivestimenti protettivi presenti nelle collezioni storiche ed indoor in metallo. Pertanto, come substrati metallici sono stati scelti l'acciaio, l'ottone e l'argento sterling, mentre come rivestimenti organici sono stati scelti una resina acrilica (Paraloid® B72) e una lacca a base nitrocellulosica (Zaponlack).

Un protocollo analitico multimodale è stato condotto sulle formulazioni gel e sui campioni in metallo prima e dopo l'intervento di pulitura, al fine di valutare l'efficienza e l'affidabilità dei nuovi metodi. In generale, i risultati ottenuti hanno dimostrato che entrambi i sistemi di pulitura garantiscono un'efficace rimozione dei materiali organici ed una moderata pulitura della corrosione. Questo risultato garantirebbe un intervento versatile, modulando tempi di applicazione e reiterazione dei gel, che è una caratteristica desiderata per la pulitura controllata di collezioni storiche in metallo.

In un'ottica ambiziosa, i risultati ottenuti nel corso della ricerca di dottorato sono stati condivisi con i restauratori e la comunità scientifica, al fine di promuovere lo studio e l'uso tali metodi e materiali innovativi, stimolando al contempo l'interesse per la ricerca di approcci di produzione più sostenibili (ad esempio, EDDS prodotto senza l'uso di bromuro di etilene) su scala industriale.

Parole chiave: collezioni storiche in metallo, bio-pulitura, organogel, Chimica Verde, rivestimenti organici, corrosione.

Chapter 1

Historical metal care: innovative green cleaning systems to bridge over traditional methods

This chapter is based on Passaretti, A., Cuvillier, L., Sciutto, G., Guilminot, E., & Joseph, E. (2021) Biologically derived gels for the cleaning of historical and artistic metal heritage *Applied Sciences*, *11*(8), 3405. DOI: 10.3390/app11083405.

1.1 Metal heritage: an overview

In the motley world of cultural heritage (CH), metals are among the main actors since the emergence of metalworking of gold, silver, and copper, which can be traced back to the 9th millennium BCE (Kristiansen and Larsson, 2005). Due to their peculiar chemo-physical properties, their aesthetic potential, and their monetary value and consequent importance on social status, metals had, and still have, a wide spectrum of applications in art through the ages. Artistic, cultural, and historical records are handed down through generations thanks to metal paintings, sculptures, decorative arts, musical instruments, jewellery, utensils, weapons, scientific and technical instruments, and so forth (Giumlia-Mair and Lucchini, 2005; Chiavari *et al.*, 2008; Bertolotti *et al.*, 2012; Felix *et al.*, 2020; Meier, 2022; Russo *et al.*, 2022; Molina *et al.*, 2023; Passaretti, Cuvillier, Künzi, *et al.*, 2023). Such a massive presence in cultural heritage has inevitably yielded a plethora of studies on metals in order to safeguard this inheritance.

From a broad perspective, the core problem for the preservation of metals lies in the spontaneous process of corrosion towards which they naturally tend over time (Chilton, 1971). Indeed, corrosion is a thermodynamically favoured phenomenon, which alters metals' original aspect and features, and represents a tremendous economic loss in whichever sector, as well as a conservation issue in the heritage field, because of its irreversible destructive action (De Marco *et al.*, 2017). Several aspects can influence metal corrosion dynamics. Along with the basic dual presence of water and oxygen that act as electrolyte and oxidant, respectively, in the electrochemical process of natural corrosion (Maréchal *et al.*, 2007), other exposure conditions rule and meddle the phenomenon. Factors such as burial soil composition, marine proximity, microbiological activity, atmospheric pollutants (e.g., nitric and sulphur oxides, hydrogen sulphide), display or storage furnishing (e.g., emission of formic acid), artificial and natural light, and, in general, alloys and object complexity play a role in metal detrimental processes (Hosseinpour and Johnson, 2017; Eggert and Fischer, 2021; Pinna, 2021; Thickett, 2021).

It is remarkable that each metal and alloy represents a unique case in terms of susceptibility to the surrounding caustic and detrimental factors (Hosseinpour and Johnson, 2017). Understanding how metals get altered within specific environments (e.g., outdoor, indoor, marine, industrial) and in contact with other materials (e.g., display cases, composite objects, organic protective films) is essential for heritage preservation. The topic raised great interest, as in the literature it is possible to trace along the decades numerous studies focusing on corrosion mechanisms (Maréchal *et al.*, 2007; Qiu and Leygraf, 2011; Tissot *et al.*, 2016; Monnier *et al.*, 2019), organic materials ageing (Mills and White, 1987; Perera, 2003; Artesani *et al.*, 2020; Molina, Cano and Ramírez-Barat, 2023b), and multi-modal investigation of model samples and heritage objects (Degrigny *et al.*, 2007; Martina *et al.*, 2012; Catelli *et al.*, 2018; Petiti *et al.*, 2020; Siatou *et al.*, 2022) in order to predict metal behaviour and establish specific guidelines for long-term conservation.

When referring to historical metal collections, which are the general target of this research study, the art pieces are usually displayed or stored indoors, and are predominantly composed of iron-, copper-, and silver-based alloys (Angelini and Argyropoulos, 2008). This family of artefacts includes objects of different provenance, ranging from ethnographic collections to scientific systems, from musical instruments to silverware (Angelini and Argyropoulos, 2008; Letardi, 2013). In addition to the large variety of historical artefacts, they are frequently made of multiple materials (i.e., composite objects) that may require specific care and preventive conservation conditions (Molina *et al.*, 2023). Normally, historical metal collections are composed of pieces that were housed and/or employed indoors, and are typically free from thick corrosion layers, because well-preserved, functional, and shiny surfaces may have been desired during their use through the time (Angelini and Argyropoulos, 2008; Molina *et al.*, 2023). Nevertheless, regular inspection, preventive care, and maintenance are required from conservator-restorers (CRs) for the long-term safeguard of such collections (Angelini and Argyropoulos, 2008; Watkinson, 2010).

1.2 Traditional conservation methods for historical metals

1.2.1 Tackling the effects of indoor metal corrosion

From a preventive perspective, despite the utopian willingness to artificially control the micro-environment surrounding art pieces, not all pivotal agents in corrosion can be simultaneously monitored, adjusted, or even avoided (Prosek *et al.*, 2013). In this scenario, historical collections are most sensitive to relative humidity (RH) conditions because of the key role of water in natural corrosion phenomena (Monnier *et al.*, 2019). Indeed, it is generally assumed that metals are considerably affected by potential damages when RH raises above 60%, since water vapour condenses and settles on substrates, igniting the so-called "wet-dry" cycle of corrosion (Evans and Taylor, 1972; Maréchal *et al.*, 2007; Angelini and Argyropoulos, 2008). Furthermore, substrates made of silver, copper, lead, or zinc are strongly altered in the presence of indoor gases, such as sulphur oxides or hydrogen sulphide, leading to the formation of species considered harmful or unesthetic (Watkinson, 2010; Degrigny *et al.*, 2016; Letardi, 2021). In particular, when referring to silver and copper-based alloys, the corrosion phenomenon ignited by the presence of gaseous sulphur compounds is defined "tarnishing" and it is characterised by the formation of a thin film (i.e., up to hundreds of nanometres) which has a substantial impact on the aesthetic of the substrate due to its typically dark and dull appearance (Kuhn and Kelsall, 1983; Schalm *et al.*, 2016; de Figueiredo Junior *et al.*, 2021).

When corrosion is already formed on the surface of historical metals, conservators can opt for different intervention methods in order to tackle such alteration, which can be undesired either for aestheticism or harmfulness reasons (Turner-Walker, 2008). Stabilisation or removal of altered layers present can be achieved by metal CRs work. The first treatment is aimed at converting detrimental corrosion products into more stable phases while keeping an aesthetically acceptable aspect according to CR standards (Turner-Walker, 2008; Joseph, Simon, *et al.*, 2012). However, this procedure is not commonly applied to indoor historical pieces, but rather explored in the case of archaeological or outdoor-set metals (Comensoli *et al.*, 2017; Kergourlay *et al.*, 2018; James and Joseph, 2021). On the contrary, corrosion removal is a preferred practice on historical collections, although it needs careful preliminary consideration (Angelini and Argyropoulos, 2008). Indeed, due to the inherent artistic, historical, aesthetic, and monetary value, the preservation of the original surface of artworks is generally prioritised, despite the possible presence of alterations (Gillies and Seyb, 2013). Nonetheless, when the appearance, functionality, or long-term conservation are endangered by artwork condition, it is inevitable to remove such detrimental surface layers (Mari Yanagishita, 2012; Siano *et al.*, 2012; Gillies and Seyb, 2013). Thus, when corrosion removal is considered, a preliminary evaluation of the alteration exhibited (e.g., noble or detrimental patina) and the intervention methodology to be applied are crucial, in order to not damage treated metal substrates or possible associated materials (i.e., composite objects), lose information about object history, decorations, or authenticity (Angelini and Argyropoulos, 2008; Turner-Walker, 2008).

Several cleaning methods are available for CR cleaning interventions on historical metals, and are normally classified as follow (Table 1.1):

- **Mechanical**: this class of interventions is based on wet or dry abrasion, and in particular it is run by means of abrasive pastes, erasers, scalpel, rotary tools, or steam when working on thin corrosion layers as normally present on historical metals. The employed tools are generally reusable for several interventions, which is considered a positive aspect. However, mechanical methods require high caution since the employed technique might be too aggressive on the treated substrate, marking it irreparably with scratches or provoking excessive loss of surface information (e.g., decorations). Because of the lack of control and consequent extreme attention needed, mechanical methods are reported as time-consuming practices. Tools and materials employed in mechanical cleaning can leave post-treatment residues that are often removable by simple dry brushing or solvents, yet the situation is more challenging in the presence of metal porosities or inlays. (Argyropoulos, 2008; Plé and Schröter, 2020; Basilissi *et al.*, 2022).
- **Chemical**: mainly water solutions made of acids, solvents, and complexing agents. The category includes a vast number and heterogeneity of substances, ranging from thiourea, sodium or ammonium thiosulphate, Deep Eutectic Solvents (DES), and primarily synthetic complexing agents such as ethylenediaminetetraacetic acid disodium salt (Na_2EDTA), diethylenetriaminepentaacetic acid (DTPA), or triammonium citrate (TAC). When unstrained chemical solutions are employed, it is complicated to limit the intervention area and adjust the cleaning performance as sought. Moreover, chemical methods require an attentive closing clearing or rinsing phase to remove any residual chemical remains that may over-clean and corrode the metal, interacting with the substrate in an uncontrolled way. Chemicals present evident drawbacks in terms of health and environmental risks because of the conventional use of volatile and toxic substances that would require the use of personal protective equipment (PPE), ventilation systems in the workshops, and specific waste treatments, which are often demanding and expensive requirements for professionals to comply with. Nevertheless, these products are popular among CRs for metal cleaning despite the numerous drawbacks because of their efficiency, extensive availability, and affordability. (Angelini and Argyropoulos, 2008; Contreras-Vargas, Ruvalcaba-Sil and Rodriguez-Gómez, 2013; Palomar, Ramírez Barat, *et al.*, 2016; Albelda-Berenguer, Monachon and Joseph, 2019; Selwyn and McKinnon, 2021; Tsurumaki *et al.*, 2022).
- **Electrochemical**: electrochemical reduction of corrosion species by immersion in electrolytic baths (e.g., NaOH or formic acid solutions) or by application of electrolytic "pencils" (e.g., PLECO[1]) for more restricted and controlled intervention. Generally, the method implies converting corrosion products (e.g., Ag_2S) into metallic species (e.g., Ag). The procedure is highly selective since the potential applied is set according to the target species, thus mass loss is negligible. However, the substrate surface will still be affected by the morphology induced by the alteration compounds previously present, therefore causing surface micro-roughness that would lead to higher reactivity to caustic agents and, thus, re-corrosion. Additionally, the technique is considered expensive for a vast use in metal care and requires technical skills for the right choice of parameters. Especially in the case of electrolytic pencils, the cleaning is time-consuming and, therefore, is frequently limited to specific instances in the presence of composite and elaborate artefacts (e.g., textiles with silver threads). (Degrigny, 2010; Palomar, Ramírez Barat, *et al.*, 2016; Hindborg, 2019; Ricotta, Gagnini and Degrigny, 2022).
- **Others**: laser, plasma, and ozone cleaning are reported as alternative advanced technologies for metal cleaning. Despite granting fast and potentially adjustable cleaning, the use of these techniques is strictly limited to experts belonging to private companies that also provide the machines themselves, hence justifying the significant and prohibitive cost of such interventions. Several additional constraints and problems are reported in the literature, ranging from the over-heating of

[1] Electrolytic device developed for the local cleaning of silver tarnish (Degrigny *et al.*, 2016).

metal surfaces when exploiting laser ablation, to the excessive invasivity on metal substrates. (Hacke *et al.*, 2003; Grassini *et al.*, 2007; Mateo *et al.*, 2009; Palomar, Oujja, *et al.*, 2016; Schalm *et al.*, 2018).

Table 1.1 Comparative table of the main cleaning methods exploited on historical metal collections.

	Mechanical	**Chemical**	**Electrochemical**	**Others**
Examples	Abrasive pastes, erasers, scalpels, rotary tools, steam, cloths	Complexing agents, acids, solvents	Electrolytic reduction by immersion or electrolytic "pencils"	Laser, plasma, and ozone cleaning
Advantages	Affordable, reusable	Chance of high control (e.g., gels), affordable	Highly selective, negligible mass loss	Fast, adjustable
Drawbacks	Time-consuming, invasive to artworks, possible residues	PPE and ventilation, materials and wastes possibly harmful to operator, nature, and artwork	Cost, lack of long-term efficacy, technical skills, time-consuming	Surface heating, invasive, advanced technologies and expertise, cost

1.2.2 Organic coatings for the protection of historical metal collections

Once historical artefacts have already undergone cleaning intervention and environmental parameters are not fully controllable, a precaution to corrosion development is to shield the metallic surface from external atmospheric agents. A valid and often-exploited solution relies on the application of organic protective coatings (Angelini and Argyropoulos, 2008). Such materials provide a screening film onto metals with specific physical, mechanical, and aesthetical characteristics that allow CRs to choose coatings according to the substrate treated and the displaying environment (e.g., indoor or outdoor) (Watkinson, 2010). The products typically employed in metal conservation are both of natural (e.g., beeswax, resins) or synthetic origin (e.g., nitrocellulose lacquers, acrylic varnishes, microcrystalline waxes) (Argyropoulos, Giannoulaki, *et al.*, 2007). The second class of coatings has acquired increasing relevance in CH since they are designed mainly for industrial purposes with high-performance and durability features in order to be the most environmentally-proof as possible (Argyropoulos, Charalambous, *et al.*, 2007; Watkinson, 2010; Wolfe and Grayburn, 2017). However, being developed for the industrial sector, synthetic coatings do not always fulfil conservation ethics, for instance, regarding the reversibility of the application, the respect of aesthetic aspect of the artwork, or ease-of-use, as in the case of polyurethane varnishes (Appelbaum, 1987; Degrigny *et al.*, 2007; Cano, Lafuente and Bastidas, 2010; Watkinson, 2010). Therefore, new materials are developed in the branch of conservation sciences seeking protective films fitting CH requirements (Molina, Cano and Ramírez-Barat, 2023a). In particular, it is noteworthy the current awareness towards the design and investigation of innovative coatings that merge the compelling features of nanomaterials and naturally-based substances (e.g., waxes) in a green and sustainable outlook (Giuliani *et al.*, 2018; Maria Calvino *et al.*, 2023). Despite the wide range of options provided by the industry, CRs tend to rely on materials that have been deeply tested or are commonly reported in the previous interventions, therefore resulting in being considered adequate for metal heritage safeguard (Argyropoulos, Giannoulaki, *et al.*, 2007; Watkinson, 2010). A comprehensive review of the organic coatings mostly employed by CRs and lately developed in metal conservation has been recently provided by Molina, Cano and Ramírez-Barat (2023). The authors confirm that despite the existence of new organic coatings successfully designed for metal heritage preservation,

conservator-restorers are sceptical and instead resort to "traditional" solutions that thus are more represented in metal collections, and would include (Table 1.2):

- **Acrylic resins**: coatings based on acrylic and/or methacrylic copolymers are the most employed in metal conservation. The family of Paraloid® (Acryloid® in the USA) is the most represented and counts a vast number of formulations, among which Paraloid® B72, a copolymer of ethyl methacrylate and methyl acrylate, stands out. It is undoubtedly the most extensively used coating among acrylics due to its multiple feasible applications in art conservation as consolidant, adhesive, and protective film. Indeed, it is reported to be the most employed protective coating in Europe for historical indoor alloys made of iron, copper, and silver. For outdoor artworks, Incralac® is often a preferred option. The formulation comprises Paraloid® B44, additives as levelling agents, and benzotriazole (BTA), which is a corrosion inhibitor exploited as a UV absorber. In general terms, acrylic coatings demonstrated satisfactory transparency, mechanical properties, ease-of-use, and chemical stability over time, providing acceptable long-term protection, re-treatability, and aesthetics. Despite the conventional approval by CRs, acrylic resins are proven to be affected by photo-oxidation reactions that cause critical consequences affecting the aestheticism (i.e., yellowing effect) and the resistance to degradation in the long-term. Moreover, the plethora of products available and the formulation variability through the years make a comprehensive understanding and evaluation of possible drawbacks of this class of materials difficult. Yet, as an example, Paraloid® B67 failed in metal protection and reversibility because of the long ester groups, present in its chemical formulation, that are proven to be more prone to thermal and photodegradation. (Lazzari and Chiantore, 2000; Chiantore and Lazzari, 2001; Argyropoulos, Giannoulaki, *et al.*, 2007; Wolfram, Brüggerhoff and Eggert, 2010; Down, 2015; Carmen, 2016; Mohamed and Mohamed, 2017; Švadlena and Stoulil, 2017; Artesani *et al.*, 2020).
- **Nitrocellulose lacquers**: before the advent of Paraloid®, cellulose nitrate formulations were widely exploited as protective coatings and consolidants in metal care. The most recurring evidence in the literature mentions commercial products, such as Agateen™, Frigiline™, Ercolene™, or Zaponlack. Nitrocellulose lacquers are mainly exploited for the protection and aesthetic of silver heritage due to their high protective performance in the presence of gaseous sulphides. This property also led to the application of these coatings on indoor historical copper-alloys. Evaluation tests by accelerated ageing demonstrated that nitrocellulose coatings are susceptible to the phenomenon of yellowing as the acrylic counterparts, while being less long-time effective. Contradictory results are instead reported for the long-term reversibility of such materials. (Luxford and Thickett, 2007; Heginbotham *et al.*, 2014; Eggert *et al.*, 2019; Borén, 2022; Katayon, 2022).
- **Waxes**: natural waxes (e.g., paraffin, beeswax) are nowadays abandoned options being tested as not long-lasting and even potentially dangerous for metallic substrates because of the release of organic acids by ageing (Russo *et al.*, 2023). The synthetic counterparts are mainly classified as microcrystalline and polyethylene waxes. The first category includes materials derived from petroleum refining and is mostly represented in indoor metal care by Renaissance™ and Cosmoloid H80 waxes. The second group comprises low molecular weight polyethylene polymers, such as the family of Poligen® ES (e.g., 91009, 91012). In general, synthetic waxes are often used because of their inherent hydrophobicity and thus protection against moisture; additionally, they provide a matt finishing appreciated by metal CRs. However, they can induce the darkening of metallic surfaces, accumulation of dust and other atmospheric particles, and their durability and consequently long-term protection are judged lower than acrylic varnishes, hence requiring frequent renewal. (Moffett, 1996; Watkinson, 2010; Couture-Rigert, Sirois and Moffatt, 2012; Molina, Cano and Ramírez-Barat, 2023a).

Table 1.2 Organic protective coatings most represented in indoor metal collections.

	Acrylic resins	Nitrocellulose lacquers	Waxes
Examples	Paraloid® (or Acryloid®); e.g., Paraloid® B72, B44, Incralac®	Agateen™, Frigiline™, Ercolene™, Zaponlack	Beeswax, paraffin, polyethylene (e.g., Poligen® ES) and microcrystalline (e.g., Cosmoloid H80, Reinassance™) waxes
Advantages	Transparency, mechanical properties, adhesion, chemical stability, multi-functionality, re-treatability	Protective in high-sulphide conditions	Natural options, barrier to moisture and oxygen, matt finishing
Drawbacks	Yellowing and lack of resistance to degradation in the long-term	Not long-time effective, unsure reversibility	Low durability and protection, organic acids by ageing, surface darkening, dust accumulation

Evidently, organic films are also not everlasting materials but are sensitive to detrimental factors through time, even if to a lesser degree or merely not like metals. The possible altering phenomena affecting organic coatings can be mostly linked to:

1) photo-oxidation provoked by UV radiation of light sources, for instance, which leads to the oxidation of double bonds, polymer segment scission, and cross-linking (i.e., covalent bonds are formed among the molecular chains);
2) high levels of temperature and/or humidity that induce thermal degradation, provoking the so-called yellowing effect, and hydrolysis of the polymer chain;
3) biodeterioration by microbial (or higher forms of life) activity (Mills and White, 1987; Perera, 2003; Cappitelli, Zanardini and Sorlini, 2004).

All these detrimental factors affect the chemical stability of the organic coating, inducing undesired consequences, such as aspect alteration (e.g., yellowing phenomena), change in the solubility/reversibility of the material (i.e., reversibility ethics in art conservation), harmful reaction with the underlying substrate (e.g., wax production of organic acids), coating cracking or even detachment, thus producing mechanical stress to the underneath surface and failure in the protection purpose because of the eventual exposure of metals to caustic agents (Appelbaum, 1987; Smith, 1988; Perera, 2003; Siatou *et al.*, 2007; Couture-Rigert, Sirois and Moffatt, 2012; Munoz-Vinas, 2012; Molina, Cano and Ramírez-Barat, 2023a).

Therefore, the removal (and replacement) of organic coatings is inevitable once their preservative and aesthetic functions are compromised. The most employed approach to this aim is the dissolution of the no more-desired coating (Jaeger, 2008; Cagnini, Gennai and Mazzoni, 2012; Mari Yanagishita, 2012; Giuliani *et al.*, 2018). Generally, it is considered that solubility follows the basic principle of *like dissolves like*: "Chemically similar" substances, mainly in terms of intermolecular forces, are soluble in each other. Despite its simplicity, the rule aids in navigating when choosing solvents; also, CRs often rely on this principle by means of helpful solubility diagrams, such as Teas Charts, for the selection of theoretically appropriate solvents according to the case treated (Stavroudis and Doherty, 2007; Phenix, 2013). The Teas diagram, reproduced in Figure 1.1 (Chelazzi, Giorgi and Baglioni, 2018), is usually a bi-dimensional plot that schematically represents the chemical properties of solvents. In particular, the position in the chart is determined mathematically from Hansen solubility parameters developed for the study of intermolecular forces. Specifically, in the diagram space limited by the axis it is reported the contribution of dispersive (F_d), polar (F_p), and hydrogen bonding (F_h) forces of materials (Stavroudis and Doherty, 2007; Casini, Chelazzi and Baglioni, 2023).

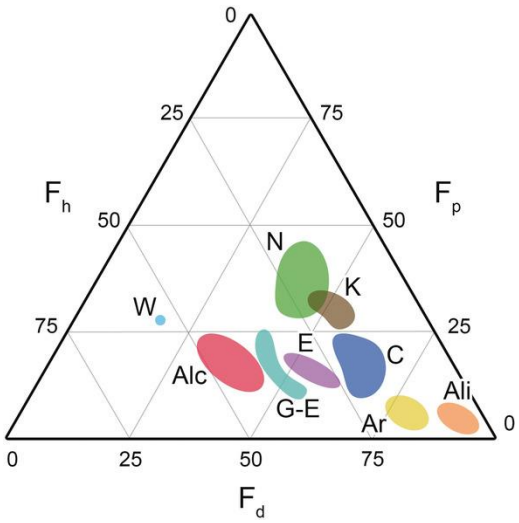

Figure 1.1 Teas solubility diagram indicating the solubility parameters of common families of solvents having similar properties: water (W), nitrogen-containing solvents (N), ketones (K), alcohols (Alc), glycol ethers and esters (G-E), esters (E), chlorinated solvents (C), aromatics (Ar), aliphatics (Ali). (Reproduced from Chelazzi, Giorgi and Baglioni, 2018).

1.3 Gels as a reliable cleaning delivery system in Cultural Heritage

The employment of neat solvents may be unsafe for users due to their potential flammability or by prolonged inhalation and exposure (Davidson, Hannigan and Bowen, 2021; Kurnianto *et al.*, 2023). This scenario, unfortunately, matches with the figure of conservators, who often employ toxic solvents such as xylene, acetone, white spirit, turpentine, in a confined workplace and possibly avoiding the precautional use of PPE, fume hoods, or ventilation systems (Varnai *et al.*, 2011). Furthermore, in art conservation, one of the leading priorities is the safety of the artwork itself. This entails the importance not only of suitable products but also of an appropriate application methodology for the security of CRs during interventions (Brandi, 1963; Appelbaum, 1987). In the case of metal heritage, the presence of a corrosion layer turns the substrate into highly porous and thus drastically more water/solvent sensitive. The substrate micro-porosity leads also to a less precise and flawed post-treatment rinsing of unstrained cleaning products employed. Moreover, chemicals (e.g., solvents, acids, chelators) can be potentially corrosive if not properly handled and retained (Heitz, 1974; Di Marino *et al.*, 2018). To minimise such potential inherent drawbacks of unstrained chemical cleaning, delivery systems are a valid alternative for art conservation, to assure a controlled release of the loaded treating solutions and solvents.

Nowadays, several methodologies are available to CRs in order to avoid the use of neat solvents and unrestrained active solutions on artworks. Delivery systems such as (micro)emulsions (Fratini and Carretti, 2013; Brajer *et al.*, 2014; Chelazzi, Giorgi and Baglioni, 2018; Lo Dico *et al.*, 2018) and gel formulations (Cremonesi, 2013; Mazzoni *et al.*, 2014; Chelazzi *et al.*, 2018; Casini, Chelazzi and Baglioni, 2023) are widely reported in the literature as suitable methodologies in art conservation. In particular, the latter class is considered as most reliable, tailorable, and performing, and therefore gels have been adopted in the development of the research study presented in this doctoral dissertation.

Gels are biphasic systems made of at least two components: a polymer and a fluid phase. The polymer, acting as thickening agent, forms a three-dimensional network in the liquid medium (Rogovina, Vasil'ev and Braudo, 2008). The cross-linked system entraps the liquid, limiting simultaneously its unstrained dispersion by evaporation and excessive release. The liquid is retained in the network through interactions between the polymer chains. According to their chemical nature, these interactions can be reversible thanks to weak bonds (i.e., hydrogen bonds, van der Waals) or irreversible in presence of covalent bonding. The different bonding leads to the formation of physical and chemical gels, respectively, presenting dissimilar chemical features (Fratini and Carretti, 2013). Namely, the inherent forces within chemical gels are stronger than the adhesive forces between gel and substrate to be treated. This implies an easier detachment of such formulation from the target, thereby avoiding extra steps of clearance to remove potential residues (Baglioni *et al.*, 2019). Finally, gel systems can be classified according to the fluid contained inside the polymer matrix:

in presence of water, they are called "hydrogels", while non-aqueous formulations, hence loaded with organic solvents or oils, are defined as "organogels" or "solvent-gels (Fratini and Carretti, 2013).

In the last decades of the twentieth century, Richard Wolbers introduced gel systems to the world of art conservation (Wolbers, 1988, 1992). During workshops with conservator-restorers, he presented several pioneering solutions for the cleaning of paintings. Viscous solvent-gels able to retain polar solvents (e.g., ethanol, xylene) in a Carbopol (934, 940, 950) matrix by surfactant action of Ethomeen® C-25 or C-12 together with water; emulsions of polar and non-polar solvents held together thanks to the addition of an emulsifier (Brij® 35, Triton™ X-100, TWEEN® 20); hydrogels loaded with enzymes to achieve a very selective cleaning of undesired materials. In all cases, a fundamental phase was the clearance by dry cotton swabbing followed by the use of neat solvents, selected according to the substrate (e.g., white spirit, water, xylene, Shellsol T), in order to remove any residual presence of the treatment (Byrne, 1991). His work focused on paintings, which are water- and solvent-sensitive substrates, and demonstrated that gel formulations are ideal for high-controlled and less invasive cleaning interventions in art conservation (Byrne, 1991; Wolbers, 2000).

The captivating and promising evidence on canvas paintings encouraged the diffusion of cleaning gelled systems to several other CH sectors, including wall paintings and stone care (Cushman and Wolbers, 2007; Barberà Giné and Marín Ortega, 2017; Toreno *et al.*, 2018; Van Loon *et al.*, 2019). For paper, textile, or wood substrates, the employment of gels became an essential methodology able to replace the conventional cleaning procedure by immersion into water solution that was not optimal for extremely sensitive materials (Mazzuca *et al.*, 2014; Delattre, Bouvet and Le Bourg, 2017; Rapti *et al.*, 2017).

Nowadays gel-based cleaning protocols are recognised as well-grounded and effective methodologies by CRs, thanks to their high retention and interesting rheological properties that allow a spatially precise and time-controlled intervention, while providing more ease in handling during application and clean-up phases (Guilminot *et al.*, 2018; Prati *et al.*, 2019; Baij, Hermans, *et al.*, 2020). In addition, gelled systems can potentially adsorb undesired substances to be removed (i.e., soiling, corrosion products, and degraded organic materials) in the polymeric matrix (Giordano and Cremonesi, 2021; Theodorakopoulos *et al.*, 2023). Eventually, gels drastically hamper evaporation of volatile components (i.e., solvents), hence reducing active agents quantities needed for the intervention, while creating a safer work environment by limiting operator exposure to potential harmful substances' vapours (e.g., acetone, ligroin, xylene) (Chelazzi *et al.*, 2018).

Nevertheless, the use of gels on metal artworks is still anecdotal, even though there is the need for localised treatments, considering how heterogenous they can be: composite artifacts, gilded artworks, painted metals, etcetera (Guilminot *et al.*, 2019). Furthermore, the use of gels would provide several advantages such as the reduction of solvent vapour inhalation and the prevention of surface scratches induced by mechanical procedures (Duncan, Berrie and Weiss, 2017). The main critical aspect of gel implementation in metal care might be attributed to potential rigidity of such systems. Most of the time, indeed, it implicates a non-even contact and adhesion on the surface, which, for metals, can be complex in terms of shape (e.g., curves, vertical position) and morphology (e.g., due to corrosion). However, the high modularity of gels eases the feasibility of satisfactory results on metals alike on other substrates, as demonstrated by the literature (Duncan, Berrie and Weiss, 2017; Guilminot *et al.*, 2019; Yiming *et al.*, 2019; Guilminot, 2023).

1.4 The advent of Green Chemistry principles in Art Conservation

As evident to scientific and civil community, in the last decades greater concern, and therefore attention, is addressed to the impact of everyday habits, methodologies, goods, and materials on the environment and on human health. The field of Cultural Heritage is not excluded from this issue and is reasoning about the sustainability of its well-grounded practices adopted in conservation practices (Merriman, 2008; De Silva and Henderson, 2011; Kumar and Sagar, 2017). Indeed, despite using little quantities compared to the industrial sector, the regular exploitation of toxic active agents (e.g., EDTA, TAC, xylene, methyl ethyl ketone MEK) or petroleum-derived products (e.g., white spirit, synthetic coatings) piles up at global scale

with other field activities, such as pharmaceuticals, fuel, food industry, and so forth, generating concern (Calvo-Flores *et al.*, 2018). Indeed, the iteration of unsustainable and harmful practices in art conservation causes at first an impact on operators' health, and in a second instance, especially if wastes are not correctly disposed, also on the environment and global health (Duan *et al.*, 2017). From this perspective, the growing concern is legitimate around turning the page from several materials and methods considered harmful or pollutant, yet traditionally exploited in CH, towards the so-called "greener" substitutes (Del Curto and Turrina, 2023). The term "green" gathers a wide range of safe and responsible alternatives that can be selected and recognised using twelve factors listed in the journal *Green Chemistry* (Anastas and Eghbali, 2010), earlier discussed by Paul Anastas and John Warner in 1998 (Anastas and Warner, 1998). The principles are nowadays to be considered as cornerstones to face environmental and global health problems, converting traditional methods and substances into more sustainable alternatives. The Green Chemistry principles confront aspects such as renewable origin, recyclability, relative energy consumption and biodegradability; hazardousness (e.g., toxicity and flammability) of products and related wastes; availability on a large scale and affordability (Table 1.3). As discussed in the scientific paper (Anastas and Eghbali, 2010), a critical and pivotal point in the green inversion is that new alternatives have to display properties and performances analogous to traditional substances and methodologies to be considered as valid substituents.

Table 1.3 Resuming table listing the twelve principles of Green Chemistry defined by Paul Anastas and John Warner in 1998 (Anastas and Warner, 1998).

1	Waste prevention	**7**	Use of Renewable Feedstocks
2	Atom Economy	**8**	Reduce Derivatives
3	Less Hazardous Chemical Syntheses	**9**	Catalysis
4	Designing Safer Chemicals	**10**	Design for Degradation
5	Safer Solvents and Auxiliaries	**11**	Real-time analysis for Pollution Prevention
6	Design for Energy Efficiency	**12**	Inherently Safer Chemistry for Accident Prevention

1.4.1 Seeking for "bio" building-blocks for cleaning gels in metal care

The majority of publications for metal conservation mentions the use of synthetic polymers and artificial active agents (e.g., organic solvents, chelators) for the design of cleaning formulations. In 2014, a set of indoor bronze sculptures were successfully treated via Carbopol solvent-gel applications to remove layer-by-layer dirt, protective waxes, and corrosion species (Smith, 2017). While water-based formulations made of the synthetic polymer poly(vinyl alcohol) (PVA) were designed by Baglioni et al. as part of the NANORESTART project and successfully assessed on copper alloys (Parisi *et al.*, 2018; Guaragnone *et al.*, 2020). Despite the evident and captivating potential, high attention must be addressed to waste management and the correlated ecological impact for such solutions. For instance, PVA is readily water-soluble, but inadequate disposal can cause pollution of groundwaters, and its biodegradation is achieved by very specific bacteria, barely represented in nature (Chiellini *et al.*, 2003; Feldman, 2020). Another critical point is the sustainability of gelling agents' production. Although bio-derived from cellulose, often the synthesis of cellulose-based polymers cannot be considered green, since it may require reagents hazardous for the aquatic environment (e.g., chloroacetic acid used for the synthesis of carboxymethyl cellulose) (Duplat *et al.*, 2009).

In contrast, scarcer is the literature on bio-derived and biodegradable gel systems, both in art and more specifically in metal conservation; yet new research evidence is reported in the last years (Paragraph 1.4.2).

When operating with gel cleaning systems, the green sieve should be directed towards all formulation components, namely, thickening agents (i.e., polymers) and additional active constituents, such as solvents and complexing agents. Utmost care should be paid in the choice of the materials, considering features ranging from the original derivation of the sources to their recyclability and degradability (Jiménez-González *et al.*, 2004; Tabone *et al.*, 2010; Yates and Barlow, 2013). In particular, the doctoral research presented in this manuscript was addressed towards the exploitation of "bio", namely potentially bio-sourced and biodegradable, gel components. A more exhaustive overview and explanation of this concept is proposed in the paragraphs that follow.

1.4.1.1. Bio-polymers

Biopolymers are naturally occurring polymers (e.g., polyhydroxyalkanoates PHAs, agar, chitosan) or derived from bio-based monomers (e.g., polylactic acid PLA, polybutylene succinate PBS) (Kaplan, 1998; Zhu, Romain and Williams, 2016). Their most evident green quality is that starting resources are not petroleum-based, contrary to traditional materials such as polypropylene (PP), polystyrene (PS), or high-density polyethylene (HDPE) (Kaplan, 1998). Biopolymers appear as valid candidates to replace petrochemical counterparts, however, the generally high cost of production and significant amount of raw material required for their production draw boundaries to a wider diffusion (Rattana and Gheewala, 2019). They are broadly employed for biomedical applications, such as suture threads (Knutson *et al.*, 2017) and drug carriers (Li *et al.*, 2018) because of their human-compatibility and natural deterioration without any side effects. Furthermore, they are diffused in fields ranging from food industry to waste management, passing through cosmetics and household products (Keshavarz and Roy, 2010; Peelman *et al.*, 2013; Bayer *et al.*, 2014; Calabrò and Grosso, 2018; Onen Cinar *et al.*, 2020). It is important to remark that not all bio-sourced (i.e., derived from microbes, fungi, or plants) polymers are implicitly owned with biodegradability, as in the case of conventional nylon despite being manufactured from polyamides derived from castor oil plants (Leja and Lewandowicz, 2010; Zhu, Romain and Williams, 2016). Evidently, the global evaluation of polymers and biopolymers is complex when investigated under the point of view of Green Chemistry principles. Therefore an increasing number of publications is focused on life cycle analysis (LCA) of polymers for a better understanding of sustainability and safety of such materials (Yates and Barlow, 2013; Ramesh and Vinodh, 2020).

1.4.1.2 Bio-solvents

As seen in the case of organic protective coatings for metal heritage, solvents are indispensable chemical tools in art conservation, as much as in a broad spectrum of sectors, including pharmaceuticals, food industry, household products, cosmetics, paint industry, etc. Therefore, it appears obvious to put these substances under review, not only for possible consequences on direct users but also for the potential impact on a wider scale in the environment, and consequently, on global health. The topic is crucial and reached the attention of renowned institutions such as the World Health Organization that pointed out problems derived from certain substances and drew up localised restrictions on their use, to mitigate the consequential hazard (Calvo-Flores *et al.*, 2018).

In the world of cultural heritage, besides the spheres of human and nature health, the evaluation of the potential harm on the artworks themselves is central, even overriding compared to the abovementioned factors. Considering art conservation from the Green Chemistry outlook, water could be ascribed among the greenest solvents commonly employed, being harmless for operators and environment, readily available, and not expensive. Nonetheless, several reactions cannot be performed with water alone due to solubility factors (e.g., removal of non-polar coatings). In addition, for metals, it is important to remind that water is a key player in the spontaneous natural process of corrosion, implying the willingness of substituting it with more substrate-friendly organic alternatives (Maréchal *et al.*, 2007). Besides water, a solvent (or mixture) satisfying even a few of the Green Chemistry principles can be rated as "green" weighed against its conventional counterparts. Thus, a proper comparative assessment should be carried out, considering the three macro-subjects of health, safety, and nature, according to one of the numerous scoring-guides

proposed in the literature (Anastas and Eghbali, 2010; Prat, Hayler and Wells, 2014; Calvo-Flores *et al.*, 2018).

Bio-solvents may be counted in the category of greener solvent alternatives. They are produced from readily renewable feedstocks, by fermentation or chemical transformation of biomass derivatives (Calvo-Flores *et al.*, 2018). This implies the valorisation of sources otherwise considered as wastes, increasing the greenness score of this class of chemicals. Bio-ethanol, bio-butanol, ethyl lactate, gamma-valerolactone, and biodiesel are some bio-solvents that can be mentioned as useful greener alternatives to conventional counterparts used in metal care (Calvo-Flores *et al.*, 2018). As in the case of bio-polymers, not all bio-solvents can be inherently considered innocuous for the environment and human health. For instance, bio-butanol has inherent low acute toxicity that makes the solvent accepted in several sectors as in art conservation (Gettens and Stout, 1966), however, its fumes can induce noxious effects by lengthened inhalation, thus, despite the bio-origin, this solvent is harmful under the irrevocable criterion of human health (Calvo-Flores *et al.*, 2018)

1.4.1.3 Bio-chelators

Lastly, when aiming to remove corrosion and tarnishing species form metal substrates, complexing agents are often required in chemical cleaning solutions. So far metal CRs resorted to non-renewable, pollutant, and toxic compounds such as ethylenediaminetetraacetic acid (EDTA) and diethylenetriaminepentaacetic acid (DTPA) (Oviedo and Rodríguez, 2003; Xie, 2009). Seeking for naturally produced and biodegradable chelators to be loaded in bio-gel formulations, it is necessary to rely on microbial metabolic activity. The literature shows indeed a new impulse in this research branch of Conservation Science, aimed at taking advantage of the natural processes of certain organisms to complex metal ions present in the surrounding environment for vital purposes (Fomina *et al.*, 2005; Albelda-Berenguer, Monachon and Joseph, 2019). From one side, the exploitation of living microorganisms, such as the fungi *Beauveria bassiana* and the fungal strain *Alternaria* sp., is of high interest in metal conservation, because of their ability to complex metallic ions dangerous for their survival (Hong and Simon, 2007; Joseph, Cario, *et al.*, 2012). Their activity have been successfully exploited for the cleaning and protection (i.e., formation of metal oxalates) of historical metallic heritage (Joseph, Cario, *et al.*, 2012; Comensoli *et al.*, 2019). However, these methods set limitations in terms of storage conditions of the living organisms, environmental parameters (i.e., temperature and relative humidity) of application to promote microbial activity, and, most importantly, CRs hesitation towards their exploitation for prejudiced safety reasons. Hence, the exploitation of non-living microbial solutions could be a more favourable bio-option to be explored, trying to overcome all previously mentioned limitations. To this purpose, previous research has demonstrated the efficacy and reliability of microbial extracts for heritage conservation. In particular, successful and encouraging results were obtained by cleaning solutions of bio-derivates like citric acid (Palomar, Ramírez Barat, *et al.*, 2016; Guilminot, 2023) and siderophores (Rapti *et al.*, 2017, 2021, 2023; Albelda-Berenguer, Monachon and Joseph, 2019; Ganesan *et al.*, 2022), which were proposed as more responsible complexing agents than traditional EDTA or DTPA for the treatment or cleaning of altered substrates, such as waterlogged wood, textile, paper, and metals. The mentioned substances are microbial metabolites commonly available in nature and their biodegradability is well-documented (Sauer *et al.*, 2008; Liaud *et al.*, 2014).

1.4.2 Bio-based cleaning gels for heritage conservation

1.4.2.1 Hydrogels

Polysaccharides are the main bio-polymers utilised as thickening agents in hydrogels for metal heritage cleaning. Namely, agar, gellan gum, and xanthan gum are the most represented in the literature, and the resulting formulations all belong to the class of physical gels, since water is physically retained within the gel network by hydrogen bonding of the polymer polar groups (Dalvi-Isfahan, Hamdami and Le-Bail, 2017). A short overview of gel preparation, features, and applications for the cleaning of metals is proposed here to display the multiple potentials of such systems. Although employing bio-derived and biodegradable polymers, the final formulations are frequently loaded with active solutions not belonging to the category

of "green" materials. Therefore, the mention of such solutions is rather intentioned to show the potential of the bio-gelling agents with the aim of fostering their implementation with a greener attitude.

- **Agar** is extracted from red seaweed membranes, in particular *Gelidium* sp., *Pterocladia* sp. and *Gracilaria* sp. (Tamura and Takagi, 2017). The primary compound is agarose, which is however more often found impurified together with agaropectin, being less expensive (Cremonesi, 2013). It forms rigid hydrogels when heated above 90 °C and cooled down, and provides satisfying results when directly applied hot on the target, as in a sol-gel state, since it still has the chance to conform to the artefact surface (Guilminot *et al.*, 2019). The heating procedure, which is normally performed twice to achieve a well-interconnected network (Medina-Esquivel *et al.*, 2008), can discourage CRs from the use of agar, especially when working out of their ateliers, hypothetically with no heating devices or electricity available. Furthermore, agar gels cannot be formed directly out of acidic or basic solutions because the polymer would incur hydrolysis (Armisén and Gaiatas, 2009). Yet, several non-neutral solutions and solvents can be absorbed by immersion once the gel is created (Giraud *et al.*, 2021). A new commercial product Nevek® has been recently developed and is reported as particularly advantageous in metal cleaning, because it reduces the preparation time of conventional agar gels being a ready-to-use double gellified agar with 5% ethanol that mitigates microbial growth during storage (Guilminot *et al.*, 2019).
  In the literature, several methods based on agar are mentioned for the successful cleaning of metal heritage. In the case of archaeological silver horns, an agar gel was initially pre-formed and subsequently impregnated with the active solution for their cleaning (Marchand *et al.*, 2013). On the contrary, in the case of inlays on copper-alloys, an agar hydrogel was formulated directly loaded with the complexing solution after buffering the starting mixture at neutral pH (Fays, 2018). Agarose rigid gels resulted in being the ideal solution for the careful electrolytic cleaning of Japanese lacquer objects, in order to face the complex combination of metal inlays present, namely tin, lead, and iron. The gel provided good localised electrolytic reduction treatment exclusively on the corroded areas, without affecting and altering the surrounding water-sensitive lacquers (Wolbers, Rivers and Yamashita, 2014). Similarly, agar formulations have been tested for the electrochemical cleaning of silver threads and silver leaves, however low efficiency was achieved on non-flat artefacts due to gel rigidity and tendency to crack (Létrange *et al.*, 2017; São João, Branco and Leite Fragoso, 2017).
  In light of the large exploitation in Cultural Heritage, as much as in food and other numerous industrial sectors, the recent shortage of agar supplies is not surprising, in addition to the unpredictability of its production due to the dependence on marine conditions (i.e., warmth, infesters). Therefore, despite the moderate usage of this thickening agent in art conservation, it is important to be aware of these issues, and try to adopt a greener and responsible attitude by choosing other gels whenever possible (Tamura and Takagi, 2017).
- **Gellan gum** is a polysaccharide produced by the bacterium *Sphingomonas elodea* (Wolbers, 2017). As agar, it can be employed for the formulation of rigid gels, that are best-performing when applied warm, and are compatible with impregnation of acidic and basic solutions once prepared, yet some references report the incompatibility of the polymer with complexing agents (Fays, 2018; Guilminot *et al.*, 2019).
  A commercial derivative-form, Phytagel®, is suitable to cold preparation and has been successfully used for the stabilisation of copper artifacts (Domon Beuret *et al.*, 2015). The polysaccharide was selected because of its adherence on vertical surfaces, ease of removal, and compatibility with the chosen active agents to be englobed (i.e., microorganisms). In addition to transparency, which was considered an asset since it allowed the monitoring of the treatment, its gelling properties are exhibited even at low concentration (0.5 to 5 g/L), and the obtained gellan-based formulations were stable in a wide pH range (Domon Beuret *et al.*, 2015).
- **Xanthan gum** is a thickening agent biosynthesised by the bacterium *Xanthomonas campestris* by fermentation of sucrose or glucose (Varghese *et al.*, 2020). It is compatible with aqueous solutions in a broad range of pH, yet it is less effective in gelling basic solutions (Guilminot *et al.*, 2019). The

inherent high viscosity of xanthan gels complicates the definition of the treated area as much as hard the removal afterwards from the metallic substrates (Fays, 2018; Guilminot *et al.*, 2019). The studies mention the rigorous clearance by neat water necessarily employed for a perfect elimination of any formulation remains, thus compromising one of the primary goals of gelled cleaning systems regarding the avoidance of unstrained solvents. Recent test interventions carried out on archaeological silver-plated copper alloy coins and historical heritage (i.e., tarnished silver object with reliefs, painted aluminium aircraft wrecks, and lead artefacts) confirmed that, although providing cleaning, xanthan-based formulations show the abovementioned drawbacks in relation to the significant amount of residues left on the treated surfaces (Guilminot, 2023).

1.4.2.2. Organogels

Organogels have been explored mostly for the highly-controlled cleaning of paintings and graphic documents, being multi-component artefacts and strongly sensitive to solvents (Baglioni *et al.*, 2015; Pianorsi *et al.*, 2017; Prati *et al.*, 2018). On the contrary, literature reports sporadic evidence regarding their application in the branch of metals (Duncan, Berrie and Weiss, 2017; Yiming *et al.*, 2019). Eventually, rare is the attention addressed towards the design of bio-derived solvent-formulations for the cleaning of artworks, and in these situations, the bio-polymer polyhydroxybutyrate (PHB) was chosen as thickening agent (Samorì *et al.*, 2016; Walsh-Korb, Ruiz-Fourcade and Avérous, 2017; Prati *et al.*, 2019; Yiming *et al.*, 2019). To briefly mention PHB green features, the polymer can be naturally synthesised by several microorganisms (e.g., *Alcaligenes* spp., *Bacillus* spp., *Azotobacter* spp., *Pseudomonas* spp.) from renewable feed-stocks rich in sugars, it is completely biodegradable, non-pollutant, and biocompatible (Yilmaz, Soran and Beyatli, 2005; Scalioni, Gutiérrez and Felisberti, 2017).

In the first case study here reported, PHB was employed together with alginic acid to create a functionalised organogel for the treatment of archaeological wooden findings (Walsh-Korb, Ruiz-Fourcade and Avérous, 2017). The core idea was the addition of iron chelators to the gel to examine the potential for the innovative development of *in situ* applications. Regrettably, to enhance polyhydroxybutyrate solubility, chloroform was employed to obtain lower molar mass polymer chains. This intermediate step would represent a critical drawback for large-scale use in conservation, due to the severe health danger associated with chloroform (Fawell, 2000). Its use and the unclear outcomes highlighted the need of improving the preparation protocol and exploring different chelating agents.

Samorì et al. (2016) introduced to CH the first fully bio-based organogels made from the bio-polymer polyhydroxybutyrate (PHB) and γ-valerolactone (GVL), which is a bio-sourced, non-toxic, and biodegradable solvent (Calvo-Flores *et al.*, 2018; Gao *et al.*, 2020). The resulting gel systems led to the removal of terpenic resin from oil paintings, leaving only little residues of GVL detected by solid-phase microextraction (SPME) that did not appear concerning in terms of retention into underlying layers (Prati *et al.*, 2018). However, the unwanted deposition of solvent on the object is a weakness, especially when referring to rigid gels that are expected to be highly retentive (Samorì *et al.*, 2016). It is a crucial point that attracted the attention of supplementary studies (Baij, Buijs, *et al.*, 2020), and lead to an additional implementation of the PHB-GVL formulation involving the use of cutting-edge electrospun material, interposed between gel and painting, in order to further minimise solvent residues (Jia *et al.*, 2020).

Another PHB-organogel was designed exploiting ethyl lactate (EL), a naturally produced, low-toxic, and readily biodegradable solvent (Pereira, Silva and Rodrigues, 2011; Kua *et al.*, 2016). The obtained PHB-EL gelled system performed satisfactorily to remove dammar from the surface of oil paintings (Prati *et al.*, 2019). Compared to the outcome yielded by the neat solvent applied by cotton-swabbing, the low mechanical stress provoked by the application of the gelled system is remarkable. In addition, a small amount of EL residues after gel treatment were evidenced by SPME analysis, in spite of solvent's inherent low vapour pressure (Prati *et al.*, 2019).

Despite not being fully bio-derived, it is noteworthy to mention one last green gel derived from polyhydroxybutyrate, because applied for the cleaning of metal heritage. The gel involved the use of biodiesel (BD), which is a renewable option to bypass the reliance on fossil-fuels (Gu and Jérôme, 2013;

Calvo-Flores *et al.*, 2018), and in this study was evaluated as an innovative greener candidate among non-polar solvents (Yiming *et al.*, 2019). As biodiesel itself is not able to create a gel out of PHB, the formulation included also the solvent dimethyl carbonate (DMC) to dissolve the polymer. The PHB-DMC/BD system was designed for the application on bronzes for the removal of wax coatings (Yiming *et al.*, 2019). Previous tests demonstrated that dimethyl carbonate alone does not affect non-polar materials (i.e., wax); therefore, the sole action of biodiesel for the removal of such coating was proven. However, the research pointed out also the well-known non-volatility of biodiesel, which appears as the main drawback of such procedure. Indeed, even if retained in a gelled system, biodiesel tended towards leaving residues on the metal surface, implicating an additional clearance step with free DMC to remove undesired remains (Yiming *et al.*, 2019).

Recently, dimethyl carbonate was exploited for the removal of dammar coatings present on paintings by means of a bio-derived organogel loaded with the aforementioned solvent (Çakmak *et al.*, 2022). The system was designed by using thiol-ene photopolymerization (TEP) from three bio-based building blocks, namely isosorbide, pyrogallol, limonene. However, pyrogallol is considered relatively toxic for human health, as pointed out by the research's authors, making questionable the greenness of the developed formulation despite the use of bio-sourced materials and the cleaning performance (Çakmak *et al.*, 2022).

1.5 HELIX project: towards bio-gel systems for historical metal cleaning

The research study presented in this manuscript has been carried out within the framework of the HELIX project (Investigating metal bioremediation for the preservation of historical metal artworks; project 2020–2024, P.I. Edith Joseph) funded by the Swiss National Science Foundation (SNSF) (grant number 205121_188755). A ground-breaking interdisciplinary approach, merging natural sciences and art conservation, is the integral principle of the research project HELIX, which has been developed at the Haute Ecole Arc Conservation-Restauration and the University of Neuchâtel in Switzerland, in collaboration with international partners as the University of Bologna (Ravenna, Italy) and the Laboratory Arc'Antique (Nantes, France). The project was aimed to design novel gel formulations for the cleaning of altered historical metals with a greener and innovative approach (Passaretti, Cuvillier, Guilminot, *et al.*, 2023).

As a preliminary and essential step, a world-wide survey was conducted within the framework of the HELIX project with the aim of comprehending materials and related problematics that experts in the field of historical metal conservation were more frequently facing and dealing with. In particular, the proposed questionnaire was specifically focused on the cleaning praxes of indoor historical artefacts made of iron-, copper-, and silver-based alloys, which are the target objects of HELIX and of the research here presented. The survey was spread through numerous wide-reaching networks in 2020 and gathered evidence of regular practices in metal heritage care, helping to better address the research in order to meet end-users' expectations and concerns, while respecting green chemistry guidelines. The participants (over 60 persons) mentioned corrosion and organic coatings removal as main issues in their daily work. As expected, in the category of organic coatings, they listed Paraloid®, nitrocellulose lacquers, and waxes as principal products in their workshop and on the treated objects. Remarkably, despite the global trend into more sustainable materials and methods, no feedback reported the use of green or bio-solvents, as well as the exploitation of gels for the cleaning of neither the metallic substrates nor the protective organic coatings potentially present. Numerous were the reasons deducible to explicate the rare use of green solutions for metal care. The relatively high price of greener alternatives, the unawareness of either risks related to traditional methods or existence of reliable substitute products, and the effort required to change long-established habits in favour of unprecedented approaches emerged as most rated deterrents towards the green conservation transition.

In response to this outcome, innovative greener solutions for metal care were investigated in close contact with conservator-restorers. In particular, bio-gel formulations were designed for the removal of undesired or altered materials of both inorganic (i.e., corrosion) and organic nature (i.e., protective coatings) possibly present on historical metal artefacts, specifically iron-, copper- and silver-based alloys. Both hydro- and solvent-gels were explored, and this doctoral dissertation presents specifically the results obtained in the

exploration of novel organogel formulations. Great attention was addressed towards the system components, namely, thickening agents (i.e., biopolymers), solvents (i.e., water and bio-solvents), and complexing agents (i.e., metabolites), with the purpose of selecting only potentially bio-sourced, naturally biodegradable, and non- or low-toxic materials. More in detail, the research here proposed is developed as follows:

- In **Chapter 2** a first selection of the bio-components for the double-target formulations is addressed. In particular, the use of the bio-solvent ethyl lactate is explored in combination with several bio-derived polymers. The research was aimed to the removal of two classes of polar protective coatings, namely an acrylic (i.e., Paraloid® B72) and a nitrocellulose (i.e., Zaponlack) lacquers, being widely exploited for the protection of historical metal heritage.
- After selecting a basic formulation according to the cleaning action on the organic material and the handling properties, **Chapter 3** proposes the first multi-functional organogel designed for the cleaning of corroded iron-based artworks presenting acrylic-based material to be concurrently removed. The siderophore deferoxamine B is thus explored in the gelled system as a bio-based alternative complexing agent.
- In line with the perspective adopted for the concurrent removal of undesired substances, **Chapter 4** presents a new green complexing agent in the field of metal conservation, namely ethylenediamine-N,N'-disuccinic acid (EDDS) that was investigated embedded in a bio-gel for the cleaning of altered brass presenting additionally a nitrocellulose lacquer (i.e., Zaponlack). It is remarkable that EDDS is employed in the field of metal conservation for the first time within the framework of the HELIX project.
- In light of the outcomes obtained, preliminary considerations for the implementation of the bio-gel loaded with EDDS for the cleaning of sterling silver are presented in **Chapter 5**. The attention was focused on the visual and colorimetric appearance that is considered a crucial parameter by conservators when working on these collections.
- Finally, in **Chapter 6,** some general conclusions are reported, together with possible future developments considering the results obtained within the research presented.

Bibliography

Albelda-Berenguer, M., Monachon, M. and Joseph, E. (2019) Siderophores: From natural roles to potential applications. 1st edn, Advances in Applied Microbiology. 1st edn. Elsevier Inc. Available at: https://doi.org/10.1016/bs.aambs.2018.12.001.

Anastas, P. and Eghbali, N. (2010) 'Green Chemistry: Principles and Practice', Chem. Soc. Rev., 39(1), pp. 301–312. Available at: https://doi.org/10.1039/B918763B.

Anastas, P.T. and Warner, J.C. (1998) 'Green chemistry', Frontiers, 640(1998), p. 850.

Angelini, E. and Argyropoulos, V. (2008) 'PROMET state-of-the-art approach for protecting, preserving, and interpreting metals from museums in the Mediterranean basin', in V. Argyropoulos (ed.) Metals and Museums in the Mediterranean. Protecting, Preserving and Interpreting. TEI (Athens), pp. 23–37.

Appelbaum, B. (1987) 'Criteria for Treatment: Reversibility', Journal of the American Institute for Conservation, 26(2), pp. 65–73. Available at: https://doi.org/10.1179/019713687806027852.

Argyropoulos, V., Giannoulaki, M., et al. (2007) 'A survey of the types of corrosion inhibitors and protective coatings used for the conservation of metal objects from museum collections in the Mediterranean basin', in Strategies for Saving our Cultural Heritage. Proceedings of the International Conference on

Conservation Strategies for Saving Indoor Metallic Collections, Cairo (Egypt). TEI of Athens, Athens, pp. 166–170.

Argyropoulos, V., Charalambous, D., et al. (2007) 'Testing of a new wax coating Poligen ES 91009®and corrosion inhibitor additives used for improving coatings for historic iron alloys', in Degrigny C, Langh R van, Joosten I, Ankersmit B (eds) METAL 07: proceedings of the ICOM-CC metal WG Interim meeting, Amsterdam, ICOM-CC, Amsterdam, pp. 10–15.

Argyropoulos, V. (2008) 'Past and current conservation practices: The need for innovative and integrated approaches', in V. Argyropoulos (ed.) Metals and Museums in the Mediterranean. Protecting, Preserving and Interpreting. TEI (Athens), pp. 55–75.

Armisén, R. and Gaiatas, F. (2009) 'Agar', in Handbook of Hydrocolloids. Elsevier, pp. 82–107. Available at: https://doi.org/10.1533/9781845695873.82.

Artesani, A. et al. (2020) 'Recent Advances in Protective Coatings for Cultural Heritage–An Overview', Coatings, 10(3), p. 217. Available at: https://doi.org/10.3390/coatings10030217.

Baglioni, P. et al. (2015) 'Organogel formulations for the cleaning of easel paintings', Applied Physics A, 121(3), pp. 857–868. Available at: https://doi.org/10.1007/s00339-015-9364-0.

Baglioni, P. et al. (2019) 'Smart Soft Nanomaterials for Cleaning', in Nanotechnologies and Nanomaterials for Diagnostic, Conservation and Restoration of Cultural Heritage. Elsevier, pp. 171–204. Available at: https://doi.org/10.1016/B978-0-12-813910-3.00009-4.

Baij, L., Hermans, J., et al. (2020) 'A review of solvent action on oil paint', Heritage Science, 8(1), p. 43. Available at: https://doi.org/10.1186/s40494-020-00388-x.

Baij, L., Buijs, J., et al. (2020) 'Quantifying solvent action in oil paint using portable laser speckle imaging', Scientific Reports, 10(1), p. 10574. Available at: https://doi.org/10.1038/s41598-020-67115-1.

Barberà Giné, A. and Marín Ortega, S. (2017) 'The removal of Paraloid B-72 coatings with aqueous gelled systems: Roman frescoesfrom Empúries, Catalonia', in L. V. Angelova et al. (eds) Gels in the Conservation of Art. London: Archetype Publications, pp. 363–365.

Basilissi, G. et al. (2022) 'Evaluation of a dry method using erasers for silver--copper alloy tarnish cleaning and comparison with traditional methods', Journal of the American Institute for Conservation, 61(2), pp. 112–128.

Bayer, I.S. et al. (2014) 'Direct Transformation of Edible Vegetable Waste into Bioplastics', Macromolecules, 47(15), pp. 5135–5143. Available at: https://doi.org/10.1021/ma5008557.

Bertolotti, G. et al. (2012) 'Micro-Raman study of copper hydroxychlorides and other corrosion products of bronze samples mimicking archaeological coins', Analytical and Bioanalytical Chemistry, 402(4), pp. 1451–1457. Available at: https://doi.org/10.1007/s00216-011-5268-9.

Borén, E. (2022) A GREENER SOLUTION Investigating the potential use of Green Solvents to remove cellulose nitrate lacquer from silver objects. University of Gothernburg. Available at: https://hdl.handle.net/2077/72648.

Brajer, I. et al. (2014) 'The removal of aged acrylic coatings from wall paintings using microemulsions', in J. Bridgland (ed.) ICOM-CC 17th Triennial Conference Preprints. Melbourne, Australia: Paris: International Council of Museums, p. 8. Available at: https://flore.unifi.it/retrieve/handle/2158/937931/43204/1103_087_BRAJER_ICOM-CC_2014.pdf.

Brandi, C. (1963) Teoria del Restauro.

Byrne, A. (1991) 'WOLBERS CLEANING METHODS: INTRODUCTION', AICCM Bulletin, 17(3–4), pp. 3–11. Available at: https://doi.org/10.1179/bac.1991.17.3-4.001.

Cagnini, A., Gennai, S. and Mazzoni, M.D. (2012) 'La Banderuola di Palazzo Vecchio: storia, vicende conservative, restauro', OPD restauro, pp. 13–32. Available at: https://opificiodellepietredure.cultura.gov.it/pubblicazioni/opd-restauro-n-24-2012/.

Çakmak, Y. et al. (2022) 'Isosorbide, pyrogallol, and limonene-containing thiol-ene photocured bio-based organogels for the cleaning of artworks', Journal of Cultural Heritage, 55, pp. 391–398. Available at: https://doi.org/10.1016/j.culher.2022.04.013.

Calabrò, P.S. and Grosso, M. (2018) 'Bioplastics and waste management', Waste Management, 78, pp. 800–801. Available at: https://doi.org/10.1016/j.wasman.2018.06.054.

Calvo-Flores, F.G. et al. (2018) 'Green and Bio-Based Solvents', Topics in Current Chemistry, 376(3), p. 18. Available at: https://doi.org/10.1007/s41061-018-0191-6.

Cano, E., Lafuente, D. and Bastidas, D.M. (2010) 'Use of EIS for the evaluation of the protective properties of coatings for metallic cultural heritage: a review', Journal of Solid State Electrochemistry, 14(3), pp. 381–391. Available at: https://doi.org/10.1007/s10008-009-0902-6.

Cappitelli, F., Zanardini, E. and Sorlini, C. (2004) 'The Biodeterioration of Synthetic Resins Used in Conservation', Macromolecular Bioscience, 4(4), pp. 399–406. Available at: https://doi.org/10.1002/mabi.200300055.

Carmen, L.I. (2016) 'Biodeterioration of acrylic polymers Paraloid B-72 and B-44: Report on field trials', Anatolian Archaeological Studies, 15, pp. 283–289.

Casini, A., Chelazzi, D. and Baglioni, P. (2023) 'Advanced methodologies for the cleaning of works of art', Science China Technological Sciences [Preprint]. Available at: https://doi.org/10.1007/s11431-022-2348-7.

Catelli, E. et al. (2018) 'Can hyperspectral imaging be used to map corrosion products on outdoor bronze sculptures?', Journal of Spectral Imaging [Preprint]. Available at: https://doi.org/10.1255/jsi.2018.a10.

Chelazzi, D. et al. (2018) 'Gels for the Cleaning of Works of Art', in. Washington, DC, USA: ACS Publications, pp. 291–314. Available at: https://doi.org/10.1021/bk-2018-1296.ch015.

Chelazzi, D., Giorgi, R. and Baglioni, P. (2018) 'Microemulsions, Micelles, and Functional Gels: How Colloids and Soft Matter Preserve Works of Art', Angewandte Chemie International Edition, 57(25), pp. 7296–7303. Available at: https://doi.org/10.1002/anie.201710711.

Chiantore, O. and Lazzari, M. (2001) 'Photo-oxidative stability of paraloid acrylic protective polymers', Polymer, 42(1), pp. 17–27. Available at: https://doi.org/10.1016/S0032-3861(00)00327-X.

Chiavari, C. et al. (2008) 'Atmospheric corrosion of historical organ pipes: The influence of environment and materials', Corrosion Science, 50(9), pp. 2444–2455. Available at: https://doi.org/10.1016/j.corsci.2008.06.045.

Chiellini, E. et al. (2003) 'Biodegradation of poly (vinyl alcohol) based materials', Progress in Polymer Science, 28(6), pp. 963–1014. Available at: https://doi.org/10.1016/S0079-6700(02)00149-1.

Chilton, J.P. (1971) 'The Corrosion of Metals', Journal of the Royal Society of Arts, 119(5181), pp. 614–629. Available at: https://www.jstor.org/stable/41370804%0A.

Comensoli, L. et al. (2017) 'Use of Bacteria To Stabilize Archaeological Iron', Applied and Environmental Microbiology. Edited by M.A. Elliot, 83(9). Available at: https://doi.org/10.1128/AEM.03478-16.

Comensoli, L. et al. (2019) 'The potential of microorganisms for the conservation-restoration of iron artworks', in Metal 2019, 9th interim meeting of the ICOM-CC metals working group. Neuchâtel, Switzerland, pp. 242–249. Available at: https://www.dora.lib4ri.ch/empa/islandora/object/empa%3A19840.

Contreras-Vargas, J., Ruvalcaba-Sil, J.L. and Rodriguez-Gómez, F.J. (2013) 'Effects of the cleaning of silver with acidified thiourea solutions', in Conference proceedings of Metal, pp. 223–228.

Couture-Rigert, D.E., Sirois, P.J. and Moffatt, E.A. (2012) 'An investigation into the cause of corrosion on indoor bronze sculpture', Studies in Conservation, 57(3), pp. 142–163. Available at: https://doi.org/10.1179/2047058412Y.0000000004.

Cremonesi, P. (2013) 'Rigid gels and enzyme cleaning', in New Insights into the Cleaning of Paintings: Proceedings from the Cleaning 2010 International Conference, Universidad Politecnica de Valencia and Museum Conservation Institute.

Del Curto, D. and Turrina, A. (2023) 'Towards a Reasoned Glossary of Green Conservation: A Semantic Review of Green-Oriented Terms in the Field of Cultural Heritage', Sustainability, 15(16), p. 12104. Available at: https://doi.org/10.3390/su151612104.

Cushman, M. and Wolbers, R. (2007) 'A new approach to cleaning iron stained marble surfaces', WAAC newsletter, 29(2), pp. 23–28.

Dalvi-Isfahan, M., Hamdami, N. and Le-Bail, A. (2017) 'Effect of freezing under electrostatic field on selected properties of an agar gel', Innovative Food Science & Emerging Technologies, 42, pp. 151–156. Available at: https://doi.org/10.1016/j.ifset.2017.06.013.

Davidson, C.J., Hannigan, J.H. and Bowen, S.E. (2021) 'Effects of inhaled combined Benzene, Toluene, Ethylbenzene, and Xylenes (BTEX): Toward an environmental exposure model', Environmental Toxicology and Pharmacology, 81, p. 103518. Available at: https://doi.org/10.1016/j.etap.2020.103518.

Degrigny, C. et al. (2007) 'Characterisation of corrosion product layers on atmospherically corroded historic ferrous objects: application to the armour of the Palace Armoury, Valletta, Malta', Strategies for Saving our Cultural Heritage, pp. 31–39.

Degrigny, C. (2010) 'Use of electrochemical techniques for the conservation of metal artefacts: a review', Journal of Solid State Electrochemistry, 14(3), pp. 353–361. Available at: https://doi.org/10.1007/s10008-009-0896-0.

Degrigny, C. et al. (2016) 'A new electrolytic pencil for the local cleaning of silver tarnish', Studies in Conservation, 61(3), pp. 162–173. Available at: https://doi.org/10.1179/2047058415Y.0000000015.

Delattre, C., Bouvet, S. and Le Bourg, E. (2017) 'Gellan gum and agar compared to aqueous immersion for cleaning paper', in L. V. Angelova et al. (eds) Gels in the Conservation of Art. London: Archetype Publications, pp. 57–61.

Lo Dico, G. et al. (2018) 'Microemulsion Encapsulated into Halloysite Nanotubes and their Applications for Cleaning of a Marble Surface', Applied Sciences, 8(9), p. 1455. Available at: https://doi.org/10.3390/app8091455.

Domon Beuret, E. et al. (2015) 'Biopatines: des champignons au service des alliages cuivreux', in Cahier n°22 - XXVIIIe Journées des restaurateurs en archéologie. Arles, October 2014. ARAAFU. Paris, France, pp. 45–48. Available at: http://mediatheque-numerique.inp.fr/Bibliographies/Biopatines-un-traitement-ecologique-et-durable-pour-stabiliser-la-corrosion-sur-des-surfaces-en-alliages-cuivreux.

Down, J.L. (2015) 'The evaluation of selected poly(vinyl acetate) and acrylic adhesives: A final research update', Studies in Conservation, 60(1), pp. 33–54. Available at: https://doi.org/10.1179/2047058414Y.0000000129.

Duan, W. et al. (2017) 'Environmental behavior and eco-toxicity of xylene in aquatic environments: A review', Ecotoxicology and Environmental Safety, 145, pp. 324–332. Available at: https://doi.org/10.1016/j.ecoenv.2017.07.050.

Duncan, T.T., Berrie, B.H. and Weiss, R.G. (2017) 'Soft, Peelable Organogels from Partially Hydrolyzed Poly(vinyl acetate) and Benzene-1,4-diboronic Acid: Applications to Clean Works of Art', ACS Applied Materials & Interfaces, 9(33), pp. 28069–28078. Available at: https://doi.org/10.1021/acsami.7b09473.

Duplat, V. et al. (2009) 'Steel versus Paper : The Conservation of a Piece of Modern Art Consisting of a Rust Print on Paper', Journal of Paper Conservation, 10(3), pp. 26–34.

Eggert, G. et al. (2019) 'Metal conservation, cellulose nitrate and the Oddy test', in C. Chemello, L. Brambilla, and E. Joseph (eds) Metal 2019 Proceedings of the Interim Meeting of the ICOM-CC Metals Working Group. International Councils of Museums - Committee for Conservation, p. 473.

Eggert, G. and Fischer, A. (2021) 'The formation of formates: a review of metal formates on heritage objects', Heritage Science, 9(1), p. 26. Available at: https://doi.org/10.1186/s40494-021-00499-z.

Evans, U.R. and Taylor, C.A.J. (1972) 'Mechanism of atmospheric rusting', Corrosion Science, 12(3), pp. 227–246. Available at: https://doi.org/10.1016/S0010-938X(72)90671-3.

Fawell, J. (2000) 'Risk assessment case study—Chloroform and related substances', Food and Chemical Toxicology, 38, pp. S91–S95. Available at: https://doi.org/10.1016/S0278-6915(99)00129-5.

Fays, M. (2018) « D'or, d'argent et de pate noire : incrustations révélées » étude et conservation-restauration de cinq objets islamiques en alliage cuivreux incrustés. Institut National du Patrimoine. Available at: https://mediatheque-numerique.inp.fr/documentation-oeuvres/memoires-diplome-restaurateurs-patrimoine/dor-dargent-pte-noire-incrustations-revelees-etude-conservation-restauration-cinq-objets-islamiques-en-alliage-cuivreux-incrustes-issus.

Feldman, D. (2020) 'Poly(Vinyl Alcohol) Recent Contributions to Engineering and Medicine', Journal of Composites Science, 4(4), p. 175. Available at: https://doi.org/10.3390/jcs4040175.

Felix, V.S. et al. (2020) 'Analysis of silver coins from colonial Brazil by hand held XRF and micro-XRF', Applied Radiation and Isotopes, 166, p. 109409. Available at: https://doi.org/10.1016/j.apradiso.2020.109409.

de Figueiredo Junior, J.C.D. et al. (2021) 'The Cleaning of Silver Objects With a Basic Solution of Sodium Glycinate: A Study on Artificially and Naturally Tarnished Silver', Studies in Conservation, 66(7), pp. 375–383. Available at: https://doi.org/10.1080/00393630.2020.1859876.

Fomina, M. et al. (2005) 'Role of oxalic acid overexcretion in transformations of toxic metal minerals by Beauveria caledonica', Applied and Environmental Microbiology, 71(1), pp. 371–381. Available at: https://doi.org/10.1128/AEM.71.1.371-381.2005.

Fratini, E. and Carretti, E. (2013) 'Chapter 10. Cleaning IV: Gels and Polymeric Dispersions', in Nanoscience for the Conservation of Works of Art, pp. 252–279. Available at: https://doi.org/10.1039/9781849737630-00252.

Ganesan, S. et al. (2022) 'Microbes for Archaeological Wood Conservation', CHIMIA, 76(9), p. 772. Available at: https://doi.org/10.2533/chimia.2022.772.

Gao, F. et al. (2020) 'Replacement strategies for non-green dipolar aprotic solvents', Green Chemistry, 22(19), pp. 6240–6257. Available at: https://doi.org/10.1039/D0GC02149K.

Gettens, R.J. and Stout, G.L. (1966) Painting Materials. A Short Encyclopaedia. New York: Dover Publications, Inc.

Gillies, J.C. and Seyb, I. (2013) 'La Fée aux Fleurs: Investigation and Conservation of a 19th Century Outdoor Cast Iron Sculpture', in METAL 2013: Interim Meeting of the ICOM-CC Metal Working Group, Conference Proceedings, 16-20 September 2013, Edinburgh, Scotland, pp. 147–152.

Giordano, A. and Cremonesi, P. (2021) 'New Methods of Applying Rigid Agar Gels: From Tiny to Large-scale Surface Areas', Studies in Conservation, 66(8), pp. 437–448. Available at: https://doi.org/10.1080/00393630.2020.1848272.

Giraud, T. et al. (2021) 'Use of gels for the cleaning of archaeological metals. Case study of silver-plated copper alloy coins', Journal of Cultural Heritage, 52, pp. 73–83. Available at: https://doi.org/10.1016/j.culher.2021.08.014.

Giuliani, C. et al. (2018) 'Chitosan-based coatings for corrosion protection of copper-based alloys: A promising more sustainable approach for cultural heritage applications', Progress in Organic Coatings, 122(March), pp. 138–146. Available at: https://doi.org/10.1016/j.porgcoat.2018.05.002.

Giumlia-Mair, A. and Lucchini, E. (2005) 'Surface analyses on modern and ancient copper based fakes', Surface Engineering, 21(5–6), pp. 406–410. Available at: https://doi.org/10.1179/174329305X64402.

Grassini, S. et al. (2007) 'Advanced plasma treatment for cleaning and protecting precious metal artefacts', in Strategies for saving our cultural heritage. Proceedings of the international conference on conservation strategies for saving indoor metallic collections, Cairo. TEI of Athens, Athens, pp. 127–131.

Gu, Y. and Jérôme, F. (2013) 'Bio-based solvents: An emerging generation of fluids for the design of eco-efficient processes in catalysis and organic chemistry', Chemical Society Reviews, 42(24), pp. 9550–9570. Available at: https://doi.org/10.1039/c3cs60241a.

Guaragnone, T. et al. (2020) 'PVA-based peelable films loaded with tetraethylenepentamine for the removal of corrosion products from bronze', Applied Materials Today, 19, p. 100549. Available at: https://doi.org/10.1016/j.apmt.2019.100549.

Guilminot, E. et al. (2018) 'Projet collaboratif sur l'utilisation des gels pour le traitement des métaux : démarche et fonctionnement', in Journées des Restaurateurs en Archéologie. Journée d'Étude, de Recherche et d'Innovation. Lyon, France, p. 14.

Guilminot, E. et al. (2019) 'Use of Gels for the treatment of Metals', in C. Chemello, L. Brambilla, and E. Joseph (eds) Metal 2019 Proceedings of the Interim Meeting of the ICOM-CC Metals Working Group. International Councils of Museums - Committee for Conservation, p. 473.

Guilminot, E. (2023) 'The Use of Hydrogels in the Treatment of Metal Cultural Heritage Objects', Gels, 9(3), p. 191. Available at: https://doi.org/10.3390/gels9030191.

Hacke, A.-M. et al. (2003) 'Investigation into the nature of metal threads in a Renaissance tapestry and the cleaning of tarnished silver by UV/Ozone (UVO) treatment', Journal of materials science, 38, pp. 3307–3314.

Heginbotham, A. et al. (2014) 'An evaluation of protective coatings for brass in indoor environments, with an emphasis on Boulle marquetry', in Furniture finishes: past, present and future of transparent wood coatings. Proceedings of 12th International Symposium on wood and furniture conservation: Stichting Ebenist, Amsterdam, pp. 14–15.

Heitz, E. (1974) 'Corrosion of Metals in Organic Solvents', in Advances in Corrosion Science and Technology. Boston, MA: Springer US, pp. 149–243. Available at: https://doi.org/10.1007/978-1-4615-9059-0_3.

Hindborg, K. (2019) 'Electrolytic Cleaning of Silver Threads-Effects of Electrolytes on the Condition of Silk'.

Hong, L. and Simon, J.D. (2007) 'Current Understanding of the Binding Sites, Capacity, Affinity, and Biological Significance of Metals in Melanin', The Journal of Physical Chemistry B, 111(28), pp. 7938–7947. Available at: https://doi.org/10.1021/jp071439h.

Hosseinpour, S. and Johnson, M. (2017) 'Vibrational Spectroscopy in Studies of Atmospheric Corrosion', Materials, 10(4), p. 413. Available at: https://doi.org/10.3390/ma10040413.

Jaeger, T. (2008) 'Short Communication Removal of Paraffin Wax in the Re-treatment of Archaeological Iron', Journal of the American Institute for Conservation, 47(3), pp. 217–223. Available at: https://doi.org/10.1179/019713608804539619.

James, S. and Joseph, E. (2021) 'Microbial-Driven Stabilisation of Archaeological Iron Artefacts', Corrosion and Materials Degradation, 2(2), pp. 274–292. Available at: https://doi.org/10.3390/cmd2020015.

Jia, Y. et al. (2020) 'Organogel Coupled with Microstructured Electrospun Polymeric Nonwovens for the Effective Cleaning of Sensitive Surfaces', ACS Applied Materials & Interfaces, 12(35), pp. 39620–39629. Available at: https://doi.org/10.1021/acsami.0c09543.

Jiménez-González, C. et al. (2004) 'Expanding GSK's Solvent Selection Guide?application of life cycle assessment to enhance solvent selections', Clean Technologies and Environmental Policy, 7(1), pp. 42–50. Available at: https://doi.org/10.1007/s10098-004-0245-z.

Joseph, E., Cario, S., et al. (2012) 'Protection of metal artifacts with the formation of metal-oxalates complexes by Beauveria bassiana', Frontiers in Microbiology, 2(JAN). Available at: https://doi.org/10.3389/fmicb.2011.00270.

Joseph, E., Simon, A., et al. (2012) 'Spectroscopic characterization of an innovative biological treatment for corroded metal artefacts', Journal of Raman Spectroscopy, 43(11), pp. 1612–1616. Available at: https://doi.org/10.1002/jrs.4164.

Kaplan, D.L. (1998) 'Introduction to Biopolymers from Renewable Resources', in Biopolymers from Renewable Resources. Berlin, Heidelberg: Springer Berlin Heidelberg, pp. 1–29. Available at: https://doi.org/10.1007/978-3-662-03680-8_1.

Katayon, M. (2022) 'The Use of Gels for the Removal of Cellulose Nitrate Lacquer on Silver'.

Kergourlay, F. et al. (2018) 'Stabilization treatment of cultural heritage artefacts: In situ monitoring of marine iron objects dechlorinated in alkali solution', Corrosion Science, 132, pp. 21–34. Available at: https://doi.org/10.1016/j.corsci.2017.12.028.

Keshavarz, T. and Roy, I. (2010) 'Polyhydroxyalkanoates: bioplastics with a green agenda', Current Opinion in Microbiology, 13(3), pp. 321–326. Available at: https://doi.org/10.1016/j.mib.2010.02.006.

Knutson, C.M. et al. (2017) 'Polymeric Medical Sutures: An Exploration of Polymers and Green Chemistry', Journal of Chemical Education, 94(11), pp. 1761–1765. Available at: https://doi.org/10.1021/acs.jchemed.6b00835.

Kristiansen, K. and Larsson, T.B. (2005) 'L'âge du Bronze, une période historique', Annales. Histoire, Sciences Sociales, 60(5), pp. 975–1007. Available at: https://doi.org/10.1017/S039526490001934X.

Kua, Y.L. et al. (2016) 'Ethyl lactate as a potential green solvent to extract hydrophilic (polar) and lipophilic (non-polar) phytonutrients simultaneously from fruit and vegetable by-products', Sustainable Chemistry and Pharmacy, 4, pp. 21–31. Available at: https://doi.org/10.1016/j.scp.2016.07.003.

Kuhn, A.T. and Kelsall, G.H. (1983) 'Methods for the Testing of Tarnish', British Corrosion Journal, 18(4), pp. 168–173. Available at: https://doi.org/10.1179/000705983798273552.

Kumar, R. and Sagar, P. (2017) 'Preface on Green Conservation of the Museum Objects', in T. Gupta, B. Mistry, and B.S. Gupta (eds) A treatise on Recent Trends and Sustainability in Crafts & Design. Excel India, pp. 118–124.

Kurnianto, A.A. et al. (2023) 'The Correlation of Blood Xylene Levels and Neurological Disorders among Informal Car Painters', Journal of Chemical Health Risks, 13(1), pp. 195–205.

Lazzari, M. and Chiantore, O. (2000) 'Thermal-ageing of paraloid acrylic protective polymers', Polymer, 41(17), pp. 6447–6455. Available at: https://doi.org/10.1016/S0032-3861(99)00877-0.

Leja, K. and Lewandowicz, G. (2010) 'Polymer biodegradation and biodegradable polymers-a review.', Polish Journal of Environmental Studies, 19(2).

Letardi, P. (2013) 'Electrochemical measurements in the conservation of metallic heritage artefacts: an overview', in Corrosion and Conservation of Cultural Heritage Metallic Artefacts. Elsevier, pp. 126–148. Available at: https://doi.org/10.1533/9781782421573.2.126.

Letardi, P. (2021) 'Testing New Coatings for Outdoor Bronze Monuments: A Methodological Overview', Coatings, 11(2), p. 131. Available at: https://doi.org/10.3390/coatings11020131.

Létrange, A. et al. (2017) 'Comparison of three hydrogels for cleaning tarnished silver threads using electrochemical treatment', in L. V. Angelova et al. (eds) Gels in the Conservation of Art. London: Archetype Publications, pp. 369–371.

Li, Z. et al. (2018) 'Novel supramolecular organogel based on β-cyclodextrin as a green drug carrier for enhancing anticancer effects', Journal of Molecular Liquids, 250, pp. 19–25. Available at: https://doi.org/10.1016/j.molliq.2017.11.154.

Liaud, N. et al. (2014) 'Exploring fungal biodiversity: organic acid production by 66 strains of filamentous fungi', Fungal Biology and Biotechnology, 1(1), pp. 1–10. Available at: https://doi.org/10.1186/s40694-014-0001-z.

Van Loon, A. et al. (2019) 'The Development of an Aqueous Gel Testing Procedure for the Removal of Lead-Rich Salt Crusts on the Surface of Paintings by Giovanni Antonio Pellegrini (1675–1741) in the "Golden Room" of the Mauritshuis', in. Berlin/Heidelberg, Germany: Springer, pp. 283–296. Available at: https://doi.org/10.1007/978-3-319-90617-1_16.

Luxford, N. and Thickett, D. (2007) 'Preventing silver tarnish--lifetime determination of cellulose nitrate lacquer', Metal, 7, pp. 88–93.

Marchand, G. et al. (2013) 'Study of the conservation treatment applied to the archaeological horn silver artifacts', in Interim Meeting for the International Council of Museums Committee for Conservation Metal Working Group, Metal 2013. Edinburgh, Scotland: International Councils of Museums - Committee for Conseravtion and Historic Scotland, pp. 245–250.

De Marco, A. et al. (2017) 'High resolution estimates of the corrosion risk for cultural heritage in Italy', Environmental Pollution, 226, pp. 260–267. Available at: https://doi.org/10.1016/j.envpol.2017.03.066.

Maréchal, L. et al. (2007) 'Study of the atmospheric corrosion of iron by ageing historical artefacts and contemporary low-alloy steel in a climatic chamber: comparison with mechanistic modelling', in Corrosion of Metallic Heritage Artefacts. Elsevier, pp. 131–151. Available at: https://doi.org/10.1533/9781845693015.131.

Mari Yanagishita (2012) 'Il restauro della grande Croce del Pollaiolo: un intervento all'interno del cantiere organizzato per l'Altare di San Giovanni', in Mandragora (ed.) E l'informe si fa forma... : studi intorno a Santa Maria del Fiore in ricordo di Patrizio Osticresi. Florence, Italy, pp. 281–286.

Maria Calvino, M. et al. (2023) 'Beeswax/halloysite microparticles embedded within a geopolymeric layer for the protective coating of steel', Materials Letters, 330, p. 133257. Available at: https://doi.org/10.1016/j.matlet.2022.133257.

Di Marino, D. et al. (2018) 'Corrosion of metal electrodes in deep eutectic solvents', Electrochemistry Communications, 90, pp. 101–105. Available at: https://doi.org/10.1016/j.elecom.2018.04.011.

Martina, I. et al. (2012) 'Micro-Raman characterisation of silver corrosion products: instrumental set up and reference database', E-Preserv Sci, 9, pp. 1–8.

Mateo, M.P. et al. (2009) 'Laser cleaning of varnishes and contaminants on brass', Applied Surface Science, 255(10), pp. 5579–5583.

Mazzoni, M. et al. (2014) 'Laponite micro-packs for the selective cleaning of multiple coherent deposits on wall paintings: The case study of Casina Farnese on the Palatine Hill (Rome-Italy)', International Biodeterioration & Biodegradation, 94, pp. 1–11. Available at: https://doi.org/10.1016/j.ibiod.2014.06.004.

Mazzuca, C. et al. (2014) 'Gellan hydrogel as a powerful tool in paper cleaning process: A detailed study', Journal of Colloid and Interface Science, 416, pp. 205–211. Available at: https://doi.org/10.1016/j.jcis.2013.10.062.

Medina-Esquivel, R. et al. (2008) 'Measurement of the Sol–Gel Transition Temperature in Agar', International Journal of Thermophysics, 29(6), pp. 2036–2045. Available at: https://doi.org/10.1007/s10765-007-0332-6.

Meier, J. (2022) 'Keris Blade Protection – A Comparison of Traditional and Contemporary Coatings', in Metal 2022, proceedings of the interim meeting of the ICOM-CC metals working group.

Merriman, N. (2008) 'Museum collections and sustainability', Cultural trends, 17(1), pp. 3–21.

Mills, J.S. and White, R. (1987) 'Fundamental aspects of deterioration', in The Organic Chemistry of Museum Objects. Elsevier, pp. 134–140. Available at: https://doi.org/10.1016/B978-0-408-11810-1.50016-7.

Moffett, D.L. (1996) 'Wax Coatings on Ethnographic Metal Objects: Justifications for Allowing a Tradition to Wane', Journal of the American Institute for Conservation, 35(1), p. 1. Available at: https://doi.org/10.2307/3179934.

Mohamed, W.A. and Mohamed, N.M. (2017) 'Testing Coatings for Enameled Metal Artifacts', International Journal of Conservation Science, 8(1).

Molina, M.T. et al. (2023) 'Protective Coatings for Metals in Scientific—Technical Heritage: The Collection of the Spanish National Museum of Science and Technology (MUNCYT)', Heritage, 6(3), pp. 2473–2488. Available at: https://doi.org/10.3390/heritage6030130.

Molina, M.T., Cano, E. and Ramírez-Barat, B. (2023a) 'Protective coatings for metallic heritage conservation: A review', Journal of Cultural Heritage, 62, pp. 99–113. Available at: https://doi.org/10.1016/j.culher.2023.05.019.

Molina, M.T., Cano, E. and Ramírez-Barat, B. (2023b) 'Testing protective coatings for metal conservation: the influence of the application method', Heritage Science, 11(1), p. 94. Available at: https://doi.org/10.1186/s40494-023-00937-0.

Monnier, J. et al. (2019) 'The long term indoor atmospheric corrosion of iron : rust layer characterisation To cite this version : HAL Id : hal-02270518 The long term indoor atmospheric corrosion of iron : rust layer characterisation'.

Munoz-Vinas, S. (2012) Contemporary Theory of Conservation. Routledge. Available at: https://doi.org/10.4324/9780080476834.

Onen Cinar, S. et al. (2020) 'Bioplastic Production from Microalgae: A Review', International Journal of Environmental Research and Public Health, 17(11), p. 3842. Available at: https://doi.org/10.3390/ijerph17113842.

Oviedo, C. and Rodríguez, J. (2003) 'EDTA: The chelating agent under environmental scrutiny', Quimica Nova, 26(6), pp. 901–905. Available at: https://doi.org/10.1590/S0100-40422003000600020.

Palomar, T., Ramírez Barat, B., et al. (2016) 'A comparative study of cleaning methods for tarnished silver', Journal of Cultural Heritage, 17, pp. 20–26. Available at: https://doi.org/10.1016/j.culher.2015.07.012.

Palomar, T., Oujja, M., et al. (2016) 'Evaluation of laser cleaning for the restoration of tarnished silver artifacts', Applied Surface Science, 387, pp. 118–127.

Parisi, E.I. et al. (2018) 'Film forming PVA-based cleaning systems for the removal of corrosion products from historical bronzes', Pure and Applied Chemistry, 90(3), pp. 507–522. Available at: https://doi.org/10.1515/pac-2017-0204.

Passaretti, A., Cuvillier, L., Guilminot, E., et al. (2023) 'Biocleaning of historical metal artworks: innovative green gels amended with microbial derivatives', Frontiers in Materials, 10. Available at: https://doi.org/10.3389/fmats.2023.1277972.

Passaretti, A., Cuvillier, L., Künzi, C.-A., et al. (2023) 'Multi-analytical characterisation of Art Déco dinanderie: single point and map analysis of Jean Dunand's metal artworks', in RAA2023-11th International Conference on the Application of Raman Spectroscopy in Art and Archaeology.

Peelman, N. et al. (2013) 'Application of bioplastics for food packaging', Trends in Food Science & Technology, 32(2), pp. 128–141. Available at: https://doi.org/10.1016/j.tifs.2013.06.003.

Pereira, C.S.M., Silva, V.M.T.M. and Rodrigues, A.E. (2011) 'Ethyl lactate as a solvent: Properties, applications and production processes – a review', Green Chemistry, 13(10), p. 2658. Available at: https://doi.org/10.1039/c1gc15523g.

Perera, D.Y. (2003) 'Physical ageing of organic coatings', Progress in Organic Coatings, 47(1), pp. 61–76. Available at: https://doi.org/10.1016/S0300-9440(03)00037-7.

Petiti, C. et al. (2020) 'Effects of cleaning procedures on the long-term corrosion behavior of bronze artifacts of the cultural heritage in outdoor environment', Environmental Science and Pollution Research, 27(12), pp. 13081–13094. Available at: https://doi.org/10.1007/s11356-020-07814-4.

Phenix, A. (2013) 'Effects of Organic Solvents on Artists Oil Paint Films: Swelling', New Insights into the Cleaning of Paintings: Proceedings from the Cleaning 2010 International Conference, Universidad Politecnica de Valencia and Museum Conservation Institute [Preprint]. Available at: https://doi.org/10.5479/si.19492359.3.1.

Pianorsi, M.D. et al. (2017) 'Organogels for the cleaning of artifacts', Pure and Applied Chemistry, 89(1), pp. 3–17. Available at: https://doi.org/10.1515/pac-2016-0908.

Pinna, D. (2021) 'Microbial Growth and its Effects on Inorganic Heritage Materials', in E. Joseph (ed.) Microorganisms in the Deterioration and Preservation of Cultural Heritage. Cham: Springer International Publishing, pp. 3–35. Available at: https://doi.org/10.1007/978-3-030-69411-1_1.

Plé, E. and Schröter, J. (2020) 'Le nettoyage des bronzes dorés', Technè. La science au service de l'histoire de l'art et de la préservation des biens culturels, (49), pp. 117–121.

Prat, D., Hayler, J. and Wells, A. (2014) 'A survey of solvent selection guides', Green Chem., 16(10), pp. 4546–4551. Available at: https://doi.org/10.1039/C4GC01149J.

Prati, S. et al. (2018) 'Sustainability in art conservation: a novel bio-based organogel for the cleaning of water sensitive works of art', Pure and Applied Chemistry, 90(2), pp. 239–251. Available at: https://doi.org/10.1515/pac-2017-0507.

Prati, S. et al. (2019) 'Cleaning oil paintings: NMR relaxometry and SPME to evaluate the effects of green solvents and innovative green gels', New Journal of Chemistry, 43(21), pp. 8229–8238. Available at: https://doi.org/10.1039/C9NJ00186G.

Prosek, T. et al. (2013) 'Real-time monitoring of indoor air corrosivity in cultural heritage institutions with metallic electrical resistance sensors', Studies in Conservation, 58(2), pp. 117–128. Available at: https://doi.org/10.1179/2047058412Y.0000000080.

Qiu, P. and Leygraf, C. (2011) 'Initial oxidation of brass induced by humidified air', Applied Surface Science, 258(3), pp. 1235–1241. Available at: https://doi.org/10.1016/j.apsusc.2011.09.080.

Ramesh, P. and Vinodh, S. (2020) 'State of art review on Life Cycle Assessment of polymers', International Journal of Sustainable Engineering, 13(6), pp. 411–422. Available at: https://doi.org/10.1080/19397038.2020.1802623.

Rapti, S. et al. (2017) 'Removing iron stains from wood and textile objects: assessing gelled siderophores as novel green chelators', in L. Angelova and R. Ormsby, Bronwyn Townsend, Joyce Wolbers (eds) Gels in the Conservation of Artconservation. London: Archetype Publications, pp. 343–348.

Rapti, S. et al. (2021) 'Siderophores and their Applications in Wood, Textile, and Paper Conservation', in Microorganisms in the Deterioration and Preservation of Cultural Heritage. Cham: Springer International Publishing, pp. 301–339. Available at: https://doi.org/10.1007/978-3-030-69411-1_14.

Rapti, S. et al. (2023) 'Desferrioxamine B: Investigating the Efficacy of Hydrogels and Ethanol Gels for Removing Akaganeite and Maghemite from Dry Wooden Substrates', Forests, 14(2), p. 247. Available at: https://doi.org/10.3390/f14020247.

Rattana, S. and Gheewala, S.H. (2019) 'Environment impacts assessment of petroleum plastic and bioplastic carrier bags in Thailand', Journal of Sustainable Energy & Environment, 10, pp. 9–17.

Ricotta, N., Gagnini, A. and Degrigny, C. (2022) 'Analysis of heterogeneous tarnish on silver-based alloys using the Pleco for local, controlled electrolytic cleaning', in Metal 2022, proceedings of the interim meeting of the ICOM-CC metals working group.

Rogovina, L.Z., Vasil'ev, V.G. and Braudo, E.E. (2008) 'Definition of the concept of polymer gel', Polymer Science - Series C, 50(1), pp. 85–92. Available at: https://doi.org/10.1134/S1811238208010050.

Russo, S. et al. (2022) 'Revealing degradation patterns: Imaging Techniques for the study of metal soap formation on painted metal objects', in Metal 2022, proceedings of the interim meeting of the ICOM-CC metals working group.

Russo, S. et al. (2023) 'But aren't all soaps metal soaps? A review of applications, physico-chemical properties of metal soaps and their occurrence in cultural heritage studies', Heritage Science, 11(1), p. 172. Available at: https://doi.org/10.1186/s40494-023-00988-3.

Samorì, C. et al. (2016) 'The Green Attitude in Art Conservation: Polyhydroxybutyrate-based Gels for the Cleaning of Oil Paintings', ChemistrySelect, 1(15), pp. 4502–4508. Available at: https://doi.org/10.1002/slct.201601180.

São João, J., Branco, L.C. and Leite Fragoso, S. (2017) 'Trials fo agar gels and task-specific salts for the electrochemical reduction of silver sulphide on silver leaf', in L. V. Angelova et al. (eds) Gels in the Conservation of Art. London: Archetype Publications, pp. 287–291.

Sauer, M. et al. (2008) 'Microbial production of organic acids: expanding the markets', Trends in Biotechnology, 26(2), pp. 100–108. Available at: https://doi.org/10.1016/j.tibtech.2007.11.006.

Scalioni, L. V., Gutiérrez, M.C. and Felisberti, M.I. (2017) 'Green composites of poly(3-hydroxybutyrate) and curaua fibers: Morphology and physical, thermal, and mechanical properties', Journal of Applied Polymer Science, 134(14), pp. 1–13. Available at: https://doi.org/10.1002/app.44676.

Schalm, O. et al. (2016) 'The corrosion process of sterling silver exposed to a Na2S solution: monitoring and characterizing the complex surface evolution using a multi-analytical approach', Applied Physics A, 122(10), p. 903. Available at: https://doi.org/10.1007/s00339-016-0436-6.

Schalm, O. et al. (2018) 'How effective are reducing plasma afterglows at atmospheric pressure in removing sulphide layers: Application on tarnished silver, sterling silver and copper', Surface and Interface Analysis, 50(1), pp. 32–42. Available at: https://doi.org/10.1002/sia.6329.

Selwyn, L. and McKinnon, W.R. (2021) 'Silver and Acid-thiourea Silver Dips: Rinsing and Aging Monitored by Electrochemistry', Studies in Conservation, 66(2), pp. 98–112. Available at: https://doi.org/10.1080/00393630.2020.1773056.

Siano, S. et al. (2012) 'Laser cleaning in conservation of stone, metal, and painted artifacts: state of the art and new insights on the use of the Nd:YAG lasers', Applied Physics A, 106(2), pp. 419–446. Available at: https://doi.org/10.1007/s00339-011-6690-8.

Siatou, A. et al. (2007) 'Testing new coating systems for the protection of metal collections exposed in uncontrolled museum environment', in Strategies for Saving our Cultural Heritage. Proceedings of the International Conference on Conservation Strategies for Saving Indoor Metallic Collections., Cairo. TEI of Athens, Athens, pp. 115–120.

Siatou, A. et al. (2022) 'A Methodological Approach for Multi-Temporal Tracking of Silver Tarnishing', in Proceedings of the 4th ACM International workshop on Structuring and Understanding of Multimedia heritAge Contents. New York, NY, USA: ACM, pp. 5–13. Available at: https://doi.org/10.1145/3552464.3555686.

De Silva, M. and Henderson, J. (2011) 'Sustainability in conservation practice', Journal of the Institute of Conservation, 34(1), pp. 5–15. Available at: https://doi.org/10.1080/19455224.2011.566013.

Smith, R.D. (1988) 'Reversibility: A Questionable Philosophy', Restaurator, 9(4). Available at: https://doi.org/10.1515/rest.1988.9.4.199.

Smith, S.S. (2017) 'Layer by layer: the removal of complex soiling on a collection of modern art bronzes using buffered pH-adjusted aquous gels', in L. V. Angelova et al. (eds) Gels in the Conservation of Art. London: Archetype Publications, pp. 349–355.

Stavroudis, C. and Doherty, T. (2007) 'A novel approach to cleaning II: extending the Modular Cleaning Program to solvent gels and free solvents, part 1', WAAC newsletter, 29(3), pp. 9–15.

Švadlena, J. and Stoulil, J. (2017) 'Evaluation of protective properties of acrylate varnishes used for conservation of historical metal artefacts', Koroze a ochrana materiálu, 61(1), pp. 25–31.

Tabone, M.D. et al. (2010) 'Sustainability Metrics: Life Cycle Assessment and Green Design in Polymers', Environmental Science & Technology, 44(21), pp. 8264–8269. Available at: https://doi.org/10.1021/es101640n.

Tamura, M. and Takagi, K. (2017) 'Towards the sustainable use of agar / agarose in conservation: a case study of the Izu peninsula, Japan', in L. V. Angelova et al. (eds) Gels in the Conservation of Art. London, UK: Archetype Publications, pp. 152–154.

Theodorakopoulos, C. et al. (2023) 'Cleaning testing of nineteenth-century plaster surface models with thin polyacrylamide-based gel layers attached to flexible polyethylene films', Heritage Science, 11(1), p. 95. Available at: https://doi.org/10.1186/s40494-023-00924-5.

Thickett, D. (2021) 'Oxygen Depletion Testing of Metals', Heritage, 4(3), pp. 2377–2389. Available at: https://doi.org/10.3390/heritage4030134.

Tissot, I. et al. (2016) 'Corrosion of silver alloys in sulphide environments: a multianalytical approach for surface characterisation', RSC Advances, 6(57), pp. 51856–51863. Available at: https://doi.org/10.1039/C6RA05845K.

Toreno, G. et al. (2018) 'Biological colonization on stone monuments: A new low impact cleaning method', Journal of Cultural Heritage, 30, pp. 100–109. Available at: https://doi.org/10.1016/j.culher.2017.09.004.

Tsurumaki, A. et al. (2022) 'Removal of Copper Corrosion Products by Using Green Deep Eutectic Solvent and Bio-Derivative Cellulose Membrane', Polymers, 14(11), p. 2284. Available at: https://doi.org/10.3390/polym14112284.

Turner-Walker, G. (2008) A practical guide to the care and conservation of metals. Taichung City, Taiwan: Headquarters Administration of Cultural Heritage, Council for Cultural Affairs.

Varghese, S.A. et al. (2020) 'Natural polymers and the hydrogels prepared from them', in Hydrogels Based on Natural Polymers. Elsevier, pp. 17–47. Available at: https://doi.org/10.1016/B978-0-12-816421-1.00002-1.

Varnai, V.M. et al. (2011) 'Upper respiratory impairment in restorers of cultural heritage', Occupational Medicine, 61(1), pp. 45–52. Available at: https://doi.org/10.1093/occmed/kqq170.

Walsh-Korb, Z., Ruiz-Fourcade, S. and Avérous, L. (2017) 'Responsive bio-based gels for the preservation and treatment of archaeological wooden objects', in R. Angelova, L.V., Ormsby, B., Townsend, J.H., Wolbers (ed.) Gels in the Conservation of Art. London, UK: Archetype Publications, pp. 294–296.

Watkinson, D. (2010) 'Preservation of Metallic Cultural Heritage', in Shreir's Corrosion. Elsevier, pp. 3307–3340. Available at: https://doi.org/10.1016/B978-044452787-5.00172-4.

Wolbers, R. (2000) 'Cleaning Painted Surfaces: Aqueous methods', in. Archetype Publications, p. 198.

Wolbers, R. (2017) 'Terminology and properties of selected gels', in L. V. Angelova et al. (eds) Gels in the Conservation of Art. London: Archetype Publications, pp. 381–394.

Wolbers, R., Rivers, S. and Yamashita, Y. (2014) 'Corroded applied lead-based decoration (hyomon) on Japanese lacquer: Principles and case studies', Studies in Conservation, 59(sup1), pp. S191–S194. Available at: https://doi.org/10.1179/204705814X13975704319316.

Wolbers, R.C. (1988) 'Notes for workshop on new methods in the cleaning of paintings'.

Wolbers, R.C. (1992) 'Recent developments in the use of gel formulations for the cleaning of paintings', in Restoration'92: conservation, training, materials and techniques: latest developments. Preprints to the conference held at the RAI International Exhibition and Congress Centre, Amsterdam, 20-22 October 1992, pp. 74–75.

Wolfe, J. and Grayburn, R. (2017) 'A review of the development and testing of Incralac lacquer', Journal of the American Institute for Conservation, 56(3–4), pp. 225–244. Available at: https://doi.org/10.1080/01971360.2017.1362863.

Wolfram, J., Brüggerhoff, S. and Eggert, G. (2010) 'Better than Paraloid B-72? Testing Poligen®waxes as coatings for metal objects', Proceedings of the METAL [Preprint].

Xie, C.Z. (2009) Environmental impacts of effluent containg EDTA from dairy processing plants. The University of Waikato. Available at: http://waikato.researchgateway.ac.nz/.

Yates, M.R. and Barlow, C.Y. (2013) 'Life cycle assessments of biodegradable, commercial biopolymers—A critical review', Resources, Conservation and Recycling, 78, pp. 54–66. Available at: https://doi.org/10.1016/j.resconrec.2013.06.010.

Yilmaz, M., Soran, H. and Beyatli, Y. (2005) 'Determination of poly-β-hydroxybutyrate (PHB) production by some Bacillus spp.', World Journal of Microbiology and Biotechnology, 21(4), pp. 565–566. Available at: https://doi.org/10.1007/s11274-004-3274-1.

Yiming, J. et al. (2019) 'A new bio-based organogel for the removal of wax coating from indoor bronze surfaces', Heritage Science, 7(1), p. 34. Available at: https://doi.org/10.1186/s40494-019-0276-8.

Zhu, Y., Romain, C. and Williams, C.K. (2016) 'Sustainable polymers from renewable resources', Nature, 540(7633), pp. 354–362. Available at: https://doi.org/10.1038/nature21001.

Chapter 2

Bio-formulations for the removal of synthetic organic coatings from historical metals

2.1 Organic coatings on historical metal artworks: from sought to undesired materials

In Paragraph 1.2.2 the use of organic coatings as protection means for the long-term safeguarding of historical metallic artefacts from the irreversible and damaging process of corrosion in outlined. The discussion also mentioned the central problematics linked to ageing and deterioration phenomena affecting such materials in the long-term, altering their aesthetical (e.g., yellowing) and physico-chemical (e.g., film resistance, solubility) properties. In particular, it was pointed out the importance of respecting the reversibility principle that would guarantee coating removal – and possibly replacement – once its aesthetical features and/or protective purpose start failing.

The research study here proposed in Chapter 2 was therefore carried out to design bio-based and biodegradable gelled formulations for the removal of protective coatings, once this intervention is sought. The extensive development and assessment of the formulations were aimed at providing greener alternatives to conservator-restorers and novel inputs to be further developed in conservation science. Given the variegate spectrum of products available for art conservation, the research target was set in line with the responses gathered through the HELIX survey in 2020 (Paragraph 1.5). Namely, the design of gelled bio-formulations for the removal of acrylic varnishes and nitrocellulose lacquers was investigated. Specifically, Paraloid® B72 and Zaponlack were selected for the respective categories, being among the most traditional solutions for indoor metal care.

2.1.1 Acrylic resin – Paraloid® B72

As presented in Paragraph 1.2.2, among the category of acrylic resins, the family of Paraloid® (Acryloid® in the USA) is widely represented in art conservation, and in particular the formulation Paraloid® B72 stands out when referring to indoor historical metal artworks. Paraloid® B72 (often abbreviated in "PB72" in this dissertation) is a copolymer of methyl acrylate and ethyl methacrylate (30/70% w/w), manufactured by Rohm & Haas (USA) since the first half of the twentieth century (Farmakalidis *et al.*, 2016). The chemical structure is a linear copolymer of the two aforementioned monomers that are randomly arranged along the chain and combined by the polymerisation of the double bonds (Figure 2.1). Overtime its composition slightly varied compared to the information provided by the manufacturer, as demonstrated by the detection of additional butyl methacrylate (2.2 mol%) (Lazzari and Chiantore, 2000) or TiO_2 loaded in the formulation for higher protection against photochemical and thermal deterioration (Farmakalidis *et al.*, 2016). It is sold either already prepared in solution or in solid pellets that can be dissolved by adequate solvents, such as ethanol, acetone, ethyl acetate, ethyl lactate, butyl acetate, etcetera (Vinçotte *et al.*, 2019) to the desired concentration and viscosity according to the sought application (Chapman and Mason, 2003).

As typically for acrylic resins, Paraloid® B72 demonstrated satisfactory transparency (i.e., refractive index 1.49), mechanical properties, ease-of-use, and chemical stability over time, generally guaranteeing long-term protection, reversibility, and aesthetic (Chapman and Mason, 2003; Farmakalidis *et al.*, 2016). The material stability was tested by photo-oxidation (Chiantore and Lazzari, 2001) and thermal ageing (Farmakalidis *et al.*, 2016) in order to investigate resin reliability when affected by external deteriorating factors (e.g., UV light, high temperature).

When subjected to photo-oxidation, Paraloid® B72 showed satisfactory resistance against oxidation, which is a property ascribable to its main component methyl acrylate, as stated by the authors of the test (Chiantore and Lazzari, 2001). Photo-oxidation occurred without formation of insoluble fractions when Paraloid® B72 was irradiated by xenon light source (filtered for $\lambda < 295$ nm) up to 2500 hours. This is crucial to respect the principle of intervention reversibility in art conservation, hence guaranteeing its potential removal by appropriate solvents. The same test did not reveal cracking or other visible variations on the aged films. Interestingly, this behaviour is different from the one observed when Paraloid® B72 is subjected to UV light in the spectral region 220-300 nm, which was found to ignite a fast yellowing of the polymer (Melo *et al.*, 1999).

Finally, Farmakalidis *et al.* (2016) observed the coating behaviour when subjected to thermal ageing. After 18 days in a laboratory oven at 100 °C, Paraloid® B72 films remained soluble in the tested solvents (i.e., cyclohexane, toluene), however swelling and solubility experiments revealed a reduction in solubility of 8.7%. Lower hydrophobicity was verified measuring the contact angle on the aged material, also evidencing a change in its surface polarity. Finally, colourimetry highlighted a colour variation of the Paraloid® B72 film comparing before and after ageing (i.e., $\Delta E^* = 2.58$), which is greatly linked to b* values that increased over time (from 1.13 to 3.15), proving a yellowing effect.

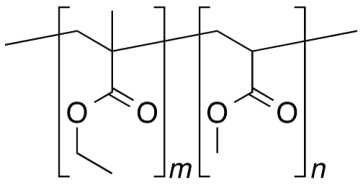

Figure 2.1 Paraloid® B72, structural formula of the methyl acrylate/ethyl methacrylate monomers in the linear copolymer chain.

2.1.2 Cellulose nitrate lacquer – Zaponlack

Nitrocellulose materials are another class of protective coatings that was largely used before the advent of Paraloid® (i.e., acrylic resins), as explained in Paragraph 1.2.2. Nowadays, they are mainly found and exploited on silver- and copper-alloys due to the relevant protection provided against gaseous sulphide compounds possibly present in indoor environments (Molina, Cano and Ramírez-Barat, 2023a).

Within the framework of this research, Zaponlack (often abbreviated in "ZL" in this manuscript), a lacquer fabricated in Germany, was selected as nitrocellulose-based coating. Poor reference literature is available about this specific product; therefore a general discussion is here addressed about the category of cellulose nitrate lacquers.

Nitrocellulose coatings were developed after the First World War by the reaction of nitric acid (HNO_3) and cellulose in the presence of the dehydrating agent sulfuric acid (H_2SO_4) (Fernández de la Ossa *et al.*, 2011). During the synthesis, approximately two of the cellulose hydroxyl groups (-OH) in each ring are replaced with nitrate groups (NO_3) with a degree of substitution usually in the range 1.9-2.4 (Fernández de la Ossa *et al.*, 2011). As displayed in Figure 2.2, the resulting cellulose nitrate molecule is characterised by the presence of nitrate ester ($-ONO_2$) and hydroxyl (-OH) groups that determine the polarity of the compound. Indeed, it is well-known in the field of heritage conservation that nitrocellulose materials can be dissolved (i.e., for application or removal) by means of polar organic solvents such as esters and ketones (e.g., acetone, ethyl acetate, diethyl carbonate) (Borén, 2022). In lowly-nitrated nitrocellulose formulations (i.e., low degree of substitution, 1.9-2.1), the polymer is dissolved in a solvent – or a mixture of them – and are generally used as coatings for several purposes (e.g., nail varnishes, wood lacquers). The presence of the so-called "lacquers thinners" (i.e., solvents) allows to obtain low-viscosity formulations that are easily spreadable and provide a final glossy film of nitrocellulose on the treated substrates after evaporation (Moity *et al.*, 2016).

This class of coatings, as already mentioned, is still favoured when aiming to protect copper- and especially silver-based artefacts (Molina, Cano and Ramírez-Barat, 2023a). Indeed, its optical qualities, good adhesion

to metallic surfaces, and, most relevantly, low permeability to corrosive gases, such as hydrogen sulphide (H_2S), make this family of organic coatings appealing in conventional metal care praxes (Borén, 2022).

However, high concern is expressed regarding its instability over time. Indeed, the material is prone to photochemical deterioration by a combination of hydrolysis and oxidation reactions mainly initiated by UV radiation. The high photo-sensitivity of nitrocellulose is well-documented, especially when exposed to wavelengths between 360-400 nm, which justifies its use indoors (Shashoua, Bradley and Daniels, 1992; Molina, Cano and Ramírez-Barat, 2023a). The deterioration of nitrocellulose is auto-catalytic. When the polymer starts to deteriorate, the bonds break causing the release of gaseous nitrogen dioxide (NO_2), which catalyses the deterioration process by oxidation (Shashoua, Bradley and Daniels, 1992). The process leads to chain scission along the backbone of the molecule with a resulting decrease in molecular weight and viscosity (i.e., the material is more brittle) while registering an increase of polarity (i.e., failure in long-term reversibility) (Shashoua, Bradley and Daniels, 1992; Luxford and Thickett, 2007).

With the aim of utilising ethyl lactate for the removal of nitrocellulose lacquers from metals, previous literature reports its efficient exploitation in dissolving this class of materials also at the industrial level for paints, dyes, and varnishes (Nikles *et al.*, 2001; Calvo-Flores *et al.*, 2018). In particular, the suitability of ethyl lactate for the dissolution of Zaponlack was already discussed in a Master's degree dissertation by Borén (2002). The study focused on the research of greener solvents for the removal Zaponlack lacquer from silver model samples. The cleaning assays were performed using a large number of solvents (e.g., ethyl acetate, dimethyl carbonate), including ethyl lactate, and with different application methods (i.e., cotton swabbing and poultice). In all cases, ethyl lactate performed in a satisfactory way for the removal of the nitrocellulose lacquer. In parallel, no evident alterations were observed on the test samples derived from the interaction between the organic solvent and the metallic substrate (Borén, 2022).

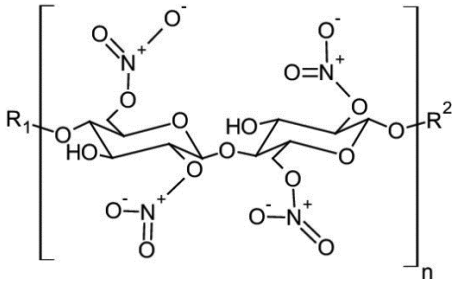

Figure 2.2 Structural formula of the cellulose nitrate polymer.

2.2 Mock-up preparation

In order to assess the removal of the aforementioned synthetic coatings (i.e., Paraloid® B72 and Zaponlack), iron- and copper-based alloys were chosen as substrates being the most representative for indoor historical metal collections, as reported in the literature (Angelini and Argyropoulos, 2008) and by the answers collected through the world-wide survey conducted within the framework of the HELIX project in 2020. Specifically, mild steel and brass (Cu 66%, Zn 34% by X-ray fluorescence analysis) coupons were employed to evaluate the cleaning performance of the novel formulations proposed. Metal sheets of 30 × 30 × 1 mm^3 and 50 × 50 × 1 mm^3 purchased from Tartaix Métaux Outillage (France) were drilled in the centre of the sheet's upper edge, creating a hole of 2 mm in diameter that was used to hang the mock-ups in batches in a climatic chamber for artificial ageing. The drilled coupons were then degreased by cotton swabbing using subsequently ethanol (96.0 – 97.2%) and acetone (≥99.5%) from Sigma Aldrich. Afterwards, the coupons were coated by brush with two thin criss-cross layers of protective coatings. In agreement with the abovementioned HELIX survey and the literature (Molina, Cano and Ramírez-Barat, 2023a), the selected coatings were differently associated to the chosen substrates. In particular, steel was coated with the acrylic resin Paraloid® B72 from CTS (10% w/v solution in ethyl acetate (≥99.7%) from Sigma Aldrich) and brass with the nitrocellulose lacquer Zaponlack from Carl Roth. The resulting coated mock-ups were firstly left

to dry in uncontrolled conditions, then placed into a climatic chamber for the artificial ageing of the coatings (Figure 2.3). In order to obtain a large number of mock-ups in the same ageing conditions for reproducibility, the metallic sheets were hung by nylon threads connected to the climatic chamber grills, keeping a distance of 2 cm between them, and placing them perpendicularly to the ventilation system. The protocol employed in the climatic chamber consisted of a cyclic program of a wet phase (38 °C at 80% RH) for 16 hours followed by a dry phase (23 °C at 55% RH) of 8 hours, repeated daily for three months (Degrigny, 2008).

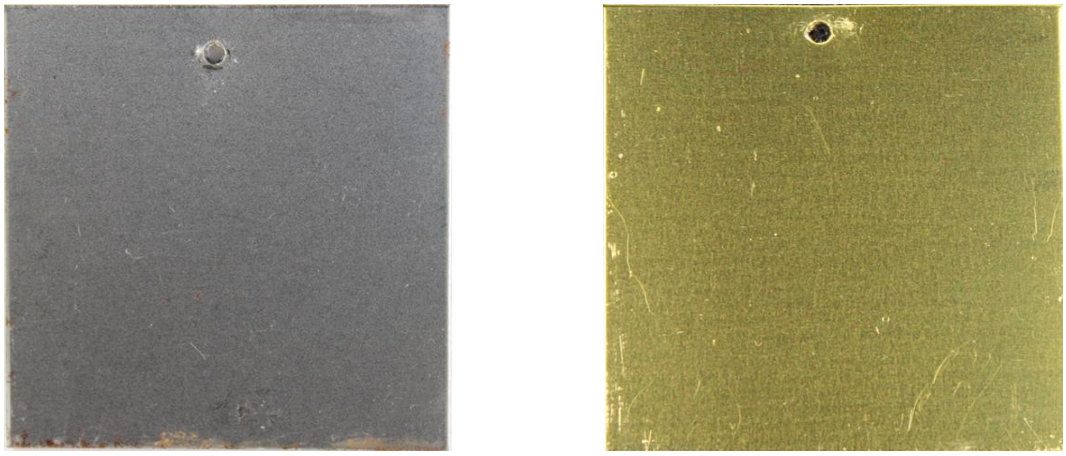

Figure 2.3 Mild steel (left) and brass (right) mock-ups coated with Paraloid® B72 and Zaponlack, respectively, after artificial ageing. The shown metal sheets are 50 × 50 × 1 mm^3.

2.3 Ethyl lactate as a key actor in the removal of the organic coatings

The solvent ethyl lactate was the first building block selected for the design of the sought greener organogels. The choice was made surveying the previous literature reporting the successful exploitation of ethyl lactate in dissolving both classes of selected organic coatings, namely acrylic and nitrocellulose lacquers.

Tested as an alternative solvent for the preparation of acrylic resins, namely Paraloid® B72 and B44, ethyl lactate was able to dissolve both products (Vinçotte *et al.*, 2019). Nevertheless, the solvent was not sufficiently volatile (i.e., vapour pressure 0.27 kPa at 20 °C) compared to other traditionally employed solvents (e.g., acetone vapour pressure is 24.66 kPa at 20 °C) for this purpose. Its use as a varnish diluent would pose concerns about the potential consequences derived from residual ethyl lactate entrapped in the coating once applied (Vinçotte *et al.*, 2019).

Concerning nitrocellulose lacquers, a recent thesis dissertation by Evelina Borén evaluated, among others, the exploitation of ethyl lactate as a greener mean for the removal of Zaponlack from silver heritage (Borén, 2022). Compared to acetone as a conventional solvent, ethyl lactate demonstrated good efficiency in removal when applied by poultice cloth (2 minutes × 2) or cotton swabbing on both fresh and aged Zaponlack samples. The same author did not highlight any corrosive effect on the silver substrates due to the interaction with ethyl lactate, which is in line with other evidence in the literature, and encouraging for its exploitation to clean altered metal collections (Pereira, Silva and Rodrigues, 2011; Dolzhenko, 2020).

In parallel with its proven efficacy in dissolving the organic coatings, the solvent has inherent green features that accomplish multiple of the twelve Green Chemistry principles (Anastas and Warner, 1998). Ethyl lactate, indeed, belongs to the family of lactates, which is a group of environmentally-benign solvents that are progressively becoming protagonists in numerous sectors (Gu and Jérôme, 2013). They derive from lactic acid that can be manufactured by biomass in a renewable way. According to the microorganisms involved in the process, it can be produced either as pure (R)- or (S)- enantiomer or as a racemate through

fermentation of hexoses and other carbohydrates (Ghaffar *et al.*, 2014). Thanks to the advantageous bio-origin and similar chemical properties, lactates are gaining consideration for the substitution of more hazardous and toxic substances like toluene, xylene, or methyl ethyl ketone (MEK) (Nikles *et al.*, 2001; Kerton and Marriott, 2013). Their replacement with lactates ensures safer workplaces, as in the potential scenario of CRs daily activity (Pereira, Silva and Rodrigues, 2011).

Among the most exploited lactates, ethyl lactate (ethyl 2-hydroxypropanoate) stands out (Figure 2.4). Examining the solvent through the filter of greenness and sustainability, it is produced by the reaction of ethanol with lactic acid through the fermentation of biomass, wherein water is the sole by-product (Gu and Jérôme, 2013). The solvent origin is thus sustainable and renewable, moreover requiring low costs for the production (Gu and Jérôme, 2013). Ethyl lactate is characterised by low toxicity (i.e., present as an additive in food) and readily biodegradability into water and carbon dioxide (Pereira, Silva and Rodrigues, 2011; Kua *et al.*, 2016). Some toxicological and physico-chemical properties of ethyl lactate of interest to evaluate the suitability and impact in CRs workshops are reported in Table 2.1 along with other traditional solvents (i.e., MEK, acetone, water).

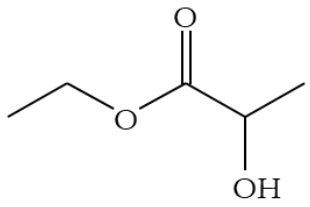

Figure 2.4 Structural formula of the bio-solvent ethyl lactate (EL).

Table 2.1 Toxicological and physico-chemical properties of interest for ethyl lactate and some traditional solvents. Data provided by the European Chemicals Agency (ECHA) and Merck.

	Toxicity (inhalation threshold)	*Boiling point (at 100 atm)*	*Vapour pressure (at 20 °C)*
Methyl ethyl ketone (MEK)	106 mg/m³	79.6 °C	10 kPa
Acetone	200 mg/m³	56.1 °C	24 kPa
Water	-	100 °C	2.34 kPa
Ethyl lactate	**1.739 mg/m³**	**138.6 °C**	**0.27 kPa**

Ethyl lactate is classified as a polar protic solvent (Volpi, 2017). The proximity between hydroxyl and carbonyl groups (Figure 2.4) determines intra-molecular hydrogen bonding that makes the solvent highly miscible in water (Aparicio and Alcalde, 2009). The Teas chart reported in Figure 2.5 proposes ethyl lactate position according to Hansen solubility parameters (Stavroudis and Doherty, 2007) and in relation to other conventional solvents. Overall, ethyl lactate arranges close to solvents such as isopropanol and ethanol because of the molecular properties aforementioned (i.e., especially polar (F_p) and hydrogen bonding (F_h) forces), while showing polar forces similar to solvents such as MEK, which would explain the use of EL as replacement solution (Nikles *et al.*, 2001). Ethyl lactate demonstrates an ability to dissolve both polar and non-polar species as confirmed by the significant exploitation for the formulation of industrial dyes, paints, and varnishes (Nikles *et al.*, 2001; Kua *et al.*, 2016; Calvo-Flores *et al.*, 2018). Finally, ethyl lactate is characterised by low vapour pressure (i.e., 0.27 kPa at 20 °C) and high boiling point (138.6 °C at 100 atm), which are features that would guarantee a safe work environment, when compared to other traditional solvents with similar dissolving properties (Table 2.1).

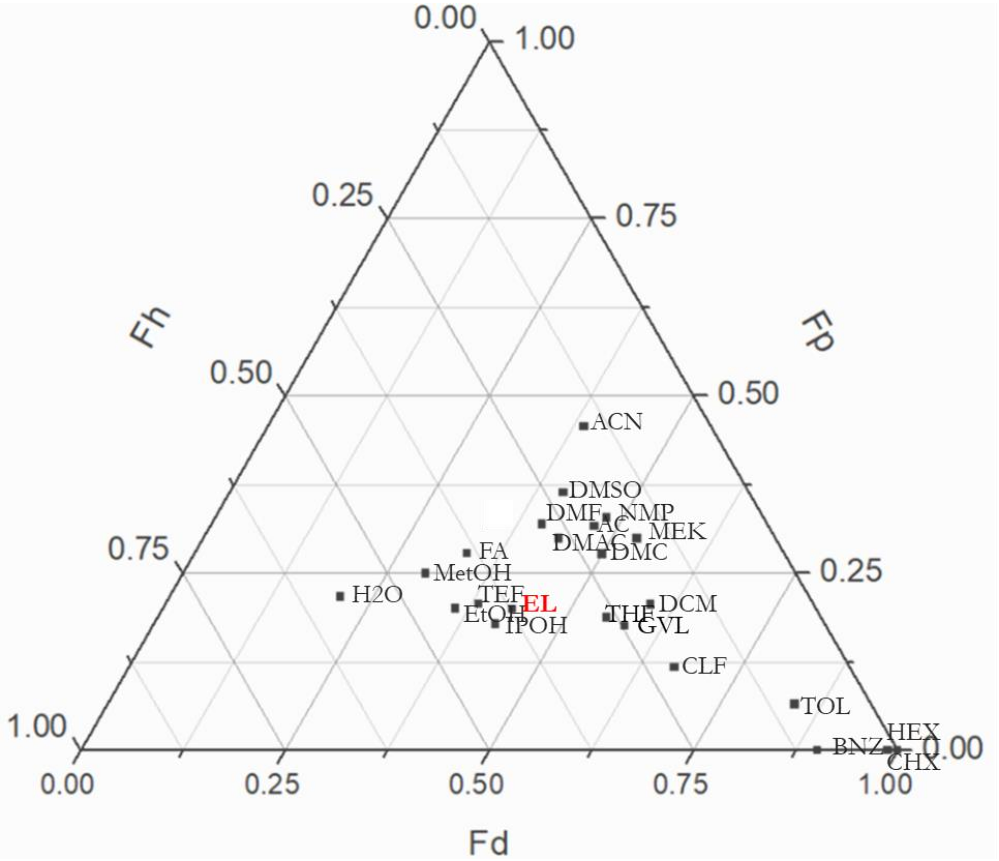

Figure 2.5 Teas solubility diagram showing the position of ethyl lactate (EL, in red) in relation to other traditional solvents. The bi-plot is delimited by three axis reporting the contribution of dispersive (F_d), polar (F_p), and hydrogen bonding (F_h) forces of solvents. The other labels stand for: acetone (AC), acetonitrile (ACN), benzene (BNZ), chloroform (CLF), cyclohexane (CHX), dichloromethane (DCM), dimethyl sulfoxide (DMSO), dimethylacetamide (DMAC), dimethylformamide (DMF), dimethyl carbonate (DMC), ethanol (EtOH), formic acid (FA), gamma-valerolactone (GVL), isopropanol (IPOH), methanol (MetOH), methyl ethyl ketone (MEK), N-methyl pyrrolidone (NMP), n-hexane (HEX), tetrahydrofuran (THF), toluene (TOL), trichlorotrifluoroethane (TFE), water (H2O).

Appealed by its assets, several articles have been published on the potential insertion of ethyl lactate in art conservation. For instance, as previously mentioned, it was tested as an innovative greener solvent for the preparation of Paraloid® resins (Vinçotte *et al.*, 2019). On the other side, quite a few studies have been carried out on its cleaning efficacy. Its value is well-noted in the removal of graffiti inks from underlying original supports and already exploited in industry (Calvo-Flores *et al.*, 2018) as well as in art conservation (Esson, Scott and Hayes, 2018). In the latter case, the solvent demonstrated not only efficiency in the cleaning but also a satisfactory selectivity towards specific binders without impacting the subjacent original paint. Similarly, the solvent was exploited for the cleaning of differently stained photographs (ELattar *et al.*, 2021). Marks linked to self-adhesive notes and tapes, used in the past, were successfully removed by cotton swabs soaked in ethyl lactate without causing any harm to the object or leaving residues. Post-treatment assessment did not highlight any surface alteration in terms of pH, colour, or topography of the photographs, nor the degradation of the gelatine binder present. Finally, ethyl lactate led to satisfactory removal of natural terpenic varnishes from oil paintings when loaded in a bio-derived gel system named by the authors of the study "PHB-EL" (i.e., polyhydroxybutyrate PHB, ethyl lactate EL) (Prati *et al.*, 2019). The employment of a fully bio-sourced gelled formulation was of clear interest and in line with the research presented in this manuscript, therefore the PHB-EL gel was tested for its implementation among the category of chemical methods for the cleaning of metal artworks (Paragraph 2.4).

2.3.1 Preliminary test

In a preliminary phase, the reliability on the use of ethyl lactate was evaluated in relation to the metallic substrates to be treated. Published literature reports the reliable use of the organic solvent on metals (Pereira, Silva and Rodrigues, 2011; Dolzhenko, 2020; Borén, 2022), however it is a common praxis to ascertain the suitability of a material prior to use it on metal artefacts, as addressed by the so-called "Oddy test" introduced by Andrew Oddy and co-workers in the early 1970s (Thickett and Lee, 2004). In this research study, the test was aimed to verify the possible adverse effects provoked by the interaction between metals (i.e., steel and brass) and the organic solvent (i.e., ethyl lactate) through an over-exposure compared to the one employed when cleaning with the proposed formulations (i.e., maximum total time of 20 minutes, Paragraph 2.8.1).

Initially, mild steel and brass 30 × 30 × 1 mm^3 coupons (Tartaix Métaux Outillage, France) were degreased by cotton swabbing using subsequently ethanol (96.0 – 97.2%) and acetone (≥99.5%) from Sigma Aldrich. The coupons were then half-immersed into a crystallising dish containing ethyl lactate for 90 minutes, while the other halves of the coupons were kept untreated as controls (Figure 2.6). Eventually, the immersed surfaces were quickly dried with a cotton swab.

Figure 2.6 Mild steel (left) and brass (right) coupons half-immersed into a crystallising dish containing ethyl lactate for 90 minutes.

After the 90-minute immersion in ethyl lactate, as reported by photographic evidence (Figure 2.7, A and B), there was no clear distinction between the coupon areas subjected to immersion in ethyl lactate and the controls if observed by the naked eye. When inspected by optical microscopy with 50× magnification, no manifest surface alteration was found on the immersed coupon halves, but possibly the presence of fewer marks related to dirt and grease that apparently were not entirely removed by the sole preliminary cotton swabbing by ethanol and acetone (Figure 2.7). Finally, colorimetric data collected on the two halves of the tested metals are consistent with the interpretation achieved by optical microscopy. Indeed, when relating the immersed halves and the controls, a minimal colour difference (ΔE*) was noticeable; namely, ΔE* was calculated as 0.16 (±0.42) and 1.59 (±0.23) for steel and brass coupons, respectively.

The preliminary test did not evidence any negative interaction occurring between ethyl lactate and the metallic pieces employed in this study, therefore the solvent could be selected and the research for adequate carrier systems could be explored.

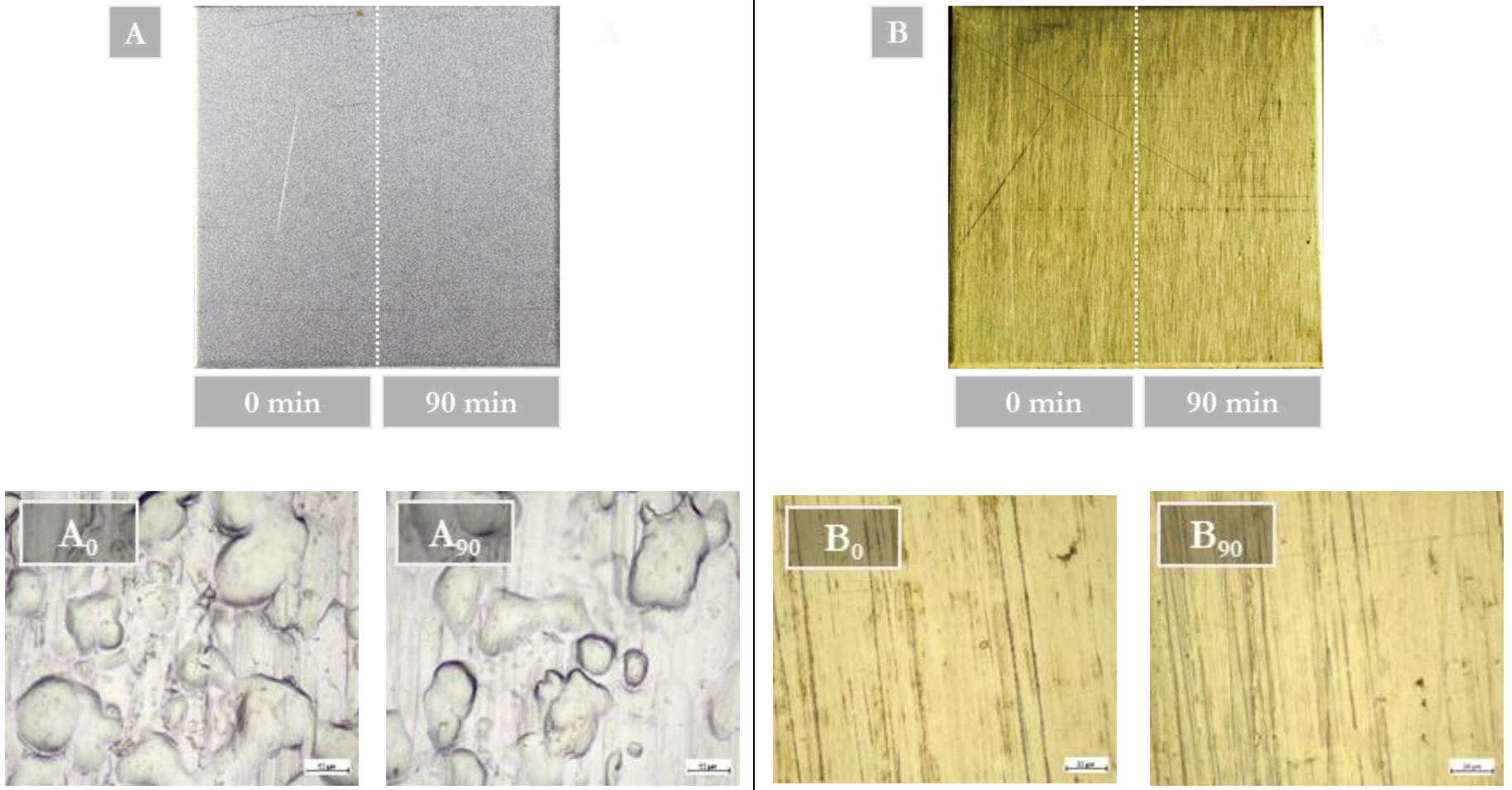

Figure 2.7 Photographs of steel (A) and brass (B) coupons (30 × 30 × 1 mm³) after being half-immersed into ethyl lactate for 90 minutes. Optical microscope images in bright field of untreated (A_0 and B_0) and treated (A_{90} and B_{90}) steel and brass surfaces, respectively. The scale bar for microscope pictures indicates 20 μm.

2.4 PHB-EL formulation

2.4.1 Polyhydroxybutyrate (PHB)

Multiple bio-derived polymers were chosen for the design of a gelled system retaining ethyl lactate for the removal of organic coatings. The first presented is polyhydroxybutyrate (PHB), which belongs to the family of polyhydroxyalkanoates (PHAs), and therefore, to the esters class. From a green perspective, it is fundamental to mention that polyhydroxyalkanoates can be produced by more than 300 bacteria and archaea species, in both oxic and anoxic environments, indexing this class of materials among the bio-polymers. Their synthesis occurs either during the growth phase or under stress conditions (e.g., depletion of vital nutrients) while being in surplus of carbon (Khatami *et al.*, 2021). Indeed, PHA is hoarded as intracellular granules in the cytoplasm and kept as energy storage. Furthermore, PHAs' natural degradation into carbon dioxide, water, and biomass requires about two months (Hassan *et al.*, 2013), awarding this class of polymers with additional inherent features in line with the Green Chemistry principles (Anastas and Warner, 1998). Nonetheless, the current cost of PHAs is nearly six times higher than conventional fossil-sourced plastics, clearly restricting and compromising the implementation of these biopolymers on a wider scale (Khatami *et al.*, 2021).

More precisely, polyhydroxybutyrate (PHB) is a semi-crystalline polymer synthesised by several microorganisms (e.g., *Alcaligenes* spp., *Bacillus* spp., *Azotobacter* spp., *Pseudomonas* spp.), which exploit renewable feedstocks rich in sugars for their metabolic activity (Yilmaz, Soran and Beyatli, 2005; Scalioni, Gutiérrez and Felisberti, 2017). Being bio-sourced, it can be classified as bio-polymer, moreover it is completely biodegradable when exposed to active biological environments, non-pollutant, and biocompatible (Yilmaz, Soran and Beyatli, 2005; Scalioni, Gutiérrez and Felisberti, 2017; McAdam *et al.*, 2020).

As a member of the PHAs, polyhydroxybutyrate is characterised by the presence of a methyl group (CH_3) and an ester linkage group (−COOR), as displayed in Figure 2.8. These molecular features and the fact that PHBs are short-chain length polymers (i.e., 3-5 carbon atoms in the monomer chain) determine the hydrophobicity, thermoplasticity, brittleness, and stiffness of polyhydroxybutyrate derivatives (McAdam *et al.*, 2020). Moreover, such chemo-physical properties are similar to petroleum-derived counterparts, such as polypropylene (PP) and polyethylene (PE), making this class of bio-polymers a potential greener alterative to pollutant plastics (McAdam *et al.*, 2020). Evidently, these characteristics narrow the application window of such material according to the exploitation purposes. Therefore, blends of polyhydroxybutyrate with other polymers are a solution often utilised in industry to compensate its undesirable properties (e.g., brittleness) while enhancing the greenness of the resulting plastics, as in the case of PHB blends with poly(ethylene oxide) (PEO) or poly(vinylphenol) (PVP), but it can also be found in association with green polysaccharides such as chitin and chitosan (Leja and Lewandowicz, 2010). Finally, from a chemical perspective, PHB bio-polymers are soluble in polar solvents (e.g., chloroform, dichloromethane, acetic acid (Jirage *et al.*, 2013)) but not in water, being an hydrophobic molecule (Balaji, Gopi and Muthuvelan, 2013).

In the sporadic applications in art conservation, the form poly-3-hydroxybutyrate (i.e., three carbon atoms in the monomer chain) was employed as a thickening agent (Samorì *et al.*, 2016; Walsh-Korb, Ruiz-Fourcade and Avérous, 2017; Prati *et al.*, 2019; Yiming *et al.*, 2019). In particular, as previously mentioned in this manuscript, a PHB-EL (i.e., loaded with ethyl lactate) gelled system was developed in the field of conservation science for the effective cleaning of varnished paintings (Samorì *et al.*, 2016; Volpi, 2017; Prati *et al.*, 2019), therefore its potential exploitation in metal conservation was of high appeal.

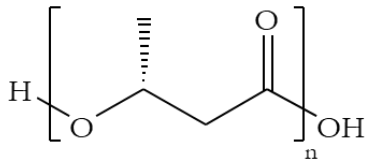

Figure 2.8 Structural formula of the bio-polymer polyhydroxybutyrate (PHB).

2.4.2 The PHB-EL system

For the synthesis of the PHB-EL formulation was employed the bio-polymer poly-3-hydroxybutyrate (PHB) purchased from Biomer and the bio-solvent ethyl lactate (≥98%) (EL) from Sigma Aldrich in a mixture 7% w/v, as reported in the reference literature (Volpi, 2017; Prati *et al.*, 2019). The mixture was stirred in a covered glass petri dish at about 110 °C for a few minutes until the PHB powder got dissolved and the mixture gained in thickness. The resulting mixture was finally left to cool down to room temperature before application (i.e., 23.8 ±2.4 °C, laboratory conditions in this study) (Figure 2.9). Once cool, the measured pH in the PHB-EL formulation was acidic with a value around 4, which is linked to the presence of the organic solvent (i.e., pH ethyl lactate = 4 (Merck, 2024a)). The pH value reported by the supplier Sigma-Aldrich, and confirmed when measured by pH meter, was unexpected since the predicted pKa of ethyl lactate is 13.21 ± 0.20 (Chemical Book, 2024), thus legitimising a pH close to neutral. The evidence, instead, may suggest the presence of contaminants in the solvent that could not be identified in this study.

Figure 2.9 Photography of the PHB-EL gel formulation in a glass petri dish once at room temperature (i.e., 23.8 ±2.4 °C) (on a white background).

2.5 Agar-water/EL formulation

2.5.1 Agar

Agar was already introduced in this manuscript when reporting some examples of bio-polymers exploited in water-based formulations (see 1.4.2.1 Hydrogels, page 45). As a short reminder, agar is a natural polysaccharide extracted from several red seaweed membranes (Tamura and Takagi, 2017). Its primary component is agarose (Figure 2.10) which is frequently found in association with agaropectin. These two polysaccharides are characterised by the same monomer but present different structures. Agarose is a linear polymer consisting of alternating β-D-galactose and 3,6-anhydro-L-galactose rings connected by alternate α-(1,3) and β-(1,4) glycosidic bonds. On the other side, agaropectin is a heterogeneous agarose in which some 3,6-anhydro-L-galactose units are substituted by L-galactose-6-sulphate or by methoxy or pyruvate groups. Being the agar gelation process mainly driven by agarose, the presence of an agaropectin fraction and their proportion can differently alter and especially reduce the polymer gelation properties (Bertasa *et al.*, 2020). It is also known that the type of seaweed and the growing environment, as much as the extraction method employed, strongly affect the ratio between the two components, and consequently gelation and rheological properties of agar (Bertasa *et al.*, 2020). However, the co-presence of purified (agarose) and unpurified (agaropectin) polysaccharides generally reduces the cost of agar, making its use in art conservation more accessible for routine cleaning interventions (Cremonesi, 2013).

The gels obtained from agar are defined as semi-rigid, thermo-reversible, and hydrophilic systems (Sansonetti *et al.*, 2020). They are prepared by simple heating of the bio-polymer powder in appropriate ratios with water or neutral solutions (Guilminot *et al.*, 2019). As broadly discussed in a previous section (page 45), several methodologies based on agar gels are reported in the literature as successful mean for the cleaning of metal heritage, including objects made of iron-, copper-, and silver-alloys, which are the targets of this thesis dissertation (Marchand *et al.*, 2013; Wolbers, Rivers and Yamashita, 2014; Létrange *et al.*, 2017; São João, Branco and Leite Fragoso, 2017; Fays, 2018).

The wide exploitation of agar gels in CH and its physical properties make this polymer accepted nowadays by CRs in their conservation and restoration interventions, therefore it is of high interest to further research and explore the potential of this bio-polymer. As said, agar is normally employed in form of hydrogels, and previous researches tested its suitability as a carrier for water-based non-neutral solutions like citric acid, nitric acid, and NaOH (Giraud *et al.*, 2021). In this case, the study did not yield to the formation of stable agar systems neither when the non-neutral solutions were directly added during the heating phase, nor when pre-formed agar gels were left immersed in the solutions. On the contrary, a positive outcome is reported when the so-called Deep Eutectic Solvents (DES) were employed, specifically a mixture of choline chloride and urea (Jia *et al.*, 2021). Firmly restrained inside an agar matrix, in total absence of water, the resulting gel was successfully applied for the removal of proteinaceous materials from paintings.

Following such literature evidence, the study here presented was oriented towards the tentative design of an agar gel loaded with ethyl lactate exploring multiple methods with the goal of achieving an innovative fully bio-sourced and biodegradable formulation.

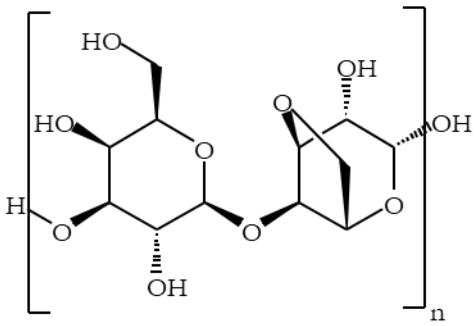

Figure 2.10 Structural formula of the bio-polymer agarose.

2.5.2 Design of the Agar-water/EL system

Multiple agar w/v concentrations and water/EL ratios were tested in order to explore the best combination for the making of the gel, as reported in Table 2.2. The design was addressed in order to load the system with the maximum concentration of ethyl lactate, being the component interest for the removal of the organic coatings, while obtaining a stable gel despite the presence of the acidic solvent (i.e., potential hydrolysis of the agar polymer (Armisén and Gaiatas, 2009)).

A first series of attempts investigated the possibility of forming an agar gel loaded with ethyl lactate by simple addition of all components (i.e., "all-at-once" formulation), namely agar powder, deionised water, and ethyl lactate, in a glass petri dish placed on a hot plate at about 90-100 °C under magnetic stirring. Although several formulations were explored (Table 2.2), an optimal mixture gelation could be achieved in none of the cases (Figure 2.11, a), contrary to regular agar hydrogels.

Therefore, the same set of formulations was then investigated by initially forming a standard agar hydrogel and afterwards adding ethyl lactate while the gel was still viscous (above 40 °C (Medina-Esquivel *et al.*, 2008)), aiming to verify a potential compatibility among the components by simply changing the preparation protocol. The tests yielded no uniform gelation of the agar powder when employing high concentrations of the polymer (i.e., 6% w/v), resulting in fragile and non-retaining formulations when manipulated. Similarly,

high ratios of ethyl lactate/water did not achieve the formation of gelled systems, possibly due to acidic hydrolysis induced by the presence of ethyl lactate (Armisén and Gaiatas, 2009). On the contrary, when lowering both variables, gelation occurred. In general, the formulations at 3% w/v resulted in being fragile when handled for the application and not as retentive as the formulations at 4% w/v that was preferred consequently in this study. Finally, among the tested formulations at 4% w/v, the gel loaded with ethyl lactate in ratio 1:3 (v/v) with water was chosen compared to 1:4 because it allowed to work with a higher concentration of ethyl lactate, which is the desired active agent acting on the removal of the selected organic coatings.

Table 2.2 Resuming table of the tests carried out to design the agar-water/EL formulation. The results show the outcome for still-warm (above 40 °C) agar hydrogels loaded with ethyl lactate. Green and red cells indicate formulations leading or not to agar gelation, respectively. The blue cell shows the formulation (i.e., agar hydrogel 4% w/v loaded with ethyl lactate (1:3 v/v)) selected as best performing in terms of solution retention, ease in handling, and ethyl lactate content. Grey cells report tests not carried out. The same set of experiments was run also for "all-at-once" formulation, resulting in being unsuccessful for all combinations.

		Agar hydrogel		
		3% w/v	**4% w/v**	**6% w/v**
Ratio EL/water (v/v)	**1:4**	Lower EL amount	Lower EL amount	No gel
	1:3	Poor handling	✓	No gel
	1:2	Poor retention and handling	No gel	No gel
	1:1	No gel	Not tested	Not tested

Once chosen the agar hydrogel 4% w/v loaded with ethyl lactate (1:3 v/v) as ideal formulation, different application and post-treatment methods were explored in order to define an adequate implementation of the system. When preliminarily tested on 3 × 3 cm^2 coupons, the main weakness registered was linked to the crucial need of mechanical action by dry cotton swabbing at the end of the cleaning process to appreciate evidence of the removal of the organic coatings present on both iron and brass sheets. Indeed, the impression was that the gel system was rather softening and swelling the organic material but could not remove it by gel detachment from the mock-up. Willing to overcome – or reduce – the need of mechanical action, other application ways were explored to improve the cleaning system efficiency. For example, application by gentle friction with a gel pre-formed in a cut plastic syringe (i.e., gel diameter about 1 cm) was assayed (Figure 2.11, b). However, the protocol resulted in being even less performing, probably due to the absence of a prolonged localised application of the gel despite using the same intervention time. Another procedure assessed exploited the potential of the agar formulation to be applied when still warm and viscous (Guilminot, 2023). The application method resulted in being possible and the loaded water/EL solution did not get dispersed uncontrolled on the test coupon (Figure 2.11, c), however no advantages in the removal of the coatings could be registered, since the use of dry cotton swab was still necessary at the end of the procedure.

Figure 2.11 Attempts for the design of agar-water/EL formulation. (a) Glass petri dish containing agar powder, deionised water, and ethyl lactate, after being heated and stirred on a hot plate. No homogeneous gelation was achieved. (b) Agar hydrogel 4% w/v loaded with ethyl lactate (1:3 v/v) formed in a plastic syringe. (c) Agar hydrogel 4% w/v loaded with ethyl lactate (1:3 v/v) applied while still warm on a mild steel coupon (30 × 30 × 1 mm^3) coated with Paraloid® B72.

A final attempt was carried out exploiting the immersion method, which is reported as a feasible option to be tested when non-neutral solutions are employed (Giraud *et al.*, 2021; Guilminot, 2023). Therefore, a pre-formed agar hydrogel 4% w/v was immersed for 24 hours in ethyl lactate in a closed glass petri dish with the goal of retaining a higher amount of solvent compared to the water/EL 3:1 system. At the end of the immersion process, the gel appeared shrunk compared to its original size, and the consistence was firmer when cut with a metallic spatula for the application. When compared to an agar hydrogel 4% w/v loaded with ethyl lactate (3:1 v/v) and prepared using a glass petri dish with the same diameter (i.e., lid diameter of 50 mm), the EL-immersion gel quarters were visibly smaller in size and, most relevantly, the system did not yield an effective removal of the Paraloid® B72 coating, contrary to the counterpart despite adopting the same cleaning protocol (i.e., single application of 5 minutes), as shown in Figure 2.12.

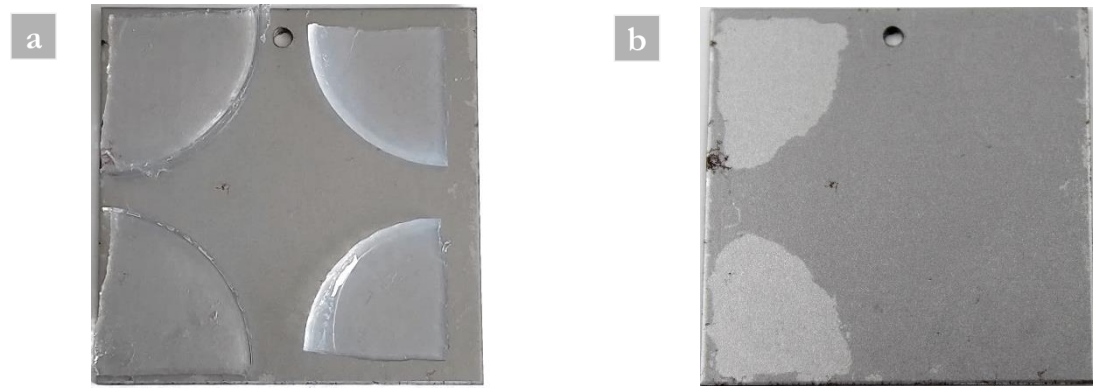

Figure 2.12 Mild steel coupon (50 × 50 × 1 mm^3) coated with Paraloid® B72 during (a) and after (b) 5-min cleaning with agar hydrogels (4% w/v) loaded with ethyl lactate (1:3 v/v) when the gel was still warm (left side of the mock-up) and agar hydrogel immersed for 24 hours in ethyl lactate (right side). The gels were initially prepared using a glass petri dish with the same diameter (i.e., lid diameter of 50 mm).

In conclusion, for the synthesis of the agar-water/EL system was initially prepared an agar (AgarArt, CTS) hydrogel with the addition of deionised water at a concentration of 4% w/v. The mixture was stirred in a covered glass petri dish at about 90-100 °C until gelation occurred. Once removed the petri dish from the hot plate, and while the mixture was still above the sol-gel transition temperature of around 40 °C (Medina-Esquivel *et al.*, 2008), ethyl lactate (≥98%, Sigma Aldrich) was added in a volume ratio of 1:3 in regard to

the deionised water already present in the agar gel. The resulting mixture was manually stirred by a metallic spatula for a few seconds, and finally let cool down to room temperature before application (i.e., 23.8 ±2.4 °C) (Figure 2.13). The measured pH in the formed agar-water/EL system was 5.

Figure 2.13 Photography of the Agar-water/EL 3:1 gel formulation in a glass petri dish once at room temperature (i.e., 23.8 ±2.4 °C) (on a white background).

2.6 PLA-EL formulation

2.6.1 Polylactic acid (PLA)

Polylactides (PLAs) are produced from lactic acid by the fermentation of renewable resources such as corn, potato, and starch (Ozkoc and Kemaloglu, 2009; Leja and Lewandowicz, 2010). In addition to their bio-derived origin, this class of polymers is slowly biodegradable (i.e., breaks down into H_2O and CO_2 within few years), compostable, renewable, energy-saving compared to petroleum-based counterparts (i.e., it requires 25 – 55% less energy), and known for being very low or non-toxic (Leja and Lewandowicz, 2010; Nurazzi *et al.*, 2022; Taib *et al.*, 2023).

Since lactic acid is a chiral molecule with both levo- and dextro-types of isomers, three forms of polylactic acid can be manufactured: poly-L-lactic acid (PLLA), poly-D-lactic acid (PDLA), and poly-D,L-lactic acid (PDLLA) (Li *et al.*, 2020). In general, polylactic acid (PLA) is a linear polyester and its monomer molecular structure is displayed in Figure 2.14 (Ozkoc and Kemaloglu, 2009).

The different proportion of D and L isomers present in the numerous PLAs available determines properties such as degree of crystallinity, inherent viscosity, brittleness, stiffness (Bragagni *et al.*, 2013; Nurazzi *et al.*, 2022). For instance, poly-L-lactic acid (PLLA) is of high interest thanks to its mechanical properties similar to those of petroleum-based polystyrene (PS) and polyethylene terephthalate (PET) (Nurazzi *et al.*, 2022). However, the inherent hardness and brittleness of PLLA hinders its exploitation in the biomedical field for orthopaedic and dental surgery (Leja and Lewandowicz, 2010). To overcome this limitation, blends of PLAs can be manufactured according to the application purposes and the desired features (e.g., drug delivery, tissue engineering (Li *et al.*, 2020). For instance, the stereo-complex PDLLA, synthesised from enantiomeric PLAs (i.e., PDLA and PLA blend), showed higher hydrolysis resistance and melting temperature (i.e., 220-230 °C) than pure PLLA and PDLA (i.e., 170-180 °C), which is reported as a limiting factor for the exploitation of pure PLA isomers in certain biomedical applications (Leja and Lewandowicz, 2010). Finally, due to the presence of ester (−COOR) and methyl (CH_3) functional groups in the polymer structure (Figure 2.14), polylactic acid is characterised by high polarity and hydrophobicity (Nurazzi *et al.*, 2022).

The scientific literature, reporting the use of this polymer in the field of cultural heritage, is very scarce. PLA was investigated mainly to exploit it as a protective film on stone heritage, looking for a bio-sourced and biodegradable alternative to traditional synthetic coatings. In particular, Ocak et al. (2009) verified poor capability of polylactic acid for the protection of marble surfaces against the phenomenon of sulphatation in the presence of environments rich in SO_2 (Ocak *et al.*, 2009) The same author investigated the potential of PLA-montmorillonite nanocomposite fillers to protect marbles against air pollution. The study

demonstrated higher impermeability to water and its vapour for the stone substrate treated by the nanomaterial (Ocak *et al.*, 2015).

Furthermore, Giuntoli *et al.* (2012) studied several PLA-based systems for their suitability as protective films on marble against ageing. A general enhancement of the water-repellent behaviour of the substrate was registered thanks to PLA inherent hydrophobicity, while UV radiation led, in some cases, to a detachment between the polymer layer and marble. Finally, the research demonstrated that PLA polymers coming from the L-enantiomer provided higher protection against water compared to those obtained from a racemic mixture of L- and D-lactide (Giuntoli *et al.*, 2012).

In the research proposed in this dissertation, polylactic acid was experimented as a carrier for the cleaning of metal substrates present in indoor historical collections. The goal was to design a gelled system loaded with ethyl lactate, in light of the evidence reported by the previous literature (Punet *et al.*, 2017).

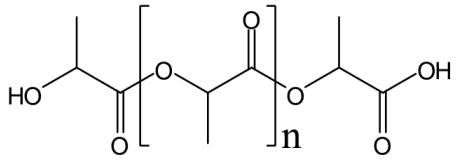

Figure 2.14 Structural formula of polylactic acid (PLA).

2.6.2 Design of the PLA-EL formulation

Previous literature stated the reliability of polylactic acid as scaffolding in tissue engineering (Punet *et al.*, 2017). In particular, the chance of achieving a rigid PLA-based organogel is reported when the polymer is solubilised in ethyl lactate at concentration 4-10% w/v at about 40-50 °C. In general, the ability of ethyl lactate in dissolving PLA is also reported in art conservation literature, showing an undesired swelling of the polymer when cleaning by EL (Kampasakali *et al.*, 2021).

Relying on this encouraging evidence and in light of the polymer greenness, a first constraint was encountered when approaching to the purchase of the specific polymer reported in the research of Punet *et al.*, (2017), namely, poly-L/DL lactic acid 70/30 from Purasorb. Indeed, the sale of this (and similar) products resulted in being extremely sectorial and unrealistic for research out of biomedical engineering and pharmaceutical industry. Clearly, the impossibility of procuring the desired PLA partially compromised the research development and, more in general, needs to be considered as a critical limitation when fostering exploration and exploitation of greener alternatives, such as PLA, in art conversation for a turnover in the CRs activity.

In order to overcome this constraint, multiple PLA alternatives were surveyed, seeking suitable features for the design of a PLA-EL gelled system. The polymers at disposal and their specifications provided by the supplier (Merck) are listed in Table 2.3, together with the denomination (letters from A to D) given for an easier mentioning in the text. The sequence of experiments carried out with PLA are summarised for clarity in Table 2.4.

Table 2.3 Tested polylactic acids and related specifications provided by the supplier (Merck).

	A	**B**	**C**	**D**
Brand name	PLA, Goodfellow	Resomer® R 203 H	Resomer® R 207 S	Resomer® L 206 S
Enantiomer	PLLA	PDLA	PDLA	PLLA
Molecular weight	unknown	18,000-24,000	209,000	unknown
Form	pellets	amorphous	amorphous	granular
Inherent viscosity	unknown	0.25-0.35 dL/g	1.3-1.7 dL/g	0.8-1.2 dL/g
Glass-transition	unknown	Tg 48-52 °C	Tg 53-57 °C	Tg 60-65 °C

All polymers were initially tested following the gelation protocol adopted in the reference paper by Punet *et al.* (2017) (i.e., 4% w/v in ethyl lactate at about 40 °C). The obtained mixtures were rather liquid in the case of polymer B and C, whereas no dissolution was achieved for A and D, not even when increasing the temperature up to 100 °C to promote the reaction. Consequently, product A and D were excluded from further testing and the design of the PLA-EL system focused on the exploitation of polymers B and C investigating higher %w/v concentrations to gain in stiffness.

When testing 20% w/v concentrations, PLA B resulted rather liquid compared to C, therefore the formulation design focused on the latter polymer to have a system easier to handle and potentially better retentive. Interestingly, for both polymers (i.e., B and C) dissolution occurred also when the mixture in ethyl lactate 20% w/v was prepared at room temperature (i.e., 23.8 ±2.4 °C, registered average temperature in the laboratory over one year). Consequently, this method was accepted in line with the Green Chemistry principle "Design for Energy Efficiency" (Anastas and Warner, 1998), not requiring the use of heat and therefore electricity, and providing a solution ready-to-prepare *in situ* for CRs when out of their workshops.

Once selected polymer C, the w/v percentage of the PLA-EL system was further increased up to 30% to avoid dripping effects that would make the formulation hard to handle as well as to apply it on smooth or vertical metallic surfaces. Despite the high content of thickening agent, the PLA-EL formulation at 30% w/v did not yield a rigid gel system, contrary to what was expected from the literature (Punet *et al.*, 2017). Nevertheless, the formulation had the best characteristics achievable among the explored solutions in terms of solvent retention, ease-in-use, and stiffness when manipulated by metallic spatula, therefore it was selected and investigated for metal cleaning. Finally, in order to improve the ease-in-removal after application, Japanese paper (6 g/m², CTS) was assayed to detach the PLA-EL system in a more controlled way.

Table 2.4 Table resuming the tests carried out to design the PLA-EL system. Green and red cells indicate formulations leading or not to PLA dissolution in the set conditions, respectively. The increasing texture of the formulation, when manipulated by a metallic spatula, is represented by an increasing number of "+". The blue cell shows the formulation (i.e., PLA-EL 30% w/v formed at room temperature (i.e., 23.8 ±2.4 °C) (RT) selected as best performing in terms of solution retention, ease in handling, and consistence. Grey cells report tests not carried out.

		PLA type			
Formulation [% w/v in EL]	*Temperature [°C]*	**A**	**B**	**C**	**D**
4%	40	Not dissolved	Dissolved	Dissolved	Not dissolved
	60	Not dissolved	Dissolved	Dissolved	Not dissolved
	80	Not dissolved	Dissolved	Dissolved	Not dissolved
	100	Not dissolved	Dissolved	Dissolved	Not dissolved
20%	60	Not tested	+	++	Not tested
	RT	Not tested	+	++	Not tested
25%	RT	Not tested	Not tested	+++	Not tested
30%	RT	Not tested	Not tested	++++	Not tested

In conclusion, for the synthesis of the PLA-EL system, polylactide acid (PLA) Resomer® R 207 S from Merck was mixed together with the bio-solvent ethyl lactate (≥98%) (EL) from Sigma Aldrich in a concentration 30% w/v. Few seconds of manual stirring with a metallic spatula at room temperature (i.e., 23.8 ±2.4 °C) were sufficient to homogenise the mixture (Figure 2.15). The measured pH in the resulting PLA-EL formulation was acidic (i.e., pH 4) in accordance with the presence of ethyl lactate (Merck, 2024a).

Figure 2.15 Photography of the PLA-EL formulation in a glass petri dish (on white background).

2.7 Characterisation of the formulations

2.7.1 Rheology

The mechanical properties of the formulations loaded with ethyl lactate were investigated via rheology by amplitude sweep analysis. The technique allows to examine the behaviour of viscoelastic systems, such as gels, when subjected to oscillatory shear deformations at gradually increasing strain amplitudes. The test provides information about the formulation nature (i.e., gel-structured or liquid) and mechanical features (i.e., rigidity, malleability, tendency to crack) and was performed for all formulations developed within this doctoral research project, following the previous literature (Carretti *et al.*, 2008; Prati *et al.*, 2019; Yiming *et*

al., 2019). When using amplitude sweep analysis, the stress response of the sample is plotted in a cartesian graph as a function of the shear strain and storage (G') and loss (G") moduli. More in detail, storage and loss moduli provide information about the behaviour of the analysed system according to its elastic and viscous fractions, respectively (Janmey, Georges and Hvidt, 2007; Samorì *et al.*, 2016).

In the case of the PHB-EL and agar-water/EL formulations, the rheometer registered values for the storage modulus G' (i.e., formulation stiffness) approximately an order of magnitude higher than the loss modulus G" (i.e., formulation viscosity) over the linear viscoelastic (LVE) region (Figure 2.16, green and blue plots, respectively). This region is distinguishable by a plateau trend for the storage G' modulus curve, and represents the range of shear strain tested for which the sample structure does not get destroyed. The data collected for PHB-EL and agar-water/EL systems in the LVE region showed that G' > G", which is distinctive for viscoelastic solids characterised by strong interaction forces, leading to describe the two samples as gel-like structured in rheology (Grattoni *et al.*, 2001). When comparing their strengths (i.e., stiffness) over the LVE region, it was manifest that the PHB-based gel had stronger structure than the agar one in light of the recorded G' values presented n Figure 2.16. When examining the limit of the LVE region, named yield point (τ_y) in rheology, the response of the PHB-EL gel displayed a yield point around a strain $\gamma = 0.02\%$, whereas in the case of the agar-water/EL gel the LVE plateau trend was still present over two additional orders of magnitude of shear strain, presenting a yield point at $\gamma = 4\%$. The recorded τ_y values indicated that the agar-water/EL gel was less prone to structural destruction, prior to complete collapse (i.e., G' = G"), compared to the PHB-based one when stimulated in the set conditions. After leaving the LVE region, a gradual drop of the G' curve occurred in the case of the PHB-EL gel until G' = G", stating a non-brittle fracturing form of the sample. On the contrary, the agar-water/EL gel curve dropped sharply closely after τ_y showing a more brittle behaviour in the same interval. For both systems, the rheometer registered a tendency of G" value to raise before the crossover point (i.e., G' = G") that is indicative for micro-cracks not extended throughout the entire material prior to the breakdown of sample structure. Such breakdown moment happens when storage and loss moduli curves cross each other, hence when G' = G". The conjunction point between the two curves is denominated flow point (τ_f) and was calculated at strain $\gamma = 1.5\%$ and $\gamma = 50\%$ for PHB-EL and agar-water/EL gels, respectively (Figure 2.16). The data highlighted that the agar-water/EL gel got entirely ruptured at higher strains than the poly-3-hydroxybutyrate-based system. After the crossover point, the viscous portion prevails on the response behaviour of the examined samples.

In contrast to the previous two formulations, PLA-EL resulted in having values of G" > G' in the LVE region, when analysed by amplitude sweep under the same rheological conditions (Figure 2.16, orange). PLA-EL exhibited a fluid state across the entire deformation range due to the registered relation between storage and loss moduli. Hence it cannot be defined as gel, like the aforementioned formulations, but rather as a viscoelastic liquid under the set measuring conditions. In particular, the value recorded for the storage modulus of PLA-EL in the LVE region (i.e., G' = 850 Pa) was approximately one order of magnitude inferior to the agar-water/EL gel and even two orders when compared to the PHB-EL gel, describing the PLA-EL formulation as weakly structured when related to the other systems. Its viscoelastic linearity is constant along high shear strain values (i.e., mechanical stress), reaching the yield point τ_y (i.e., linearity limit) around a strain $\gamma = 100\%$, which is several orders of magnitude greater than τ_y of PHB-EL (i.e., $\gamma = 0.02\%$) and agar-water/EL (i.e., $\gamma = 4\%$). Finally, because of the fluid nature of the PLA-EL formulation, no flow point τ_f (i.e., G' = G") could be detected in relation to the impossibility of fracturing the sample in the set experimental conditions (Figure 2.16).

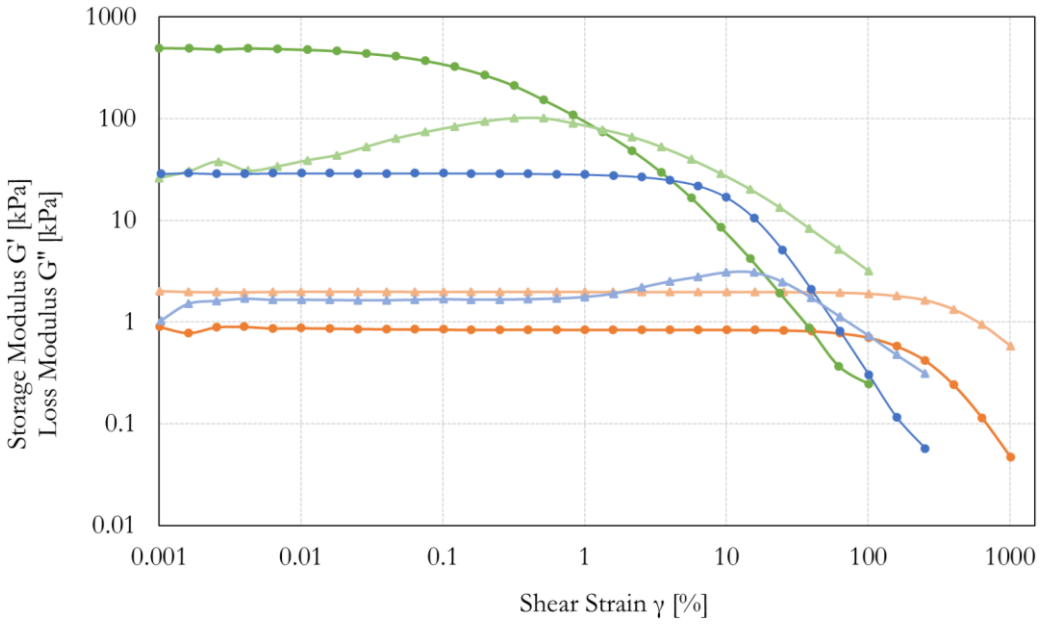

Figure 2.16 Strain dependence of storage modulus G' (circles, darker hue) and loss modulus G" (triangles, lighter hue). The amplitude sweep curves for PHB-EL (green), agar-water/EL (blue), and PLA-EL (orange) systems are plotted.

Table 2.5 Rheological response of the ethyl lactate-based formulations by amplitude sweep analysis.

Formulation	**PHB-EL**	**Agar-water/EL**	**PLA-EL**
LVE region	G' > G"	G' > G"	G" > G'
Definition	viscoelastic solid (gel)	viscoelastic solid (gel)	viscoelastic liquid (fluid)
Yield point (τ_y)	γ = 0.02%	γ = 4%	γ = 100%
Flow point (τ_f)	γ = 1.5%	γ = 50%	absent

As a conclusive evaluation of the rheological properties of the three formulations proposed (Table 2.5), considering the sought use as cleaning systems on metal artefacts, the very poor rheological features of the PLA-EL system show a material that potentially would be hard to handle and apply, and that would leave post-treatment residues, because of the low stiffness and viscous nature. However, PLA-EL can provide high adaptability to the target metal geometry.

On the contrary, the PHB-EL and agar-water/EL gels showed interesting properties such as the stiffness that indicates possible easy handling for operators and potentially no cleaning residues after gel removal. The formulation stiffness might also imply poor adaptability to the probable unevenness of metallic surfaces, especially for the strong structure of the PHB-EL gel. Nevertheless, the rheological behaviour registered for this gel is in line with the previous literature related to this system that was successfully applied in art conservation for the cleaning of paintings supporting an effective exploitation also on metals (Prati *et al.*, 2019).

Similarly, the exploitation of the agar-water/EL gel in metal cleaning seems promising from the mechanical point of view, especially when further compared to a plain agar hydrogel. Indeed, an additional amplitude sweep study was run on a traditional fully water-based version (i.e., agar hydrogel) of the agar system employing the same concentration (i.e., 4% w/v) and the same experimental conditions. The results obtained by rheology are displayed in Figure 2.17 and summarised in Table 2.6. Firstly, in both cases the

instrument measured values of G' > G" in the LVE region, which is characteristic for viscoelastic solids, defining the two systems as gels under the rheological perspective, as expected. However, the analysis detected for the plain agar hydrogel a storage modulus G' value approximately one order of magnitude higher than the value associated to the agar-water/EL gel, highlighting a more accentuated stiffness and strength in the case of the bare hydrogel (Figure 2.17). Differently, the plateau trend for the storage G' modulus curve in the LVE region showed its linearity limit (i.e., yield point) around a strain $\gamma = 0.2\%$ for the plain hydrogel, whereas it reached the yield point at $\gamma = 4\%$ for the agar gel loaded with ethyl lactate. The τ_y values indicated that the system loaded with ethyl lactate was less prone to structural destruction compared to the plain agar 4% hydrogel. Moreover, a more intense raising bump in the G" curve was clearly detected before the crossover point (i.e., G' = G") in the case of the plain agar hydrogel, which was indicative of a higher structural susceptibility to micro-cracks in the system compared to the formulation loaded with ethyl lactate (Figure 2.17). The final material breakdown was occurring at flow points calculated at strain $\gamma = 5.7\%$ for the plain agar hydrogel and $\gamma = 50\%$ for the agar-water/EL counterpart (Figure 2.17). The recorded data highlighted that the structure of the gel with ethyl lactate got entirely destructed at higher strains than the plain hydrogel, demonstrating appealing properties, such as a higher adaptability to the metal surface unevenness and a lower tendency in brittleness hence towards leaving possible post-cleaning residues.

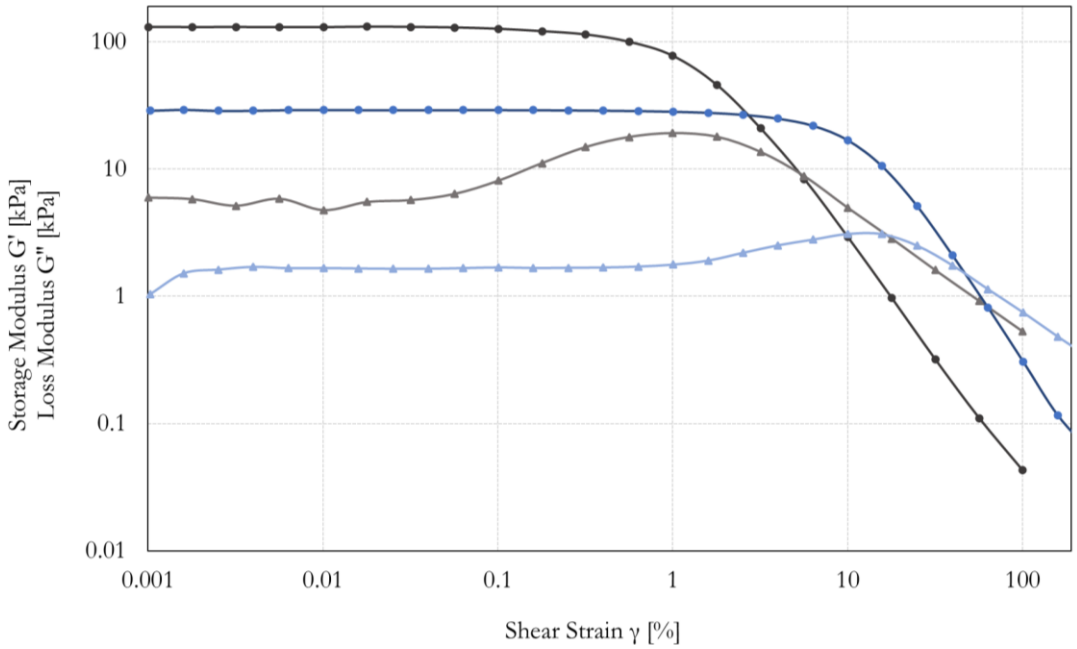

Figure 2.17 Strain dependence of storage modulus G' (circles, darker hue) and loss modulus G" (triangles, lighter hue). The amplitude sweep curves for agar-water/EL 4% w/v and agar-water 4% w/v gels are plotted in blue and black, respectively.

Table 2.6 Rheological response of agar 4% w/v hydrogels loaded (i.e., water/EL 3:1) or not with ethyl lactate (EL) by amplitude sweep analysis.

Formulation	**Agar-water/EL (4% w/v)**	**Agar-water (4% w/v)**
LVE region	G' > G"	G' > G"
Definition	viscoelastic solid (gel)	viscoelastic solid (gel)
Yield point (τ_y)	γ = 4%	γ = 0.2%
Flow point (τ_f)	γ = 50%	γ = 5.7%

2.7.2 Cryo-Scanning electron microscopy (Cryo-SEM)

Cryo-SEM analysis permitted to examine the inner structure of still-moist EL-based systems. Indeed, compared to conventional scanning electron microscopy (SEM), the cryo-technique allows to work on initially still-moist samples that did not lose the original structure caused by a slow evaporation of the liquid fraction retained; on the contrary, the gels are instantly frozen by liquid nitrogen slush, hence preserving their initial structure (Rahbani *et al.*, 2013).

All specimens showed different inner structures (Figure 2.18) and this observation was consistent and deducible from the different behaviours recorded when analysed under the same experimental conditions by rheology.

To the best of the author's knowledge, no previous research was carried out on PHB-based gels by cryo-SEM analysis. In the field of conservation science, a study on the cleaning system PHB-GVL (i.e., gamma-valerolactone GVL) observed the dry gel by means of Scanning Electron Microscopy in low vacuum mode revealing spherical morphology in sample's surface (Samorì *et al.*, 2016). When using cryo-SEM analysis, instead, the inner features of the PHB-EL system could be observed, showing a densely interconnected network under 8000× magnification (Figure 2.18, a). The pores were not equally sized, showing a diagonal aperture measured in the order of 10^{-1} – 10^{-2} μm. Additionally, the cavities were not homogeneously distributed in the gel, probably explaining the high stiffness registered by rheology. At higher magnification (25000×, Figure 2.18, b), the technique could recognise an almost plate-like structure that created rather blocky pores in the PHB-EL formulation.

On the contrary, agar-water/EL and PLA-EL systems showed more circular porosities in their inner sections (Figure 2.18, d and f, respectively). The agar-based formulation was characterised by a sponge-like structure (Figure 2.18, c), in line with the previous literature on agar hydrogels (Rahbani *et al.*, 2013; Ivashchenko, 2022). Differently than in the case of PHB-EL gel, the scaffolding around pores was visible also in areas where cavities are not fully uncovered after sublimation etching, therefore they were plausibly well dispersed in the agar-water/EL gel. The general dimension of agar-system holes was also in accordance with the references (i.e., approximately in the range 10^{-1} - 1 μm), despite not being homogenous all over the sample (Figure 2.18, d) (Rahbani *et al.*, 2013; Ivashchenko, 2022). Compared to a plain agar hydrogel 4% w/v analysed under the same cryo-SEM conditions, the system loaded with ethyl lactate seemed denser in the structure, by the presence of membranes inside the pores that are visually absent in the conventional agar hydrogel (Figure 2.19). This evidence might justify the higher resistance to shear strain compared to simple agar hydrogel recorded by rheological measurements.

Finally, as previously mentioned, the PLA-EL showed circle-shaped inner structures by cryo-SEM observation. In relation to the agar-water/EL system, however, the cavities appeared more spherical, with an aperture diameter of approximately 1-3 μm, and not disposed on a layered scaffolding in the case of PLA-EL (Figure 2.18, e). Possibly, the solvent droplets were englobed in such sponge-like structure of the PLA-EL formulation before performing the sublimation process necessary for the cryo-SEM analysis.

Finally, in the PLA-EL system, the structural cavities resulted in being surrounded by foil-like membranes rather than chained to each other as in the PHB-EL and agar-water/EL structures (Figure 2.18, F).

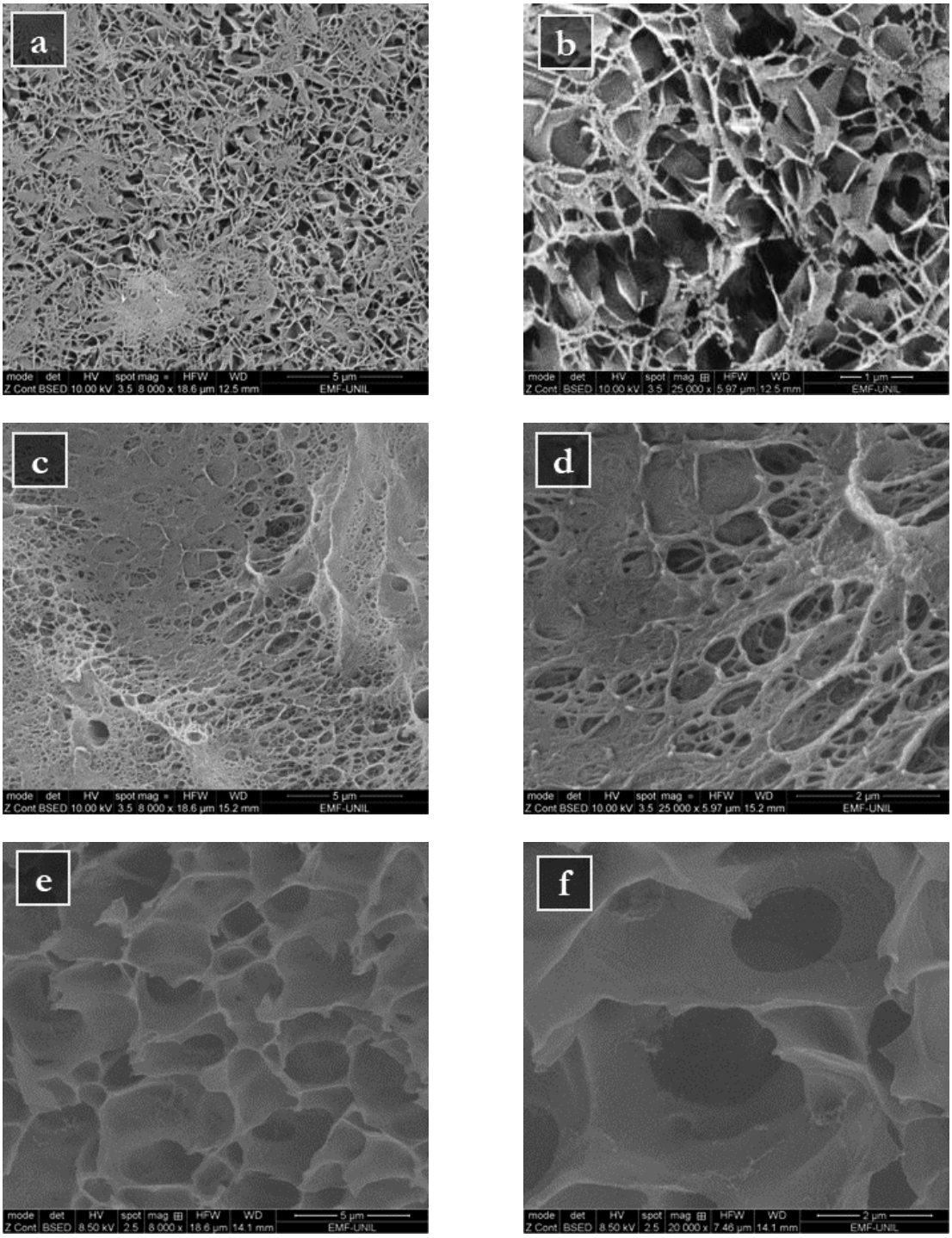

Figure 2.18 Cryo-SEM back-scattered electrons (BSE) images of the inner structure of PHB-EL (a, b), agar-water/EL (c, d), and PLA-EL (e, f) systems after sublimation etching and platinum coating. The scale bar indicates 5 and 2 μm for images on the left and on the right, respectively.

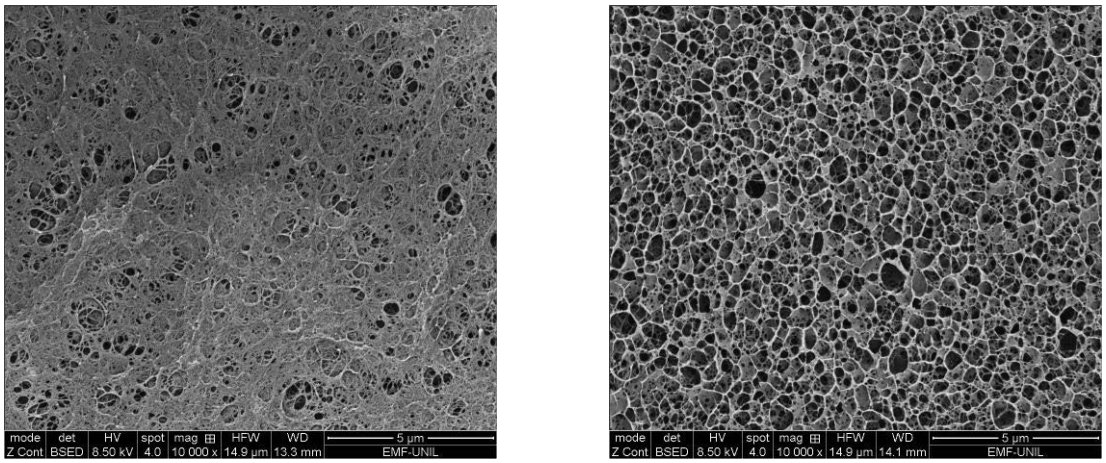

Figure 2.19 Cryo-SEM back-scattered electrons (BSE) images of the inner structure of agar-water/EL (left), and agar-water 4% w/v (right) gels after sublimation etching and platinum coating. The scale bar indicates 5 µm.

2.7.3 Thermogravimetric analysis (TGA)

Ethyl lactate-based systems were analysed by thermogravimetric analysis (TGA) in order to evaluate the evaporation of the liquid phase embedded compared to the sole ethyl lactate solvent or when in solution with deionised water (1:3 v/v, as in the agar-water/EL system), according to the related formulations. The analysis was an isothermal run at 40 °C, hence the registered weight loss could be attributed entirely to the evaporation of the liquid fraction present in the samples, and in none of the cases to the polymers employed in the formulations. Indeed, poly-3-hydroxybutyrate, agar, and polylactic acid are in solid state at the temperature reached during the analysis (i.e., 40 °C) (Leja and Lewandowicz, 2010; McAdam *et al.*, 2020; Giordano, Caruso and Lazzara, 2022). Therefore, the TGA curves displayed in Figure 2.20 were calculated as weight loss percentages considering exclusively samples' liquid fraction in order to correctly compare the obtained results. Additionally, the calculated first derivative of the TGA isothermal curves are shown in SM-Figure 1 to help the reader with the visualisation of mass loss trends (i.e., evaporation rates) over time for each sample.

In general, the thermogravimetric analysis proved that neat ethyl lactate (Figure 2.20, red dashed line) or in solution with deionised water (Figure 2.20, blue dashed line) were always more prone to evaporation compared to the related gelled systems over time in the same set of conditions. Specifically, after 60 minutes of isothermal run, ethyl lactate reached 14% of its initial weight when free, whereas the measured value was twice as large (i.e., 29%) when EL was restrained in the PHB-based gel (Figure 2.20, green solid line) and even about four times as large (i.e., 52% of its initial weight) when restrained in the PLA-EL formulation (Figure 2.20, yellow solid line). A possible explanation to the registered behaviours might come from cryo-SEM analysis. As previously seen, the two systems were characterised by different inner structures. In particular, PLA-EL showed a structure where cavities were surrounded by foil-like membranes, whereas the PHB-EL gel had a rather inter-chained network (Figure 2.18). It might be assumed that the first structure better retained the liquid fraction that was entrapped in the spherical pores observed by cryo-SEM for the PLA-EL system. Potentially, sequential etching by progressive short-time sublimation might be performed on the samples' surface in the cryo-SEM chamber to observe the type and distribution of pores at the surface. This outcome would help to corroborate or reject the possible explanation here provided.

Differently, in the case of the agar-water/EL gel (Figure 2.20, blue solid line), the evaporation rate of the whole liquid fraction (i.e., EL/water 1:3 v/v) was higher than the sole ethyl lactate (Figure 2.20, red dashed line), as shown by the related TGA curve trends. This outcome could be ascribed to the presence of water that is characterised by higher vapour pressure (i.e., 2.34 kPa at 20 °C) (Huang, 2018) than ethyl lactate (i.e.,

0.27 kPa at 20 °C) (Merck, 2024a). When comparing the agar-water/EL 3:1 system to the related free solution (Figure 2.20, blue dashed line), the outcome was in line with previous observations, since the agar system hampered the evaporation of the loaded solution. Indeed, in the case of the free water/EL 3:1 solution, a complete evaporation, hence a weight reaching zero, occurred within 55 minutes of TGA isothermal in the set conditions; on the contrary to the agar system that kept about 10% of solvents starting weight within the 60-minute range of analysis.

In general, the analysis verified that the investigated formulations were able to delay the unwanted loss of active solution in the atmosphere in the explored conditions. However, the values obtained cannot be considered quantitatively as evaporation rates, being affected by factors such as the different geometry of samples (i.e., thickness, surface) and possible partial evaporation of the retained solution in preparation of the analysis. Nonetheless, they provided information about the efficient retention of the active solutions, reducing the quantities to be used in a potential cleaning intervention.

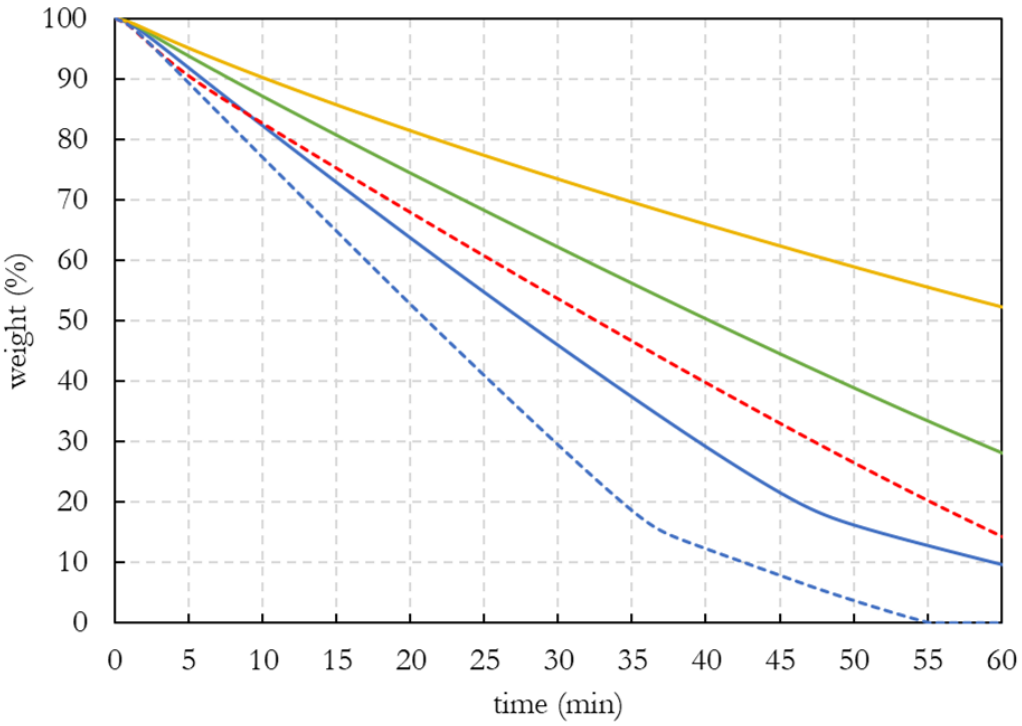

Figure 2.20 Isothermal TGA scan at 40 °C in nitrogen atmosphere comparing the weight loss of neat EL (red, dashed) and water/EL (3:1) solution (blue, dashed) to PHB-EL (green, solid), PLA-EL (yellow, solid), and agar-water/EL (blue, solid) formulations. The showed TGA curves were calculated considering samples' liquid fraction solely.

2.8 Cleaning assessment and evaluation

2.8.1 Cleaning protocol

The cleaning performance of the formulated solvent-based solutions was evaluated and compared by modulation of application time and renewals. Based on the literature related to the exploitation of the PHB-EL gel for the cleaning of paintings, short-time applications were effective for the removal of aged organic coatings (Volpi, 2017). Therefore, PHB-EL, agar-water/EL, and PLA-EL were similarly assayed on mock-up triplicates by intervals of 5 and 10 minutes, with or without reiteration (i.e., 5-min × 2 and 10-min × 2).

Four areas of 2 × 2 cm² were defined on the 5 × 5 cm² mock-up surface, and the cleaning protocol was set in triplicates as reported graphically in Figure 2.21.

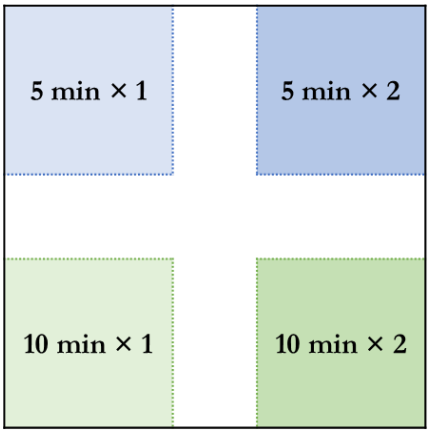

Figure 2.21 Graphical representation of 2 × 2 cm² mock-up areas cleaned by PHB-EL, agar-water/EL, and PLA-EL formulations. Application of 5 (top, blue) and 10 minutes (bottom, green), without (left, lighter hue) and with reiteration (right, darker hue).

The method of application and removal of the tested formulations needed to be adapted to the texture of the systems when manipulated by spatula (Figure 2.22), as summarised in Table 2.7.

Specifically, PHB-EL and agar-water/EL's stiffness and rigidity allowed to cut 2 × 2 cm² size gels for the cleaning assessment. Furthermore, the gels could be prepared achieving a thickness of around 2 mm in order to have higher reproducibility within each series of gel formulations. This thickness was employed according to preliminary studies performed on the PHB-EL gel that verified a good adaptability of the gel to metal substrates, while obtaining an easy-to-handle and non-brittle system when detached after treatment (i.e., solvent evaporation) (Hammond, 2021). The cut gels were then applied onto the established mock-up areas and gently pressed with the spatula to maximise the contact and avoid air bubbles between the gel and the metal sheet.

On the contrary, due to its rather liquid nature, the PLA-EL formulation was tested defining the area to be treated by cutting some Japanese paper (6 g/m², CTS) of around 2 × 2 cm² size. Once the paper was arranged on the mock-up test areas, a layer of PLA-EL was applied by metallic spatula. However, unlike the previous two formulations, the thickness of the PLA-EL layer could not be ascertained to be even among all applications (i.e., same amount of formulation in function of treated areas), causing a rather approximative comparison of the cleaning results a priori. Similarly, assaying to apply a precise aliquot of PLA-EL formulation each time with the use of a micropipette, the viscosity of the system did not allow to employ this application method. Possibly, the use of a double-side open mould, masking the mock-up areas while retaining the formulation within each test area, could have helped to use always the same quantity of PLA-EL within the experiment for better reproducibility.

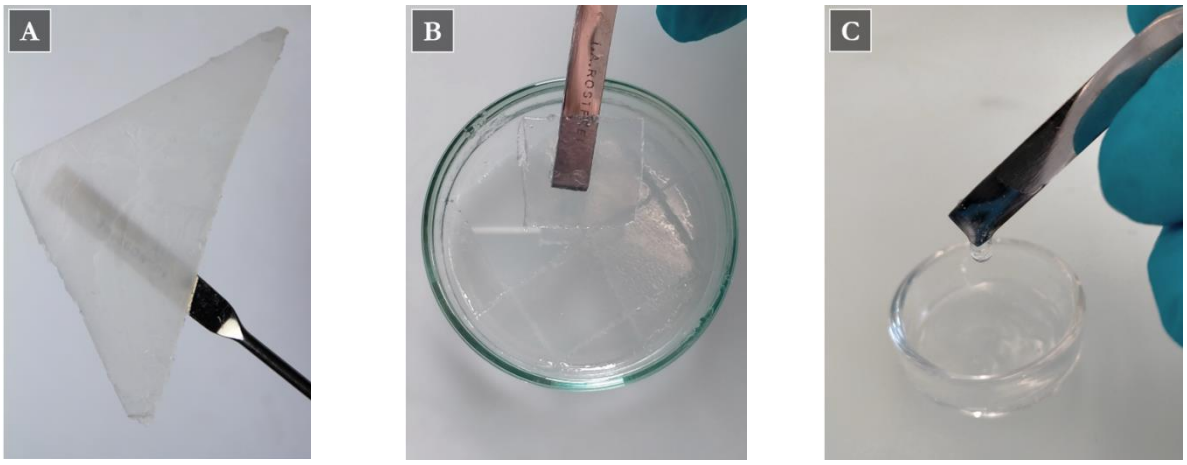

Figure 2.22 Appearance of PHB-EL (A), agar-water/EL (B), and PLA-EL (C) formulations when manipulated with a metallic spatula before application.

After application, the PHB-EL and agar-water/EL gels were detached in one move by a spatula, and the mock-up surface was cleaned by gentle dry cotton-swabbing to remove possible gel residues and swollen organic coatings. In the case of the PLA-EL solution, firstly Japanese paper and overlaying PLA-EL system were detached from mock-ups by tweezer. Secondly, potential swollen coating and formulation residues were taken away by alternate dry and wet (i.e., deionised water) cotton swabbing. Indeed, the wet cleaning assured the removal of the PLA-based system, being a highly hydrophobic polymer (Nurazzi *et al.*, 2022).

Table 2.7 Protocols employed for the application and removal of the different formulations.

Formulation	*Application method*	*Post-application protocol*
PHB-EL	Cut and application by metallic spatula	Dry cotton swabbing
Agar-water/EL	Cut and application by metallic spatula	Dry cotton swabbing
PLA-EL	1. Collection by metallic spatula 2. Application on Japanese paper	1. Removal of Japanese paper and overlaying PLA-EL by tweezers 2. Alternate dry and wet (deionised water) cotton swabbing

In the described cleaning protocol, the ethyl lactate concentration, which was the active agent in this work, was not identical among the three formulations, since each polymer required a different percentage of the organic solvent. Similarly, as discussed, a precise thickness of formulation employed could not be maintained in the case of the PLA-EL solution, which required, in addition, a different post-application protocol for its removal. All these factors led to an approximative qualitative interpretation of the data when comparing the investigated methods. It did not allow to compare objectively the three formulations among themselves, but rather focussing the discussion on the cleaning yields by comparison to application times (i.e., 5 and 10 minutes) and reiterations (i.e., none or one) employed in the frame of the individual formulations.

2.8.2 Multi-analytical protocol for the assessment of coating removal

2.8.2.1 Visual appearance

The cleaning yielded on the mock-ups via the three formulations proposed was visually evident already by the naked eye. Marked differences could be appreciated not only when comparing the various outcomes within the same formulation, but also when examining overall the post-cleaning appearance of the metallic sheets despite being differently treated, as displayed in Figure 2.23.

As a broad initial observation, as expected from the literature, ethyl lactate could dissolve both organic coatings, Paraloid® B72 and Zaponlack. The cleaning differences observed are therefore linked to the delivery system employed.

Focusing the attention on the spatial precision, it was possible to notice that for both sets of mock-ups (i.e., Fe PB72 and Brass ZL), the perimeter of the areas (2 x 2 cm^2) treated by PHB-EL gel was well defined and the edges were neat. Lower was the definition achieved when employing the PLA-EL system in spite of the use of Japanese paper that could have helped to better retain the formulation during the application. Extremely poor surface definition was observed on areas cleaned by the agar-water/EL gel, especially when operating on Zaponlack removal. Additionally, when detaching the agar-water/EL system, the nitrocellulose lacquer looked merely swollen by the treatment and scarcely removed from the metallic sheet only thanks to the closing step of dry cotton swabbing that provided a mechanical action.

For all formulations, the short-time (i.e., 5 minutes) cleaning by single application appeared visually not sufficient for the complete removal of both types of organic coatings. In this case, a swelling effect was rather noticed on the metallic sheets, with consequential redeposition and spread of the lacquers due to the mechanical action provoked by dry cotton swabbing during the final clearing step.

The agar-water/EL gel applied on steel mock-ups provoked a manifest staining effect on the metallic substrate, especially when the gel was renewed for a second application (i.e., 5- and 10-minute × 2). In light of the preliminary test outcome (Paragraph 2.3.1) and the absence of such marks when employing PLA- and PHB-based systems, the stains should be ascribed to a negative interaction possibly occurring between steel sheets and water present in the agar-based systems. Finally, the agar-water/EL gel did not provide a visually successful removal of the nitrocellulose lacquer when applied on brass mock-ups. The little cleaning obtained was rather gained by the mechanical action of the cotton buds employed after treatment on the partially swollen lacquer.

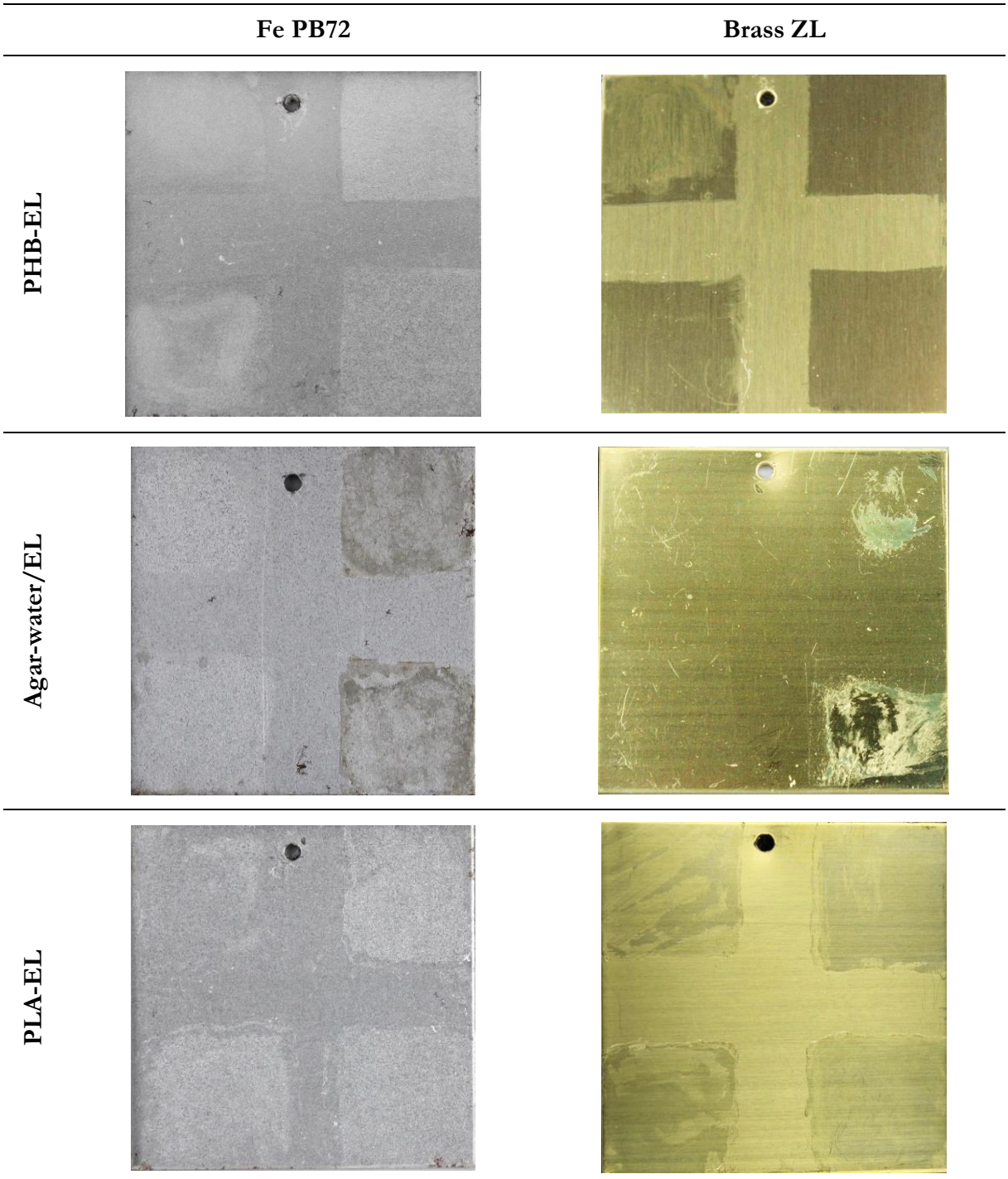

Figure 2.23 5 × 5 cm² mock-ups made of mild steel coated with Paraloid® B72 (column "Fe PB72") and brass coated with Zaponlack (column "Brass ZL") after cleaning. Resulting 2 × 2 cm² mock-up areas cleaned by PHB-EL (first row), agar-water/EL (second row), and PLA-EL (third row) formulations. Cleaning by 5- (mock-up top half) and 10-minute (mock-up top half) applications, without (mock-up left side) and with reiteration (mock-up right side), was performed as graphically drafted in Figure 2.21.

2.8.2.2 Optical microscopy

Microscopic observation under UV light could easily emphasise mock-up surface features after cleaning, thanks to the coatings' fluorescence under the experimental conditions.

In general, as displayed in Figure 2.24 for brass mock-ups coated with Zaponlack, PHB-EL appeared the best performing formulation. Very sporadic blue spots (i.e., ZL fluorescence) can be identified on the treated areas when a single application was employed, and none when the gel was renewed in a second application. On the contrary, in the case of brass zones cleaned by PLA-EL formulation, a persistent blueish hue is visually recognisable in all areas except for the cleaning of 10 minutes with reiteration, suggesting a residual presence of Zaponlack as supposed by naked eye inspection. Finally, areas cleaned by agar-water/EL exhibited clearly a blue coloration linked to the substantial presence of the nitrocellulose lacquer after treatment. In the case of the cleaning carried out with two applications of 10 minutes each, a partial removal of ZL coating could be observed, as also reported by overall visual appearance of the treated area. Remarkably, no perceptible alteration of the metallic surface was evidenced for none of the applications when observing the cleaned brass mock-ups in bright field.

Concerning the steel series (Figure 2.25), overall the metallic sheets appeared more affected by coating residues after cleaning, possibly due to the more pronounced surface roughness compared to brass. This aspect was further investigated by examining bare iron coupons in the same microscopy conditions, and blue shades were observed on the surface flaws despite the complete absence of a coating (SM-Figure 2). This effect of reflection of a blue component in the light employed for microscopy observation would result in potentially jeopardising the actual identification of Paraloid® B72 residues. To by-pass this limit, Fourier-transform infrared spectroscopy (FTIR) was employed to monitor and detect the presence of residual coating on the treated areas, as discussed in the next paragraphs (page 105).

In general, PHB-EL and PLA-EL systems resulted as most effective for the removal of Paraloid® B72 from mild steel sheets. Especially when employed by two consecutive applications, the perception of coating residues under UV light was lower and the cleaning yielded was more homogeneous compared to one single application. In the case of agar-water/EL, bright blue residues or more generally a blueish hue was still visible in all cleaned areas, ascribable to swollen PB72 that got broadly redeposited on the metallic sheet after treatment. Moreover, moving from the goal of coating removal, it was distinctly manifest the alteration occurred on the steel substrate after agar-water/EL application when observing the areas cleaned by two gel applications in bright field (Figure 2.26), as already visible with the naked eye.

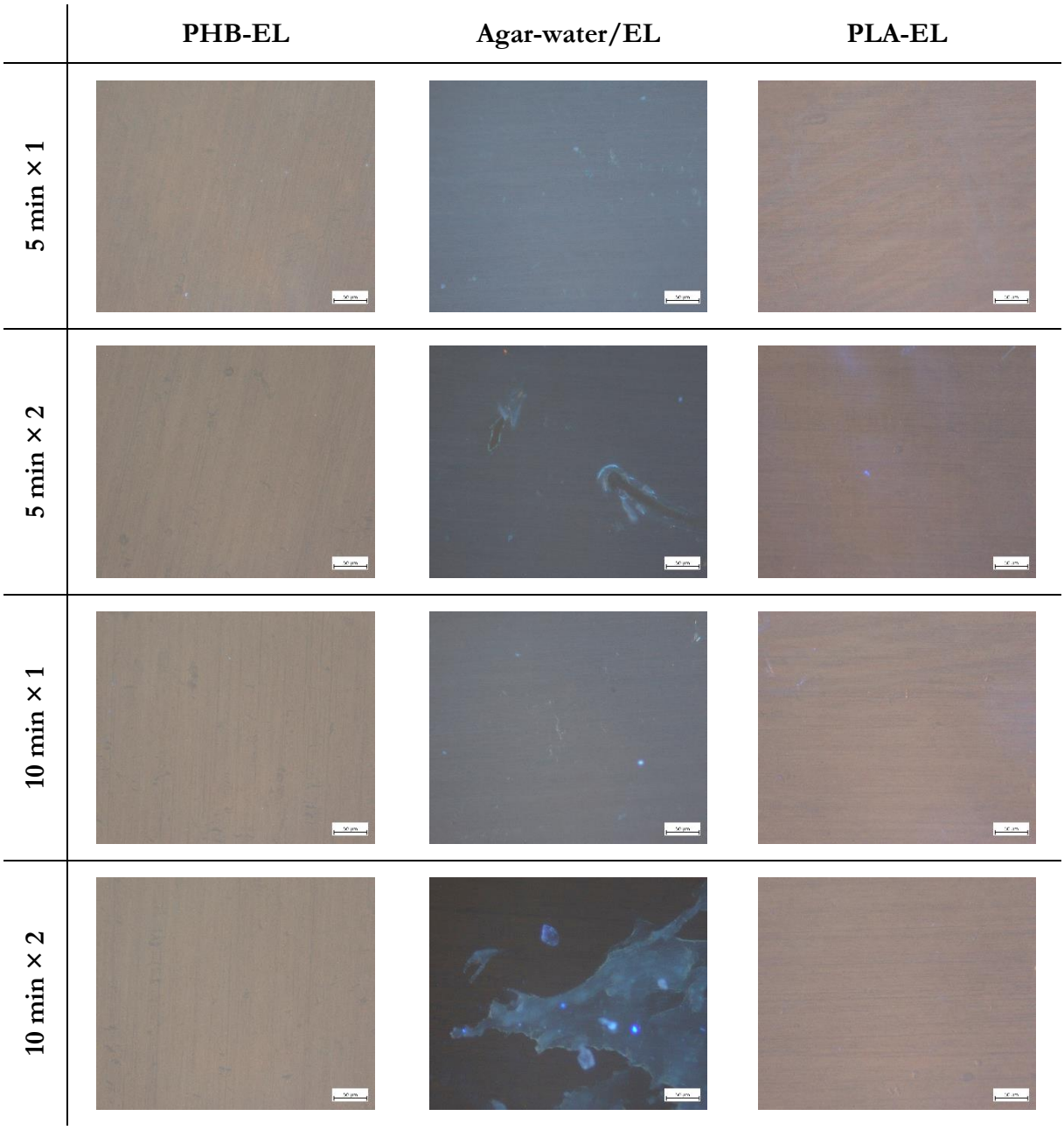

Figure 2.24 Optical microscope images acquired under UV light of brass mock-ups coated with Zaponlack after cleaning. The figure reports the cleaning outcomes for PHB-EL (left column), agar-water/EL (central column), and PLA-EL (right column) formulations applied 5 and 10 minutes without (first and third rows, respectively) and with renewal (second and fourth rows, respectively). The scale bar indicates 50 μm.

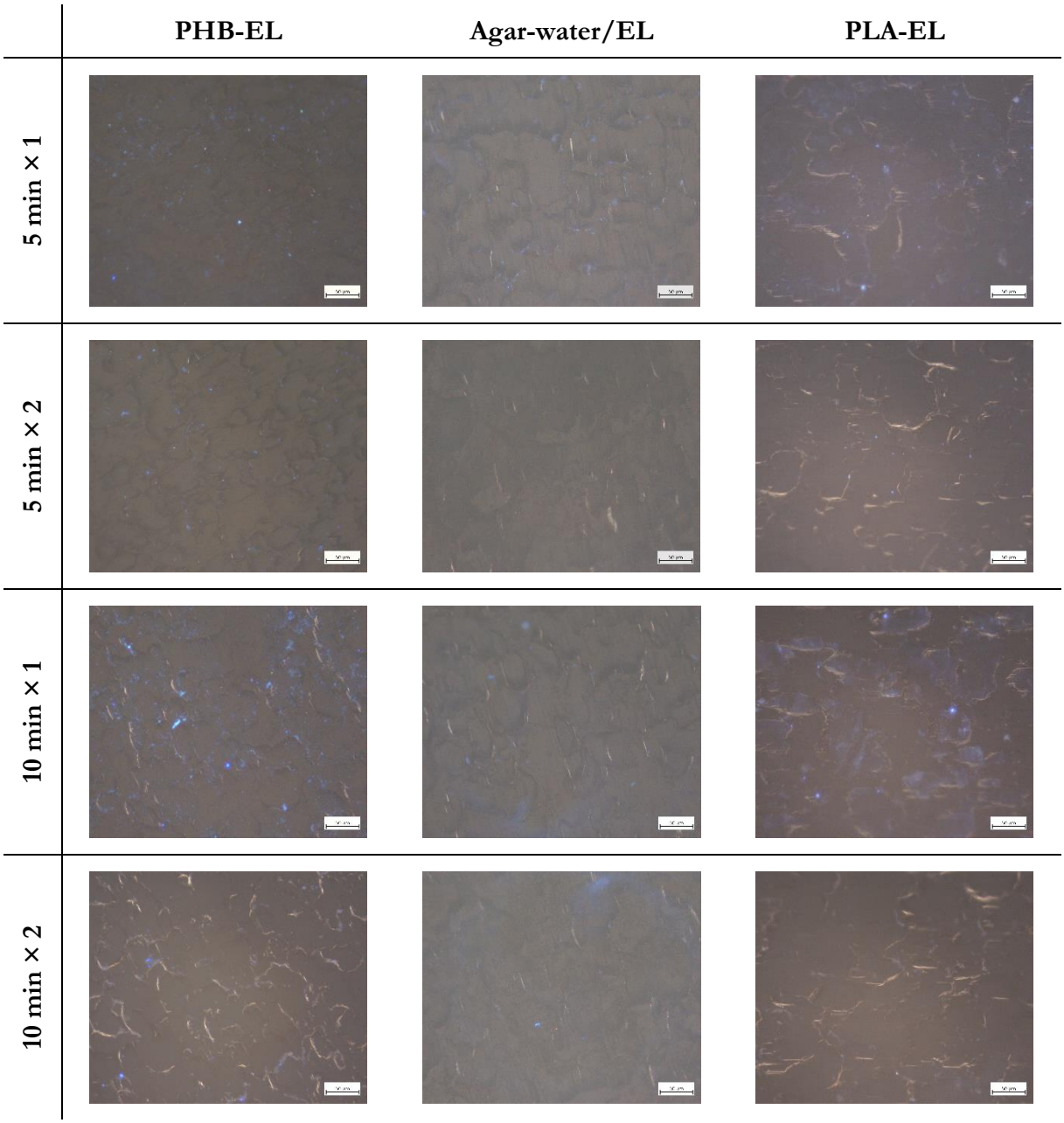

Figure 2.25 Optical microscope images acquired under UV light of mild steel mock-ups coated with Paraloid® B72 after cleaning. The figure reports the cleaning outcomes for PHB-EL (left column), agar-water/EL (central column), and PLA-EL (right column) formulations applied 5 and 10 minutes without (first and third rows, respectively) and with renewal (second and fourth rows, respectively). The scale bar indicates 50 μm.

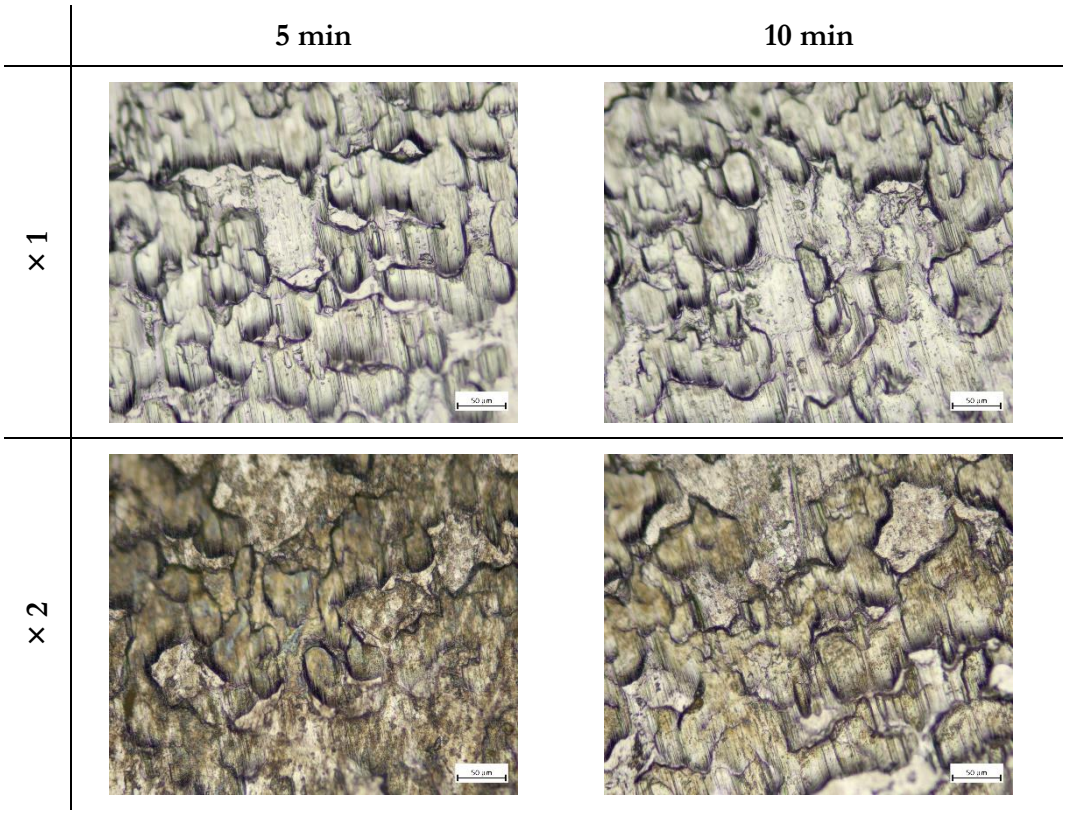

Figure 2.26 Optical microscope images in bright field of mild steel mock-ups coated with Paraloid® B72 after cleaning with agar-water/EL. The figure displays the cleaning outcomes for the applications of 5 (left column) and 10 minutes (right column), without (first row) and with gel renewal (second row). The scale bar indicates 50 μm.

2.8.2.3 Colorimetry

Colorimetric data were collected on the mock-up triplicates, before and after each cleaning, to compare the outcomes obtained with the same formulation but with different application times and renewals. The evaluation was addressed without comparing the post-cleaning data to bare mild steel and brass coupons because the mock-ups employed in this study were coated and artificially aged for 3 months (page 229). The process had inevitably affected also the metallic substrates – despite being protected by the coatings – making the comparison altered. Therefore, the analysis was focused on the detection of possible surface changes or alterations, noticeable by colorimetry, derived from the use of the proposed formulations, namely, PHB-EL, agar-water/EL, and PLA-EL systems.

Due to the large number of data and the multiple variables to be taken into account (i.e., formulation renewal, application time), statistics was applied to colorimetric information. At first, analysis of variance (ANOVA) was applied to colorimetric data to consider exclusively statistically relevant factors. Afterwards, the Tukey's HSD (i.e., Honestly Significant Difference) test was applied to the resulting data to make a pairwise comparison. This approach was selected in accordance with the literature, and will be reproposed throughout the manuscript for the evaluation of colorimetric data, since L*, a*, and b* are independent variables (Ragain and Johnston, 2000; Lo Monaco *et al.*, 2011; Kim *et al.*, 2013).

Working on data collected from mild steel mock-ups coated with Paraloid® B72, Table 2.8 reports the variation of colorimetric coordinates comparing before and after cleaning, whereas raw data are available in SM-Table 2. The Tukey's HSD test verified a significant discrimination for L*, a*, and b* values, when relating data obtained after single or double application of agar-water/EL gel on the test mock-ups ($p < 0.001$). Indeed, as also visually evident by optical microscopy, coupon areas treated by the agar-based system

got altered when cleaned by double application, losing brightness (i.e., -3.11 (±1.50) for 5-minute and -0.30 (±0.57) for 10-minute protocol, with gel reiteration) while acquiring yellow-reddish shades typical of iron corrosion species (Table 2.8). In the case of the PHB-EL gel, the Tukey's HSD test verified significant difference ($p < 0.001$) among L* and a* values when comparing one or two gel applications employing the same application time (i.e., 5 or 10 minutes). This outcome would prove that the cleaning performance, obtained by the PHB-EL system on mild steel mock-up coated with PB72, was rather related to gel renewal than application time. Finally, L* values were considered relevant when comparing 5-minute protocol with or without PLA-EL renewal on mild steel mock-ups presenting PB72 ($p < 0.05$).

The same statistical method (i.e., ANOVA and Tukey's HSD test) was applied also to colorimetric data collected from brass mock-ups coated with Zaponlack after cleaning, which are reported in SM-Table 3 (raw data) and Table 2.9 (comparison after-before). The analysis demonstrated that both L* and a* coordinates could not be considered as discriminant variables ($p > 0.05$) for the distinction of colorimetric results obtained for all tested formulations (i.e., PHB-EL, agar-water/EL, and PLA-EL). Only b* values resulted statistically relevant to distinguish the cleaning performance of the agar-water/EL gel when applied twice for 10 minutes compared to all other cleaning interventions by the same gel ($p < 0.05$). This result would evidence that only when operating by long and repeated application, the agar-water/EL system could provide an appreciable cleaning effect on the nitrocellulose coating, as also observed by optical microscopy. The colorimetric coordinate b* was recognised as a significant variable for the distinction of data related to PLA-EL when comparing measurements obtained for one or two applications of 10-minutes ($p < 0.05$). Finally, no colorimetric coordinates could discriminate the cleaning data related to PHB-EL gel from a statistical perspective.

Table 2.8 Variation of CIELab coordinate values of mild steel mock-ups coated with Paraloid® B72, comparing before and after cleaning. ΔL*, Δa* Δb*, and related ΔE* SCI values are reported along with their standard deviation into brackets.

	Cleaning time	Number of applications	ΔL*	Δa*	Δb*	ΔE*
PHB-EL	5 min	1	1.77 (±0.25)	0.21 (±0.06)	0.83 (±0.11)	1.96 (±0.23)
		2	5.60 (±0.48)	0.02 (±0.02)	0.72 (±0.10)	5.64 (±0.48)
	10 min	1	0.82 (±0.67)	0.29 (±0.05)	1.24 (±0.06)	1.52 (±0.36)
		2	6.74 (±0.48)	-0.01 (±0.01)	0.66 (±0.03)	6.77 (±0.48)
Agar-water/EL	5 min	1	8.17 (±0.20)	-0.04 (±0.02)	0.83 (±0.00)	8.21 (±0.20)
		2	-3.11 (±1.50)	0.54 (±0.01)	5.63 (±0.23)	6.45 (±0.75)
	10 min	1	7.72 (±0.39)	-0.01 (±0.01)	0.99 (±0.01)	7.78 (±0.39)
		2	-0.30 (±0.57)	0.57 (±0.08)	5.07 (±0.64)	5.12 (±0.64)
PLA-EL	5 min	1	3.71 (±1.92)	-0.03 (±0.04)	0.29 (±0.34)	3.73 (±1.91)
		2	8.99 (±0.52)	0.01 (±0.01)	1.06 (±0.16)	9.05 (±0.51)
	10 min	1	6.21 (±0.73)	-0.02 (±0.02)	0.51 (±0.06)	6.23 (±0.72)
		2	7.22 (±0.61)	0.08 (±0.02)	1.46 (±0.13)	7.37 (±0.60)

Table 2.9 Variation of CIELab coordinate values of brass mock-ups coated with Zaponlack, comparing before and after cleaning. ΔL*, Δa* Δb*, and related ΔE* SCI values are reported along with their standard deviation into brackets.

	Cleaning time	Number of applications	ΔL*	Δa*	Δb*	ΔE*
PHB-EL	5 min	1	-5.20 (±2.39)	1.26 (±0.20)	2.25 (±0.67)	5.80 (±2.16)
		2	-2.78 (±0.97)	1.59 (±0.20)	4.42 (±0.94)	5.46 (±0.91)
	10 min	1	-4.28 (±0.76)	2.16 (±0.13)	6.85 (±1.34)	8.36 (±1.16)
		2	-1.43 (±2.31)	1.32 (±0.11)	3.58 (±1.19)	4.07 (±1.32)
Agar-water/EL	5 min	1	-0.27 (±0.64)	0.04 (±0.08)	-0.96 (±0.21)	1.00 (±0.27)
		2	1.38 (±0.93)	0.57 (±0.64)	-0.35 (±0.31)	1.53 (±0.87)
	10 min	1	2.66 (±0.10)	-0.23 (±0.06)	0.21 (±0.24)	2.68 (±0.10)
		2	0.83 (±1.41)	0.84 (±0.44)	2.66 (±1.62)	2.91 (±1.54)
PLA-EL	5 min	1	-0.93 (±0.34)	0.91 (±0.15)	2.02 (±0.22)	2.40 (±0.23)
		2	2.06 (±0.08)	0.96 (±0.23)	2.48 (±0.10)	3.36 (±0.11)
	10 min	1	0.00 (±0.66)	1.44 (±0.30)	5.03 (±0.29)	5.24 (±0.30)
		2	0.45 (±0.14)	1.13 (±0.25)	1.80 (±0.14)	**2.8** ±0.18)

2.8.2.4 Eddy current measurements

Measurements by Eddy current were performed to evaluate the thickness of the organic coatings (i.e., Paraloid® B72 and Zaponlack) residually present on metal coupons (i.e., mild steel and brass, respectively) after cleaning.

In general, the method ascertained the reduction of the coatings' thickness after application, as shown in Table 2.10 for mild steel mock-ups, coated with Paraloid® B72, and in Table 2.11 for brass mock-ups, coated with Zaponlack. However, the technique did not provide relevant information to discriminate the performance obtained by the several formulations (i.e., PHB-EL, agar-water/EL, and PLA-EL) and time/reiterations explored in the research.

In the case of the removal of Paraloid® B72 from mild steel coupons, indeed, no significant separation of outcomes was obtained screening of the collected data by Tukey's HSD test. The only exception was in the case of PLA-EL applied once for 5 or 10 minutes ($p < 0.05$). When considering data related to the cleaning obtained by agar-water/EL gel, the Eddy current device registered a decrease in the initial coating thickness, followed by an increment of the thickness in mock-up areas cleaned by 5 and 10 minutes with double gel application (Table 2.10). Potentially, this outcome could have been linked to the alteration of the metal substrate by formation of corrosion phases, as suggested by optical microscopy (Figure 2.26). However, statistical analysis did not ascertain a significant difference among the measurements obtained for areas treated by agar-water/EL gel.

A similar scenario was obtained when observing Eddy current data collected from brass mock-ups coated with Zaponlack (Table 2.11). No relevant separation of data linked to the cleaning by PHB-EL gel was verified by Tukey's HSD test. A relevant discrimination was proven by statistical analysis only for the measurements registered on mock-ups treated by agar-water/EL gel by single or double 10-minute application and by PLA-EL system applied once for 5 minutes vs twice for 10 minutes. However, after cleaning by PHB-EL and PLA-EL systems, the values recorded were mostly negative in relation to the

calibration performed on a bare brass coupon with same dimensions (50 × 50 × 1 mm^3), as required by the measuring device (Table 2.11). On one side, when employing the PHB-EL gel, the obtained values and related standard deviations were still in a range of acceptance if compared to the instrumental error (i.e., ±0.7 μm + 1% of measured value). On the other side, this consideration was not valid when considering brass areas cleaned by PLA-EL formulation.

The unexpected response of the device for brass mock-ups and the poor distinction among the several times and application reiterations employed with each system (i.e., PHB-EL, agar-water/EL, and PLA-EL) would suggest that the Eddy current measurements did not provide helpful information to monitor the cleaning performance. Fourier-transform infrared spectroscopy was therefore applied to analyse cleaned mock-ups, attempting to track some trends supported by statistical analysis (i.e., PCA) (page 105).

Table 2.10 Average Paraloid® B72 layer thickness (μm) measured by Eddy current on coated mild steel mock-ups before and during the cleaning protocol addressed by PHB-EL, agar-water/EL, and PLA-EL systems, respectively. Values are correlated with their standard deviation.

Formulation	Application Time	Number of gels	Coating thickness (μm)
PHB-EL	0 minutes	0	1.91 (± 0.68)
	5 minutes	1	0.64 (±0.41)
		2	0.12 (± 0.41)
	10 minutes	1	0.32 (±0.46)
		2	0.02 (± 0.28)
Agar-water/EL	0 minutes	0	2.07 (± 0.44)
	5 minutes	1	0.60 (± 0.68)
		2	1.05 (± 0.59)
	10 minutes	1	0.62 (± 0.54)
		2	0.70 (± 0.95)
PLA-EL	0 minutes	0	2.32 (± 0.71)
	5 minutes	1	1.19 (±1.16)
		2	0.48 (± 0.85)
	10 minutes	1	0.13 (±0.60)
		2	-0.01 (± 0.77)

Table 2.11 Average Zaponlack layer thickness (μm) measured by Eddy current on coated brass mock-ups before and during the cleaning protocol addressed by PHB-EL, agar-water/EL, and PLA-EL systems, respectively Values are correlated with their standard deviation.

Formulation	Application Time	Number of gels	Coating thickness (μm)
PHB-EL	0 minutes	0	2.26 (±0.31)
	5 minutes	1	-0.05 (±0.23)
		2	-0.22 (±0.20)
	10 minutes	1	-0.20 (±0.28)
		2	-0.21 (±0.29)
Agar-water/EL	0 minutes	0	2.73 (±0.30)
	5 minutes	1	2.59 (±0.45)
		2	0.99 (±1.20)
	10 minutes	1	1.70 (±0.54)
		2	0.83 (±2.25)
PLA-EL	0 minutes	0	2.33 (±0.64)
	5 minutes	1	0.13 (±0.31)
		2	-0.81 (±0.33)
	10 minutes	1	-0.90 (±0.55)
		2	-1.14 (±0.29)

2.8.2.5 X-Ray Fluorescence (XRF) spectroscopy

Elemental analysis by X-ray fluorescence (XRF) spectroscopy was carried out on the three EL-loaded formulations before and after cleaning application for both steel and brass mock-ups. The study was aimed to reveal any potential presence of Fe, Cu, or Zn following the interaction between the formulations and the metallic sheets. The detection of such elements would be considered a weakness when intervening selectively on the removal of organic protectives, since no action on the metallic substrate is desired.

The XRF analysis did not highlight any relevant difference between pre- and post-treatment on the formulations except for the agar-water/EL samples after application on steel mock-up coated with Paraloid® B72. Figure 2.27 displays the XRF spectrum collected from the gel after one application of 10 minutes, where peaks detected at approximately 6.4 and 7 keV correspond to the Kα1 and Kα2 lines characteristic for iron. The presence of iron was a peculiar case for agar-water/EL on the steel mock-ups and highlighted a negative interaction occurring between gel and substrate, as already evidenced in the result discussion so far. In the same XRF spectrum, it is possible to notice a signal at approximately 3.7 keV ascribable to a contamination linked to calcium, and finally a triplet of signals recorded in the spectral region above 16 keV, which are characteristic for the instrument X-ray tube anode in molybdenum.

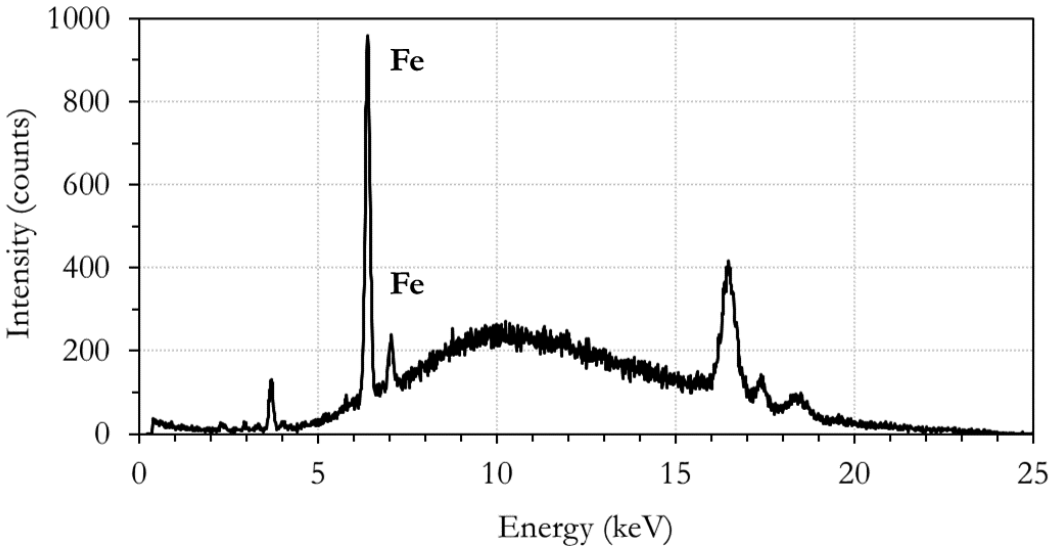

Figure 2.27 XRF spectrum of agar-water/EL after one application of 10 minutes on steel mock-up coated with Paraloid® B72. Signals related to iron are labelled "Fe".

2.8.2.6 Fourier-transform infrared (FTIR) spectroscopy - Formulations

Initially, reference FTIR spectra were collected for all formulations before and after application on the mock-ups in order to verify the successful cleaning action of the proposed systems by Fourier-transform infrared (FTIR) spectroscopy performed in ATR mode. In particular, the solvent-based formulations were let dry in order to eliminate any unwanted spectral information related to solvents originally present in the systems (i.e., ethyl lactate and water, according to the examined formulation).

The reference FTIR spectrum for dry PHB-EL gel was in high accordance with the literature for poly-3-hydroxybutyrate (Danis *et al.*, 2015; Wei, McDonald and Stark, 2015; Kang and Yun, 2022) and it is presented in Figure 2.28. The most diagnostic bands for the dry PHB-EL system are listed and attributed in Table 2.12, based on the interpretation provided by the previous literature (Danis *et al.*, 2015; Wei, McDonald and Stark, 2015; Kang and Yun, 2022). The acquired spectrum was necessary for the interpretation of the data collected from PHB-EL gels after cleaning application on test mock-ups with the purpose to ascertain the ability of the system to dissolve, and especially, retain the coating to be removed.

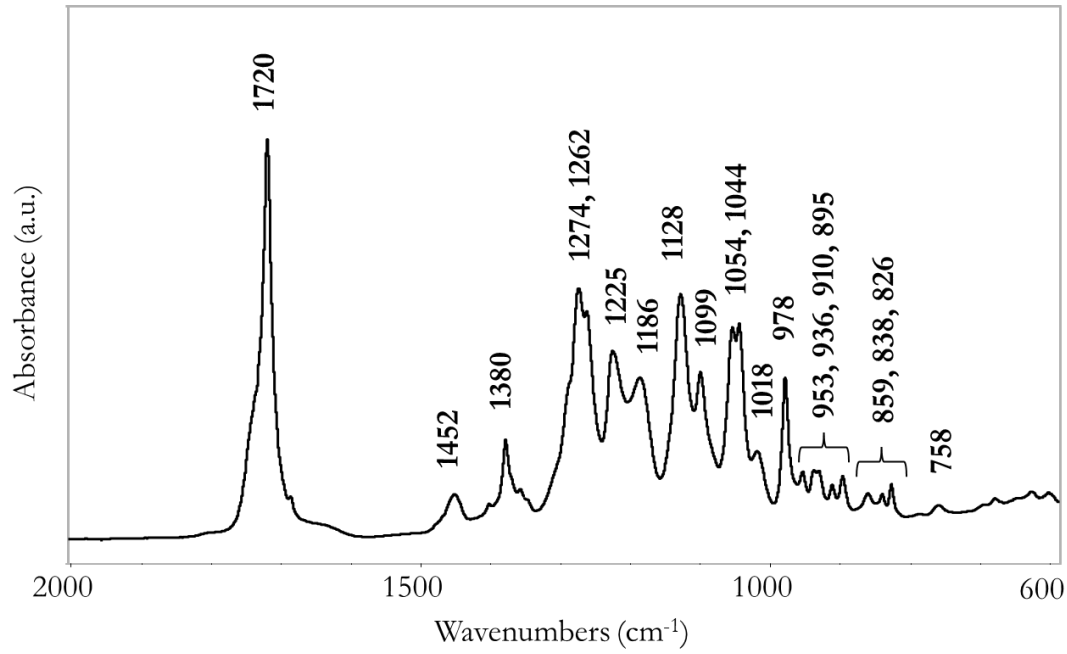

Figure 2.28 ATR-FTIR spectrum of dry and non-used PHB-EL gel. The wavenumbers of peaks diagnostic for the gel are reported above the spectrum.

Wavenumber		Assignment
1720	vs	ν(C-O)
1452	w	δ(CH_3), δ(CH_2)
1380	m	δ(C-H), δ(CH_3)
1274	s	ν(C-O-C), δ(CH_2)
1225	m	ν(C-O-C), δ(CH_2)
1186	m	ν(C-O-C)
1128	s	ν(C-O-C)
1054	s	ν(C-O-C)
978	s	δ(CH_2)

vs = very strong, s = strong, m = medium, w = weak signal; ν = stretching, δ= bending. All values are expressed in cm^{-1}.

Table 2.12 Characteristic FTIR signals detected for dry PHB-EL gel (Danis *et al.*, 2015; Wei, McDonald and Stark, 2015; Kang and Yun, 2022).

Therefore, FTIR spectroscopy was performed in ATR mode on the surface of PHB-EL gels after being in contact (i.e., 5 minutes) with the coated metal mock-ups (i.e., mild steel and brass) to verify the potential absorbance of the swollen coatings (i.e., Paraloid® B72 and Zaponlack, respectively) in the cleaning system.

Paraloid® B72 was not detected analysing the PHB-EL gel after one application of 5 minutes on mild steel mock-ups (i.e., coated with PB72), even after letting the gel dry to avoid the unwanted spectral information related to ethyl lactate. Therefore, used PHB-EL gels were submitted to extraction by acetone (≥99.5%, Sigma Aldrich) to solubilise potential deposits of the acrylic coating entrapped in the system. Analysis by means of FTIR spectroscopy on the collected extraction residue provided the successful identification of Paraloid® B72 when compared to the reference spectrum of the material, as reported in Figure 2.29. Despite the overlapping with FTIR bands diagnostic also for poly-3-hydroxybutyrate, the extraction residue was characterised by the typical signals for Paraloid® B72, as identifiable by the band at about 1720 cm^{-1}, corresponding to C=O stretching vibration, and similar patterns in the fingerprint regions between 1480-

1350 cm^{-1} and 1300-900 cm^{-1} that are linked respectively to C-H bending and C–O stretching vibrations (Derrick, Stulik and Landry, 2000).

On the other hand, when performing FTIR analysis directly on the dry PHB-EL gel used in one 5-minute application on coated (i.e., ZL) brass coupons, Zaponlack could be detected due to the absorption band at about 1644 cm^{-1} (i.e., asymmetric NO_2 stretching vibration) characteristic for nitrocellulose lacquers (Brock *et al.*, 2018). As shown in Figure 2.30, the signal did not overlap with any spectral features related to the PHB-matrix, thus ascertaining the presence of the lacquer on the gelled system after cleaning application.

Collected FTIR data demonstrated that the PHB-EL formulation could tackle the organic coatings already with a short-time application (i.e., 5 minutes) and was able to absorb both swollen Paraloid® B72 and Zaponlack, detaching from the corresponding mock-ups (i.e., mild steel and brass, respectively). This result was considered a desired feature that would limit or even exclude the need of post-cleaning actions (e.g., cotton swabbing using a solvent) to entirely remove the undesired materials.

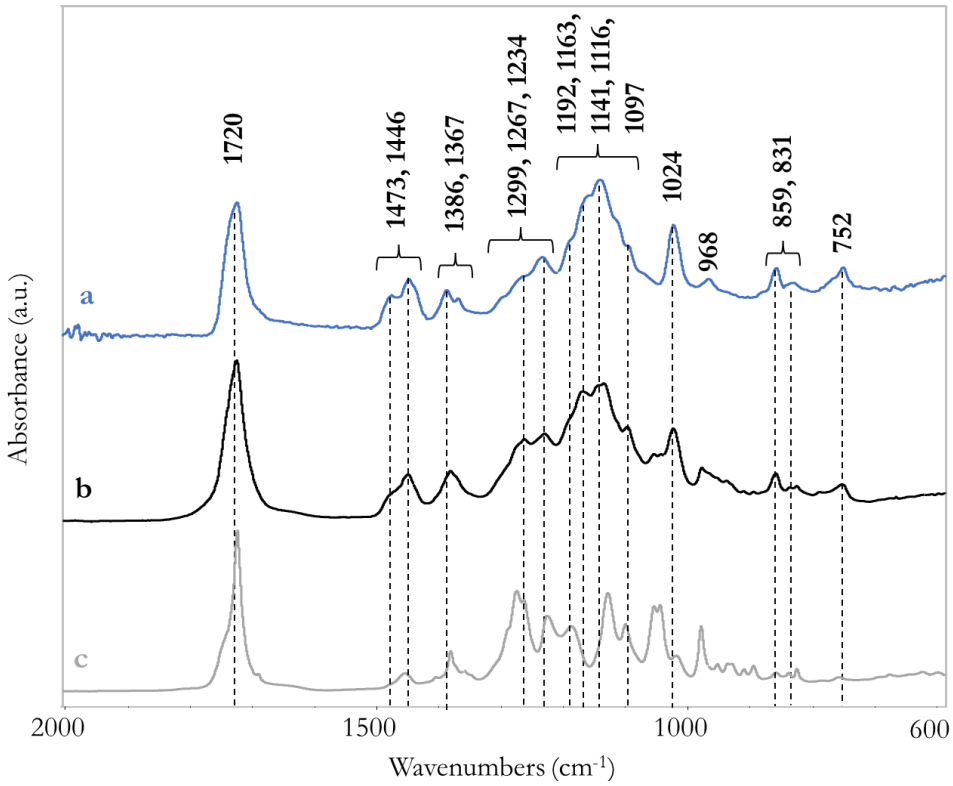

Figure 2.29 ATR-FTIR spectra of Paraloid® B72 powder (a), extraction residue from PHB-EL gel after one application of 5 minutes on a mild steel mock-up coated with Paraloid® B72 (b), and dry non-used PHB-EL gel (c). IR bands related to Paraloid® B72 (a) also detected for the extraction residue (b) are highlighted by dashed lines and related wavenumbers are reported.

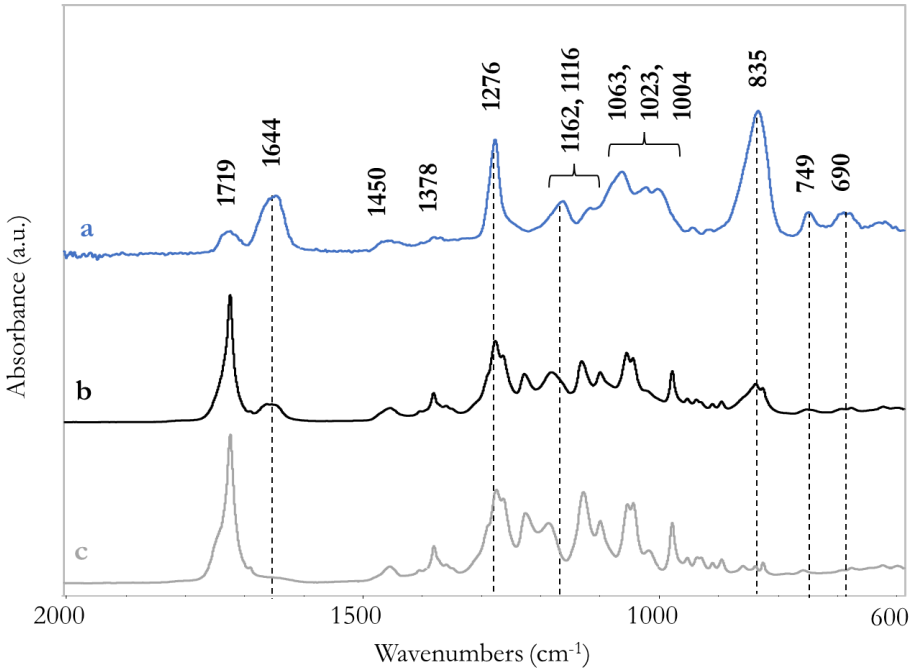

Figure 2.30 ATR-FTIR spectra of Zaponlack (a), PHB-EL gel after one application of 5 minutes on a brass mock-up coated with Zaponlack (b), and dry non-used PHB-EL gel (c). IR bands related to Zaponlack (a) also detected for the gel after cleaning application (b) are highlighted by dashed lines and related wavenumbers are reported.

Moving to the outcome obtained for the agar-water/EL gel, at first a reference spectrum for the non-used and dry system was acquired by Fourier-transform infrared spectroscopy in ATR mode. The collected spectrum is displayed in Figure 2.31 and corresponded well to spectra reported in the literature for agar powder and derived gels (Table 2.13) (Gómez-Ordóñez and Rupérez, 2011; Zamora-Mora *et al.*, 2014; Yarnpakdee, Benjakul and Kingwascharapong, 2015). Yet, a surprising additional signal was detected for the agar-water/EL system at about 1727 cm^{-1}. This vibration is diagnostic for C=O stretching modes that could not be related to ethyl lactate, since the analysis was carried out on dry gel samples. On the contrary, the IR vibration was possibly attributed to the presence of alginic acid in the commercial agar powder (AgarArt, CTS), which is normally used by CRs as in this research study (Gómez-Ordóñez and Rupérez, 2011). Alginic acid is a derivative of brown seaweeds that can act as thickening agent, therefore it could be possibly present as an additive in the AgarArt product. Furthermore, this bio-sourced polymer has cross-linking properties towards metal cations, such as iron(III) (Massana Roquero *et al.*, 2022). This evidence may further explain the interaction between agar-water/EL gels and mild steel substrates, resulting in an anaesthetic and unsought alteration of the treated metals (Figure 2.26). Additional assessments may be foreseen using pure agar and not a commercial product normally employed by CRs to investigate this phenomenon.

For both cleaning applications, namely on mild steel mock-ups coated with Paraloid® B72 and brass coupons coated with Zaponlack, Fourier-transform infrared spectroscopy performed in ATR mode on used agar-water/EL gels did not yield a successful identification of the organic coatings. The investigation was repeated for all applications times explored in this research (i.e., 5 and 10 minutes with single or double cleaning application) submitting the used gels to extraction by acetone (≥99.5%, Sigma Aldrich) to solubilise potential deposits of the coatings. Nonetheless, FTIR analysis could not identify none of the organic coatings and only spectral noise was recorded.

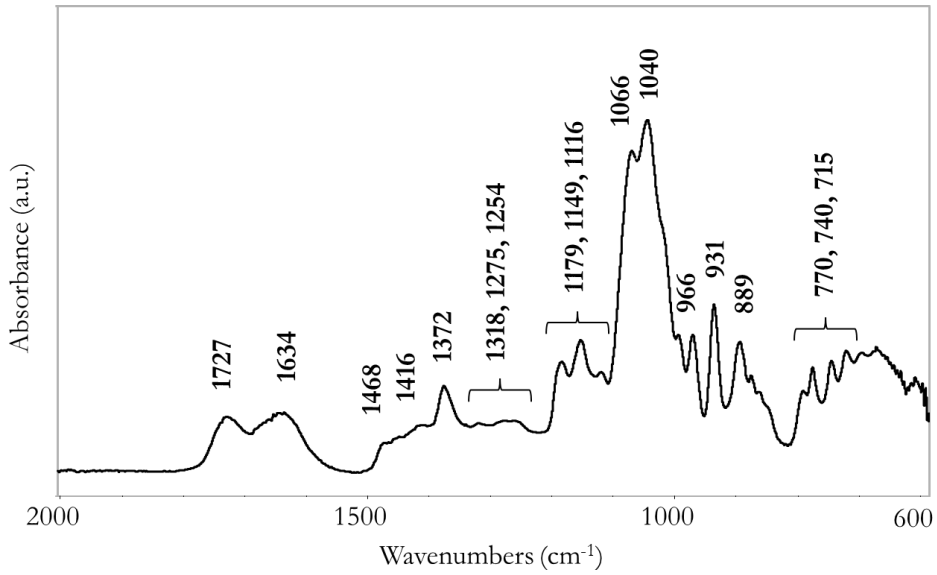

Figure 2.31 ATR-FTIR spectrum of dry and non-used agar-water/EL gel. The wavenumbers of peaks diagnostic for the gel are reported above the spectrum.

Wavenumber		Assignment
1727	m	ν(C=O)
1634	m	ν(C=O) [amide I]
1372	m	δ(C-C)
1149	m	ν(C-O)
1040	vs	ν(C-C), δ(C-O)
931	m	ν(C-O-C) [3,6-anhydro-galactose]
889	m	δ(C-H)

vs = very strong, m = medium signal; ν = stretching, δ= bending. All values are expressed in cm^{-1}.

Table 2.13 Characteristic FTIR signals detected for dry agar-water/EL gel (Gómez-Ordóñez and Rupérez, 2011; Zamora-Mora *et al.*, 2014; Yarnpakdee, Benjakul and Kingwascharapong, 2015).

Finally, the dry PLA-EL formulation was analysed by ATR-FTIR spectroscopy, and the resulting spectrum is presented in Figure 2.32. The employment of ethyl lactate in the formulation did not alter the polymer when comparing the FTIR spectral pattern of PLA-EL to polylactic acid (Tudorachi, Lipsa and Mustata, 2012; Mistretta *et al.*, 2019). A good matching could be ascertained with the reference literature for this polymer and signal assignment for the PLA-EL system is proposed in Table 2.14 according to previous publications (Tudorachi, Lipsa and Mustata, 2012; Mistretta *et al.*, 2019).

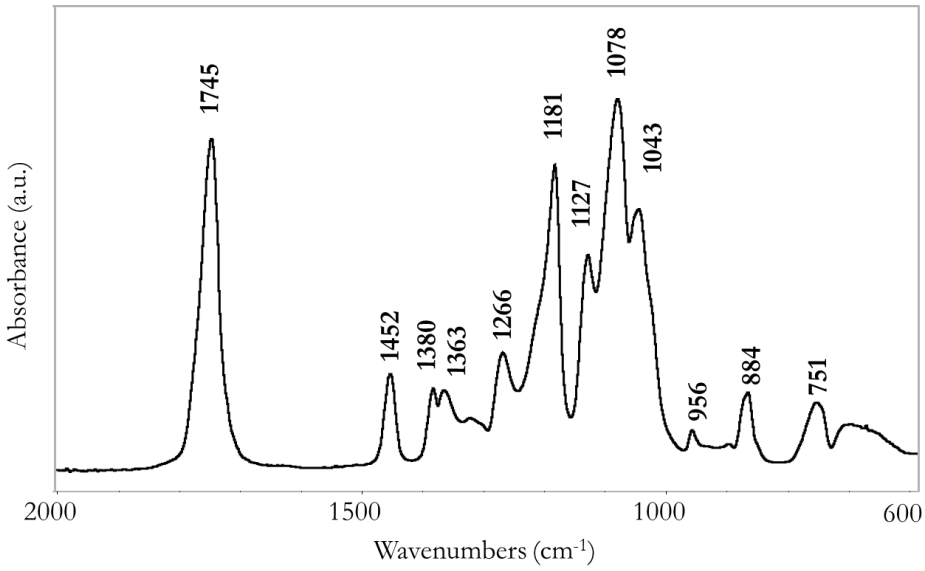

Figure 2.32 ATR-FTIR spectrum of dry and non-used PLA-EL system. The wavenumbers of peaks diagnostic for the formulation are reported above the spectrum.

Wavenumber		Assignment
1745	vs	δ(C=O)
1452	m	δ(CH_3)
1380	m	δ(CH_3)
1266	m	δ(CH_2)
1181	vs	ν(C-O)
1127	s	ν(C-O)
1078	vs	ν(C-O)
884	m	δ(C-H)

vs = very strong, s = strong, m = medium signal; ν = stretching, δ= bending. All values are expressed in cm^{-1}.

Table 2.14 Characteristic FTIR signals detected for dry PLA-EL system (Tudorachi, Lipsa and Mustata, 2012; Mistretta *et al.*, 2019).

The analysis performed on dry PLA-EL after application on mild steel mock-ups coated with Paraloid® B72 did not yield the identification of the coating on the surface of the cleaning system due to the predominant FTIR features of the polymer (SM-Figure 3). The process of extraction by polar solvents (e.g., acetone in the previous cases here presented) at room temperature (i.e., 23.8 ±2.4 °C) could not be performed in the case of the PLA-EL system since the polymer would result equally dissolved as Paraloid® B72.

On the other hand, Zaponlack was successfully identified on the surface of used PLA-EL system (i.e., 5-minute application on brass coated mock-ups) after getting dry (Figure 2.33). In particular, the presence of the nitrocellulose lacquer was confirmed by the IR peaks at about 1644, 1276, and 835 cm^{-1} all linked to NO_2 stretching vibrations that could be ascribed to Zaponlack, retained after cleaning application, on the PLA-EL system (Brock *et al.*, 2018).

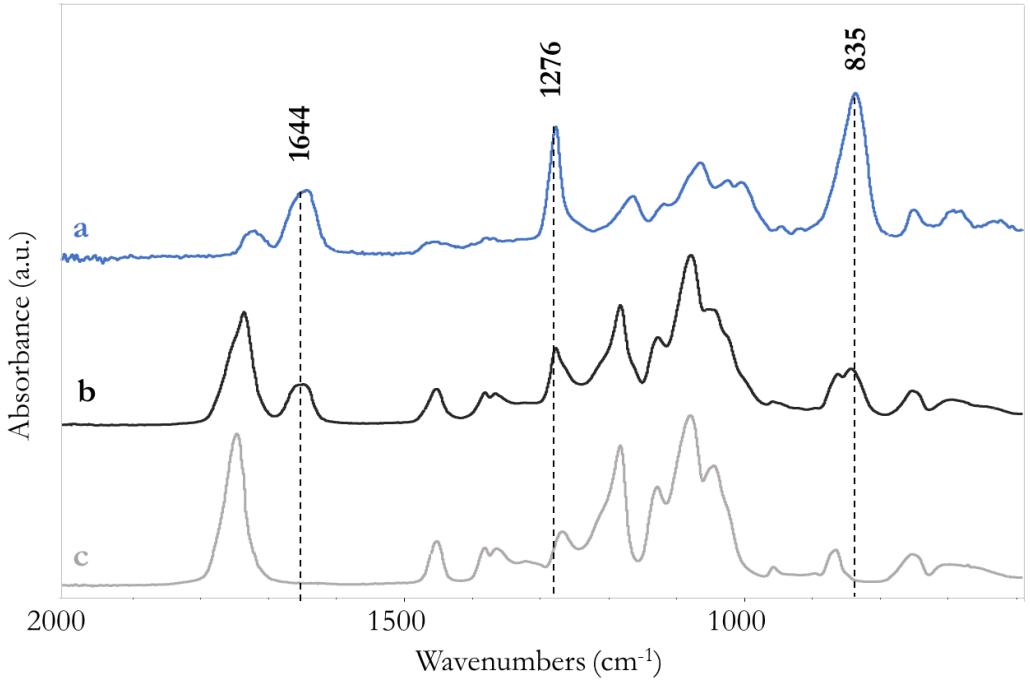

Figure 2.33 ATR-FTIR spectra of Zaponlack (a), PLA-EL system after one application of 5 minutes on a brass mock-up coated with Zaponlack (b), and dry non-used PLA-EL system (c). IR bands related to Zaponlack (a) also detected for the formulation after cleaning application (b) are highlighted by dashed lines and related wavenumbers are reported.

In conclusion, FTIR analysis performed on the proposed bio-based cleaning systems demonstrated the ability of the PHB-EL formulation to absorb both swollen Paraloid® B72 and Zaponlack, detaching them already when working with a short-time cleaning intervention (i.e., 5 minutes). In the case of the PLA-EL system, only the presence of Zaponlack could be tracked on the formulation after cleaning, whereas Paraloid® B72 spectral features were possibly overlapping the FTIR spectrum of the polymer not allowing to obtain informative outcomes. However, the ability of the PLA-EL formulation to retain the swollen Zaponlack might be ascribed also to the Japanese paper employed for its application on mock-ups. Finally, the agar-water/EL gel did not demonstrate a positive ability in entrapping swollen coatings in the gelled matrix during the cleaning application. This evidence might be linked to the hydrophobicity of the organic coatings to be removed (i.e., used also as water-repellent films for protection) in the presence of water in the agar-based system.

2.8.2.7 Fourier-transform infrared (FTIR) spectroscopy – Mock-ups

Finally, FTIR spectroscopy in reflectance mode was performed on mock-up replicates to monitor the cleaning effect achieved by the several times and reiteration tested by the use of PHB-EL, agar-water/El, and PLA-EL systems. Due to the large number of spectra to be compared, FTIR data were elaborated by Principal Component Analysis (PCA) for a better readability of the information collected at each step of cleaning. Additionally, FTIR reference spectra collected from bare metal sheets (i.e., mild steel and brass) were considered in the analysis as references to assess the cleaning level. Finally, the spectral ranges were reduced to 2000-1000 cm^{-1} and 1800-1200 cm^{-1}, when working respectively on mild steel and brass related data, in order to focus the interpretation on the regions of interest to detect the residual presence of Paraloid® B72 and Zaponlack, respectively.

The results found for the series of mild steel mock-ups coated with Paraloid® B72 are presented in Figure 2.34 (related raw data are displayed in SM-Figure 4), which displays the score (a) and loading (b) plots

obtained by PCA when considering PC1 versus PC2. Looking at the loading plot, both principal components were characterised by a range of wavenumbers between 1750-1680 cm^{-1}, which were read as negative contributions of these variables on the loadings plot for PC1 and PC2, respectively. This set of wavenumbers could be ascribed to C=O stretching vibration at about 1727 cm^{-1} diagnostic for Paraloid® B72 in this study (Derrick, Stulik and Landry, 2000). Low discrimination among data could be read in the related score plot (Figure 2.34, a). Indeed, the PCA result would suggest a residual presence of the PB72 coating especially for mock-ups cleaned by one application of 5 minutes employing the PLA-EL formulation (i.e., grey dots in the score plot). In all the other cases, the spectral features obtained by FTIR spectroscopy were similar, gathering together the data of differently cleaned mock-up areas. In particular, these data were positioned close to those collected for bare mild steel coupons (i.e., light purple dots) in the score plot, evidencing a satisfactory cleaning of the treated mock-up areas.

Moving to the series of brass mock-ups coated with Zaponlack, Figure 2.35 shows the score (a) and loading (b) plots resulting from PCA applied to FTIR data (related raw spectra are displayed in SM-Figure 5), when considering principal components 1 and 2. In this case, PC1 was mostly characterised by the sets of wavenumbers between 1620 and 1680 cm^{-1} and between 1260 and 1300 cm^{-1} that positively affected the related loadings along the axis. The mentioned spectral regions were relevant in this study because contained the diagnostic FTIR signals for NO_2 stretching vibrations, which were linked to the presence of Zaponlack (Fernández de la Ossa *et al.*, 2011; Brock *et al.*, 2018). On the other hand, in the loading plot, PC2 was characterised by a separation along the axis given principally by wavenumbers in the range 1730-1780 cm^{-1}, read as a positive contribution of these variables on the loadings plot (Figure 2.35). This range of variables (i.e., wavenumbers) could be attributed to C=O bending vibrations related to the presence of polylactic acid in this study, according to the literature (Tudorachi, Lipsa and Mustata, 2012; Mistretta *et al.*, 2019).

Following the interpretation of the loading plot, it was possible to visualise on the score plot that the majority of FTIR data collected from brass-ZL mock-up sectors, cleaned by agar-water/EL gel, were characterised by a residual presence of nitrocellulose lacquer (Figure 2.35, a). In parallel, several FTIR spectra collected from mock-ups cleaned by means of the PLA-EL system were affected by the residual undesired presence of the bio-polymer used for the cleaning system (i.e., grey and dark purple dots in the score plot) (Figure 2.35, a). Finally, most of the FTIR data related to mock-up areas cleaned by PHB-EL were grouping together with the bare untreated references, yet without demonstrating a significant discrimination among the several timing and repetitions explored (Figure 2.35, a).

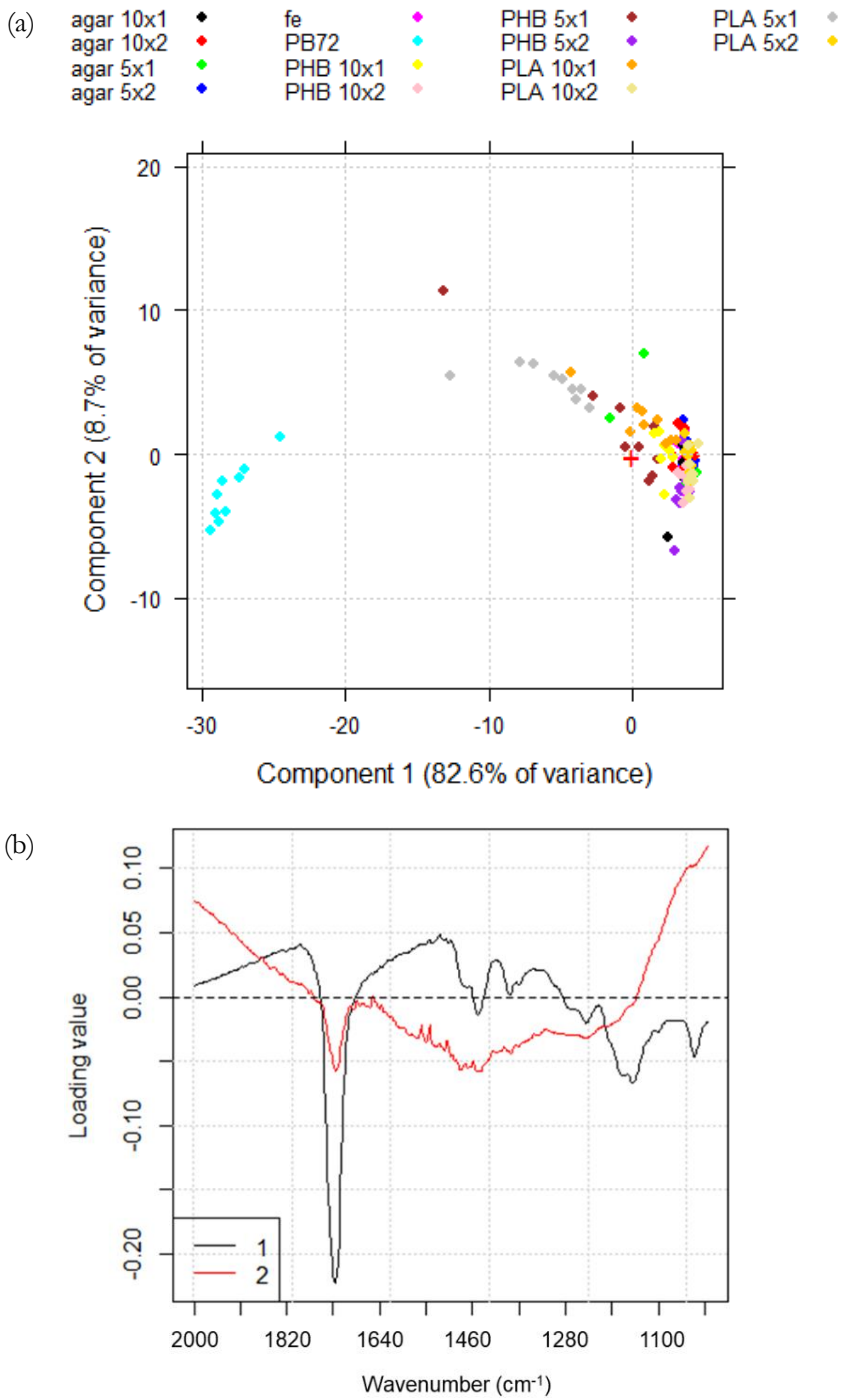

Figure 2.34 Score (a) and loading (b) plots obtained from PCA applied to FTIR spectra recorded on bare mild steel mock-ups (fe) and mild steel mock-ups, coated with Paraloid® B72, before (PB72) and after cleaning with agar-water/EL (agar), PHB-EL (PHB), and PLA-EL (PLA) systems by one (×1) or two (×2) applications of 5 or 10 minutes each, as reported in the key above the score plot in alpha-numeric order (a). (b) Related PC1 (black) and PC2 (red) loading plot.

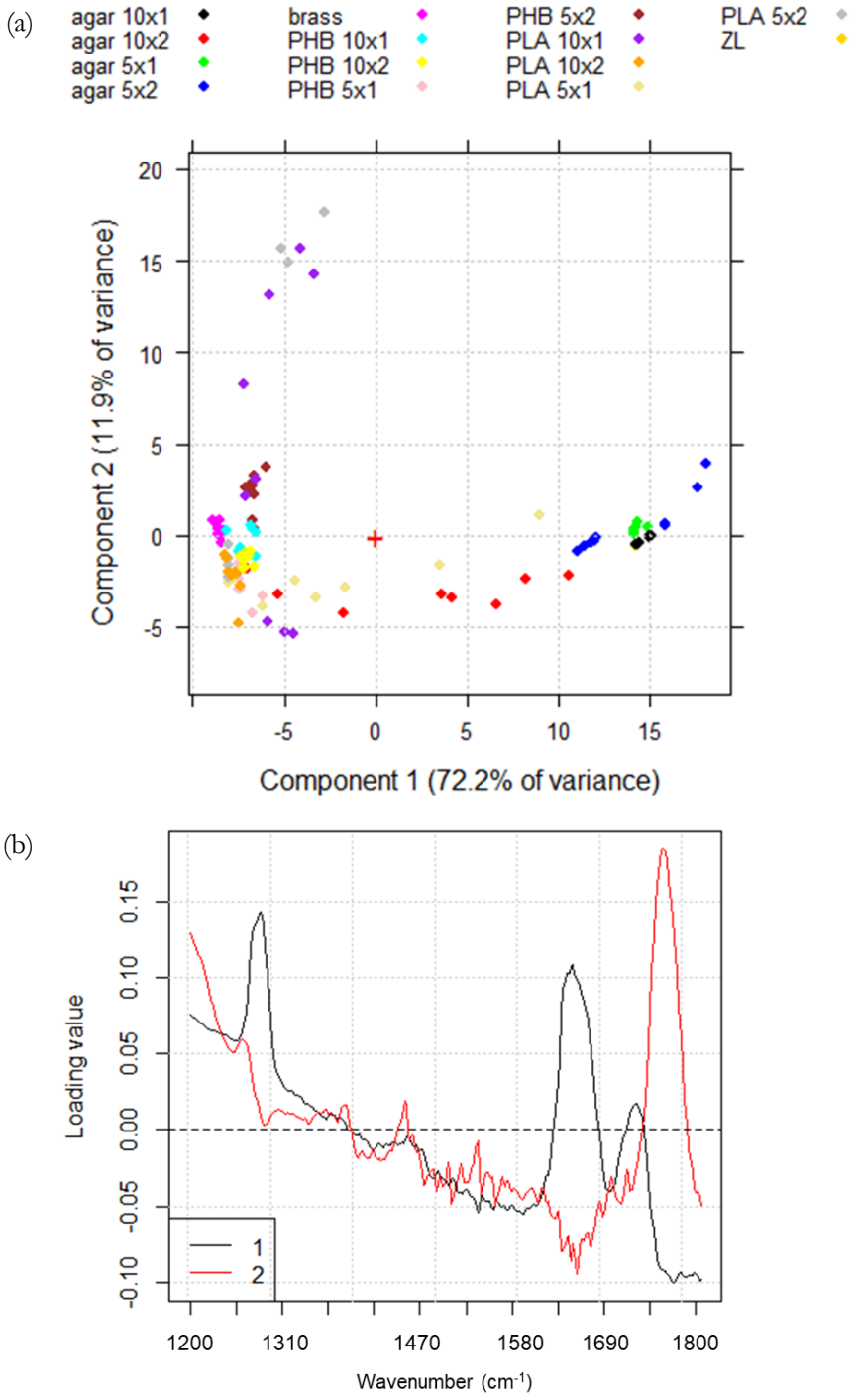

Figure 2.35 Score (a) and loading (b) plots obtained from PCA applied to FTIR spectra recorded on bare brass mock-ups (brass) and brass mock-ups, coated with Zaponlack, before (ZL) and after cleaning with agar-water/EL (agar), PHB-EL (PHB), and PLA-EL (PLA) systems by one (×1) or two (×2) applications of 5 or 10 minutes each, as reported in the key above the score plot in alpha-numeric order (a). (b) Related PC1 (black) and PC2 (red) loading plot.

2.9 Conclusions

In Chapter 2 three different formulations were designed in order to provide potentially new methods for the bio-cleaning of altered historical metals. The attention was addressed towards the selection three bio-sourced and biodegradable polymers, namely poly-3-hydroxybutyrate (PHB), agar, and polylactic acid (PLA), used as thickening agents in the formulations. In parallel, the bio-solvent ethyl lactate (EL) was chosen as active agent for the treatment of altered artefacts. In particular, previous evidence demonstrated that the organic solvent is able to dissolve two organic coatings often present on indoor historical metal heritage. Specifically, the acrylic resin Paraloid® B72 and the nitrocellulose lacquer Zaponlack.

Three formulations could be designed: PHB-EL, agar-water/EL, and PLA-EL systems. The formulations were initially characterised demonstrating different structures and features. In particular PHB-EL and agar-water/EL systems were recognised as stiff gels by rheology, whereas the same analysis classified the PLA-EL system as a viscous liquid. The different nature of the formulations determined also different ways of application and clearing approaches in order to better handle and employ the systems and avoid post-treatment residues.

Mild steel and brass mock-ups coated with Paraloid® B72 and Zaponlack, respectively, were used as model samples for the assessment of formulations' cleaning performance. The cleaning protocol tested in this study included one or two applications of 5 or 10 minutes for each system and was performed in triplicates.

Already by visual and optical microscopy inspection it was possible to appreciate the different cleaning outcomes obtained. In particular, a general alteration of mild steel coupons treated by agar-water/EL gel was noticed. X-ray fluorescence spectroscopy verified the presence of iron exclusively in the case of agar-water/EL used on steel mock-ups and corroborated the hypothesis of a negative interaction occurring between gel and substrate, possibly related to water and/or the unexpected presence of alginic acid in the commercial product. Colorimetry applied to the treated steel mock-ups further proved a loss in brightness, while acquiring yellow-reddish shades typical of iron corrosion species.

Colorimetry supported by statistical analysis (i.e., Tukey's HSD test) could discern that the cleaning performance, obtained by the PHB-EL system on mild steel mock-up coated with PB72, was rather linked to gel renewal than application time. On the contrary, no colorimetric coordinates could discriminate the several cleaning data related to PHB-EL gel applied to coated (i.e., Zaponlack) brass from a statistical perspective; no significant trends could be discerned for the cleaning action of PLA-EL formulation by colorimetry.

Fourier-transform infrared spectroscopy was performed on the proposed bio-based cleaning systems, before and after application on the test mock-ups. The analysis demonstrated the ability of the PHB-EL formulation to absorb both swollen Paraloid® B72 and Zaponlack, detaching them already after one short-time application (i.e., 5 minutes). In the case of the PLA-EL system, only Zaponlack could be identified on the used formulation, whereas Paraloid® B72 spectral features were possibly hidden by the FTIR spectrum of the PLA polymer. Finally, the agar-water/EL gel did not show the ability of entrapping swollen coatings in the gelled matrix during the cleaning application. This evidence was linked to the hydrophobicity of the organic coatings to be removed in the presence of water in the agar-based system. Finally, the same spectroscopic technique, applied to the differently cleaned mock-ups, could provide useful information about the cleaning achieved and potential formulation residues. The analysis of FTIR spectra was supported by Principal Component Analysis (PCA), in light of the large amount of data collected.

Bibliography

Anastas, P.T. and Warner, J.C. (1998) 'Green chemistry', Frontiers, 640(1998), p. 850.

Angelini, E. and Argyropoulos, V. (2008) 'PROMET state-of-the-art approach for protecting, preserving, and interpreting metals from museums in the Mediterranean basin', in V. Argyropoulos (ed.) Metals and Museums in the Mediterranean. Protecting, Preserving and Interpreting. TEI (Athens), pp. 23–37.

Aparicio, S. and Alcalde, R. (2009) 'The green solventethyl lactate: an experimental and theoretical characterization', Green Chem., 11(1), pp. 65–78. Available at: https://doi.org/10.1039/B811909K.

Armisén, R. and Gaiatas, F. (2009) 'Agar', in Handbook of Hydrocolloids. Elsevier, pp. 82–107. Available at: https://doi.org/10.1533/9781845695873.82.

Balaji, S., Gopi, K. and Muthuvelan, B. (2013) 'A review on production of poly β hydroxybutyrates from cyanobacteria for the production of bio plastics', Algal Research, 2(3), pp. 278–285. Available at: https://doi.org/10.1016/j.algal.2013.03.002.

Bertasa, M. et al. (2020) 'Agar gel strength: A correlation study between chemical composition and rheological properties', European Polymer Journal, 123, p. 109442. Available at: https://doi.org/10.1016/j.eurpolymj.2019.109442.

Borén, E. (2022) A GREENER SOLUTION Investigating the potential use of Green Solvents to remove cellulose nitrate lacquer from silver objects. University of Gothernburg. Available at: https://hdl.handle.net/2077/72648.

Bragagni, M. et al. (2013) 'Selection of PLA polymers for the development of injectable prilocaine controlled release microparticles: Usefulness of thermal analysis', International Journal of Pharmaceutics, 441(1–2), pp. 468–475. Available at: https://doi.org/10.1016/j.ijpharm.2012.11.007.

Brock, F. et al. (2018) 'Testing the Effectiveness of Protocols for Removal of Common Conservation Treatments for Radiocarbon Dating', Radiocarbon, 60(1), pp. 35–50. Available at: https://doi.org/10.1017/RDC.2017.68.

Calvo-Flores, F.G. et al. (2018) 'Green and Bio-Based Solvents', Topics in Current Chemistry, 376(3), p. 18. Available at: https://doi.org/10.1007/s41061-018-0191-6.

Carretti, E. et al. (2008) 'A new class of gels for the conservation of painted surfaces', Journal of Cultural Heritage, 9(4), pp. 386–393. Available at: https://doi.org/10.1016/j.culher.2007.10.009.

Chapman, S. and Mason, D. (2003) 'Literature Review: The Use of Paraloid B-72 as a Surface Consolidant for Stained Glass', Journal of the American Institute for Conservation, 42(2), pp. 381–392. Available at: https://doi.org/10.1179/019713603806112813.

Chemical Book (2024) Ethyl lactate. Available at: https://www.chemicalbook.com/ProductChemicalPropertiesCB5292231_EN.htm (Accessed: 25 February 2024).

Chiantore, O. and Lazzari, M. (2001) 'Photo-oxidative stability of paraloid acrylic protective polymers', Polymer, 42(1), pp. 17–27. Available at: https://doi.org/10.1016/S0032-3861(00)00327-X.

Cremonesi, P. (2013) 'Rigid gels and enzyme cleaning', in New Insights into the Cleaning of Paintings: Proceedings from the Cleaning 2010 International Conference, Universidad Politecnica de Valencia and Museum Conservation Institute.

Danis, O. et al. (2015) 'Preparation of poly(3-hydroxybutyrate-co-hydroxyvalerate) films from halophilic archaea and their potential use in drug delivery', Extremophiles, 19(2), pp. 515–524. Available at: https://doi.org/10.1007/s00792-015-0735-4.

Degrigny, C. (2008) 'The search for new and safe materials for protecting metal objects', in V. Argyropoulos (ed.) Metals and Museums in the Mediterranean. Protecting, Preserving and Interpreting. TEI (Athens), pp. 179–235.

Derrick, M.R., Stulik, D. and Landry, J.M. (2000) Infrared spectroscopy in conservation science. Getty Publications.

Dolzhenko, A. V. (2020) 'Ethyl lactate and its aqueous solutions as sustainable media for organic synthesis', Sustainable Chemistry and Pharmacy, 18, p. 100322. Available at: https://doi.org/10.1016/j.scp.2020.100322.

ELattar, L. et al. (2021) 'Ethyl Lactate: A New Prospective Eco-friendly Cleaner for Silver Gelatin Prints', Egyptian Journal of Chemistry, pp. 0–0. Available at: https://doi.org/10.21608/ejchem.2021.97654.4558.

Esson, J.M., Scott, R. and Hayes, C.J. (2018) 'Chemistry and Art: Removal of Graffiti Ink from Paints Grounded in a Real-Life Scenario', Journal of Chemical Education, 95(3), pp. 400–402. Available at: https://doi.org/10.1021/acs.jchemed.7b00536.

Farmakalidis, H.V. et al. (2016) 'Accelerated thermal ageing of acrylic copolymers, cyclohexanone-based and urea-aldehyde resins used in paintings conservation', Mediterr. Archaeol. Archaeom, 16, pp. 213–228.

Fays, M. (2018) « D'or, d'argent et de pate noire : incrustations révélées » étude et conservation-restauration de cinq objets islamiques en alliage cuivreux incrustés. Institut National du Patrimoine. Available at: https://mediatheque-numerique.inp.fr/documentation-oeuvres/memoires-diplome-restaurateurs-patrimoine/dor-dargent-pte-noire-incrustations-revelees-etude-conservation-restauration-cinq-objets-islamiques-en-alliage-cuivreux-incrustes-issus.

Fernández de la Ossa, M.Á. et al. (2011) 'Analytical techniques in the study of highly-nitrated nitrocellulose', TrAC Trends in Analytical Chemistry, 30(11), pp. 1740–1755. Available at: https://doi.org/10.1016/j.trac.2011.06.014.

Ghaffar, T. et al. (2014) 'Recent trends in lactic acid biotechnology: A brief review on production to purification', Journal of Radiation Research and Applied Sciences, 7(2), pp. 222–229. Available at: https://doi.org/10.1016/j.jrras.2014.03.002.

Giordano, A., Caruso, M.R. and Lazzara, G. (2022) 'New tool for sustainable treatments: agar spray—research and practice', Heritage Science, 10(1), p. 123. Available at: https://doi.org/10.1186/s40494-022-00756-9.

Giraud, T. et al. (2021) 'Use of gels for the cleaning of archaeological metals. Case study of silver-plated copper alloy coins', Journal of Cultural Heritage, 52, pp. 73–83. Available at: https://doi.org/10.1016/j.culher.2021.08.014.

Giuntoli, G. et al. (2012) 'Fluoro-functionalized PLA polymers as potential water-repellent coating materials for protection of stone', Journal of Applied Polymer Science, 125(4), pp. 3125–3133. Available at: https://doi.org/10.1002/app.36469.

Gómez-Ordóñez, E. and Rupérez, P. (2011) 'FTIR-ATR spectroscopy as a tool for polysaccharide identification in edible brown and red seaweeds', Food Hydrocolloids, 25(6), pp. 1514–1520. Available at: https://doi.org/10.1016/j.foodhyd.2011.02.009.

Grattoni, C.A. et al. (2001) 'Rheology and Permeability of Crosslinked Polyacrylamide Gel', Journal of Colloid and Interface Science, 240(2), pp. 601–607. Available at: https://doi.org/10.1006/jcis.2001.7633.

Gu, Y. and Jérôme, F. (2013) 'Bio-based solvents: An emerging generation of fluids for the design of eco-efficient processes in catalysis and organic chemistry', Chemical Society Reviews, 42(24), pp. 9550–9570. Available at: https://doi.org/10.1039/c3cs60241a.

Guilminot, E. et al. (2019) 'Use of Gels for the treatment of Metals', in C. Chemello, L. Brambilla, and E. Joseph (eds) Metal 2019 Proceedings of the Interim Meeting of the ICOM-CC Metals Working Group. International Councils of Museums - Committee for Conservation, p. 473.

Guilminot, E. (2023) 'The Use of Hydrogels in the Treatment of Metal Cultural Heritage Objects', Gels, 9(3), p. 191. Available at: https://doi.org/10.3390/gels9030191.

Hammond, L.C. (2021) Advanced Cleaning Systems for the Conservation of Historical Metal Artworks. Università di Bologna.

Hassan, M.A. et al. (2013) 'Sustainable production of polyhydroxyalkanoates from renewable oil-palm biomass', Biomass and Bioenergy, 50, pp. 1–9. Available at: https://doi.org/10.1016/j.biombioe.2012.10.014.

Huang, J. (2018) 'A Simple Accurate Formula for Calculating Saturation Vapor Pressure of Water and Ice', Journal of Applied Meteorology and Climatology, 57(6), pp. 1265–1272. Available at: https://doi.org/10.1175/JAMC-D-17-0334.1.

Ivashchenko, O. (2022) 'Cryo-SEM and confocal LSM studies of agar gel, nanoparticle hydrocolloid, mineral clays and saline solutions', Scientific Reports, 12(1), p. 9930. Available at: https://doi.org/10.1038/s41598-022-14230-w.

Janmey, P.A., Georges, P.C. and Hvidt, S. (2007) 'Basic Rheology for Biologists', in, pp. 1–27. Available at: https://doi.org/10.1016/S0091-679X(07)83001-9.

Jia, Y. et al. (2021) 'Deep eutectic solvent and agar: a new green gel to remove proteinaceous-based varnishes from paintings', Journal of Cultural Heritage, 51, pp. 138–144. Available at: https://doi.org/10.1016/j.culher.2021.08.001.

Jirage, A.S. et al. (2013) 'Poly-β-hydroxybutyrate: intriguing biopolymer in biomedical applications and pharma formulation trends', International Journal of Pharmaceutical & Biological Archives, 4(6), pp. 1107–1118.

Kampasakali, E. et al. (2021) 'Towards Sustainable Museum Conservation Practices: A Study on the Surface Cleaning of Contemporary Art and Design Objects with the Use of Biodegradable Agents', Heritage, 4(3), pp. 2023–2043. Available at: https://doi.org/10.3390/heritage4030115.

Kang, J. and Yun, S. Il (2022) 'Chitosan-reinforced PHB hydrogel and aerogel monoliths fabricated by phase separation with the solvent-exchange method', Carbohydrate Polymers, 284, p. 119184. Available at: https://doi.org/10.1016/j.carbpol.2022.119184.

Kerton, F. and Marriott, R. (2013) Alternative Solvents for Green Chemistry, Journal of the American Chemical Society. London, UK: Royal Society of Chemistry.

Khatami, K. et al. (2021) 'Waste to bioplastics: How close are we to sustainable polyhydroxyalkanoates production?', Waste Management, 119, pp. 374–388. Available at: https://doi.org/10.1016/j.wasman.2020.10.008.

Kim, H.-K. et al. (2013) 'Effect of polishing and glazing on the color and spectral distribution of monolithic zirconia', The Journal of Advanced Prosthodontics, 5(3), p. 296. Available at: https://doi.org/10.4047/jap.2013.5.3.296.

Kua, Y.L. et al. (2016) 'Ethyl lactate as a potential green solvent to extract hydrophilic (polar) and lipophilic (non-polar) phytonutrients simultaneously from fruit and vegetable by-products', Sustainable Chemistry and Pharmacy, 4, pp. 21–31. Available at: https://doi.org/10.1016/j.scp.2016.07.003.

Lazzari, M. and Chiantore, O. (2000) 'Thermal-ageing of paraloid acrylic protective polymers', Polymer, 41(17), pp. 6447–6455. Available at: https://doi.org/10.1016/S0032-3861(99)00877-0.

Leja, K. and Lewandowicz, G. (2010) 'Polymer biodegradation and biodegradable polymers-a review.', Polish Journal of Environmental Studies, 19(2).

Létrange, A. et al. (2017) 'Comparison of three hydrogels for cleaning tarnished silver threads using electrochemical treatment', in L. V. Angelova et al. (eds) Gels in the Conservation of Art. London: Archetype Publications, pp. 369–371.

Li, G. et al. (2020) 'Synthesis and Biological Application of Polylactic Acid', Molecules, 25(21), p. 5023. Available at: https://doi.org/10.3390/molecules25215023.

Luxford, N. and Thickett, D. (2007) 'Preventing silver tarnish--lifetime determination of cellulose nitrate lacquer', Metal, 7, pp. 88–93.

Marchand, G. et al. (2013) 'Study of the conservation treatment applied to the archaeological horn silver artifacts', in Interim Meeting for the International Council of Museums Committee for Conservation Metal Working Group, Metal 2013. Edinburgh, Scotland: International Councils of Museums - Committee for Conseravtion and Historic Scotland, pp. 245–250.

Massana Roquero, D. et al. (2022) 'Iron(III)-cross-linked alginate hydrogels: a critical review', Materials Advances, 3(4), pp. 1849–1873. Available at: https://doi.org/10.1039/D1MA00959A.

McAdam, B. et al. (2020) 'Production of Polyhydroxybutyrate (PHB) and Factors Impacting Its Chemical and Mechanical Characteristics', Polymers, 12(12), p. 2908. Available at: https://doi.org/10.3390/polym12122908.

Medina-Esquivel, R. et al. (2008) 'Measurement of the Sol–Gel Transition Temperature in Agar', International Journal of Thermophysics, 29(6), pp. 2036–2045. Available at: https://doi.org/10.1007/s10765-007-0332-6.

Melo, M.. et al. (1999) 'Photodegradation of acrylic resins used in the conservation of stone', Polymer Degradation and Stability, 66(1), pp. 23–30. Available at: https://doi.org/10.1016/S0141-3910(99)00048-8.

Merck (2024) (-)-Ethyl L-lactate, properties. Available at: https://www.sigmaaldrich.com/CH/en/product/aldrich/e34102 (Accessed: 13 February 2024).

Mistretta, M.C. et al. (2019) 'Durability of Biodegradable Polymers for the Conservation of Cultural Heritage', Frontiers in Materials, 6. Available at: https://doi.org/10.3389/fmats.2019.00151.

Moity, L. et al. (2016) 'A "top-down" in silico approach for designing ad hoc bio-based solvents: application to glycerol-derived solvents of nitrocellulose', Green Chemistry, 18(11), pp. 3239–3249. Available at: https://doi.org/10.1039/C6GC00112B.

Molina, M.T., Cano, E. and Ramírez-Barat, B. (2023) 'Protective coatings for metallic heritage conservation: A review', Journal of Cultural Heritage, 62, pp. 99–113. Available at: https://doi.org/10.1016/j.culher.2023.05.019.

Lo Monaco, A. et al. (2011) 'Colour measurements of surfaces to evaluate the restoration materials', in, p. 80840P. Available at: https://doi.org/10.1117/12.889147.

Nikles, S.M. et al. (2001) 'Ethyl lactate: a green solvent for magnetic tape coating', Green Chemistry, 3(3), pp. 109–113. Available at: https://doi.org/10.1039/b101147m.

Nurazzi, N.M. et al. (2022) 'Thermogravimetric Analysis (TGA) and Differential Scanning Calorimetry (DSC) of PLA/Cellulose Composites', in Polylactic Acid-Based Nanocellulose and Cellulose Composites. Boca Raton: CRC Press, pp. 145–164. Available at: https://doi.org/10.1201/9781003160458-7.

Ocak, Y. et al. (2009) 'Protection of marble surfaces by using biodegradable polymers as coating agent', Progress in Organic Coatings, 66(3), pp. 213–220. Available at: https://doi.org/10.1016/j.porgcoat.2009.07.007.

Ocak, Y. et al. (2015) 'Sustainable bio-nano composite coatings for the protection of marble surfaces', Journal of Cultural Heritage, 16(3), pp. 299–306. Available at: https://doi.org/10.1016/j.culher.2014.07.004.

Ozkoc, G. and Kemaloglu, S. (2009) 'Morphology, biodegradability, mechanical, and thermal properties of nanocomposite films based on PLA and plasticized PLA', Journal of Applied Polymer Science, 114(4), pp. 2481–2487. Available at: https://doi.org/10.1002/app.30772.

Pereira, C.S.M., Silva, V.M.T.M. and Rodrigues, A.E. (2011) 'Ethyl lactate as a solvent: Properties, applications and production processes – a review', Green Chemistry, 13(10), p. 2658. Available at: https://doi.org/10.1039/c1gc15523g.

Prati, S. et al. (2019) 'Cleaning oil paintings: NMR relaxometry and SPME to evaluate the effects of green solvents and innovative green gels', New Journal of Chemistry, 43(21), pp. 8229–8238. Available at: https://doi.org/10.1039/C9NJ00186G.

Punet, X. et al. (2017) 'Polylactic acid organogel as versatile scaffolding technique', Polymer, 113, pp. 81–91. Available at: https://doi.org/10.1016/j.polymer.2017.02.056.

Ragain, J.C. and Johnston, W.M. (2000) 'Color acceptance of direct dental restorative materials by human observers', Color Research & Application, 25(4), pp. 278–285. Available at: https://doi.org/10.1002/1520-6378(200008)25:4<278::AID-COL8>3.0.CO;2-F.

Rahbani, J. et al. (2013) 'Characterization of internal structure of hydrated agar and gelatin matrices by cryo-SEM', ELECTROPHORESIS, 34(3), pp. 405–408. Available at: https://doi.org/10.1002/elps.201200434.

Samorì, C. et al. (2016) 'The Green Attitude in Art Conservation: Polyhydroxybutyrate-based Gels for the Cleaning of Oil Paintings', ChemistrySelect, 1(15), pp. 4502–4508. Available at: https://doi.org/10.1002/slct.201601180.

Sansonetti, A. et al. (2020) 'A review in using agar gels for cleaning art surfaces', Journal of Cultural Heritage, 44, pp. 285–296. Available at: https://doi.org/10.1016/j.culher.2020.01.008.

São João, J., Branco, L.C. and Leite Fragoso, S. (2017) 'Trials fo agar gels and task-specific salts for the electrochemical reduction of silver sulphide on silver leaf', in L. V. Angelova et al. (eds) Gels in the Conservation of Art. London: Archetype Publications, pp. 287–291.

Scalioni, L. V., Gutiérrez, M.C. and Felisberti, M.I. (2017) 'Green composites of poly(3-hydroxybutyrate) and curaua fibers: Morphology and physical, thermal, and mechanical properties', Journal of Applied Polymer Science, 134(14), pp. 1–13. Available at: https://doi.org/10.1002/app.44676.

Shashoua, Y., Bradley, S.M. and Daniels, V.D. (1992) 'Degradation of cellulose nitrate adhesive', Studies in Conservation, 37(2), pp. 113–119. Available at: https://doi.org/10.1179/sic.1992.37.2.113.

Stavroudis, C. and Doherty, T. (2007) 'A novel approach to cleaning II: extending the Modular Cleaning Program to solvent gels and free solvents, part 1', WAAC newsletter, 29(3), pp. 9–15.

Taib, N.-A.A.B. et al. (2023) 'A review on poly lactic acid (PLA) as a biodegradable polymer', Polymer Bulletin, 80(2), pp. 1179–1213. Available at: https://doi.org/10.1007/s00289-022-04160-y.

Tamura, M. and Takagi, K. (2017) 'Towards the sustainable use of agar / agarose in conservation: a case study of the Izu peninsula, Japan', in L. V. Angelova et al. (eds) Gels in the Conservation of Art. London, UK: Archetype Publications, pp. 152–154.

Thickett, D. and Lee, L.R. (2004) Selection of materials for the storage or display of museum objects. British Museum London.

Tudorachi, N., Lipsa, R. and Mustata, F.R. (2012) 'Thermal Degradation of Carboxymethyl Starch–g-Poly(lactic acid) Copolymer by TG–FTIR–MS Analysis', Industrial & Engineering Chemistry Research, 51(48), pp. 15537–15545. Available at: https://doi.org/10.1021/ie300625c.

Vinçotte, A. et al. (2019) 'Effect of solvent on PARALOID® B72 and B44 acrylic resins used as adhesives in conservation', Heritage Science, 7(1), p. 42. Available at: https://doi.org/10.1186/s40494-019-0283-9.

Volpi, F. (2017) Green Strategies for the Cleaning of Works of Art Setting Up of an Analytical Protocol for the Evaluation of Cleaning. Alma Mater Studiorum Università di Bologna. Available at: https://doi.org/10.6092/unibo/amsdottorato/8050.

Walsh-Korb, Z., Ruiz-Fourcade, S. and Avérous, L. (2017) 'Responsive bio-based gels for the preservation and treatment of archaeological wooden objects', in R. Angelova, L.V., Ormsby, B., Townsend, J.H., Wolbers (ed.) Gels in the Conservation of Art. London, UK: Archetype Publications, pp. 294–296.

Wei, L., McDonald, A.G. and Stark, N.M. (2015) 'Grafting of Bacterial Polyhydroxybutyrate (PHB) onto Cellulose via In Situ Reactive Extrusion with Dicumyl Peroxide', Biomacromolecules, 16(3), pp. 1040–1049. Available at: https://doi.org/10.1021/acs.biomac.5b00049.

Wolbers, R., Rivers, S. and Yamashita, Y. (2014) 'Corroded applied lead-based decoration (hyomon) on Japanese lacquer: Principles and case studies', Studies in Conservation, 59(sup1), pp. S191–S194. Available at: https://doi.org/10.1179/204705814X13975704319316.

Yarnpakdee, S., Benjakul, S. and Kingwascharapong, P. (2015) 'Physico-chemical and gel properties of agar from Gracilaria tenuistipitata from the lake of Songkhla, Thailand', Food Hydrocolloids, 51, pp. 217–226. Available at: https://doi.org/10.1016/j.foodhyd.2015.05.004.

Yilmaz, M., Soran, H. and Beyatli, Y. (2005) 'Determination of poly-β-hydroxybutyrate (PHB) production by some Bacillus spp.', World Journal of Microbiology and Biotechnology, 21(4), pp. 565–566. Available at: https://doi.org/10.1007/s11274-004-3274-1.

Yiming, J. et al. (2019) 'A new bio-based organogel for the removal of wax coating from indoor bronze surfaces', Heritage Science, 7(1), p. 34. Available at: https://doi.org/10.1186/s40494-019-0276-8.

Zamora-Mora, V. et al. (2014) 'Chitosan/agarose hydrogels: Cooperative properties and microfluidic preparation', Carbohydrate Polymers, 111, pp. 348–355. Available at: https://doi.org/10.1016/j.carbpol.2014.04.087.

Chapter 3

Multi-target cleaning gel: an innovative green approach in historical iron care

This chapter is based on Passaretti, A., Cuvillier, L., Sciutto, G., & Joseph E., Innovative perspective for the cleaning of historical iron heritage: novel bio organogel for the combined removal of undesired organic coatings and corrosion. *Heritage Science* [under publication]

3.1 Corrosion behaviour of indoor historical iron-based heritage

As outlined in Paragraph 1.1, the core problem for the preservation and conservation of metallic heritage arises from the process of corrosion towards which they spontaneously tend (Chilton, 1971). In indoor environments, the phenomenon can be influenced by factors such as artificial and natural light, dust, and several volatile compounds present in the surrounding atmosphere, yet it is primarily driven by ambient temperature and relative humidity fluctuations (Monnier *et al.*, 2019). Indeed the natural process of atmospheric corrosion is provoked on a metal substrate in the presence of an electrolyte (i.e., condensed water) and an oxidant (i.e., oxygen in the air) (Monnier *et al.*, 2019). On iron-based substrates, the process can lead to localised or uniform corrosion. Localised corrosion exhibits alterations such as pitting, a destructive form of corrosion that provokes little holes on the metal (Santarini, 2007; Angelini and Argyropoulos, 2008). On the contrary, low-alloy steels are less affected by this form of corrosion process and more prone to uniform alteration (Santarini, 2007).

For indoor historical ferrous heritage, the process of corrosion follows the so-called "wet-dry" cycle, as Evan and Taylors described for the first time (Evans and Taylor, 1972). Calculations and mechanistic modelling have been developed in the last decades in order to investigate and predict the behaviour of iron-based objects for long-term preservation (Stratmann, 1990; Hœrlé *et al.*, 2004). Figure 3.1 (Maréchal *et al.*, 2007) displays a schematic representation of the wet-dry cycle for atmospheric corrosion over time and depending on electrolyte thickness. The modelled cycle distinguishes three stages to describe the process of atmospheric corrosion affecting iron. It starts with the wetting stage (I), when water vapour begins to condense on the metallic surface, forming a consistently growing electrolyte (i.e., water droplet). This event ignites the anodic dissolution of iron (Fe) in the presence of atmospheric oxygen, leading to the formation of ferrous ions (Fe^{2+}) (Stratmann, 1990). Concurrently, a cathodic reaction provokes the reduction of oxygen to hydroxyl species and, if already present as corrosion product on the metal substrate, lepidocrocite (γ-FeOOH, Fe(III) phase) into γ-Fe·OH·OH (Fe(II) phases) (Stratmann, 1990; Hœrlé *et al.*, 2004). Once the electrolyte gains a constant thickness, the wet stage (II) begins. The atmospheric oxygen in contact with condensed water is dissolved and diffused by the electrolyte. When oxygen reaches the formed rust layer, it oxides γ-Fe·OH·OH to Fe(III) phases. The eventual drying stage (III) begins when the condensed water thickness starts to diminish. The lowering of electrolyte thickness increases the oxygen diffusion in the water film, accelerating the damage rate, and consequently raising the concentration of corrosion products formed on the iron substrate. The model does not describe the conclusive step of re-oxidation of the rust layer, leading to the regeneration of lepidocrocite (Maréchal *et al.*, 2007). Eventually, the whole process of atmospheric corrosion affecting iron can be expressed by one chemical equation:

$$4Fe + 3O_2 + 2H_2O \rightarrow 4FeOOH$$ (Maréchal *et al.*, 2007)

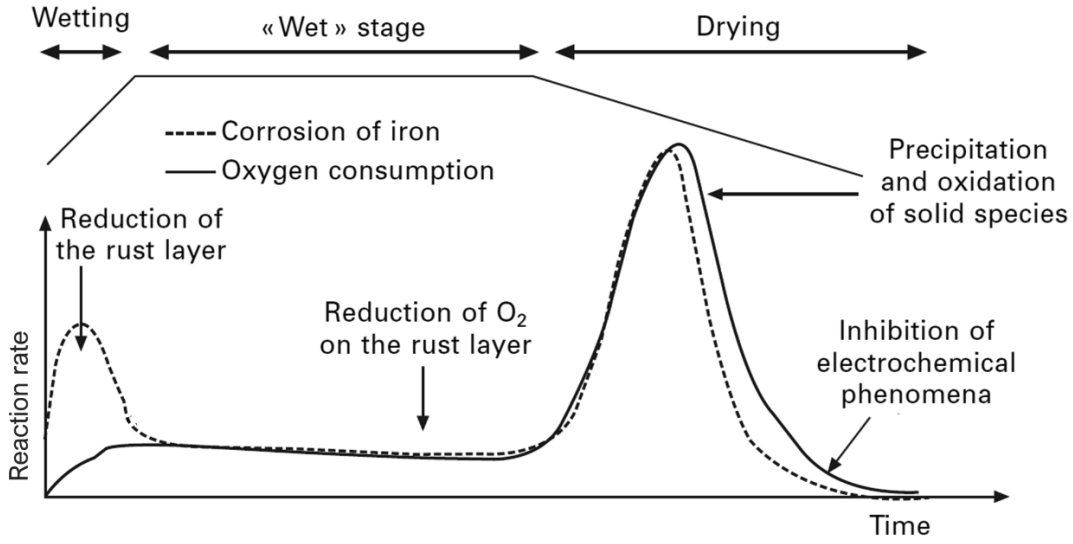

Figure 3.1 The wet-dry cycle. Variations of iron corrosion (dotted line) and oxygen consumption (solid line) rates as experimentally measured by Stratmann (Stratmann, 1990). (Reproduced from Maréchal *et al.*, 2007).

The composition of the resulting rust layer can be very heterogenous, and its identification for conservation purposes can be challenging because of the intricate stratigraphy or the different crystalline or amorphous nature of the compounds formed (Monnier *et al.*, 2019). Typically, various iron oxides and oxyhydroxides can be present: goethite (α-FeOOH), akageneite (β-FeOOH), lepidocrocite (γ-FeOOH), feroxyhyte (δ-FeOOH), ferrihydrite (hydrated oxyhydroxide of iron), maghemite (γ-Fe_2O_3), and magnetite (Fe_3O_4) (Neff *et al.*, 2006; Monnier *et al.*, 2013). Electrochemical studies have ranked the reduction activity of these phases, allowing to comprehend and differentiate between active (i.e., unstable) and non-active (i.e., stable) iron corrosion compounds (Lair *et al.*, 2006). For instance, goethite (α-FeOOH) was tested in being electrochemically inactive compared to the polymorph lepidocrocite (γ-FeOOH) that is very reactive, as illustrated in the wet-dry cycle model (Maréchal *et al.*, 2007; Santarini, 2007). In the long-term, through the cyclic corrosion of iron, lepidocrocite will be gradually transformed into the more stable form of goethite (Santarini, 2007). This ratio between non-active and active iron corrosion species, for instance goethite and lepidocrocite (α/γ), is used to empirically evaluate the stability of the alteration layer formed onto iron substrates for conservation purposes (Santarini, 2007; Monnier *et al.*, 2019).

3.2 Altered historical iron: tackling detrimental corrosion and failed or undesired organic materials

The resulting formation of reactive corrosion species on iron-based substrates can cause irreversible degradation of the affected object (Kooli *et al.*, 2018). To avoid the detrimental consequences of corrosion, several museums opt for systems to monitor and regulate environmental parameters, especially temperature and relative humidity. The prevention of significant fluctuations of these factors (e.g., changeover day-night) is critical for the preservation of historical metal objects displayed and stored indoors (Prosek *et al.*, 2013).

Alternatively, or in addition, the use of organic coatings is an effective preventive strategy to the natural process of iron corrosion, permitting to avoid the interaction between the metal substrate and the surrounding environment (Watkinson, 2010). However, as discussed in Paragraph 1.2.2, these organic materials are also sensitive to environmental detrimental factors that induce negative consequences over time. Potentially undesired impacts might occur either on the aspect of the organic material (e.g., yellowing phenomena) or on the protection purpose that, when starting to fail, causes the exposure of underlying metal to caustic agents (Perera, 2003; Couture-Rigert, Sirois and Moffatt, 2012).

Therefore, when compromised organic coatings are present, they are also frequently associated with altered underlying metal substrates (Degrigny *et al.*, 2007). In these circumstances, a possible conservation intervention is the removal of all the undesired materials present on the original metallic surface. When this option is selected, in the first place, it is necessary to eliminate the ineffective organic coatings present. This step would guarantee access for the consecutive removal of the detrimental corrosion present within and underneath the organic layer. Hence two – or more – separately addressed cleaning approaches are conventionally required, as extensively mentioned in conservation reports (Jaeger, 2008; Schmuecker, Lees and Richardson, 2011; Cagnini, Gennai and Mazzoni, 2012; Mari Yanagishita, 2012). For instance, Schmuecker et al. (2011) depicts the conservation protocol employed to clean an iron- and copper-based horse armour dated back to the 17th century. In particular, the metal plates composing the garnishment were initially cleaned with neat solvents by cotton swabbing to remove dirt, grease, and degraded protective coatings. Afterwards, mechanical soft cleaning was employed to remove the anaesthetic and detrimental corrosion present on the metallic armour (Schmuecker, Lees and Richardson, 2011). This kind of cleaning approach would guarantee a controllable intervention; nevertheless, several materials and tools, more working time, and expertise are necessary. Thus, a methodology able to tackle simultaneously, but in an adjustable way, undesired organic films and corrosion could be of interest to achieve a versatile cleaning of metal heritage. Within this scenario, previous literature has already reported the suitability and reliability of gel formulations for the controlled cleaning of altered organic materials or else harmful corrosion present on metal artefacts (Parisi *et al.*, 2018; Yiming *et al.*, 2019).

3.3 PHB-EL-DFO gel

A new green organogel was designed with the innovative outlook to simultaneously tackle inorganic compounds and organic substances as undesired materials on the surface of indoor metal artworks. Specifically, the gel formulation was aimed to concurrently remove an acrylic coating, namely Paraloid® B72, and the underlying iron corrosion, generally composed of iron oxyhydroxides such as lepidocrocite and goethite (Neff *et al.*, 2006; Monnier *et al.*, 2013) possibly present on historical steel collections. These targets were selected in accordance with preliminary bibliographic research and the replies obtained through a survey conceived within the framework of the HELIX project (Cuvillier, Passaretti and Joseph, 2020) (Paragraph 1.5). In the specific case of historical iron artefacts, often acrylic-based materials are employed with a protective goal; in addition, this class of materials is often present in marker inks used on metallic surfaces to name and catalogue heritage objects that are not displayed but stored in museums.

Great attention was addressed to the selection of the gel system components, aiming to propose a more sustainable and less harmful cleaning alternative for historical iron care. In this perspective, polyhydroxybutyrate (PHB), ethyl lactate (EL), and deferoxamine B (DFO) were employed in the formulation as thickening agent, organic solvent, and chelator, respectively (Figure 3.2). In Paragraphs 2.4.1 and 2.2, the Green Chemistry principles (Anastas and Eghbali, 2010) inherently fulfilled by polyhydroxybutyrate and ethyl lactate are mentioned and discussed. It is important to briefly recall for both chemicals the bio-derivation resulting from the microbial metabolic activity, the low or non-toxicity, and the readily biodegradability into organic innocuous substances. The following paragraph (3.3.1) reviews the properties and greenness of deferoxamine B (DFO), the siderophore newly embedded in the proposed gel formulation.

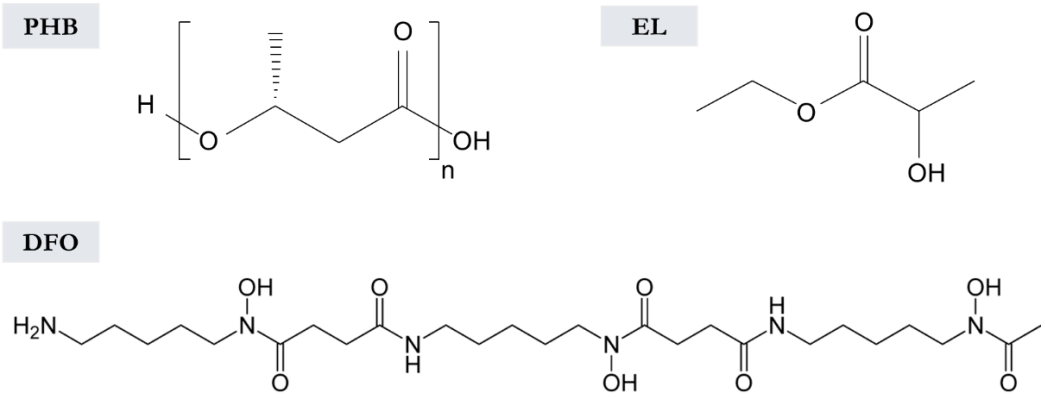

Figure 3.2 Structural formula of PHB-EL-DFO gel components: poly-3-hydroxybutyrate (PHB), ethyl lactate (EL) and deferoxamine B (DFO).

3.3.1 An insight into deferoxamine B (DFO)

Deferoxamine B is a natural compound belonging to the category of siderophores (from the Greek, "iron carriers"). This denomination recalls the activity of microorganisms and plants in producing and secreting siderophores to solubilise and transport primarily iron ions into their cells when growing in iron-deficient environments (Farkas, Enyedy and Csóka, 1999). In particular, deferoxamine B is mainly synthesised by the bacterium species *Streptomyces pilous,* and has a high affinity for ferric iron as expressed by the stability constant logK equal to 30.4 for Fe(III)-DFO systems (Schwarzenbach, 1960). This parameter represents the tendency towards the formation of a metal-ligand complex in a chemical equilibrium. Notably, DFO has a strong affinity for Fe(III) in comparison with the much lower stability constants measured for the complexes formed with other metal ions, such as Cu (II) (i.e., 13.73) or Zn(II) (i.e., 10.36) (Farkas, Enyedy and Csóka, 1999; Pawlaczyk and Schroeder, 2021). Deferoxamine B is a hexadentate ligand and, like most siderophores, it completes the octahedral coordination sphere of Fe(III), forming stable complexes in a molar ratio 1:1 (Schwarzenbach, 1960; Farkas, Enyedy and Csóka, 1999). DFO presents three bidentate hydroxamate functional groups (-CONHO$^-$), as displayed in Figure 3.3 (Bellotti and Remelli, 2021), which are the binding sites for the coordination with metal ions (Farkas, Enyedy and Csóka, 1999). It is remarkable to mention that exclusively the three-chelated DFO-complex exists in the pH range of 2-10 for Fe(III) (Farkas, Enyedy and Csóka, 1999). The iron-DFO complex has a vivid red colour that helps to ascertain and monitor the chelating process of the ligand (Bellotti and Remelli, 2021).

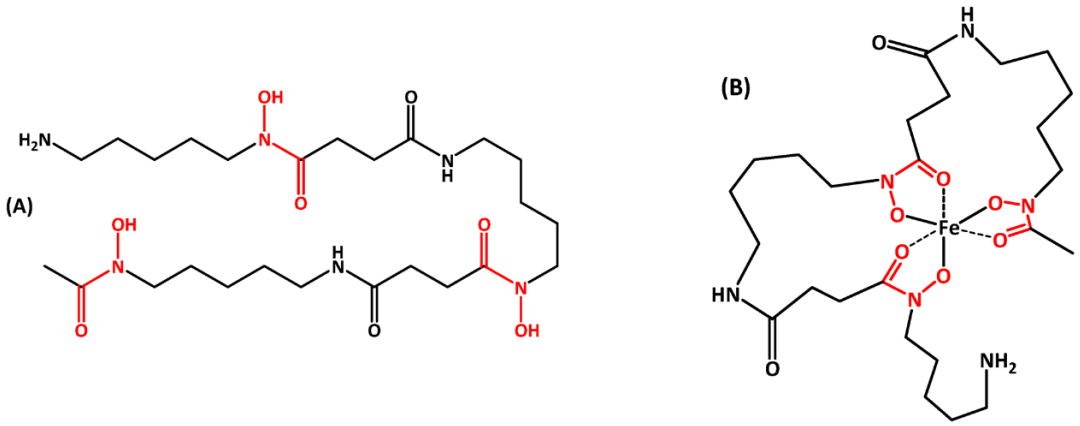

Figure 3.3 Chemical structure of deferoxamine B (DFO) (A) and iron-deferoxamine B complex (B). Hydroxamate groups, involved in metal ion chelation, are evidenced in red. (Reproduced from Bellotti & Remelli, 2021).

Regarding the aspect of greenness, the ligand is bio-synthetised by bacteria and fully biodegradable (Fazary *et al.*, 2016). DFO is non-pollutant and innocuous for the environment and the human health – considering the simple exposition to the substance, thus excluding the case of ingestion (Bentur, McGuigan and Koren, 1991; Christensen *et al.*, 2001) – appearing as a non-hazardous and safer alternative potentially able to replace the toxic chelating agents traditionally employed in metal conservation (Farkas, Enyedy and Csóka, 1999). Furthermore, literature reports that deferoxamine B inhibits Fenton reactions, hence preventing the formation of damaging hydroxyl radicals, contrary to the effect of conventional chelators, such as ethylenediaminetetraacetic acid (EDTA) and diethylenetriaminepentaacetic acid (DTPA) (Strlič, Kolar and Pihlar, 2001).

Deferoxamine B, and more in general siderophores, constitute an alternative family of greener chelators that are already exploited largely in the fields of bioremediation, medical science, and pharmacology (Hider and Kong, 2010; De Serrano, 2017; Bellotti and Remelli, 2021). In particular, it has an essential role in the therapy of patients with blood diseases (Bellotti and Remelli, 2021). The commercial drug, exploiting deferoxamine B as an active agent, is sold under the brand name Desferal® by Novartis, and it is a water-soluble injectable medication. Because of the lower cost of Desferal® compared to pure deferoxamine B, the drug afforded the opportunity to test the siderophore also in the CH field. Indeed, the high chelation efficiency and selectivity towards iron(III) determine compelling features for the exploitation of DFO in art conservation. Effective and encouraging assessments have been carried out to remove iron stains from wood, textile, and paper substrates (Albelda-Berenguer, Monachon and Joseph, 2019; Rapti *et al.*, 2021). Eventually, hydrogels were successfully amended with DFO to clean iron-contaminated waterlogged wood (Rapti *et al.*, 2023) and iron-based heritage (Cuvillier *et al.*, 2022). Recently, within the framework of the HELIX project, deferoxamine B was employed for the cleaning of altered historical iron artefacts as a greener, safer, and equally effective alternative to the conventional chelator EDTA (Cuvillier *et al.*, 2023). The study confirms the effectiveness of deferoxamine B in chelating Fe(III) also when embedded into a gel matrix (i.e., agar). The gelled DFO solution showed a lower rate of chelation over time compared to free DFO solution due to its slow release by diffusion through the gel system, which is, on the contrary, a sought feature when opting for gelled cleaning methods. Furthermore, when working with an agar hydrogel amended with DFO ($6 \cdot 10^{-2}$ M) on naturally corroded steel pieces, one application of 10 minutes provided better cleaning when the gel was applied still hot. In contrast, the action towards iron corrosion was only partially successful if used as a preformed rigid foil due to the difficulty to achieve a good contact to the target surface.

The positive outcomes, concerning the concurrent use of gel formulations and deferoxamine B, provide encouraging premises for the design of the PHB-EL-DFO organogel.

3.3.2 Design of the PHB-EL-DFO formulation

As a preliminary phase in making the new gel, the functionality of the active agent DFO embedded in the PHB-EL formulation was ascertained. Considering the chemical and physical properties of the initial gel components, it was essential to evaluate factors such as the temperature reached for the solubilisation of the polymer PHB, together with the pH and the solubility in the organic solvent EL.

First, previous research reports that the chelating action of deferoxamine B is not altered by the temperature (i.e., 100-110 °C, Paragraph 2.4.2) reached for the gelation of the polymer PHB in the presence of EL (Pawlaczyk and Schroeder, 2021; Cuvillier *et al.*, 2023). Hence, it is assumable that also for the gelation of the formulation loaded with deferoxamine B, the same temperature will be used, not causing any degradation of the chelator.

Secondly, referring to the literature, it was possible to ascertain beforehand the functionality of deferoxamine B as ligand in function of the pH. In particular, its complexing action for Fe(III), which is the target ion present in the corrosion species found on altered historical iron (i.e., oxides and oxyhydroxides of iron), is still effective at the acidic pH (i.e., pH 4) of ethyl lactate, which is the organic solvent employed

in the PHB-EL-DFO formulation (Farkas, Enyedy and Csóka, 1999; Rapti *et al.*, 2023). Indeed, it is proven that deferoxamine B chelating action performs better on iron (III) at alkaline pH (Rapti *et al.*, 2017), yet, previous studies demonstrated that equivalent effectiveness in iron chelation could also be obtained at acidic pH by repeated applications (Borer *et al.*, 2009; Rapti *et al.*, 2023).

In the third instance, the deferoxamine B used in the PHB-EL-DFO formulation comes from the commercial product Desferal® (Novartis) (Figure 3.4), which is in the form of mesylate salt, and needs to be solubilised to allow the chelation activity of the ligand contained. Therefore, solubility tests were carried out with selected green solvents: ethyl lactate, ethanol (96.0 – 97.2%), and deionised water. An aliquot of Desferal® was added in concentration 3% w/v ($2 \cdot 10^{-2}$ M) to each solvent to obtain comparable outcomes: in the case of ethyl lactate and ethanol, the drug powder was merely dispersed in the liquid phase; on the contrary, deionised water yielded a clear and transparent final solution. Subsequently, naturally corroded iron pieces were immersed for one hour in the obtained solutions to ascertain the chelating action of potentially dissolved DFO. As a comparison, Figure 3.5 a and b display the resulting solutions for ethyl lactate and deionised water, respectively. Only in the presence of water, the functionality of DFO was clearly noticeable and recognisable from the vibrant red colouration that the solution gained, typical of iron-DFO complexes (Bellotti and Remelli, 2021) (Figure 3.5, b).

It is notable that a recently published work from Rapti et al. (2023) reports that Desferal® includes some excipients that are insoluble in ethanol (Rapti *et al.*, 2023). On the contrary, the purer deferoxamine B (≥92.5%) purchased from Sigma-Aldrich is completely soluble in ethanol. The information could potentially open to a fully waterless version of the PHB-EL-DFO formulation, which would be convenient when treating an artefact on which the use of water would be strictly precluded. Nonetheless, the same research (Rapti *et al.*, 2023) verified that the efficacy of deferoxamine B in chelating iron(III) is lower in the presence of ethanol than water solutions at both alkaline and acidic pH. Moreover, pure deferoxamine B (Sigma Aldrich) has a cost of approximately eight times higher than in the form of Desferal® (Novartis). This would be a critical constraint when proposing DFO to conservator-restores as a greener alternative to replace traditional polluting and harmful chelators in their everyday work.

Therefore, in the research presented here, the minimum amount of water required for DFO solubilisation was estimated by little sequential additions of deionised water to an aliquot of Desferal®. The drug powder resulted in being wholly dissolved when the solution became clear and reached a concentration of 20% w/v (Figure 3.5, c).

Figure 3.4 Desferal® drug from Novartis: product packaging (a) and a vial of 0.5 g (b).

Figure 3.5 Resulting Desferal® solutions 3% w/v ($2 \cdot 10^{-2}$ M) in ethyl lactate (a) and deionised water (b) after one-hour immersion of naturally rusted iron pieces. Appearance of Desferal® solution in deionised water 20% w/v ($3 \cdot 10^{-1}$ M) (c).

Due to the required addition of water, a fourth factor influenced the design of the PHB-EL-DFO gel: the hydrophobicity of polyhydroxybutyrate (McAdam *et al.*, 2020). The presence of water became a decisive variable in order to determine the maximum amount of ligand that could be loaded in the organogel. Knowing the Desferal® limit of solubility in water (i.e., 20% w/v), different water solutions were added to the initial PHB-EL system (7% w/v) in a ratio 2:1, 3:1, and 6:1 v/v with ethyl lactate, as illustrated in Table 3.1. Only the latest proportion yielded a rigid gel, as desired. In the other cases, the resulting formulations were soft in consistence when cut with the spatula, not well-retentive, and not easy to handle.

Table 3.1 Resume of the tests carried out to amend the PHB-EL formulation (7% w/v) with DFO solution in water (20% w/v). Photographic evidence of resulting formulations consistence when cut and handled by spatula.

PHB-EL gel	Concentration DFO solution	Ratio EL/water	PHB-EL-DFO formulation
7% w/v	20% w/v	2:1	
		3:1	
		6:1	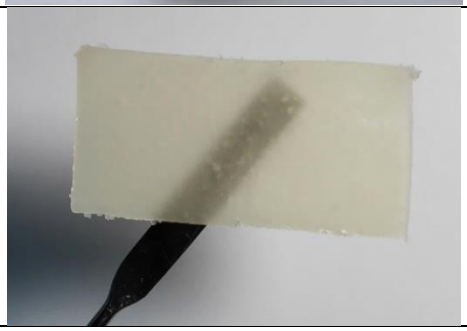

In conclusion, for the synthesis of the PHB-EL-DFO gel formulation a 20% w/v solution of deferoxamine B mesylate salt (Desferal®) (DFO) from Novartis dissolved in deionised water, was added to ethyl lactate

(≥98%) (EL) from Sigma Aldrich in a volume ratio of 1:6. The bio-polymer poly-3-hydroxybutyrate (PHB), purchased from Biomer, was then added at 7% w/v concentration. The final concentration of the DFO solution was $4 \cdot 10^{-2}$ M, which is a value in the range of other exploitations of this ligand in art conservation (Rapti *et al.*, 2017, 2023; Cuvillier *et al.*, 2022). The mixture was stirred in a covered glass petri dish at about 110 °C until the gel was formed and let cool down to room temperature (i.e., 23.8 ±2.4 °C) before application (Figure 3.6). The measured pH in the PHB-EL-DFO formulation was acidic (i.e., pH 4.8), still in the suitable range for the chelating action of deferoxamine B for Fe(III) (Farkas, Enyedy and Csóka, 1999; Rapti *et al.*, 2023).

Figure 3.6 Photography of the PHB-EL-DFO gel formulation in a glass petri dish once cooled down at room temperature (i.e., 23.8 ±2.4 °C) (on a white background).

3.3.3 Characterisation of the PHB-EL-DFO formulation

3.3.3.1 Rheology

The mechanical properties of the PHB-EL-DFO formulation were explored via rheology by amplitude sweep analysis. As seen previously in Chapter 2, the technique provides information about the behaviour of viscoelastic systems, such as gels, when exposed to oscillatory shear deformations at progressively increasing strain amplitudes. The measured stress response is plotted in a cartesian graph as a function of the shear strain and storage (G') and loss (G") moduli, which express the behaviour of elastic and viscous fractions, respectively, of the analysed system (Janmey, Georges and Hvidt, 2007; Samorì *et al.*, 2016).

For the PHB-EL-DFO formulation, the rheometer registered values for the storage modulus G' (i.e., formulation stiffness) approximately an order of magnitude higher than the loss modulus G" (i.e., formulation viscosity) over the linear viscoelastic (LVE) region (Figure 3.7, black plot). This region is illustrated as a plateau trend for the storage G' modulus curve and represents the range of shear strain tested for which the sample structure is not destroyed. The result obtained in the LVE region with G' > G" is distinctive for viscoelastic solids, which are characterised by strong interaction forces, and describes the PHB-EL-DFO samples as gel-like structured in rheology (Grattoni *et al.*, 2001). After leaving the LVE region, a gradual drop of the G' curve occurred, stating a non-brittle fracturing behaviour of the samples until reaching the crossover point (i.e., G' = G"). Considering the sought use of the PHB-EL-DFO organogel on metal artefacts, the registered stiffness and response to shear strain indicate appropriate characteristics, such as easy handling for operators and potentially no residues after gel removal. The formulation stiffness might also imply poor adaptability to the probable unevenness of metal surfaces. Nonetheless, the rheological behaviour registered for the PHB-EL-DFO gel is in line with previous literature related to similar PHB-based formulations successfully applied in art conservation, as in the case of PHB-EL gel employed for the cleaning of paintings, and PHB-DMC/BD (i.e., dimethyl carbonate and biodiesel) formulation exploited for the removal of wax on bronzes (Prati *et al.*, 2019; Yiming *et al.*, 2019).

Finally, a PHB-EL-DFO gel (Figure 3.7, black plot) and a re-heated one (Figure 3.7, orange plot) were examined by amplitude sweep to evaluate the thermoreversibility of the system (Borchard, 1998). The comparison of the resulting plots did not highlight a significant difference in the response when subjected to shear strain. As shown in Figure 3.7, the tested gels had comparable curve trends, similar G' and G"

moduli values in the LVE region and crossover points (i.e., G' = G"). The observed unaltered behaviour stated the thermoreversibility of the PHB-EL-DFO system. This feature could be of interest in a green perspective of waste reduction. Indeed, as verified, the gelled system was characterised by stiffness and consequently it was foreseen to be used by defining the desired shape and size of application by spatula cutting. However, this protocol would cause inevitably some non-used gel remains. Thus, the thermoreversibility of the PHB-EL-DFO gel would allow to effectively reassemble those gel pieces through a new melting process, guaranteeing the preservation of the original rheological properties in the re-formed cleaning system.

Finally, after the crossover point, the viscous portion (i.e., G") prevails on the response behaviour of the examined samples.

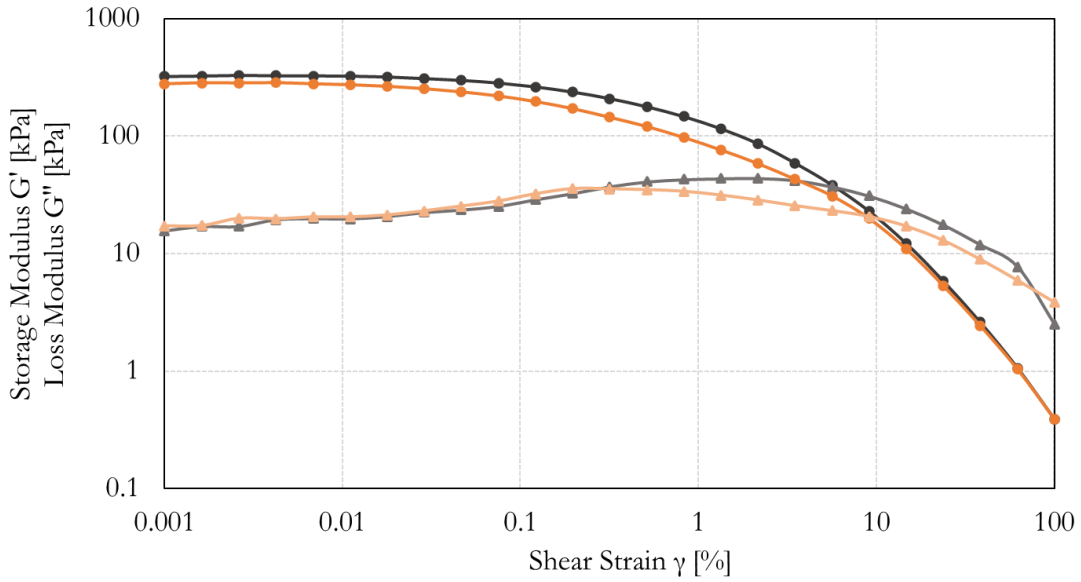

Figure 3.7 Strain dependence of storage modulus G' (circles, darker hue) and loss modulus G" (triangles, lighter hue). The amplitude sweep curves for PHB-EL-DFO formulation and re-heated formulation are plotted in black and orange, respectively.

Comparing the rheological response of the PHB-EL-DFO gel (Figure 3.8, black plot) to the PHB-EL formulation (i.e., not loaded with a DFO solution) (Figure 3.8, blue plot) subjected to the same amplitude sweep conditions, both systems showed G' > G" values over the LVE region, however their strengths (i.e., stiffness) was tested slightly different. In detail, the PHB-EL gel showed a slightly stronger structure than when retaining the DFO solution (i.e., 20% in deionised water), as presented by the G' values plotted in Figure 3.8. This outcome could possibly be linked to the hydrophobicity of poly-3-hydroxybutyrate that, in the presence of the DFO-aqueous solution might result in a structural loss in strength for the gelled system (McAdam *et al.*, 2020). However, when examining the limit of the LVE region, named yield point (τ_y) in rheology, the response of both systems was similar, presenting τ_y around a strain $\gamma = 0.02\%$ in both cases.

Observing the behaviour after the yield point, a gradual drop of the G' curves occurred for both samples, stating a non-brittle fracturing of the gels until reaching the crossover point (i.e., G' = G"). However, focusing the attention on G" curves and applying linear interpolation to the values collected during the rheological measurement, as displayed in Figure 3.8, it could be noticed that the loss modulus curve registered for the PHB-EL gel was raising before the crossover point more rapidly than in the case of the PHB-EL-DFO system. This response indicated that the PHB-EL formulation was more affected by the

phenomenon of micro-cracking before a complete structural breakdown. This last event happens when storage and loss moduli curves cross each other, hence when G' = G", and the conjunction point is denominated flow point (τ_f). In this work, the estimated τ_f for PHB-EL-DFO gel occurred approximately at strain γ = 6%, whereas it was calculated at strain γ = 1.5% for the plain PHB-EL gel. The difference was minimal, yet it would corroborate previous considerations regarding a higher stiffness and rigidity of the PHB-EL system compared to the gel loaded with the DFO solution, justifying the complete structural breakdown for PHB-EL at lower shear strains.

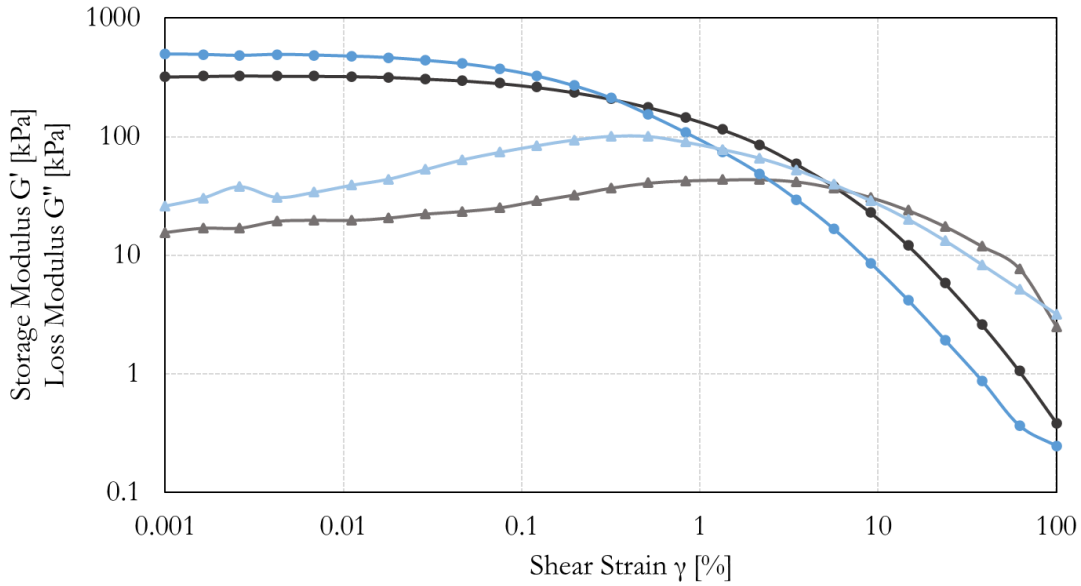

Figure 3.8 Strain dependence of storage modulus G' (circles, darker hue) and loss modulus G" (triangles, lighter hue). The amplitude sweep curves for PHB-EL-DFO and PHB-EL formulations are plotted in black and blue, respectively.

Table 3.2 Rheological response of the PHB-EL-DFO formulation compared to the plain PHB-EL gel analysed by amplitude sweep in the same conditions.

Formulation	**PHB-EL-DFO**	**PHB-EL**
LVE region	G' > G"	G' > G"
Definition	viscoelastic solid (gel)	viscoelastic solid (gel)
Yield point (τ_y)	γ = 0.02%	γ = 0.02%
Flow point (τ_f)	γ = 6%	γ = 1.5%

3.3.3.2 Cryo-Scanning electron microscopy (Cryo-SEM)

Cryo-SEM analysis was carried out to observe the inner structure of the still-moist PHB-EL-DFO gel and compare it with the PHB-EL system in order to evidence any structural variations derived from the presence of the complexing agent. The analysis was preferred to conventional scanning electron microscopy in order to avoid the slow evaporation of the liquid fraction present in the gels, which is necessary for their inspection, but would have altered their structure. On the contrary, cryo-SEM relies on the use of liquid nitrogen slush to freeze the samples instantly without modifying the inner structure (Rahbani *et al.*, 2013).

It is important to remark preliminarily that under the same experimental conditions, the PHB-EL-DFO gel did not allow to collect images at magnifications higher than 20000× without provoking damage to the samples, being more sensitive to the electron beam used for the analysis. Moreover, lower current was selected for the same reason.

Representative images acquired in back-scattered electrons (BSE) mode are reported in Figure 3.9 for both gels. In general, the two systems, analysed under the same experimental conditions, did not show significant structural differences. Indeed, the PHB-EL-DFO formulation (Figure 3.9, a and b) was characterised by a matrix densely interconnected, equal to what observed for the PHB-EL gel, as already discussed at page 83 and reported again in Figure 3.9 (c and d). Both gels presented a non-regular structure and, in accordance with previous examinations on the PHB-EL system, also the gel loaded with DFO was characterised by a plate-like structure interspersed by blocky pores. The cavities displayed a diagonal aperture that could be measured in the order of 10^{-1} – 10^{-2} μm in the case of both PHB-based systems, in the presence or not of the DFO solution. However, pores were not regularly dispersed in the PHB-EL-DFO samples (Figure 3.9, a), in line with what evidenced for the PHB-EL gel (Figure 3.9, c). Indeed, the cryo-SEM images displayed denser matrix areas, where cavities were barely visible at the magnification employed for the analysis. Such compact zones and the overall small size of pores in the PHB-EL-DFO gel would corroborate rheological measurements that stated high stiffness for the analysed samples.

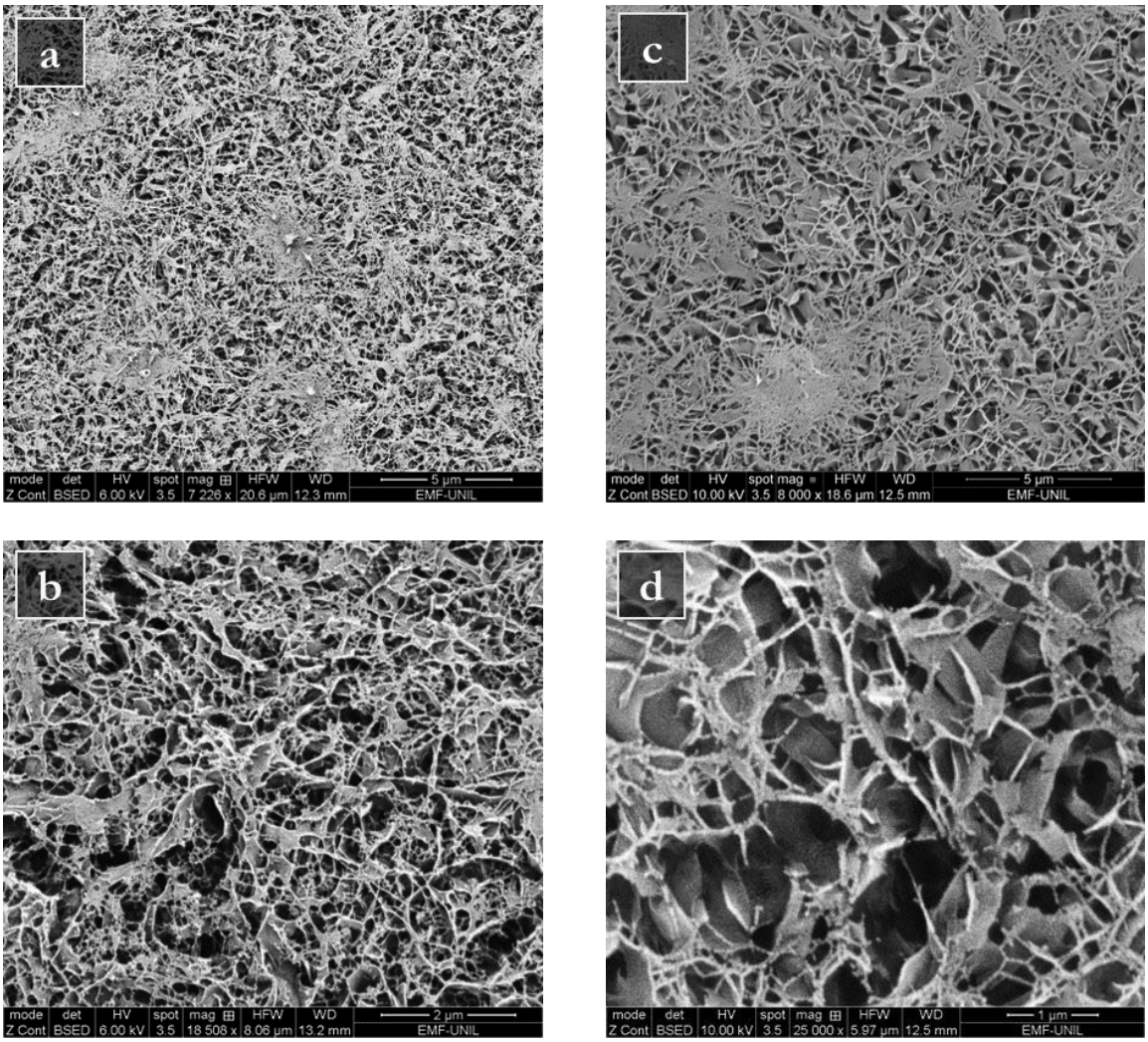

Figure 3.9 Cryo-SEM back-scattered electrons (BSE) images of PHB-EL-DFO inner structure after sublimation etching and platinum coating. Inner porosities of the PHB-EL-DFO gel (a, b) compared to the PHB-EL system (c, d). The scale bar indicates 5 µm in images a and c, 2 µm in image b, and 1 µm for image d.

3.3.3.3 Thermogravimetric analysis (TGA)

The PHB-EL-DFO gel was studied by thermogravimetric analysis (TGA) to evaluate and compare the evaporation of the embedded liquid phase and the unrestrained DFO solution (i.e., 20% in deionised water) in ethyl lactate (i.e., 1:6 v/v). The analysis was an isothermal run at 40 °C, thus the recorded weight loss could be linked entirely to the evaporation of the liquid phase present in the samples and not to polyhydroxybutyrate or deferoxamine powders, which are in a solid state at the temperature reached during the analysis (Ihnat, Vennerstrom and Robinson, 2000; McAdam *et al.*, 2020). Consequently, results shown in Figure 3.10 were calculated as weight loss percentages considering exclusively samples' liquid fraction to correctly interpret the obtained data. Additionally, the calculated first derivative of the TGA isothermal curves are displayed in SM-Figure 6 to help the visualisation of mass loss trends (i.e., evaporation rates) over time for each sample.

Thermogravimetric analysis verified that the liquid portion in the free EL-DFO-water solution (Figure 3.10, grey dashed line) was more prone to evaporation compared to when restrained in the PHB system (Figure 3.10, grey solid line) over time in the set conditions. In particular, after 60 minutes of isothermal at 40 °C, the weight of the unstrained solution dropped down to 9% of its initial value. In comparison, the EL-DFO-

water solution residually present in the gelled system was three times more, reaching approximately 28% of its starting weight.

When comparing the TGA response of plain PHB-EL gel to the PHB-EL-DFO gel considering only their liquid fractions, the two systems showed analogous behaviours over the 60-minute isothermal run, as displayed in Figure 3.10 with green and grey solid-lined plots, respectively. No significant difference could be detected and linked to the additional presence of the DFO solution.

As a final evaluation, the EL-DFO-water solution (Figure 3.10, grey dashed line) was compared to the sole ethyl lactate solvent (Figure 3.10, red dashed line), demonstrating similar rates in the set experimental conditions. However pure EL resulted in having a lower evaporation over time that could be linked to the presence of water in the EL-DFO-water sample, being water characterised by higher vapour pressure (i.e., 2.34 kPa at 20 °C) (Huang, 2018) compared to ethyl lactate (i.e., 0.27 kPa at 20 °C) (Merck, 2024a).

In general, as desired, the gelled formulation limited the unwanted loss of active solution in the atmosphere in the explored conditions. However, the values reported cannot be considered quantitatively as evaporation rates, being affected by factors such as the different geometry of the cut gel (i.e., thickness, surface) and possible partial evaporation of the solution loaded during the preparation of different specimens. Nevertheless, they provided information about the efficient retention of the active solution in the gel matrix, which can reduce the quantities to be used for a cleaning intervention.

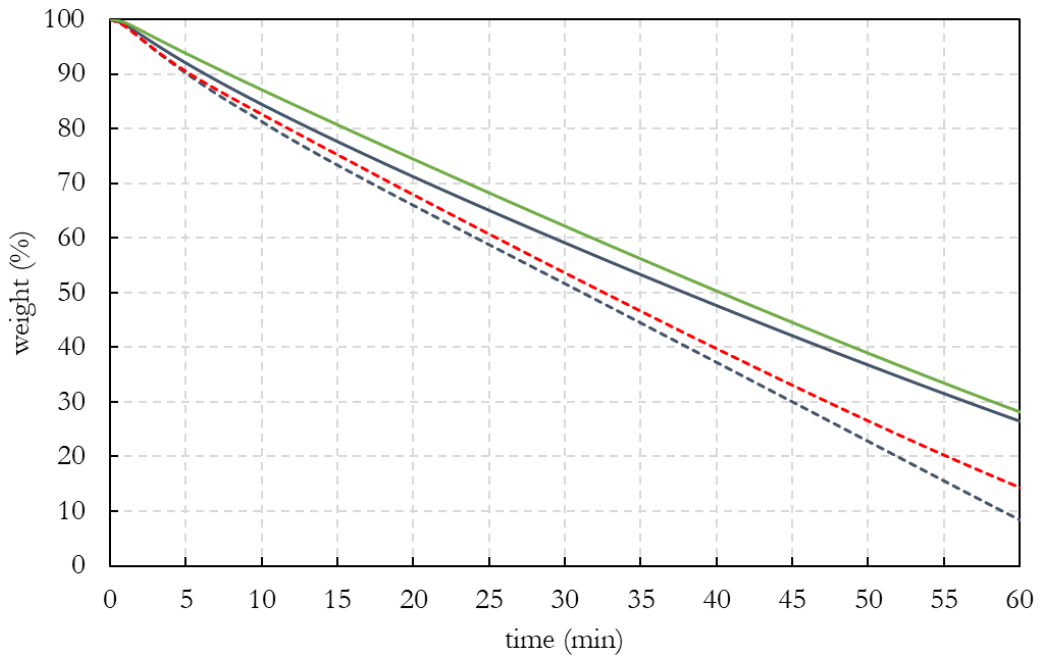

Figure 3.10 Isothermal TGA scan at 40 °C in nitrogen atmosphere comparing the weight loss of free EL-DFO-water solution (grey, dashed) to the PHB-EL-DFO gel (grey, solid). As a comparison, TGA curves for PHB-EL gel (green, solid) and neat EL solvent (red, dashed) acquired in the same experimental conditions are also reported. Data were processed considering samples' liquid fraction.

3.4 Cleaning assessment

3.4.1 Mock-up preparation

The cleaning performance of the PHB-EL-DFO organogel was assessed on steel mock-ups reproducing the co-presence of acrylic varnish (i.e., Paraloid® B72) and underlying corrosion products (i.e., iron oxyhydroxides), for their concurrent removal. For the mock-up preparation, mild steel coupons (50 × 50 ×

1 mm³) from Tartaix Métaux Outillage (France) were initially degreased by cotton swabbing using subsequently ethanol (96.0 – 97.2%) and acetone (≥99.5%) from Sigma Aldrich. Afterwards, the steel coupons were chemically aged, adjusting the protocol ASTM G48-11(2015) (Ferric Chloride Pitting Test). The metal pieces were immersed in an 11% w/v aqueous solution of iron(III) chloride hexahydrate from Carlo Erba for 24 hours. Once removed from the corrosive solution, the coupons were rinsed with deionised water, and left to dry (Figure 3.11). The protocol allowed to obtain a layer of orange-brown coloured corrosion, homogeneously distributed on the surface of mock-ups, aiding the reproducibility of the cleaning tests. Finally, the rusted coupons were coated by brush with two thin criss-cross layers of Paraloid® B72 from CTS (10% w/v solution in ethyl acetate (≥99.7%) from Sigma Aldrich), and left to dry (Figure 3.12).

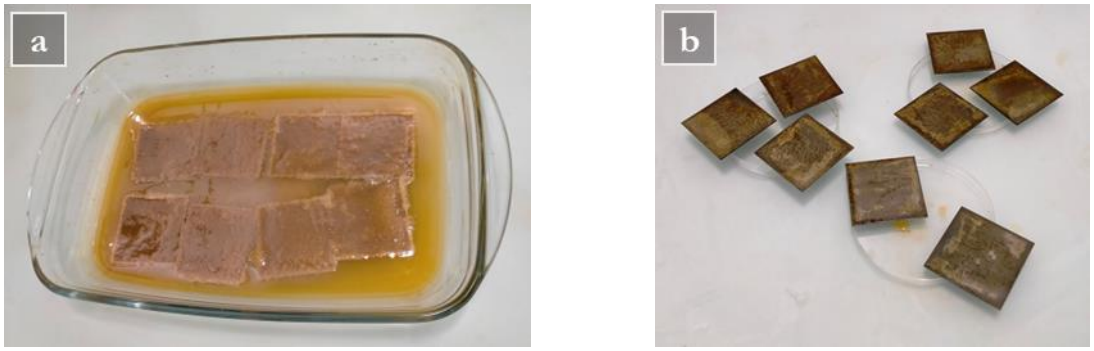

Figure 3.11 Protocol of chemical corrosion for steel coupons. Mild steel coupons (50 × 50 × 1 mm³) left in immersion in an 11% w/v solution of iron(III) chloride hexahydrate for 24 hours (a). Once removed from the corrosive solution, the coupons were rinsed with deionised water, and left to dry (b).

Figure 3.12 Mild steel coupon (50 × 50 × 1 mm³): initial aspect (left) and after ageing protocol and Paraloid® B72 coating (right).

The resulting double-target (i.e., iron corrosion compounds and organic protective film) mock-ups were characterised by Raman spectroscopy to verify the nature of the orange-brown coloured corrosion phases obtained through chemical ageing on the metallic coupons. Raman shifts typical of iron oxyhydroxides such as lepidocrocite γ-FeOOH (peaks at 248, 375, 526 and 650 cm^{-1}) and goethite α-FeOOH (245, 308 and 387 cm^{-1}) could be recognised (Figure 3.13, b-c) (Bouchard and Smith, 2003). The alternative or additional identification of akageneite (β-FeOOH, Cl) cannot be excluded when considering the overlapping signals with goethite around 310 and 395 cm^{-1}, and the use of ferric chloride hexahydrate to chemically corrode the

steel coupons (Vantelon *et al.*, 2009; Veneranda *et al.*, 2017). However, the absence of akageneite diagnostic band around 720 cm^{-1}, which is frequently used to discern between akageneite and other iron oxyhydroxides (e.g., goethite), might suggest the absence of this corrosion compound (Neff *et al.*, 2006). Additionally, Raman analysis by means of a 532-nm laser was performed to potentially favour the recognition of akageneite, according to literature (Neff *et al.*, 2006). However, the collected spectra were characterised by minor spectral features, linked to lepidocrocite, and an intense broad band detected at about 709 cm^{-1} ascribed to ferrihydrite (SM-Figure 7). Sporadically, ferric chloride hexahydrate, utilised during the chemical ageing procedure, could be detected by Raman shifts around 236, 254, 295, and 413 cm^{-1}, comparing to the collected reference spectrum (Figure 3.13, a). Finally, after coating the corroded steel pieces, additional Raman bands around 598, 836, 863, 1023, 1097 and 1111 cm^{-1} could be recognised and ascribed to Paraloid® B72, when compared to the reference spectrum collected (Figure 3.13, d-e).

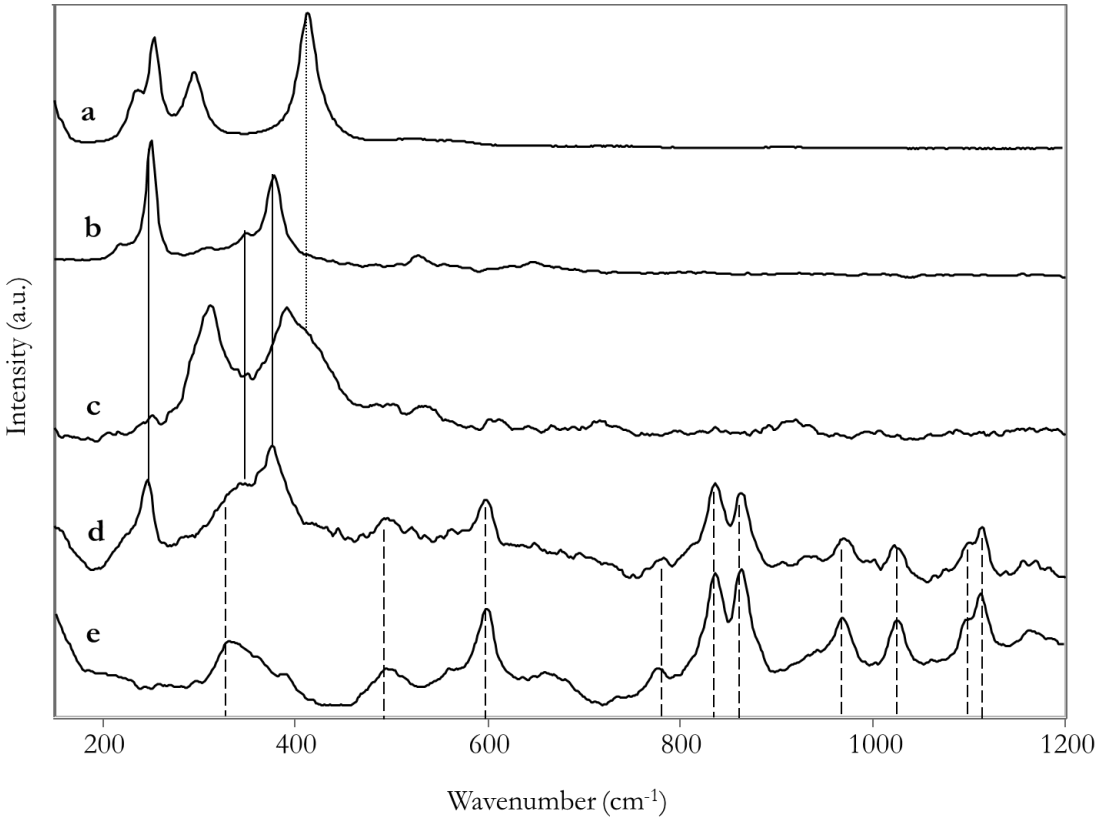

Figure 3.13 Raman spectra of ferric chloride hexahydrate (a), mild steel mock-up after chemical ageing (b, c), mild steel mock-up after chemical ageing and Paraloid® B72 coating (d), and Paraloid® B72 (e). Raman bands common among the spectra and related to ferric chloride hexahydrate (a), mild steel chemically aged (b), and Paraloid® B72 (e) are highlighted by dotted, solid, and dashed lines, respectively.

3.4.2 Cleaning protocol

The cleaning performance of the PHB-EL-DFO gel was investigated with three different application times. The organogel was assayed on triplicate mock-ups using intervals of 10, 20, and 30 minutes and by two consecutive applications, renewing the gel for each application. Longer single-application times (i.e., more than 30 minutes) were not explored because the gel would have tended to become more fragile due to solvent evaporation, and to break when removed at the end of the application, leaving residues on the treated surface. Additionally, the gradual evaporation of ethyl lactate and water would have led to poorer outcomes for Paraloid® B72 and iron corrosion removal, respectively.

After cutting in a 5-cm-diameter circle-quarter shape with a metallic spatula, the gel was applied onto mock-ups and gently pressed with the same tool to maximise the contact and avoid air bubbles between the formulation and the metal surface. On each mock-up, four equal areas were defined: three were cleaned by intervals of 10, 20, and 30 minutes respectively, and the remaining area was kept untreated as a control (Figure 3.14).

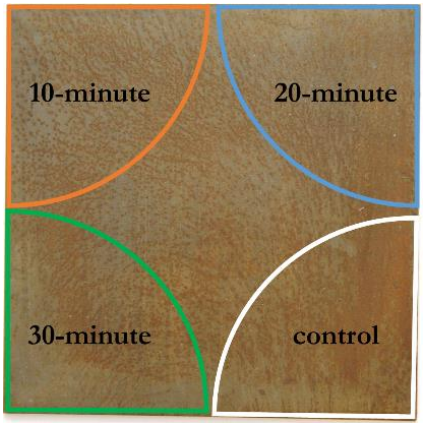

Figure 3.14 Graphical representation of the four equal areas (5-cm-diameter circle-quarters) defined on mild steel mock-ups (50 × 50 × 1 mm^3) for the PHB-EL-DFO cleaning assessment. Three areas were cleaned by intervals of 10 (top left corner, orange outline), 20 (top right corner, blue outline), and 30 minutes (bottom left corner, green outline), and a remaining area (bottom right corner, white outline) was kept untreated as a control.

After application, the gels were detached in one move by a spatula. Eventually, the mock-up surface was cleared with ethanol 70% v/v by cotton-swabbing to remove possible gel residues, swollen Paraloid® B72, and iron-DFO complexes formed during the application. Indeed, preliminary attempts demonstrated the residual presence of deferoxamine B and iron-DFO complexes, when closing the cleaning protocol solely by dry cotton swabbing, as identifiable by optical microscopy (Figure 3.15, a) and confirmed by FTIR spectroscopy applied in reflectance mode on the mock-up surface (SM-Figure 8) (Edwards *et al.*, 2005; Cozar *et al.*, 2006; Borer *et al.*, 2009). The use of an aqueous clearance solution resulted necessary to solubilise and remove the DFO-related species not entrapped on the gel surface but residually left on the metal coupon at the end of the cleaning. As displayed in Figure 3.15 b and SM-Figure 8, when clearing the same mock-up zone with ethanol 70% v/v by cotton-swabbing, the DFO-related residues are entirely removed and absent. Ethanol 70% v/v was selected as clearance solution because it is normally used by CRs to clear treated surfaces with a volatile solution that would be less prone to persist on porous substrates, such as corroded metals.

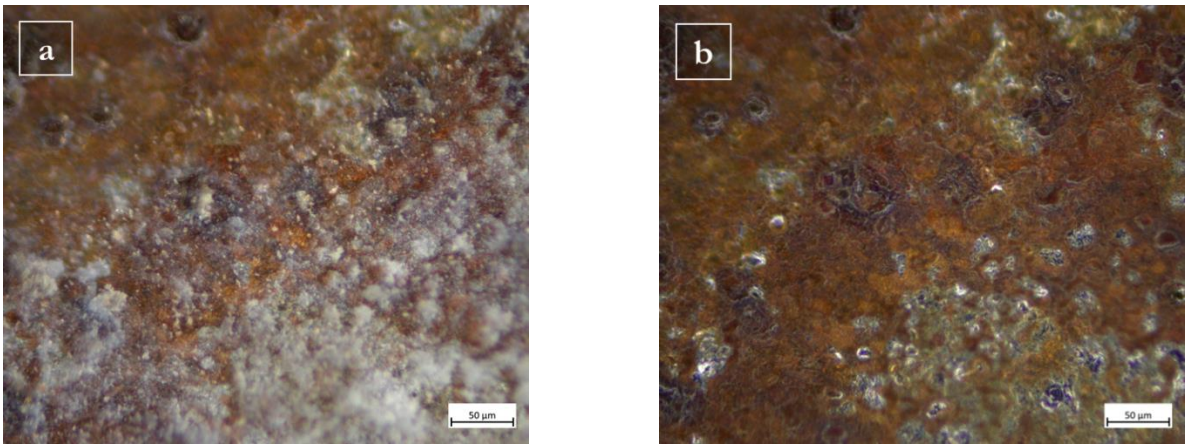

Figure 3.15 Optical microscope images, acquired in dark-field illumination, of mild steel mock-up, chemically corroded and coated with Paraloid® B72, after 10-minute PHB-EL-DFO gel application. Metal surface after dry cotton swabbing (a) and after clearing with ethanol 70% v/v solution by cotton-swabbing (b). The scale bar indicates 50 μm.

The described cleaning protocol was developed by varying only the gel application time (10, 20, or 30 minutes), while keeping constant factors such as chelating agent concentration ($4 \cdot 10^{-2}$ M) provided at each gel renewal, treated mock-up area dimensions (5-cm-diameter circle-quarter), and post-cleaning cotton-swabbing and clearance solution. Evidently, when working with a solution embedded into a gel matrix, despite providing the same concentration of active agents (i.e., DFO solution and ethyl lactate) at the start, not an equal amount will reach and interact with the target surface. This factor is due to the gel diffusion rate (Cuvillier *et al.*, 2023), which is expected to be equal for all gels employed yet leading to different outcomes in relation to the different application times tested.

3.4.3 Multi-analytical protocol for the assessment of PHB-EL-DFO gel cleaning

3.4.3.1 Visual appearance

Throughout the cleaning process, the action of the PHB-EL-DFO formulation was visually manifest and increasing with the number of gel renewals for all different application times (i.e., 10, 20, and 30 minutes) (Figure 3.16, a and SM-Figure 9). In particular, due to the gel translucence, it was possible to monitor the successful chelating action on the iron corrosion layer present on the mock-ups. Indeed, the formulation turned from whitish to bright red due to the formation of iron-DFO complexes, as reported in the literature (Bellotti and Remelli, 2021; Cuvillier *et al.*, 2022) (Figure 3.16, b).

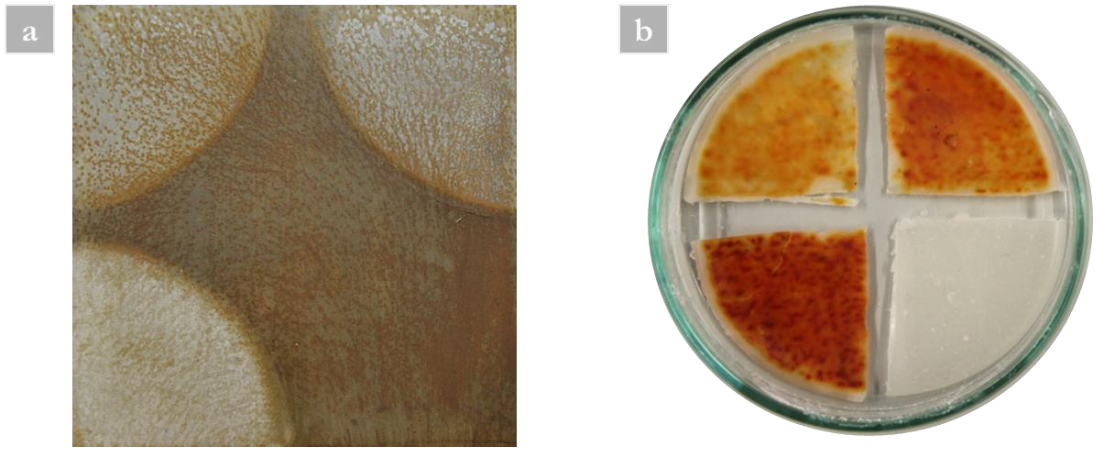

Figure 3.16 a) Chemically aged mild steel mock-up (50 × 50 × 1 mm^3), coated with Paraloid® B72, partially cleaned by PHB-EL-DFO gel. Cleaning outcomes after two gel applications of 10 (top left corner), 20 (top right corner), and 30 (bottom left corner) minutes, respectively. Bottom-right sector left untreated as a control. b) PHB-EL-DFO gels removed from the mock-up after 10 (top-left sector), 20 (top-right sector), and 30 (bottom-left sector) minutes, and PHB-EL-DFO gel not applied (bottom-right sector) as a control.

3.4.3.2 Optical microscopy

After the removal of gels and cotton swabbing of the treated zones, optical microscopy could easily emphasise the mock-up surface features. In agreement with visual observations, the treatment of 30 minutes with a gel renewal yielded a more homogeneous and efficient cleaning compared to the same protocol when opting for shorter intervals, such as 10 and 20 minutes. The mock-up zone cleaned with the 30-minute protocol showed less orange-brown rusted but more metallic grey-coloured areas, as the original appearance of the steel mock-up (Figure 3.17). No clear traces of gel residues could be observed in all treated mock-up areas. Finally, microscopic observation under UV light did not exhibit any characteristic fluorescence in the visible range, particularly the typical blue shade of Paraloid® B72, confirming the absence of possible coating remains after treatment.

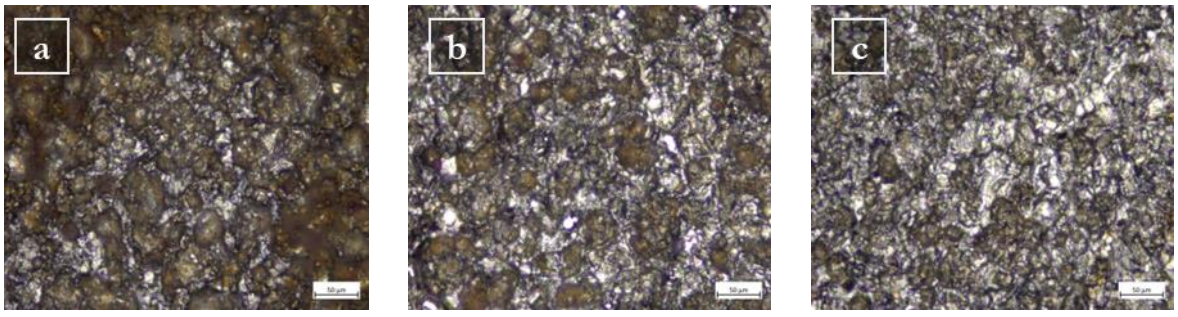

Figure 3.17 Optical microscope images (20 × magnification) in bright field of chemically aged mild steel mock-up, coated with Paraloid® B72, after two gel applications of 10 (a), 20 (b), and 30 (c) minutes, respectively. The scale bar indicates 50 μm.

3.4.3.3 Colorimetry

Colorimetric data collected on the mock-up triplicates, before and after each PHB-EL-DFO gel renewal, were consistent with the interpretation achieved by optical microscopy (raw data reported in SM-Table 4).

Comparing the CIELab coordinates, the treated areas gained brightness after cleaning intervention compared to their initial condition, as expressed by the calculated positive ΔL* values (Table 3.3). On the contrary, the obtained negative Δa* and Δb* values stated a loss in red-yellow shades on the mock-up sectors after cleaning by PHB-EL-DFO gel, referable to the removal of iron corrosion compounds thanks to the successful complexing action of deferoxamine B. As displayed in Table 3.3, this colorimetric outcome was similar for all the different application timings and was consistent with the renewal of the gel for all tested times. A final evaluation was run applying Tukey's HSD test to the colorimetric data to verify the relevance of the differences noticed among the several times and gel renewals explored in the cleaning protocol. When considering L* and a* coordinates, the analysis demonstrated that both application time and renewal were statistically relevant for the discrimination of the cleaning outcomes. It is remarkable that when comparing one application of 20 minutes to two applications of 10-min each (i.e., for a total contact time of 20 minutes) their difference was statistically relevant ($p < 0.05$), possibly showing that gel renewal was a more determinant factor rather than application time for the final cleaning outcome. This observation would be explained by both the renewal of active agent (i.e., ethyl lactate and DFO), when applying another gel, and that the intermediate clearance step could have removed residual iron-DFO complexes and swollen Paraloid® B72 when operating by 10-minute protocol. The analysis did not prove clear discrimination between the outcomes achieved by two gel applications of 20 or 30 minutes each for L* and a* coordinates ($p > 0.05$). Finally, the b* coordinate was not considered by Tukey's HSD test as a relevant factor for the distinction of the multiple cleaning outcomes.

Relating the cleaned mock-up areas to non-corroded mild steel coupons, the colour difference was still noticeable with the naked eye. In line with such perception, colorimetry, applied to cleaned sectors, confirmed a final colour difference (ΔE*) above the value of 5, which is generally considered as a threshold for clear discernment of colour difference by human eye, and thus acceptability in art conservation (Kim, Kim and Park, 2011). In general, the calculated ΔE* value decreased progressively with the number of gel renewals and for longer application times, as reported in Table 3.4. Namely, ΔE* was calculated as 19.37 (± 3.02), 15.26 (± 3.49), and 13.47 (± 2.60) for the mock-up areas treated by two PHB-EL-DFO gel applications of 10, 20, and 30 minutes respectively.

The cleaning performance evaluated by colorimetry was modest if related to the recovery of the bare steel metallic appearance. On the other hand, data showed that also when opting for long application times (i.e., 30 minutes in this study), the gelled system could provide a versatile cleaning through reiterations, preventing unsought overcleaning and guaranteeing an intervention adjustable depending on the specific case. Indeed, when treating historical metal objects, the removal of active and detrimental corrosion is typically desired while keeping a naturally aged appearance of the artefacts' surface (Cuvillier *et al.*, 2022; Guilminot, 2023).

Table 3.3 Variation of CIELab coordinates of the corroded and coated (i.e., Paraloid® B72) mild steel mock-up sectors after each cleaning step by PHB-EL-DFO gel compared to their initial condition. ΔL*, Δa*, Δb* and related ΔE* SCE values are reported along with their standard deviation into brackets.

Cleaning time	Number of gels	ΔL*	Δa*	Δb*	ΔE*
10 minutes	1	5.94 (±1.48)	-0.44 (±0.08)	-0.35 (±0.13)	5.97 (±1.47)
	2	12.48 (±1.41)	-2.21 (±0.52)	-4.48 (±0.06)	13.45 (±1.31)
20 minutes	1	10.66 (±1.89)	-1.11 (±0.01)	-3.03 (±0.06)	11.14 (±1.81)
	2	15.48 (±2.82)	-1.67 (±0.11)	-5.19 (±0.14)	16.41 (±2.66)
30 minutes	1	10.43 (±2.37)	-1.55 (±0.26)	-3.83 (±0.37)	11.22 (±2.21)
	2	17.10 (±2.06)	-2.70 (±0.61)	-7.05 (±0.84)	18.69 (±1.92)

Table 3.4 Variation of CIELab coordinates of the corroded and coated (i.e., Paraloid® B72) mild steel mock-up sectors after each cleaning step by PHB-EL-DFO gel compared to bare unaltered mild steel, used as control. ΔL*, Δa*, Δb* and related ΔE* SCE values are reported along with their standard deviation into brackets.

Cleaning time	Number of gels	ΔL*	Δa*	Δb*	ΔE*
10 minutes	1	-23.09 (±3.38)	4.93 (±2.12)	14.88 (±2.24)	27.65 (±3.06)
	2	-16.55 (±3.31)	3.16 (±1.68)	10.75 (±2.31)	19.37 (±3.02)
20 minutes	1	-17.19 (±3.06)	1.61 (±0.36)	9.25 (±1.23)	19.93 (±2.75)
	2	-12.37 (±3.99)	1.05 (±0.24)	7.09 (±1.03)	15.26 (±3.49)
30 minutes	1	-18.34 (±3.24)	2.42 (±0.76)	10.31 (±1.87)	20.94 (±2.95)
	2	-11.67 (±2.93)	1.27 (±0.41)	7.10 (±1.40)	13.47 (±2.60)

3.4.3.4 Eddy current measurements

Consistent with preceding colorimetry results, a clear reduction in the thickness of corrosion and organic coating (i.e., Paraloid® B72) present on the mock-ups was proven by Eddy current measurements. Table 3.5 displays the average values obtained on the mock-up triplicates for all areas (i.e., cleaned and untreated). In particular, higher cleaning performances, hence lower thickness, corresponded to increasing gel application times. Specifically, the device registered an average alteration thickness of 5.12 μm in the control sectors, decreasing to 3.22 μm for areas cleaned by the 10-min protocol, 2.28 μm for the 20-min protocol, and up to 1.92 μm for the 30-min protocol, respectively. The standard deviation calculated for Eddy current measurements was approximately equal for all mock-up sectors (i.e., average value around 1.39 μm) (Table 3.5). This result could be linked to the instrumental precision of the Eddy current device (i.e., ±0.7 μm + 1% of value) and mostly to common irregularity of corrosion layers present on iron, which still affect the substrate morphology also once cleaned, as already shown in Figure 3.17. Moreover, being the value consistent among the measurements, it indicated a homogeneous cleaning effect of the PHB-EL-DFO system on the altered mock-ups.

Finally, in order to consider collected data from a statistical perspective, Tukey's HSD test was applied to evaluate the outcomes yielded at the end of the three cleaning treatments (i.e., 10-, 20- and 30-minute protocols). The analysis demonstrated that Eddy current values could evidence the difference compared to the initial condition of mock-ups ($p < 0.05$), but no statistically significant discrimination was evaluated for 20- and 30-minute cleanings ($p > 0.1$). The outcome was considered in accordance with what was observed for colorimetric data employing the same statistical approach.

Table 3.5 Average alteration layer thickness (i.e., corrosion and Paraloid® B72) measured by Eddy current for chemically corroded mild steel mock-ups, coated with Paraloid® B72, left untreated as control and cleaned with 10-, 20-, and 30-minute protocols with double PHB-EL-DFO gel application. Values are reported along with their standard deviation into brackets.

Cleaning protocol	Alteration thickness (μm)
None (control)	5.12 (±1.69)
10-minute	3.22 (±1.28)
20-minute	2.28 (±1.30)
30-minute	1.92 (±1.30)

3.4.3.5 X-Ray Fluorescence (XRF) spectroscopy

Elemental analysis was carried out by means of X-ray fluorescence spectroscopy on the PHB-EL-DFO gels in order to verify the origin of the red colouration gained by the system after application on mock-ups. In particular, a comparison was addressed between the gel before and after one application of 10 minutes (Figure 3.18). The technique revealed the presence of iron only after the gel was applied on the mock-up. The XRF peaks detected at approximately 6.4 and 7.05 keV correspond to the Kα1 and Kα2 lines characteristic for iron (Figure 3.18, black spectrum), and are absent in the XRF spectrum collected for the gel before application (Figure 3.18, grey spectrum). The signal detected around 2.3 keV was associable with Kα1 and Kα2 lines of sulphur. This element is registered in the gel sample before and after application, and it is connected to the fact that deferoxamine B in the product Desferal® is in the form of mesylate salt (i.e., sulfonate groups). Finally, the signals recorded at 8.73 keV and in the spectral region above 16 keV were not linked to the gel system but to the instrument X-ray tube anode in molybdenum.

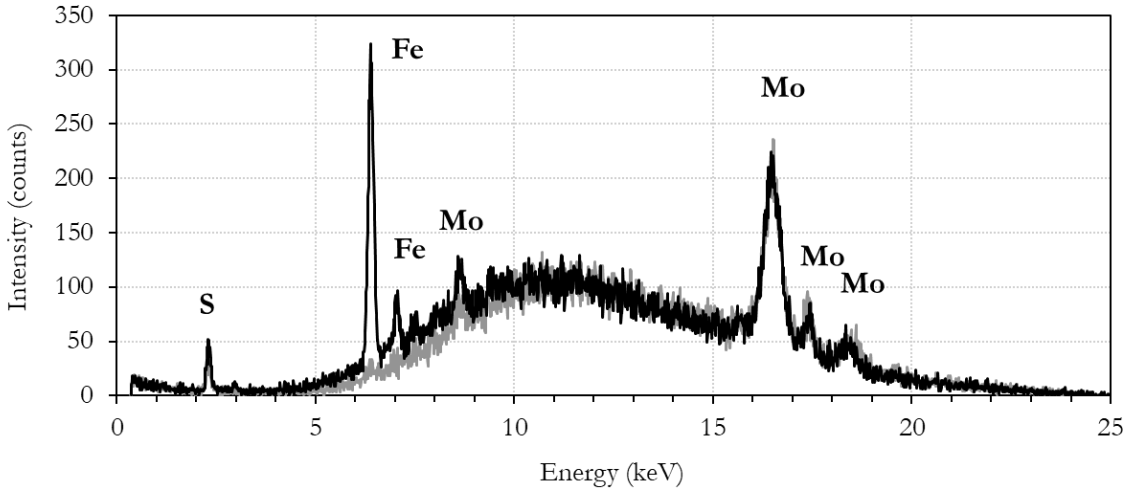

Figure 3.18 XRF spectra of PHB-EL-DFO gel before (grey) and after one application of 10 minutes on a mild steel corroded mock-up coated with Paraloid® B72 (black). Found elements are reported in the figure above the corresponding signals.

3.4.3.6 Vibrational spectroscopy: Raman and Fourier-transform infrared (FTIR) spectroscopy – Gel characterisation

Initially, reference Raman and FTIR spectra were collected for both DFO powder and iron-DFO complexes, obtained by a 1:1 molar mixture of standard ferric oxyhydroxides (FeOOH, Sigma Aldrich) in a DFO-water solution (20% w/v) (Figure 3.19). In few minutes, the solution turned from non-coloured to vivid red, as expected, because of the effective complexing action of DFO towards iron ions (Bellotti and Remelli, 2021).

Figure 3.19 Vial containing a standard powder of ferric oxyhydroxides (Sigma Aldrich) in a DFO-water solution (20% w/v).

The Raman spectra recorded for the two species are in accordance with the literature (Edwards *et al.*, 2005; Cozar *et al.*, 2006), as shown in Figure 3.20, and most diagnostic bands are listed and assigned to molecular vibrations in Table 3.6. In particular, the iron-DFO complexes resulted in being clearly discernible from DFO due to the Raman-active vibrations around 580 and 1573 cm^{-1}, respectively linked to Fe–O stretching and C=N stretching (i.e., amide functional group) vibrations derived from the complexation to Fe(III) (Cozar *et al.*, 2006). On the other hand, FTIR spectra, collected in ATR mode for the two species, are not always fitting with the spectra reported in the literature (Edwards *et al.*, 2005; Cozar *et al.*, 2006; Borer *et al.*, 2009). The spectra obtained for iron-DFO complexes frequently present additional bands related to DFO, as shown in Figure 3.21 and listed in Table 3.7. This may be due to DFO partially not being complexed to iron ions. Nonetheless, previous research demonstrated significant wavenumber variations when comparing theoretical and experimental FTIR outcomes for deferoxamine B and its iron-complexed form (Edwards *et al.*, 2005; Borer *et al.*, 2009). Moreover, when comparing IR data, the acquisition mode is a critical aspect that may determine differences in terms of peak intensity (e.g., different penetration depth of IR radiation) and position (e.g., reflective index influence when working in reflectance mode) (Hosseinpour and Johnson, 2017). Yet, the iron-DFO system could be discerned thanks to the significant shift of the FTIR band at 1622 cm^{-1} for DFO to 1637 cm^{-1} in the complexed form, linked to the C=O stretching vibration of the hydroxamate groups whose oxygen atoms bonded with Fe(III) ions (Cozar *et al.*, 2006).

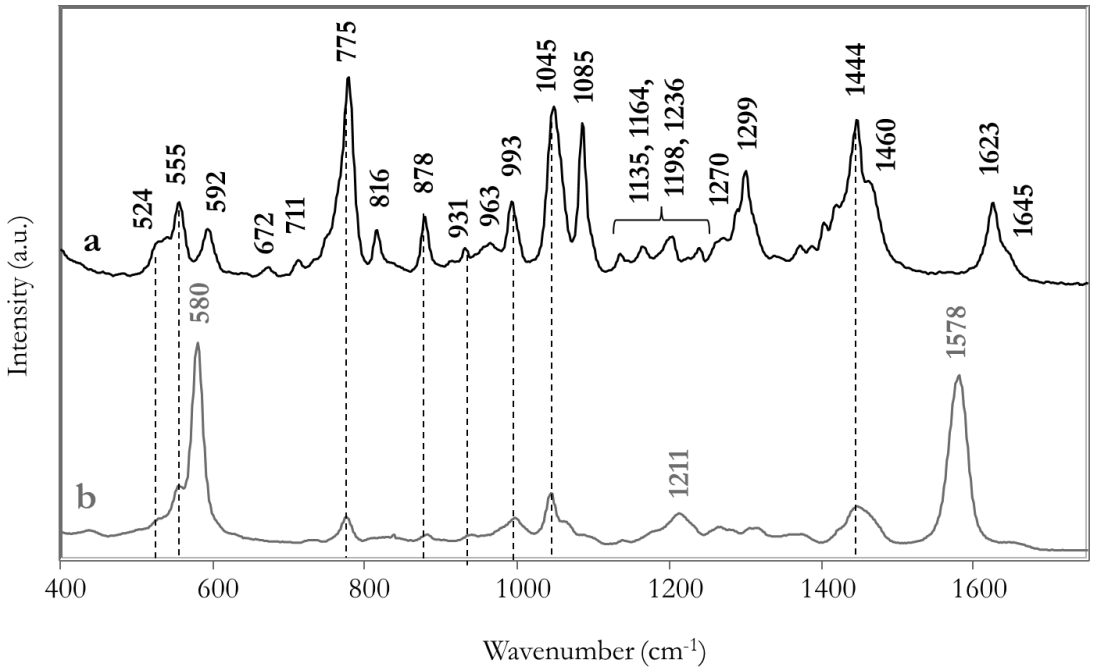

Figure 3.20 Raman spectra of DFO powder (a) and iron-DFO complexes (b). Raman bands related to DFO (a) also detected for iron-DFO complexes (b) are highlighted by dashed lines. The wavenumbers of Raman peaks diagnostic for DFO and iron-DFO complexes are reported in the figure above the respective spectra.

Table 3.6 Characteristic Raman signals detected for DFO and iron-DFO complexes (Edwards *et al.*, 2005; Cozar *et al.*, 2006).

DFO		**Fe-DFO complexes**		**Assignment**
		580	vs	ν(Fe-O)
775	vs	775	m	ν(C-N-C)
993	m	993	w	ν(C-N-C)
1045	vs	1045	m	ν(C-C), ν(N-O), ν(C-N)
1085	vs			ν(C-C), ν(N-O)
		1211	m	ν(C-C)
1299	s			ν(C-N)
1444	vs	1444	m	δ(C-H), δ(N-H)
1460	sh			δ(C-H), δ(NOH), ν(C-N)
		1578	vs	ν(C=N), δ(N-H), δ(CH_3)
1623	s			ν(C=O)

vs = very strong, s = strong, m = medium, w = weak, sh = shoulder signal; ν = stretching, δ= bending. All values are expressed in cm^{-1}.

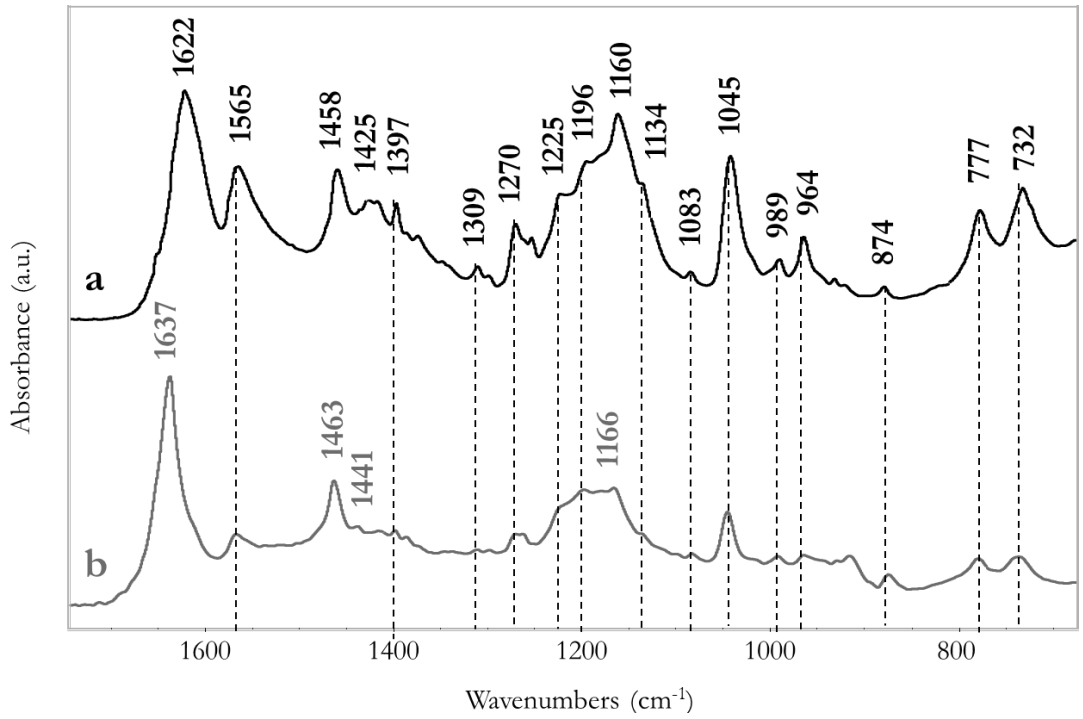

Figure 3.21 ATR-FTIR spectra of DFO powder (a) and iron-DFO complexes (b). Characteristic bands related to DFO (a) also detected for iron-DFO complexes (b) are highlighted by dashed lines. The wavenumbers of IR signals diagnostic for DFO and iron-DFO complexes are reported above the respective spectra.

Table 3.7 Characteristic FTIR signals detected for DFO and iron-DFO complexes (Edwards *et al.*, 2005; Cozar *et al.*, 2006; Borer *et al.*, 2009).

DFO		Fe-DFO complexes		Assignment
1622	vs	**1637**	vs	ν(C=O)
1565	s	1565	w	δ(N-H), ν(C-N), δ(CH_3)
1458	s	1463	m	δ(NOH), ν(CN), δ(C-H)
		1441	vw	δ(N-H), δ(C-H)
1425	m			δ(CCN), δ(CCC), δ(C-H)
1397	m	1397	vw	δ(CH_3)
1270	m	1270	w	ν(C-C)
1225	m	1225	m	ν(C-C)
1196	s	1196	m	ν(C-C)
1160	vs	1166	m	ν(C-C)
1134	sh	1134	sh	ν(SO_3)
1045	vs	1045	m	ν(C-C), ν(C-N), ν(C-O)
777	m	777	w	δ(CH_2)

vs = very strong, s = strong, m = medium, w = weak, vw = very weak, sh = shoulder signal; ν = stretching, δ= bending. All values are expressed in cm^{-1}.

As previously discussed, X-ray fluorescence spectroscopy demonstrated the presence of iron for PHB-EL-DFO gels after application. Raman spectroscopy, performed on the same samples, could link the elemental outcome to the presence of iron-DFO complexes that are formed during the cleaning process and confined within the gelled system. The analysis carried out on still-moist gels, specifically on the side that was in contact with mock-ups, revealed characteristic Raman bands distinctive for iron-DFO complexes around

580 (Fe–O stretching) and 1573 cm^{-1} (C=N stretching), which were absent on the gel surface previous application (Cozar *et al.*, 2006) (Figure 3.22).

On the contrary, FTIR did not yield a clear identification of DFO species on the used PHB-EL-DFO gel, because of the predominant spectral features related to the PHB matrix.

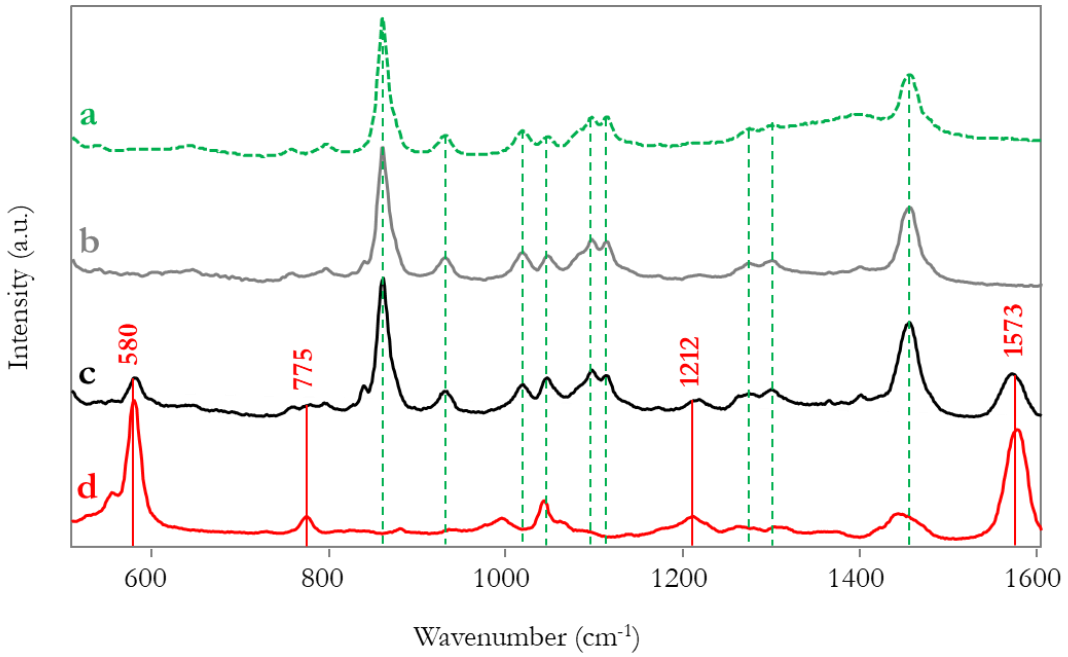

Figure 3.22 Raman spectra of ethyl lactate (a), PHB-EL-DFO still-moist gel before application (b), PHB-EL-DFO still-moist gel after one application of 10 minutes (c), and iron-DFO complexes (d). Raman bands related to ethyl lactate (a) and iron-DFO complexes (d) are highlighted by dashed and solid lines, respectively. The wavenumbers of Raman peaks diagnostic for iron-DFO complexes are reported in the figure.

Paraloid® B72 was not detected applying either Raman or FTIR spectroscopy directly on the PHB-EL-DFO gel after 10-minute application, even after letting the gel dry in order to bypass the unwanted spectral information related to solvents present in the system (i.e., ethyl lactate and water). Therefore, gels were submitted to extraction by acetone (≥99.5%, Sigma Aldrich) to solubilise potential deposits of the acrylic coating present on the used gel. The collected extraction residue could be ascribed to Paraloid® B72 by means of both Raman and FTIR spectroscopy when compared to the reference spectrum of the material, as reported in Figure 3.23 and Figure 3.24, respectively. These data confirmed that the PHB-EL-DFO formulation could tackle the organic coating already with a short-time application. Moreover, Paraloid® B72 was absorbed by the gel itself during the cleaning process on test mock-ups.

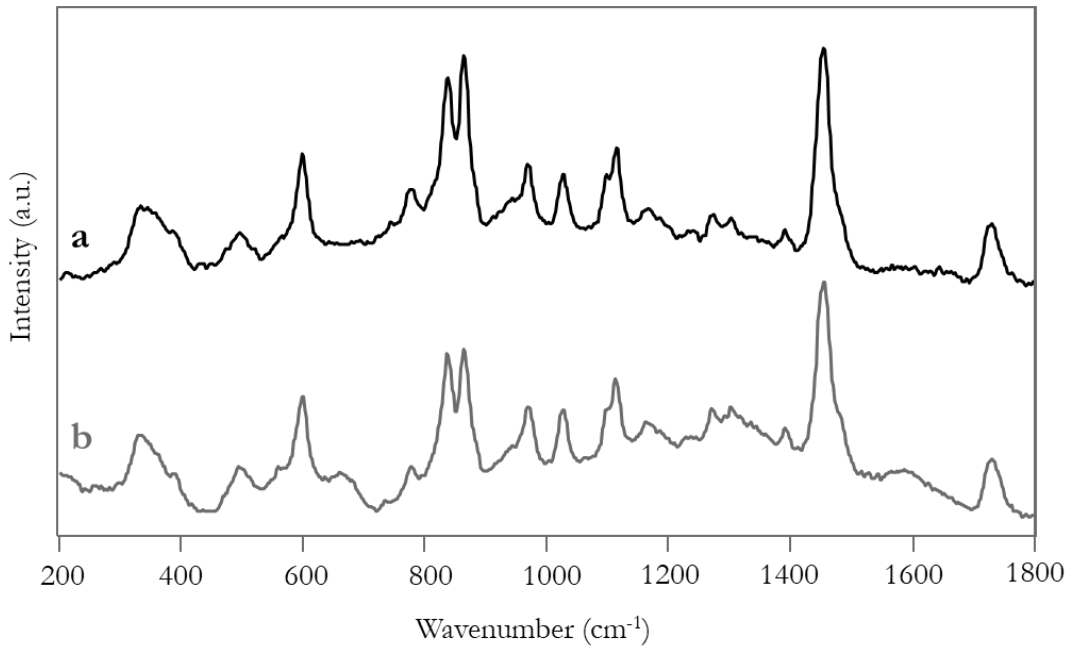

Figure 3.23 Raman spectra of Paraloid® B72 (a) and extraction residue from PHB-EL-DFO gel after one application of 10 minutes (b).

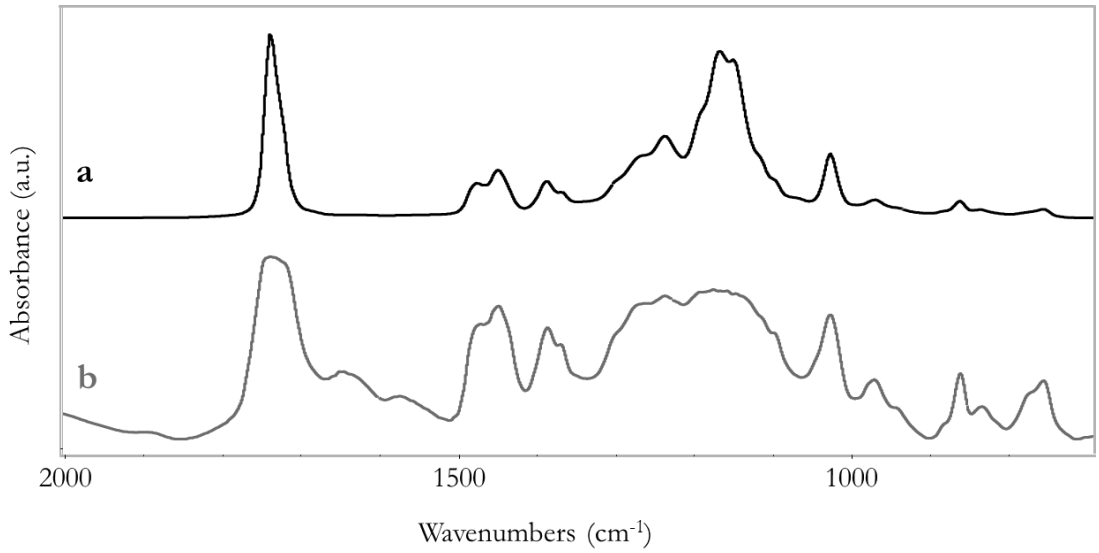

Figure 3.24 FTIR spectra, collected in reflectance mode, of Paraloid® B72 (a) and extraction residue from PHB-EL-DFO gel after one application of 10 minutes on chemically aged mild steel mock-ups coated with Paraloid® B72 (b).

3.4.3.7 Raman spectroscopy – Mock-ups

Raman spectroscopy was performed on treated areas of mock-up replicates before and after gel application.

After gel application, the collected spectra did not show the presence of Paraloid® B72 on the metal surface, potentially due to either a response under the Raman limit of detection or a complete removal of the acrylic coating. On the contrary, lattice vibrations at low wavenumbers (i.e., 88 and 143 cm^{-1}), coming from bare steel, were collected on the cleaned zones of the mock-up (Figure 3.25, a). Additionally, remaining iron

oxyhydroxides, namely lepidocrocite, could be identified thanks to the most intense and characteristic Raman peaks around 246 and 378 cm^{-1} (Figure 3.25, b). It is not straightforward to read the presence of residual iron corrosion compounds from a quantitative perspective to compare before and after cleaning. Indeed, even though the intensity of a Raman peak is proportional to the analyte concentration, factors such as matrix absorption, surface inhomogeneity and laser beam focusing complicate the quantitative interpretation of Raman data (Vandenabeele, 2013).

Overall, no significant wavenumber shifts or new Raman bands were observed on the mock-up treated areas, revealing no modification in the corrosion phases that could have potentially derived from the interaction with the PHB-EL-DFO gel. In particular, in the spectral range (500-1600 cm^{-1}) where iron-DFO complexes have the most diagnostic Raman peaks (Table 3.6), no evident vibrational bands related to these species were detected, thus underlining the absence of eventual cleaning gel residues.

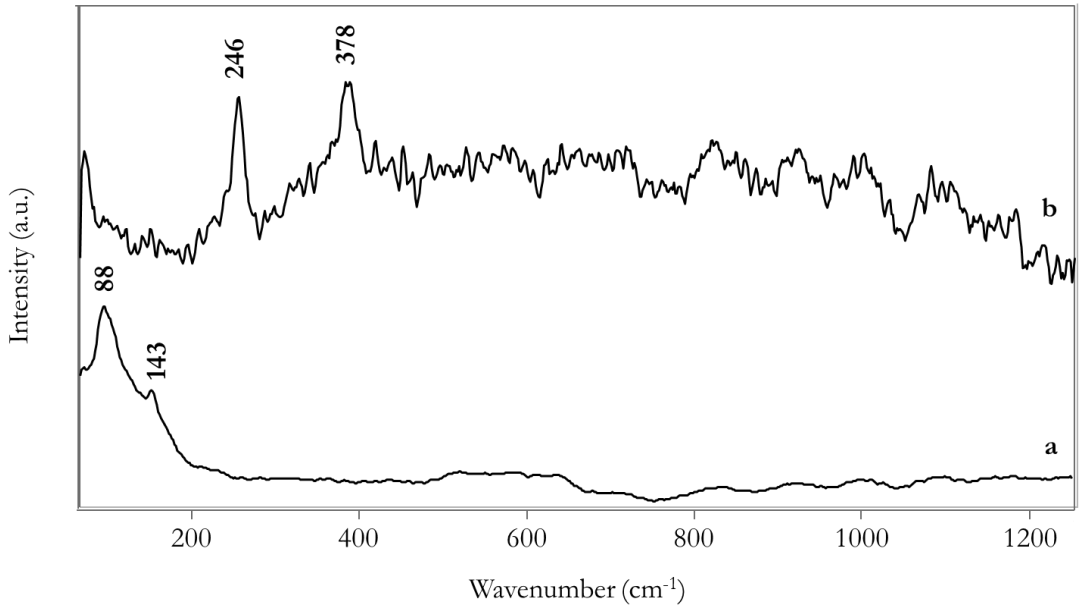

Figure 3.25 Raman spectra collected from chemically aged mild steel mock-up, coated with Paraloid® B72, after the cleaning protocol. Typical signals related to lattice vibrations (i.e., bare steel) (a) and remaining iron oxyhydroxides (i.e., lepidocrocite) (b) are reported in the figure.

3.4.3.8 Fourier-transform infrared (FTIR) spectroscopy – Mock-ups

FTIR spectroscopy in reflectance mode was applied on mock-up replicates to monitor the effect of different PHB-EL-DFO gel application times. The resulting spectra (raw data are displayed in SM-Figure 10) were elaborated by Principal Component Analysis (PCA) to ease the readability of the information collected and highlight differences related to the several applications and timings explored. Specifically, multivariate analysis was applied to FTIR spectra because the technique could provide trackable spectral features for both steel corrosion (i.e., lepidocrocite) and organic coating (i.e., Paraloid® B72) present on the model samples, resulting in being effective for the monitoring of the gel cleaning action.

In Figure 3.26, PC1 versus PC2 scatter plot allowed to obtain information on the effect of the different cleaning times and reiterations. To this aim, also FTIR data collected from bare mild steel coupons were reported as references. The related loadings plot for PC1 vs PC2 reports the spectral variables (i.e., wavenumbers) more involved in the discrimination (i.e., clusters position along the PC axes). Specifically, the presence of variables between 1710 and 1740 cm^{-1} was ascribed to the absorption band of Paraloid® B72 at about 1727 cm^{-1} related to C=O stretching vibration (Lazzari and Chiantore, 2000), whereas variables

between 1000 and 1040 cm^{-1} may be referred to iron corrosion products, which were specifically tracked by the Fe-OH bending vibration at 1025 cm^{-1}, characteristic for lepidocrocite (Petrovic, Stevula and Pisarcik, 1985). Consequently, the residual presence after cleaning of lepidocrocite and Paraloid® B72 could be displayed along PC2 positive and negative values, respectively (Figure 3.26). This outcome allowed to clearly differentiate mock-up areas cleaned by one 10- and 20-minute (Figure 3.26, black and green, respectively) and two 10-minute (Figure 3.26, red) gel applications from the others and, most relevantly, from the cluster of bare mild steel coupons used as controls (Figure 3.26, yellow). Most importantly, the result showed an overlapping of FTIR data related to bare mild steel coupons, used as reference, and mock-up areas treated with the PHB-EL-DFO gel for 30 minutes with a reiteration. This evidence would prove a successful cleaning level achieved by the innovative system with an effective removal of Paraloid® B72 and iron corrosion products, thanks to the concurrent action of ethyl lactate and DFO embedded in the gelled system.

Finally, FTIR mapping was performed on mock-up replicates after cleaning to check the potential presence of organogel residues. In particular, it was considered the FTIR band at 1045 cm^{-1}, which is characteristic for both DFO and iron-DFO complexes (i.e., C–O stretching and resonative O=C–N bond, Table 3.7), and distinguishable from other vibrational bands in the considered spectral range (Cozar *et al.*, 2006). The resulting FTIR chemigrams did not indicate the presence of DFO-related post-cleaning residues on the treated areas of the mock-ups (SM-Figure 11).

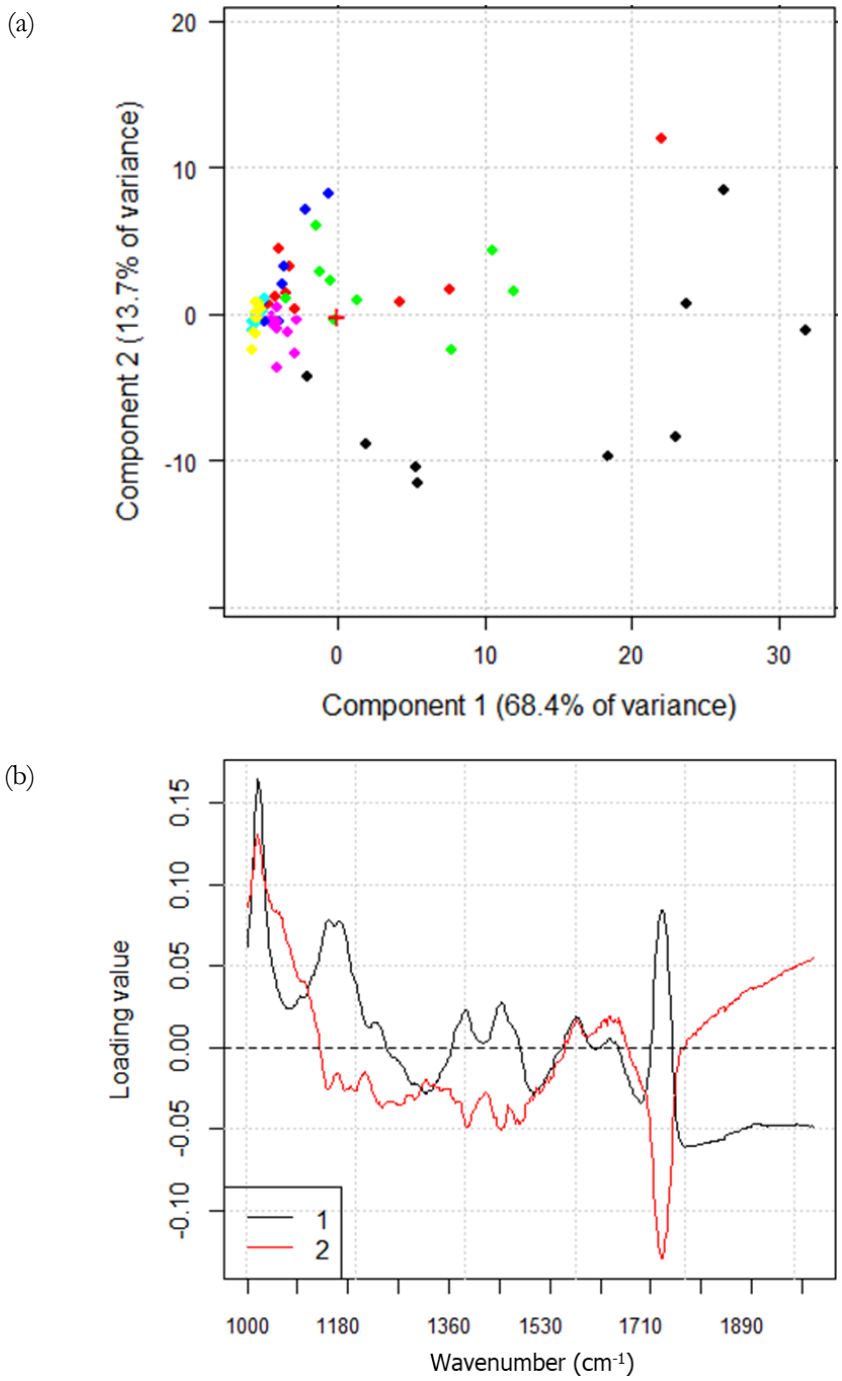

Figure 3.26 Score (a) and loading (b) plots obtained from PCA applied to FTIR spectra recorded on chemically aged mild steel mock-ups, coated with Paraloid® B72, cleaned by one 10-minute (black), two 10-minute (red), one 20-minute (green), two 20-minute (blue), one 30-minute (purple), and two 30-minute (turquoise) gel applications, and untreated bare mild steel coupons (yellow). (b) Related PC1 (black) and PC2 (red) loading plot.

3.4.3.9 Electrochemistry

Electrochemical analysis was performed on the surface of mild steel coupons to measure the polarisation resistance (*R*p) of the metallic sheets and provide some considerations on the long-term behaviour, in particular, of mock-ups cleaned by PHB-EL-DFO gel. Measurements were carried out in triplicates for mock-ups presenting different conditions (Figure 3.27):

a. Bare mild steel;
b. Bare mild steel after 3-month ageing in a climatic chamber;
c. Chemically corroded mild steel coated with Paraloid® B72 cleaned by double 30-minute application of PHB-EL-DFO gels;
d. Chemically corroded mild steel coated with Paraloid® B72, cleaned by double 30-minute application of PHB-EL-DFO gels, and finally aged for three months in a climatic chamber.

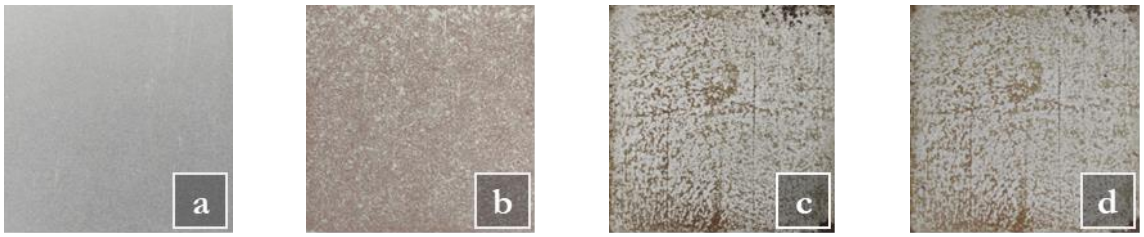

Figure 3.27 Photographs of bare mild steel coupons (50 × 50 × 1 mm^3) before (a) and after 3-month ageing in a climatic chamber (b) and chemically corroded mild steel coupons cleaned by two 30-minute applications of PHB-EL-DFO gels before (c) and after 3-month ageing in a climatic chamber (d).

Calculated average polarisation resistance values are reported in Table 3.8. It is important to mention that collected electrochemical data were not screened by statistical analysis (e.g., ANOVA) due to the scarce number of measurements available (i.e., triplicates per each coupon series). The interpretation was therefore addressed from a qualitative perspective, comparing rather magnitudes and changes among the different mock-up series.

Except for bare mild steel samples, all average *R*p values were correlated by high standard deviations, as visible in Table 3.8. Great data dispersion was considered unavoidable when working on corroded, hence irregular, surfaces such as corroded steel mock-ups; on the contrary, this effect was not registered for the flatter and more even surface of bare steel sheets. Remarkably, the impact on data dispersion was attributed exclusively to mock-up features and not to a possible uneven contact between the metal surface and the electrolyte loaded in an agarose matrix. Previous research, indeed, verified good adaptability of the gelled system to irregular metal surfaces, including corroded iron-based substrates (i.e., weathering steel) (Ramírez Barat and Cano, 2019).

In the case of bare mild steel coupons subjected to three-month ageing in a climatic chamber, a thin layer of powder-like corrosion was developed on their surface (Figure 3.27, b). The growth of a corrosion layer over the steel sheets was acting as a barrier, reducing the exposure of the bare metal surface to the electrolyte, and in consequence, increasing the measured polarisation resistance (50.3 (±41.9) kΩ cm^2) compared to the initial condition (Petiti *et al.*, 2020). Indeed, in the case of bare mild steel pieces, there were no "obstacles" (i.e., corrosion products) for the electrolyte to react with the metallic surface, hence the device registered a lower average *R*p value equal to 11.5 (±0.13) kΩ cm^2 (Table 3.8).

Focusing the attention on cleaned mild steel mock-ups, higher values of polarisation resistance were measured for the before-ageing series compared to after-ageing samples, which would be in antithesis to the explanation provided for bare steel coupons (Table 3.8). Micro-Raman spectroscopy was performed on the mock-up surfaces, without highlight differences between the several samples that were characterised by iron hydroxides corrosion products. A possible interpretation of *R*p data could be linked to the fact that cleaned mock-ups, as observed (Figure 3.27), were still presenting corrosion products that could not be removed by the PHB-EL-DFO cleaning treatment. It was therefore supposed that those species were compact and well-adherent to the metal substrate, hence possibly protective for the mock-ups (Rp = 71.6 (±58.5) kΩ cm^2). After subjecting those coupons (i.e., cleaned mock-ups) to artificial ageing in a climatic

chamber, the newly formed corrosion layer was powdery, as previously observed for bare steel pieces aged in a climatic chamber with the same protocol. The presence of such form of corrosion layer would therefore reduce the Rp value registered in this study, being not adherent and thus not protective (27.1 (±25.9) kΩ cm^2). Additionally, since the mock-ups were initially chemically etched (i.e., corroded), they were characterised by a larger specific surface than bare mild steel sheets. Consequently, when cleaned mock-up were artificially aged in the climatic chamber, the effective exposed surface was higher than the one of bare steel sheets subjected to the same ageing conditions, thus their Rp was lower (i.e., more surface was getting corroded) (27.1 (±25.9) kΩ cm^2) compared to the other series of coupons (50.3 (±41.9) kΩ cm^2) (Table 3.8).

Table 3.8 Average values of polarisation resistance (*R*p) measured for bare mild steel and chemically corroded and coated (i.e., Paraloid® B72) mild steel after cleaning by PHB-EL-DFO gel (i.e., 30-min × 2 applications). Data collected before and after ageing in a climatic chamber are reported. All values are expressed in kΩ cm^2.

	Before ageing	*After ageing*
Bare steel	11.5 (±0.1)	50.3 (±41.9)
Cleaned steel mock-ups	71.6 (±58.5)	27.1 (±25.9)

3.5 Conclusions

A new green organogel could be designed with the innovative outlook to simultaneously tackle inorganic compounds and organic substances as undesired materials on the surface of indoor steel artworks. Specifically, the cleaning targets chosen in this study were an acrylic coating (i.e., Paraloid® B72) and the underlying iron corrosion (i.e., iron oxyhydroxides).

Great attention was addressed to the selection of the gel system components in line with the Green Chemistry perspective (Anastas and Eghbali, 2010). Poly-3-hydroxybutyrate (PHB), ethyl lactate (EL), and deferoxamine B (DFO) were employed as thickening agent, organic solvent, and complexing agent, respectively. All components respected the principles of biodegradability, renewability of the source of production, and were inherently low or non-toxic. The formulation was designed considering several limiting factors, including the solubility of the DFO powder, the hydrophobicity of the PHB polymer, the DFO resistance to high temperatures reached for the gelation of the PHB-based formulation.

Mild steel mock-ups chemically corroded and coated by Paraloid® B72 were employed for the assessment of the cleaning performance of the organogel. Tukey's HSD test evidenced that colorimetric and eddy current measurements could be reliable methods for the evaluation of the cleaning outcome on steel. Most importantly, statistical analysis demonstrated that gel renewal (and possibly consecutive clearance steps) was a more relevant variable compared to application time, for the intervals explored in this research (i.e., 10, 20, 30 minutes, with and without reiteration). The final outcome did not yield a full recovery of the metallic appearance of bare steel, however normally this level of cleaning is not sought when operating on historical metals. On the contrary, a moderate, adjustable, and well-localised action could be recognised by the use of the PHB-EL-DFO system.

X-Ray fluorescence, Fourier-transform infrared and Raman spectroscopy proved the presence of iron-DFO complexes in the gel after application, ascertaining the effectiveness of the complexing solution when retained in the polyhydroxybutyrate-based system. This is an interesting outcome considering that frequently poor contact, thus interaction between cleaning system and altered metallic surfaces, is achieved when employing rigid and stiff gels (e.g., agar pre-formed gels) (Cuvillier *et al.*, 2023). Finally, the PHB-EL-DFO gel was able to tackle simultaneously the two undesired materials (i.e., corrosion products and organic

lacquer) as demonstrated by Principal Component analysis applied to FTIR spectra collected from the treated mock-ups along the cleaning assessment. In parallel, electrochemical measurements would suggest that residual corrosion products present on the surface of cleaned mock-ups were possibly well-adherent and protective against the spontaneous process of re-corrosion compared to bare mild steel substates (i.e., higher polarisation resistance).

At the moment, an aspect that can be read as a drawback is the necessary need of water for the dissolution of DFO powder (i.e., in this study, in the form of the commercial product Desferal®) and formed iron-DFO complexes after gel application. This limiting factor, however, might be possibly overcome by the use of pure deferoxamine B that was proven to be soluble in ethanol (Rapti *et al.*, 2023).

Bibliography

Albelda-Berenguer, M., Monachon, M. and Joseph, E. (2019) Siderophores: From natural roles to potential applications. 1st edn, Advances in Applied Microbiology. 1st edn. Elsevier Inc. Available at: https://doi.org/10.1016/bs.aambs.2018.12.001.

Anastas, P. and Eghbali, N. (2010) 'Green Chemistry: Principles and Practice', Chem. Soc. Rev., 39(1), pp. 301–312. Available at: https://doi.org/10.1039/B918763B.

Angelini, E. and Argyropoulos, V. (2008) 'PROMET state-of-the-art approach for protecting, preserving, and interpreting metals from museums in the Mediterranean basin', in V. Argyropoulos (ed.) Metals and Museums in the Mediterranean. Protecting, Preserving and Interpreting. TEI (Athens), pp. 23–37.

Bellotti, D. and Remelli, M. (2021) 'Deferoxamine B: A Natural, Excellent and Versatile Metal Chelator', Molecules, 26(11), p. 3255. Available at: https://doi.org/10.3390/molecules26113255.

Bentur, Y., McGuigan, M. and Koren, G. (1991) 'Deferoxamine (Desferrioxamine) New Toxicities for an Old Drug', Drug Safety, 6(1), pp. 37–46. Available at: https://doi.org/10.2165/00002018-199106010-00004.

Borchard, W. (1998) 'Properties of thermoreversible gels', Berichte der Bunsengesellschaft für physikalische Chemie, 102(11), pp. 1580–1588. Available at: https://doi.org/10.1002/bbpc.19981021115.

Borer, P. et al. (2009) 'ATR-FTIR spectroscopic study of the adsorption of desferrioxamine B and aerobactin to the surface of lepidocrocite (γ-FeOOH)', Geochimica et Cosmochimica Acta, 73(16), pp. 4661–4672. Available at: https://doi.org/10.1016/j.gca.2009.05.048.

Bouchard, M. and Smith, D.C. (2003) 'Catalogue of 45 reference Raman spectra of minerals concerning research in art history or archaeology, especially on corroded metals and coloured glass', Spectrochimica Acta Part A: Molecular and Biomolecular Spectroscopy, 59(10), pp. 2247–2266. Available at: https://doi.org/10.1016/S1386-1425(03)00069-6.

Cagnini, A., Gennai, S. and Mazzoni, M.D. (2012) 'La Banderuola di Palazzo Vecchio: storia, vicende conservative, restauro', OPD restauro, pp. 13–32. Available at: https://opificiodellepietredure.cultura.gov.it/pubblicazioni/opd-restauro-n-24-2012/.

Chilton, J.P. (1971) 'The Corrosion of Metals', Journal of the Royal Society of Arts, 119(5181), pp. 614–629. Available at: https://www.jstor.org/stable/41370804%0A.

Christensen, D.W. et al. (2001) 'Deferoxamine toxicity in hepatoma and primary rat cortical brain cultures', Human & Experimental Toxicology, 20(7), pp. 365–372. Available at: https://doi.org/10.1191/096032701680350532.

Couture-Rigert, D.E., Sirois, P.J. and Moffatt, E.A. (2012) 'An investigation into the cause of corrosion on indoor bronze sculpture', Studies in Conservation, 57(3), pp. 142–163. Available at: https://doi.org/10.1179/2047058412Y.0000000004.

Cozar, O. et al. (2006) 'IR, Raman and surface-enhanced Raman study of desferrioxamine B and its Fe(III) complex, ferrioxamine B', Journal of Molecular Structure, 788(1–3), pp. 1–6. Available at: https://doi.org/10.1016/j.molstruc.2005.04.035.

Cuvillier, L. et al. (2022) 'Exploiting Biologically Synthetized Chelators in Conservation: Gel-based Bio-cleaning of Corroded Iron Heritage Objects', in P. Mardikian, L. Näsänen, and A. Arponen (eds) Metal 2022, proceedings of the interim meeting of the ICOM-CC metals working group. Helsinki, Finland.

Cuvillier, L. et al. (2023) 'Testing of the siderophore deferoxamine amended in hydrogels for the cleaning of iron corrosion', The European Physical Journal Plus, 138(6), p. 569. Available at: https://doi.org/10.1140/epjp/s13360-023-04159-y.

Cuvillier, L., Passaretti, A. and Joseph, E. (2020) Cleaning methods for metal conservation. Available at: https://docs.google.com/forms/d/e/1FAIpQLScfxBQs2rU-Q69_sYcsvUCDOcPqiwTyKBoKFrdhT2hfFKk7ng/viewform?usp=sf_link.

Degrigny, C. et al. (2007) 'Characterisation of corrosion product layers on atmospherically corroded historic ferrous objects: application to the armour of the Palace Armoury, Valletta, Malta', Strategies for Saving our Cultural Heritage, pp. 31–39.

Edwards, D.C. et al. (2005) 'Experimental and theoretical vibrational spectroscopy studies of acetohydroxamic acid and desferrioxamine B in aqueous solution: Effects of pH and iron complexation', Geochimica et Cosmochimica Acta, 69(13), pp. 3237–3248. Available at: https://doi.org/10.1016/j.gca.2005.01.030.

Evans, U.R. and Taylor, C.A.J. (1972) 'Mechanism of atmospheric rusting', Corrosion Science, 12(3), pp. 227–246. Available at: https://doi.org/10.1016/S0010-938X(72)90671-3.

Farkas, E., Enyedy, É.A. and Csóka, H. (1999) 'A comparison between the chelating properties of some dihydroxamic acids, desferrioxamine B and acetohydroxamic acid', Polyhedron, 18(18), pp. 2391–2398. Available at: https://doi.org/10.1016/S0277-5387(99)00144-8.

Fazary, A.E. et al. (2016) 'Microbial production of four biodegradable siderophores under submerged fermentation', International Journal of Biological Macromolecules, 88, pp. 527–541. Available at: https://doi.org/10.1016/j.ijbiomac.2016.03.011.

Grattoni, C.A. et al. (2001) 'Rheology and Permeability of Crosslinked Polyacrylamide Gel', Journal of Colloid and Interface Science, 240(2), pp. 601–607. Available at: https://doi.org/10.1006/jcis.2001.7633.

Guilminot, E. (2023) 'The Use of Hydrogels in the Treatment of Metal Cultural Heritage Objects', Gels, 9(3), p. 191. Available at: https://doi.org/10.3390/gels9030191.

Hider, R.C. and Kong, X. (2010) 'Chemistry and biology of siderophores', Natural Product Reports, 27(5), p. 637. Available at: https://doi.org/10.1039/b906679a.

Hœrlé, S. et al. (2004) 'Advances in understanding atmospheric corrosion of iron. II. Mechanistic modelling of wet–dry cycles', Corrosion Science, 46(6), pp. 1431–1465. Available at: https://doi.org/10.1016/j.corsci.2003.09.028.

Hosseinpour, S. and Johnson, M. (2017) 'Vibrational Spectroscopy in Studies of Atmospheric Corrosion', Materials, 10(4), p. 413. Available at: https://doi.org/10.3390/ma10040413.

Huang, J. (2018) 'A Simple Accurate Formula for Calculating Saturation Vapor Pressure of Water and Ice', Journal of Applied Meteorology and Climatology, 57(6), pp. 1265–1272. Available at: https://doi.org/10.1175/JAMC-D-17-0334.1.

Ihnat, P.M., Vennerstrom, J.L. and Robinson, D.H. (2000) 'Synthesis and Solution Properties of Deferoxamine Amides', Journal of Pharmaceutical Sciences, 89(12), pp. 1525–1536. Available at: https://doi.org/10.1002/1520-6017(200012)89:12<1525::AID-JPS3>3.0.CO;2-T.

Jaeger, T. (2008) 'Short Communication Removal of Paraffin Wax in the Re-treatment of Archaeological Iron', Journal of the American Institute for Conservation, 47(3), pp. 217–223. Available at: https://doi.org/10.1179/019713608804539619.

Janmey, P.A., Georges, P.C. and Hvidt, S. (2007) 'Basic Rheology for Biologists', in, pp. 1–27. Available at: https://doi.org/10.1016/S0091-679X(07)83001-9.

Kim, A.-R., Kim, H.-S. and Park, S.-O. (2011) 'Measuring of the Perceptibility and Acceptability in Various Color Quality Measures', Journal of the Optical Society of Korea, 15(3), pp. 310–317. Available at: https://doi.org/10.3807/JOSK.2011.15.3.310.

Kooli, W.M. et al. (2018) 'Bacterial iron reduction and biogenic mineral formation for the stabilisation of corroded iron objects', Scientific Reports, 8(1), pp. 1–11. Available at: https://doi.org/10.1038/s41598-017-19020-3.

Lair, V. et al. (2006) 'Electrochemical reduction of ferric corrosion products and evaluation of galvanic coupling with iron', Corrosion Science, 48(8), pp. 2050–2063. Available at: https://doi.org/10.1016/j.corsci.2005.06.013.

Lazzari, M. and Chiantore, O. (2000) 'Thermal-ageing of paraloid acrylic protective polymers', Polymer, 41(17), pp. 6447–6455. Available at: https://doi.org/10.1016/S0032-3861(99)00877-0.

Maréchal, L. et al. (2007) 'Study of the atmospheric corrosion of iron by ageing historical artefacts and contemporary low-alloy steel in a climatic chamber: comparison with mechanistic modelling', in Corrosion of Metallic Heritage Artefacts. Elsevier, pp. 131–151. Available at: https://doi.org/10.1533/9781845693015.131.

Mari Yanagishita (2012) 'Il restauro della grande Croce del Pollaiolo: un intervento all'interno del cantiere organizzato per l'Altare di San Giovanni', in Mandragora (ed.) E l'informe si fa forma... : studi intorno a Santa Maria del Fiore in ricordo di Patrizio Osticresi. Florence, Italy, pp. 281–286.

McAdam, B. et al. (2020) 'Production of Polyhydroxybutyrate (PHB) and Factors Impacting Its Chemical and Mechanical Characteristics', Polymers, 12(12), p. 2908. Available at: https://doi.org/10.3390/polym12122908.

Merck (2024) (-)-Ethyl L-lactate, properties. Available at: https://www.sigmaaldrich.com/CH/en/product/aldrich/e34102 (Accessed: 13 February 2024).

Monnier, J. et al. (2013) 'Reactivity studies of atmospheric corrosion of heritage iron artefacts', in Corrosion and Conservation of Cultural Heritage Metallic Artefacts. Elsevier, pp. 285–310. Available at: https://doi.org/10.1533/9781782421573.3.285.

Monnier, J. et al. (2019) 'The long term indoor atmospheric corrosion of iron : rust layer characterisation To cite this version : HAL Id : hal-02270518 The long term indoor atmospheric corrosion of iron : rust layer characterisation'.

Neff, D. et al. (2006) 'Raman imaging of ancient rust scales on archaeological iron artefacts for long-term atmospheric corrosion mechanisms study', Journal of Raman Spectroscopy, 37(10), pp. 1228–1237. Available at: https://doi.org/10.1002/jrs.1581.

Parisi, E.I. et al. (2018) 'Film forming PVA-based cleaning systems for the removal of corrosion products from historical bronzes', Pure and Applied Chemistry, 90(3), pp. 507–522. Available at: https://doi.org/10.1515/pac-2017-0204.

Pawlaczyk, M. and Schroeder, G. (2021) ' Deferoxamine-Modified Hybrid Materials for Direct Chelation of Fe(III) Ions from Aqueous Solutions and Indication of the Competitiveness of In Vitro Complexing toward a Biological System ', ACS Omega, 6(23), pp. 15168–15181. Available at: https://doi.org/10.1021/acsomega.1c01411.

Perera, D.Y. (2003) 'Physical ageing of organic coatings', Progress in Organic Coatings, 47(1), pp. 61–76. Available at: https://doi.org/10.1016/S0300-9440(03)00037-7.

Petiti, C. et al. (2020) 'Effects of cleaning procedures on the long-term corrosion behavior of bronze artifacts of the cultural heritage in outdoor environment', Environmental Science and Pollution Research, 27(12), pp. 13081–13094. Available at: https://doi.org/10.1007/s11356-020-07814-4.

Petrovic, J., Stevula, L. and Pisarcik, M. (1985) 'Interaction between a-, b- or y-FeOOH and water at 60 C, 80 C and 100 C', Chemical paper, 39(1), pp. 59–61.

Prati, S. et al. (2019) 'Cleaning oil paintings: NMR relaxometry and SPME to evaluate the effects of green solvents and innovative green gels', New Journal of Chemistry, 43(21), pp. 8229–8238. Available at: https://doi.org/10.1039/C9NJ00186G.

Prosek, T. et al. (2013) 'Real-time monitoring of indoor air corrosivity in cultural heritage institutions with metallic electrical resistance sensors', Studies in Conservation, 58(2), pp. 117–128. Available at: https://doi.org/10.1179/2047058412Y.0000000080.

Rahbani, J. et al. (2013) 'Characterization of internal structure of hydrated agar and gelatin matrices by cryo-SEM', ELECTROPHORESIS, 34(3), pp. 405–408. Available at: https://doi.org/10.1002/elps.201200434.

Ramírez Barat, B. and Cano, E. (2019) 'Agar versus Agarose Gelled Electrolyte for In Situ Corrosion Studies on Metallic Cultural Heritage', ChemElectroChem, 6(9), pp. 2553–2559. Available at: https://doi.org/10.1002/celc.201900344.

Rapti, S. et al. (2017) 'Removing iron stains from wood and textile objects: assessing gelled siderophores as novel green chelators', in L. Angelova and R. Ormsby, Bronwyn Townsend, Joyce Wolbers (eds) Gels in the Conservation of Artconservation. London: Archetype Publications, pp. 343–348.

Rapti, S. et al. (2021) 'Siderophores and their Applications in Wood, Textile, and Paper Conservation', in Microorganisms in the Deterioration and Preservation of Cultural Heritage. Cham: Springer International Publishing, pp. 301–339. Available at: https://doi.org/10.1007/978-3-030-69411-1_14.

Rapti, S. et al. (2023) 'Desferrioxamine B: Investigating the Efficacy of Hydrogels and Ethanol Gels for Removing Akaganeite and Maghemite from Dry Wooden Substrates', Forests, 14(2), p. 247. Available at: https://doi.org/10.3390/f14020247.

Samorì, C. et al. (2016) 'The Green Attitude in Art Conservation: Polyhydroxybutyrate-based Gels for the Cleaning of Oil Paintings', ChemistrySelect, 1(15), pp. 4502–4508. Available at: https://doi.org/10.1002/slct.201601180.

Santarini, G. (2007) 'Corrosion behaviour of low-alloy steels: from ancient past to far future', in Corrosion of Metallic Heritage Artefacts. Elsevier, pp. 18–30. Available at: https://doi.org/10.1533/9781845693015.18.

Schmuecker, E., Lees, R. and Richardson, T. (2011) 'The Examination and Conservation of a 17th Century Indian Horse Armour', in P. Mardikian et al. (eds) Metal 2010: proceedings of the interim meeting of the ICOM-CC Metal Working Group, October 11-15, 2010, Charleston, South Carolina, USA. Clemson: Clemson University, pp. 120–126.

Schwarzenbach, G. (1960) 'Relationships between Metal Complex Stability and Structure of Complexing Agents', Analytical Chemistry, 32(1), pp. 6–9. Available at: https://doi.org/10.1021/ac60157a002.

De Serrano, L.O. (2017) 'Biotechnology of siderophores in high-impact scientific fields', Biomolecular Concepts, 8(3–4), pp. 169–178. Available at: https://doi.org/10.1515/bmc-2017-0016.

Stratmann, M. (1990) 'The Atmospheric Corrosion of Iron - A Discussion of the Physico-Chemical Fundamentals of this Omnipresent Corrosion Process Invited Review', Berichte der Bunsengesellschaft für physikalische Chemie, 94(6), pp. 626–639. Available at: https://doi.org/10.1002/bbpc.19900940603.

Strlič, M., Kolar, J. and Pihlar, B. (2001) 'Some preventive cellulose antioxidants studied by an aromatic hydroxylation assay', Polymer Degradation and Stability, 73(3), pp. 535–539. Available at: https://doi.org/10.1016/S0141-3910(01)00120-3.

Vandenabeele, P. (2013) Practical Raman spectroscopy: an introduction. John Wiley & Sons.

Vantelon, D. et al. (2009) 'Applications in materials science of combining Raman and X-rays at the macro- and micrometric scale', Phase Transitions, 82(4), pp. 322–335. Available at: https://doi.org/10.1080/01411590802655341.

Veneranda, M. et al. (2017) 'Characterization of archaeometallurgical artefacts by means of portable Raman systems: corrosion mechanisms influenced by marine aerosol', Journal of Raman Spectroscopy, 48(2), pp. 258–266. Available at: https://doi.org/10.1002/jrs.4997.

Watkinson, D. (2010) 'Preservation of Metallic Cultural Heritage', in Shreir's Corrosion. Elsevier, pp. 3307–3340. Available at: https://doi.org/10.1016/B978-044452787-5.00172-4.

Yiming, J. et al. (2019) 'A new bio-based organogel for the removal of wax coating from indoor bronze surfaces', Heritage Science, 7(1), p. 34. Available at: https://doi.org/10.1186/s40494-019-0276-8.

Chapter 4

Design and assessment of multi-target cleaning gel for altered historical brass

This chapter is based on
Passaretti, A., Cuvillier, L., Sciutto, G., Cano, E., Ramírez Barat, B., von Reuss, S., & Joseph E., Assessment of greener solutions for the cleaning of historical metal heritage.
Oral presentation at *InART2024 6th International Conference on Innovation in Art Research and Technology*. Oslo, Norway, June 4-7, 2024.

4.1 Corrosion behaviour of indoor brass heritage

Another family of metals commonly present in indoor historical collections includes copper and related alloys (Angelini and Argyropoulos, 2008). This class of metals is of great importance in art and technology since prehistoric times, as much as in everyday life, because of appealing inherent features ranging from good resistance to corrosion, excellent workability and mechanical properties in a wide spectrum of temperatures, and high thermal and electrical conductivity (Tuck, Powell and Nuttall, 2010; Qiu and Leygraf, 2011).

Several copper alloys are represented in the world of art, such as bronze (i.e., Cu-Sn alloys), brass (i.e., Cu-Zn alloys), and nickel silver (i.e., Cu-Zn alloy with Ni addition), which specific composition, correlated by the joined presence of minor elements (e.g., Pb, Al), provides different properties and aesthetic features to the alloys (Hughes and Rowe, 1983; Tuck, Powell and Nuttall, 2010).

The research presented in this dissertation was aimed at developing a new cleaning method for altered historical brass artefacts stored indoors. This family of metals is generally described as copper and zinc alloys, containing the latter element in a percentage between 10-45%, together with the possible presence of small quantities of Sn, Al, or Pb (Tuck, Powell and Nuttall, 2010). In general, brasses are divided in single-phase (α) and duplex (α-β) brasses according to the percentage of zinc present in the alloy, whether below or above 37%, respectively (Tuck, Powell and Nuttall, 2010).

Generally, brass is not strongly reactive in indoor environments, but slowly oxidated at room temperature overtime, leading to the formation of a complex passive layer (0.5-2 nm thickness) consisting of zinc and copper oxides, when exposed to humidified air (Qiu and Leygraf, 2011) (Figure 4.1, a). Qui and Leygraf (2011) proposed a model for the formation of this oxide layer. Once brass surface is in contact with condensed humidity droplets (i.e., water), electrochemical reactions occur dissolving Zn and Cu (i.e., anodic reaction) and generating hydroxyl ions (i.e., cathodic reaction) (Figure 4.1, b). Consequently, the dissolved metal ions react with hydroxyl ions giving aqueous metal-(OH) species that will eventually dehydrate in the form of ZnO and Cu_2O (Figure 4.1, c). The authors demonstrated the co-presence of crystalline and amorphous oxides, underlining an accelerated and localised growth of ZnO (i.e., zincite) over a following but more uniform Cu_2O (i.e., cuprite) layer formation (Qiu and Leygraf, 2011). This evidence must be linked to the different standard electrode potentials, namely, $E°$ = +0.34 V for Cu^{2+}/Cu and $E°$ = -0.76 V for Zn^{2+}/Zn, that explains the preferential oxidation of zinc over copper in a first stage.

It is also known that copper and its alloys tend to tarnish rapidly when exposed to atmospheres rich in hydrogen sulphide (Mattsson, 1958; Tuck, Powell and Nuttall, 2010). Copper sulphides (Cu_xS) can be formed on the metallic substrate where the protective metal oxide layer is absent. This formation contaminates the metal substrate, enhancing the possibility to further alteration, even when metallic objects are not exposed anymore to hydrogen sulphide sources (Mattsson, 1958).

Another alteration phenomenon reported in the literature is the process of dezincification of brasses (Tuck, Powell and Nuttall, 2010; Artesani *et al.*, 2020). During this corrosion process, zinc is preferentially dissolved and removed from affected brass alloys, provoking micro-pores and strength loss in the residual metal structure. The factors initialising this type of corrosion phenomenon on brass are high temperature, humidity, and chloride content (i.e., sea water), making this scenario less representative for historical brasses exposed indoor.

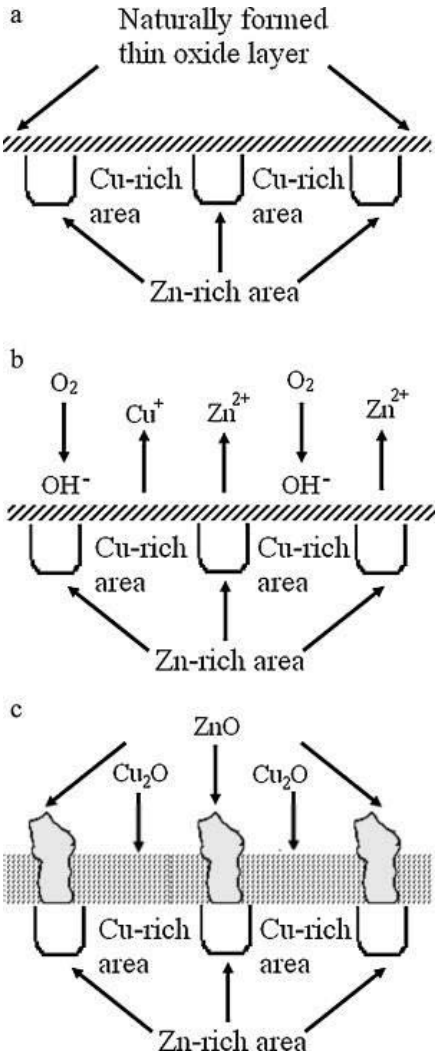

Figure 4.1 Schematic illustration of steps identified during initial oxidation of brass in humidified air. (a) Before exposure in humid synthetic air; (b) during exposure in humid synthetic air; (c) formation of corrosion products. (Reproduced from Qiu and Leygraf, 2011).

As seen in Paragraph 1.2, the prevention of corrosion products formed on metallic surfaces housed indoors is commonly sought both for aesthetics and conservation reasons (Turner-Walker, 2008). The goal is commonly achieved by regulating environmental conditions (i.e., mainly relative humidity and temperature) and/or the common CRs choice of shielding metals against caustic agents thanks to organic coatings (Watkinson, 2010; Prosek *et al.*, 2013). In particular, nitrocellulose lacquers are generally preferred in the case of brasses because of their high resistance to hydrogen sulphide possibly present in the atmosphere

(Luxford and Thickett, 2007; Heginbotham *et al.*, 2014). However, as any other organic coating, nitrocellulose is susceptible to degradation phenomena such as cracking and yellowing in the long-term, resulting in being less effective in the protection aim and no-more acceptable aesthetically (Luxford and Thickett, 2007; Heginbotham *et al.*, 2014; Eggert *et al.*, 2019). When protective coatings are compromised, the underlaying metallic substrate (i.e., brass) is exposed to potential caustic factors present in the surrounding atmosphere (i.e., humidity, hydrogen sulphide). Hence, as discussed in Paragraph 3.2, it is not surprising the co-presence of compromised coatings and altered metallic substrates when inspecting metal heritage. When conservator-restores opt for the controlled removal of both inorganic and organic undesired products in order to preserve the object in the long-term and improve the readability of the artefact, several steps of intervention are carried out (i.e., dissolution by solvents of organic materials, mechanical methods, cleaning by complexing solutions) (Jaeger, 2008; Schmuecker, Lees and Richardson, 2011; Cagnini, Gennai and Mazzoni, 2012; Mari Yanagishita, 2012). This kind of cleaning approach guarantees a more controllable intervention; nevertheless, several materials and tools, more working time, and expertise are required. The work presented in Chapter 4 is therefore aimed to explore a new methodology able to tackle concurrently undesired inorganic (i.e., brass tarnish) and organic (i.e., Zaponlack) films present on brass thanks to an adjustable and bio-based gelled cleaning system.

4.2 Mock-up preparation

The removal of tarnish layer and concurrently of nitrocellulose lacquer (i.e., Zaponlack) was evaluated on brass (Cu 66%, Zn 34% by X-ray fluorescence analysis) sheets of 50 × 50 × 1 mm^3 purchased from Tartaix Métaux Outillage (France). Coupons were preliminarily degreased by cotton swabbing using subsequently ethanol (96.0 – 97.2%) and acetone (≥99.5%) from Sigma Aldrich. Afterwards, an homogenous tarnish layer was formed following the protocol described by Hughes and Rowe (1983) in their compendium on the patination of metals (Hughes and Rowe, 1983). Despite the removal of an aesthetical patina is never the target of a cleaning intervention, being conventionally wished by the artworks' artist, in this study a patination method was selected in order to obtain an even layer of tarnish for better reproducibility and assessment of the cleaning gelled system. Clearly, the phases present in the formed patina were the real focus of the cleaning treatment, and therefore the presence of compounds that would naturally occur on brass through atmospheric indoor corrosion was desired.

The literature did not provide any information regarding the compounds created through the patination process, but rather details about the colour obtained for aesthetical reasons, therefore the patination protocol needed careful evaluation before being adopted in this study. The protocol indicating the formation of an orange-brown semi-matt finishing was explored, being the one suggesting an appearance most similar to the reality.

Aiming to artificially corrode the metal sheets, a solution of copper nitrate (20% w/v in deionised water) was employed on brass sheets as described: "*The solution is initially dabbed on vigorously with a soft cloth, to ensure that the surface is evenly "wetted". Subsequent applications should be wiped on, and used very sparingly, to inhibit the formation of green patina. After each application the article is left to dry in air. This procedure is repeated twice a day for about five days*" (Hughes and Rowe, 1983). Figure 4.2 shows the daily outcome obtained on the brass coupons.

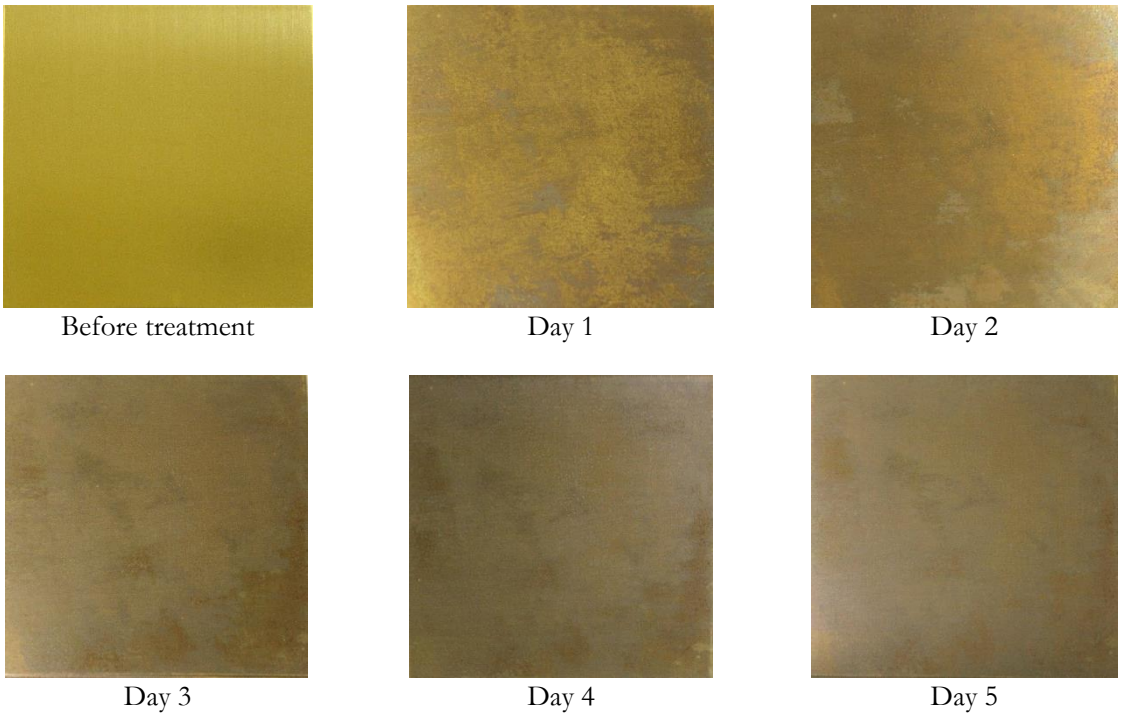

Figure 4.2 Daily monitoring of the visual appearance evolution of a brass coupon (50 × 50 × 1 mm^3) subjected to chemical ageing treatment.

It was evident that the consecutive application of the copper nitrate solution yielded a homogeneous layer of matt alteration onto the brass surface with an appearance in line with the expectation mentioned by the reference resource (Hughes and Rowe, 1983).

Colorimetry could follow the alteration process of brass sheets, as displayed in Table 4.1. Data collected day-by-day could emphasize an initial enhancement of brightness (positive ΔL*) and yellow shade (positive Δb*) of the surface possibly related to the removal of residual dirt and grease present on the brass surface. These values are then starting to invert the trend, changing towards darker (negative ΔL*) and bluer shades (negative Δb*) compared to initial CIELab coordinates, especially after 3 days of patination. In parallel, a constant increase of a* values suggested a reddish appearance of brass coupons while being patinated.

Table 4.1 Variation of CIELab coordinates of brass coupons comparing daily patination steps to initial appearance. ΔL*, Δa*, Δb* SCE values are reported along with their standard deviation into brackets.

Day	ΔL*	Δa*	Δb*
1	0.84 (±0.48)	5.29 (±0.18)	13.35 (±0.08)
2	1.05 (±0.01)	4.31 (±0.52)	3.25 (±0.56)
3	-1.00 (±0.58)	6.41 (±0.06)	-0.80 (±0.31)
4	-3.76 (±0.59)	7.29 (±0.57)	-2.14 (±0.67)
5	-3.11 (±0.84)	6.03 (±0.01)	-4.31 (±0.50)

In order to explain colorimetric data and ascertain the nature of the tarnish phases formed on brass after five days of the patination process, micro-Raman spectroscopy was performed on the metal surface (Figure

4.3). The technique could reveal the presence of several compounds normally forming on brass historical heritage when housed indoor (Paragraph 4.1). Copper oxide in the form of cuprite (Cu_2O) could be identified by the most characteristic band at about 216 cm^{-1}, correlated by signals at 94, 145, 408, and most remarkably, at 518 and 634 cm^{-1} that are markers for amorphous cuprite (Bouchard and Smith, 2003; Cakir, 2017). On the contrary, cupric oxide (CuO, tenorite) could not be tracked by the main Raman peak around 290 cm^{-1} (Cakir, 2017) in accordance with refence literature (Qiu and Leygraf, 2011). This is a positive result, being tenorite a compound whose formation is not thermodynamically favoured in normal exposing conditions, but can be formed in high-temperature oxidation and high pH conditions (Scott, 2002). On the contrary, tenorite may be found on heritage metals when an aesthetical or protective patina was desired by artists (Scott, 2002), which would not be the target of the cleaning gels here proposed.

Together with cuprite, zinc oxide (ZnO) was recognised by Raman analysis thanks to weak signals at 437 and 576 cm^{-1} (Bouchard and Smith, 2003; Dzhagan *et al.*, 2022). In particular, previous literature reports that the ratio between the two bands is an indicator for the mineral disorder (Bouchard and Smith, 2003). In relation to collected data, the technique would suggest the formation of rather amorphous zincite due to the higher relative intensity of the band at 576 cm^{-1} compared to the one at 437 cm^{-1} (Figure 4.3), in line with refence literature for brass natural oxidation (Qiu and Leygraf, 2011).

Finally, covellite (CuS) could be detected thanks to a weak Raman peak around 470 cm^{-1} (Figure 4.3), which is considered the most characteristic for the mineral (Bouchard and Smith, 2003; Dzhagan *et al.*, 2022). This product could not be linked to the patination process, yet already present on the surface of brass sheets, as an alteration product naturally occurring in the presence of hydrogen sulphide in the atmosphere (Mattsson, 1958; Tuck, Powell and Nuttall, 2010).

No manifest presence of copper nitrate (i.e., coming from the patination solution) could be detected, however a potential deposition cannot be fully excluded when considering the high fluorescence recorded in the acquired Raman spectra that might have hidden $Cu(NO_3)_2$ most intense peak at 1048 cm^{-1} (i.e., nitrate functional group), based on the reference spectrum in the same experimental conditions.

The interpretation of data acquired by Raman spectroscopy was correlated to the colorimetric outcome previously exposed. In particular, it was assumed that the enhancement of red (i.e., positive Δa^*, Table 4.1) and blue shades (i.e., negative Δb^*, Table 4.1) was linked to the formation of cuprite and zincite (red coloured minerals) together with covellite - and potentially copper nitrate residues -(blue coloured) on brass surfaces after five days of patination protocol.

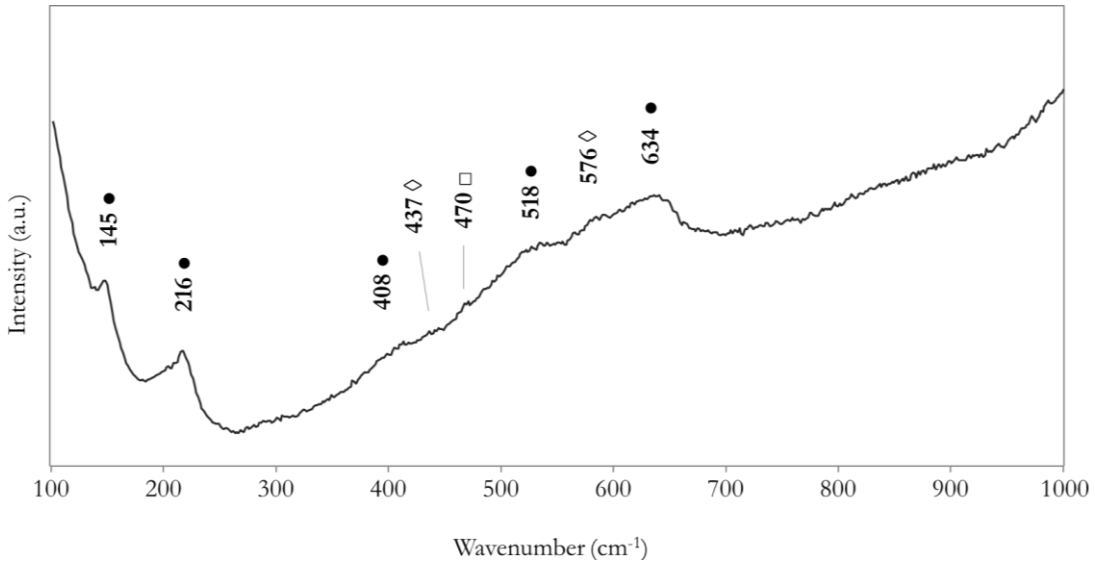

Figure 4.3 Representative Raman spectrum of brass coupon after five days of patination (i.e., chemical ageing). In the figure, signals related to cuprite (●), zincite (◊), and covellite (□) are reported.

Having ascertained the desired nature of the tarnishing products obtained on the brass sheets through patination, the resulting coupons were coated by brush with two thin criss-cross layers of protective coating. In agreement with the HELIX survey (2020) and the previous literature (Molina, Cano and Ramírez-Barat, 2023a), the nitrocellulose Zaponlack from Carl Roth was selected, being nitrocellulose lacquers highly performing on copper-based substrates for metal protection in high-sulphide indoor conditions (Paragraph 1.2.2).

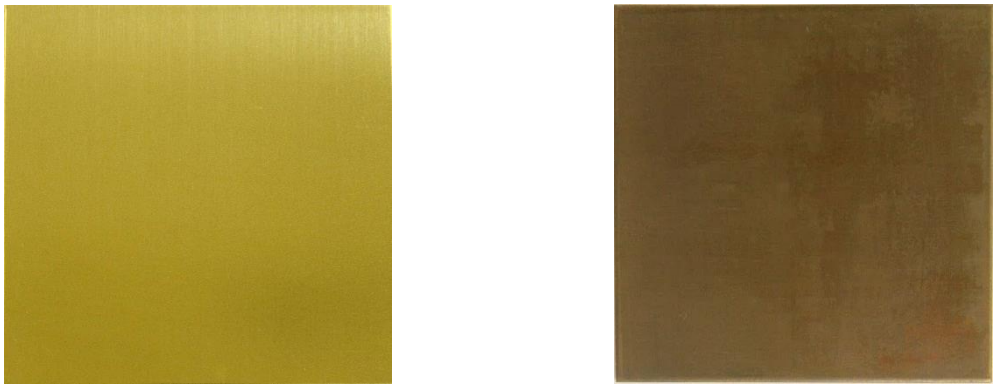

Figure 4.4 Brass mock-up (50 × 50 × 1 mm^3): initial aspect (left) and after the chemical ageing protocol and Zaponlack coating (right).

4.3 PHB-EL-EDDS gel

In line with the perspective followed for the design of the "double-target" PHB-EL-DFO system, a new bio-based organogel was designed, aiming to tackle concurrently inorganic compounds and organic substances potentially present as undesired materials on the surface of indoor historical brass heritage. Specifically, the formulation was aimed to concurrently remove a nitrocellulose lacquer (i.e., Zaponlack) and underlying brass tarnishing products (i.e., copper and zinc oxides and sulphides) possibly present on historical brass collections.

The components employed to design the innovative gel system were carefully chosen in a green perspective in terms of operator safety and environmental impact. In light of the positive results obtained for the PHB-EL-DFO gel, the bio-sourced and biodegradable poly-3-hydroxybutyrate (PHB) and ethyl lactate (EL) were employed again, together with the complexing agent ethylenediamine-N,N'-disuccinic acid (EDDS) (Figure 4.5).

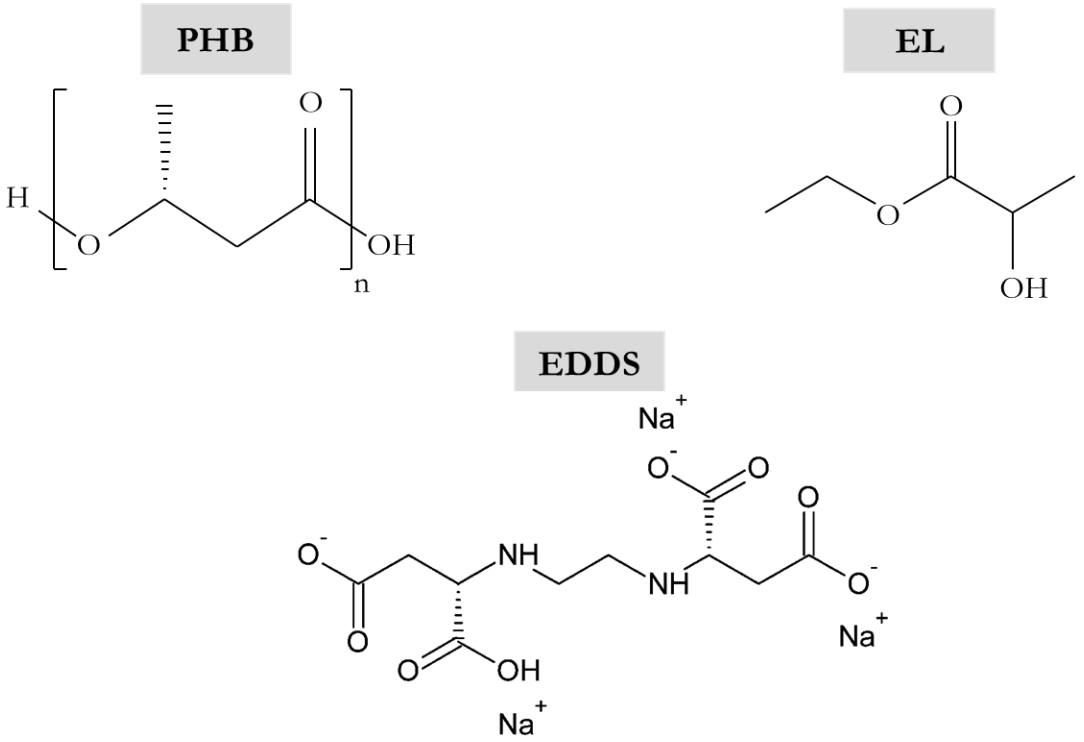

Figure 4.5 Structural formula of PHB-EL-EDDS gel components: poly-3-hydroxybutyrate (PHB), ethyl lactate (EL) and ethylenediamine-N,N'-disuccinic acid trisodium salt (EDDS).

4.3.1 An insight into ethylenediamine-N,N'-disuccinic acid (EDDS)

Ethylenediamine-N,N'-disuccinic acid, often referred to by the acronym EDDS, is a hexadentate ligand (Figure 4.6) that is gaining more and more attention in the last decades thanks to its green features that would allow the replacement of more toxic chelating agents, such as ethylenediaminetetraacetic acid (EDTA) (Orama *et al.*, 2002).

EDDS is an aminopolycarboxylic acid with isomeric structure to the more renowned EDTA, and can be found in three stereoisomeric forms [S,S], [S,R/R,S], and [R,R] due to the two chiral carbon atoms present in its structure (Figure 4.6) (Orama *et al.*, 2002; Wang *et al.*, 2022). Previous literature reports that the [S,S] isomer is rapidly and completely biodegraded and mineralised in activated sludge systems, whereas the other EDDS forms are degraded to only a limited extent (Vandevivere *et al.*, 2001; Orama *et al.*, 2002). Currently, extensive research is carried out to find methods for the recovery of used EDDS solutions (i.e., after chelating metallic ions) and to estimate the biodegradability of complexes once formed (Vandevivere *et al.*, 2001; Race, 2017). Finally, great attention is addressed towards the production of the chelating agent in a more sustainable way. Indeed, [S,S]-EDDS is mostly chemically synthesised starting from maleic acid and ethylenediamine, however previous studies demonstrated the ability of several microorganism (e.g., *Amycolatopsis japonicum, Pseudonomas*, *Acidovorax*) to produce [S,S]-EDDS by fermentation and enzymatic synthesis (Takahashi *et al.*, 1999; Wang *et al.*, 2022), fostering innovative bio-based solutions for its manufacturing.

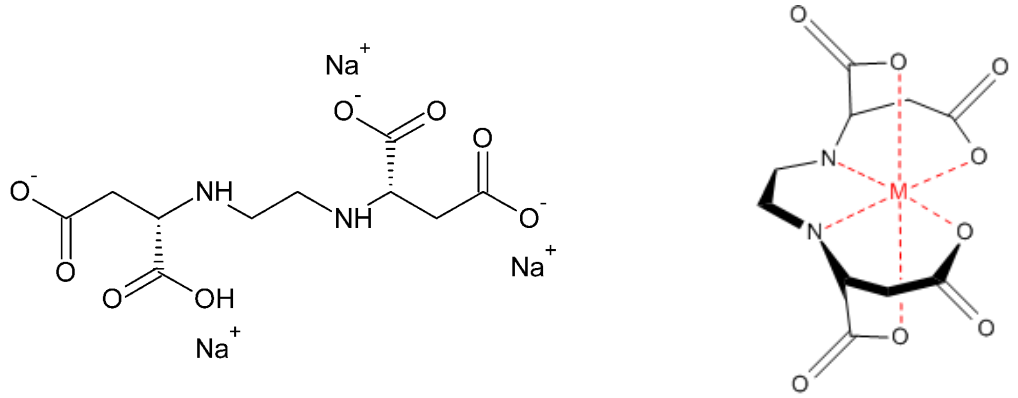

Figure 4.6 Chemical structure of ethylenediamine-N,N'-disuccinic acid trisodium salt (EDDS) (left) and metal-EDDS complexes (right).

Nowadays, ethylenediamine-N,N'-disuccinic acid is attracting research interest in detergent, cosmetic, and agrochemical industry (Orama *et al.*, 2002; Wang *et al.*, 2022). In particular, it appears as valid green candidate for the decontamination of soils from heavy metals (e.g., Cu, Pb, Zn, Cd, U), being conventional cleanup methods (e.g., EDTA solutions) rather harmful to soil properties and living organisms present herewith, because of their inherent toxicity and/or low biodegradability (Luo, Shen and Li, 2005; Chen *et al.*, 2019). In particular, EDDS demonstrated high affinity for iron, copper, and zinc ions complexation (Luo, Shen and Li, 2005), as expressed by the stability constant logK. This parameter indicates the tendency towards the formation of metal-ligand complexes in a chemical equilibrium. When considering complexes formed in a molar ratio 1:1, previous studies calculated stability constants equal to 22.0 in the case of Fe(III), 18.4 for Cu(II) ions, and 13.4 for complexes with Zn(II), without revealing distinctions related to the different EDDS chiralities (Orama *et al.*, 2002). Comparing these values to the ones reported for DFO-complexes with Fe(III) (i.e., 30.4), Cu (II) (i.e., 13.73), and Zn(II) (i.e., 10.36) (Farkas, Enyedy and Csóka, 1999; Pawlaczyk and Schroeder, 2021), it is clear that, when working on the design of a cleaning system for altered brass (i.e., Cu-Zn alloy), EDDS appeared as a more advantageous candidate to be exploited than DFO.

Figure 4.7 displays the conditional stability constants for metal-EDDS complexes (i.e., $\log K_{ML}$) in function of the pH for different ions. Being $\log K_{ML} \geq 6$ often considered as a threshold to efficient complexation, it can be estimated an approximate suitability for chelation in the pH range 3-12 towards Cu(II) ions and pH 5-12 for Zn(II) (Orama *et al.*, 2002).

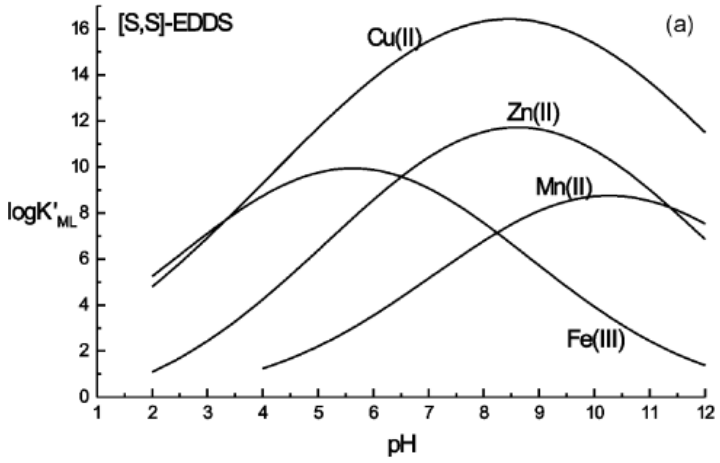

Figure 4.7 Conditional stability constants for metal-ligand (ML) complexes of [S,S]-EDDS in function of the pH. (Reproduced from Orama *et al.*, 2002).

4.3.2 Design of the PHB-EL-EDDS formulation

Few considerations were necessary before designing the new PHB-based formulation loaded with EDDS in order to ascertain the functionality of the active agent when applied through the gelled system.

Firstly, previous research reports that the chelating action of EDDS is enhanced by temperature increase (Kołodyńska, 2011; Chauhan, Pant and Nigam, 2012). In the sought application on metal objects, the formulation would be used at room temperature (i.e., 23.8 ±2.4 °C laboratory conditions in this study), therefore this factor would not be modulated. Yet, the information is relevant because ascertained that the ligand would not get altered because of the potential temperature (i.e., 100-110 °C) reached for the gelation of the polymer PHB in the presence of ethyl lactate.

Considering single gel components, it was possible to ascertain beforehand the functionality of EDDS as ligand in function of the pH. In particular, its complexing action is effective in a wide range of pH for both copper (i.e., pH 3-12 for Cu(II)) and zinc (i.e., pH 5-12 for Zn(II)) (Orama *et al.*, 2002) ions, which are the elements present in brass alloys. On the contrary, no evidence of stability constant for Cu(I) could be found in the literature. Knowing that ethyl lactate has pH 4 and the initial EDDS solution (35%) has pH around 9.2, the pH condition for EDDS efficient complexation towards Cu and Zn ions appeared respected before designing the PHB-EL-EDDS system.

The co-presence of ethyl lactate and ethylenediamine-N,N'-disuccinic acid in the PHB-based system was not evaluated as a limiting factor a priori. Previous literature reports a remarkable enhancement of copper removal from contaminated soils, when operating with EDDS solutions in the presence of ethyl lactate (Guo *et al.*, 2010). The phenomenon is explained assuming that ethyl lactate reduces the overall polarity of the aqueous EDDS solutions, weakening the competitive affinity of water molecules towards Cu ions, thus facilitating binding between EDDS and Cu cations. Specifically, an increase of Cu-EDDS stability constant (i.e., logK) from 18.4 in absence of EL, up to 26 was measured for low concentrations of EL in the EDDS solution (Guo *et al.*, 2010).

Finally, the ethylenediamine-N,N'-disuccinic acid, purchased from Sigma Aldrich, was in the form of trisodium salt solution in water at 35% concentration. Due to the presence of water, necessary for the dissolution of the salt, the hydrophobicity of poly-3-hydroxybutyrate needed to be carefully considered (McAdam *et al.*, 2020). In light of the tests carried out for the design of the PHB-EL-DFO formulation and presented in Paragraph 3.3.2, the ratio 1:6 v/v between EL and water was maintained for the new formulation loaded with EDDS, being the only one successful for the gelation of PHB-EL in the presence of water.

Not existing previous literature regarding the use of EDDS on metal heritage, the concentration of ligand to be added in the PHB-EL system was evaluated in relation to the most conventional EDTA that is normally used in a range of 10^{-3}–10^{-2} M in gelled systems (e.g., agar) (Giraud *et al.*, 2021; Guilminot, 2023). This consideration is relevant for a future comparison between the innovative PHB-EL-EDDS system and traditional cleaning methods. Considering the initial concentration of the EDDS starting solution (i.e., 35%) and the concentration for the PHB-EL system (i.e., 7% w/v), the product was diluted down to 20% in deionised water to reach a proposed final concentration of $4.8 \cdot 10^{-2}$ M in the desired PHB-EL-EDDS gel.

A first series of attempts investigated the possibility of forming the PHB-EL-EDDS system by direct addition of all components, namely polyhydroxybutyrate powder, ethyl lactate, ethylenediamine-N,N'-disuccinic acid, and deionised water, in a glass petri dish placed on a hot plate at about 100-110 °C under magnetic stirring. Although gelation could be achieved, it was impossible to manipulate and remove from the glass petri dish the resulting gel without breaking it, since the system was fragile and crumble when cut with a metallic spatula (Figure 4.8).

Figure 4.8 Appearance of the PHB-EL-EDDS formulation, formed by addition of all the components in a glass petri dish placed on a hot plate, when manipulated by metallic spatula.

The same formulation was considered changing the sequence of components addition. Firstly, a PHB-EL gel (7% w/v) was prepared and afterwards the EDDS solution (20% in water) was rapidly added to the still-viscous gel stirring manually, and finally closing the petri dish to avoid solvent evaporation while cooling to room temperature (i.e., 23.8 ±2.4 °C laboratory conditions in this study). The protocol yielded to the successful design of a rigid system that could be handled by metallic spatula for the application (Figure 4.9).

Therefore, for the conclusive synthesis of the PHB-EL-EDDS system, a PHB-EL gel was initially prepared employing the bio-polymer poly-3-hydroxybutyrate (PHB) purchased from Biomer and the bio-solvent ethyl lactate (≥98%) (EL) from Sigma Aldrich in a mixture 7% w/v. The mixture was magnetically stirred in a covered glass petri dish at about 110 °C for a few minutes until the PHB powder got dissolved and the mixture gained in thickness. In parallel, a solution of ethylenediamine-N,N'-disuccinic acid trisodium salt (Na_3EDDS 35% in water, Sigma Aldrich) was diluted in deionised water to reach a final concentration of 20% v/v. Out of heating, the EDDS solution was added in the glass petri dish while the PHB-EL gel was not rigid yet, quickly stirred manually, and finally let cool down to room temperature before application (i.e., 23.8 ±2.4 °C) (Figure 4.9). The aqueous EDDS solution was added in a volume ratio of 1:5 compared to the ethyl lactate loaded in the PHB system and the final EDDS concentration was calculated as $4.8 \cdot 10^{-2}$ M. The measured pH in the PHB-EL-EDDS formulation was varying according to the point of contact, because of the peculiar appearance, presenting EDDS reddish droplets dispersed in the gelled matrix (Figure 4.9). The pH was ranging from 5 to 8 in accordance with the fact of retaining both ethyl lactate (i.e., pH 4) and EDDS (i.e., pH 9.2 at 35% in water).

Figure 4.9 Photography of the PHB-EL-EDDS gel formulation in a glass petri dish once at room temperature (i.e., 23.8 ±2.4 °C) (on a white background).

4.3.3 Characterisation of the PHB-EL-EDDS formulation

4.3.3.1 Rheology

The mechanical properties of the PHB-EL-EDDS system were investigated resorting to rheology by amplitude sweep analysis, as already explored with the other formulations proposed in this research work.

When subjecting PHB-EL-EDDS samples to oscillatory shear deformations at gradually increasing strain amplitudes, the rheometer recorded values for the storage modulus G' (i.e., formulation stiffness) approximately an order of magnitude higher than the loss modulus G" (i.e., formulation viscosity) over the linear viscoelastic (LVE) region (Figure 4.10, orange). In particular, the LVE region, which is characterised by a plateau trend for the G' curve, shows the range of shear strain for which the sample structure does not get destroyed in the set experimental conditions. In the case of PHB-EL-EDDS samples, G' values were higher than G" values in the LVE region, which is characteristic for viscoelastic solids showing strong interaction forces, describing the system as gel-like structured in rheology (Grattoni *et al.*, 2001).

Comparing the rheological response of the PHB-EL-EDDS gel (Figure 4.10, orange) to the PHB-EL formulation not loaded with the EDDS solution (Figure 4.10, black), both systems showed G' > G" values over the LVE region, however their strengths (i.e., stiffness) was different. In particular, the PHB-EL gel demonstrated a stronger structure than the formulation loaded with EDDS solution. Similar to what observed in the case of the PHB-EL-DFO system, it was attributed this lower strength to the hydrophobicity of poly-3-hydroxybutyrate constituting the gel matrix. It is possible that the polymer, in the presence of the EDDS-aqueous solution, might yield a weaker gelled system (McAdam *et al.*, 2020).

However, when examining the limit of the LVE region, named yield point (τ_y) in rheology, the response of both systems was similar, showing τ_y around a strain $\gamma = 0.02\%$ in both cases. The two systems were similarly prone to structural destruction when stimulated in the set conditions, despite being different formulations.

Observing the behaviour after the LVE region (i.e., yield point), a gradual drop of the G' curve occurred, generally stating a non-brittle fracturing form of the samples until reaching the crossover point (i.e., G' = G"). For both formulations, the rheometer registered a tendency of G" value to raise before the crossover point, which is indicative of micro-cracks not extended throughout the entire material prior to the breakdown of sample structure. This event happens when storage and loss moduli curves cross each other, hence when G' = G". The conjunction point between the two curves is denominated flow point (τ_f) and was calculated at about strain $\gamma = 1.3\%$ and $\gamma = 1.5\%$ for PHB-EL-EDDS and PHB-EL gels, respectively. The values could not be considered as relevantly different thus proved a similar behaviour of the two systems.

Overall, the PHB-EL-EDDS system demonstrated similar behaviour as PHB-EL in response to mechanical stress (Table 4.2). In particular, the formulation was proved to be a gel (i.e., G' > G") and showed lower strength than the PHB-EL gel, possibly due to the additional presence of EDDS solution. As already discussed for the PHB-EL gel, the system loaded with EDDS showed appealing properties such as stiffness that indicates possible easy handling for operators and potentially no residues at the end of cleaning application on metals. Furthermore, the slightly lower stiffness of the formulation, compared to the gel without EDDS (i.e., PHB-EL), might imply better adaptability to the metallic surfaces to be cleaned.

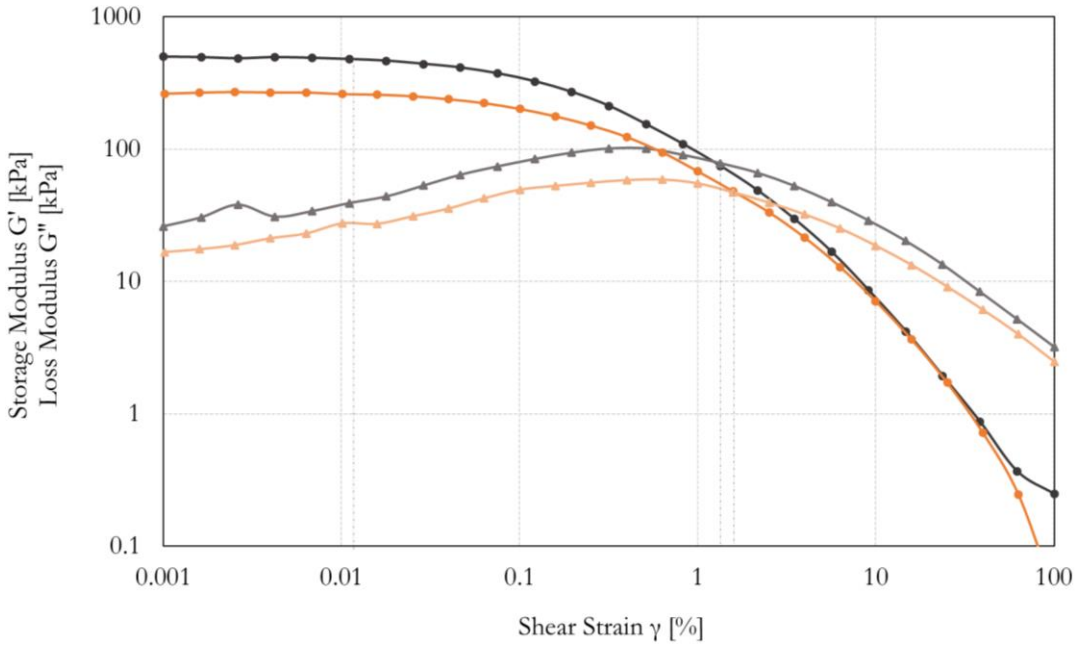

Figure 4.10 Strain dependence of storage modulus G' (circles, darker hue) and loss modulus G" (triangles, lighter hue). The amplitude sweep curves for PHB-EL-EDDS (orange) and PHB-EL (black) systems are plotted in function of shear strain percentage.

Table 4.2 Rheological response of the PHB-EL-EDDS formulation compared to the plain PHB-EL gel analysed by amplitude sweep in the same conditions.

Formulation	**PHB-EL-EDDS**	**PHB-EL**
LVE region	G' > G"	G' > G"
Definition	viscoelastic solid (gel)	viscoelastic solid (gel)
Yield point (τ_y)	γ = 0.02%	γ = 0.02%
Flow point (τ_f)	γ = 1.3%	γ = 1.5%

4.3.3.2 Cryo-Scanning electron microscopy (Cryo-SEM)

Cryo-SEM analysis was run to examine the inner structure of the still-moist PHB-EL EDDS gel and compare it with the PHB-EL system in order to evidence any structural variations derived from the presence of EDDS. It is important to highlight that under the same analytical conditions, the PHB-EL-EDDS gel did not allow to collect images at magnifications higher than 10000× without provoking damage to the sample, being more sensitive to the electron beam used for the analysis.

In general, the PHB-EL-EDDS gel matrix appeared densely interconnected under 8000× magnification, as already observed for the PHB-EL gel (Figure 4.11, A-B). In line with previous examinations on the PHB-EL system (page 83), also the gel loaded with EDDS was characterised by a plate-like structure interspersed by blocky pores with a diagonal aperture of approximately 0.5 μm (Figure 4.11, A). Pores were not homogeneously distributed in the sample, as for the PHB-EL gel. Indeed, it was possible to observe similar dense matrix areas, where cavities were barely present, in both systems, without and with the additional presence of EDDS (Figure 4.11, A-B). Such denser regions and the small size of pores in the gel would probably corroborate rheological measurements, validating the stiffness registered for the PHB-EL-EDDS system.

From a broader inspection, moving to lower magnification (174×), it was possible to see distinctly the presence of multiple droplets, arguably related to the EDDS solution entrapped in the PHB-gel matrix. The drops had various sizes, ranging from 1 to approximately 10^2 μm (Figure 4.11, C). The aspect evidenced by cryo-SEM back-scattered electrons (BSE) images collected for the PHB-EL-EDDS gel was in accordance with the appearance of emulsions, as reported in the literature (Mikula and Munoz, 2000; Xiao *et al.*, 2022). The complexing agent seemed immiscible in the PHB-based gelled formulation. Finally, it is relevant to address the attention towards the region within a droplet of EDDS solution (i.e., homogeneous and spherical element on the left of the image) and the PHB-matrix (i.e., region presenting holes on the right-side of the image), as reported in Figure 4.11, D. The image in BSE showed a gap of almost 2 μm between one element and the other one, where the polymer structure was only poorly linked to the EDDS drop.

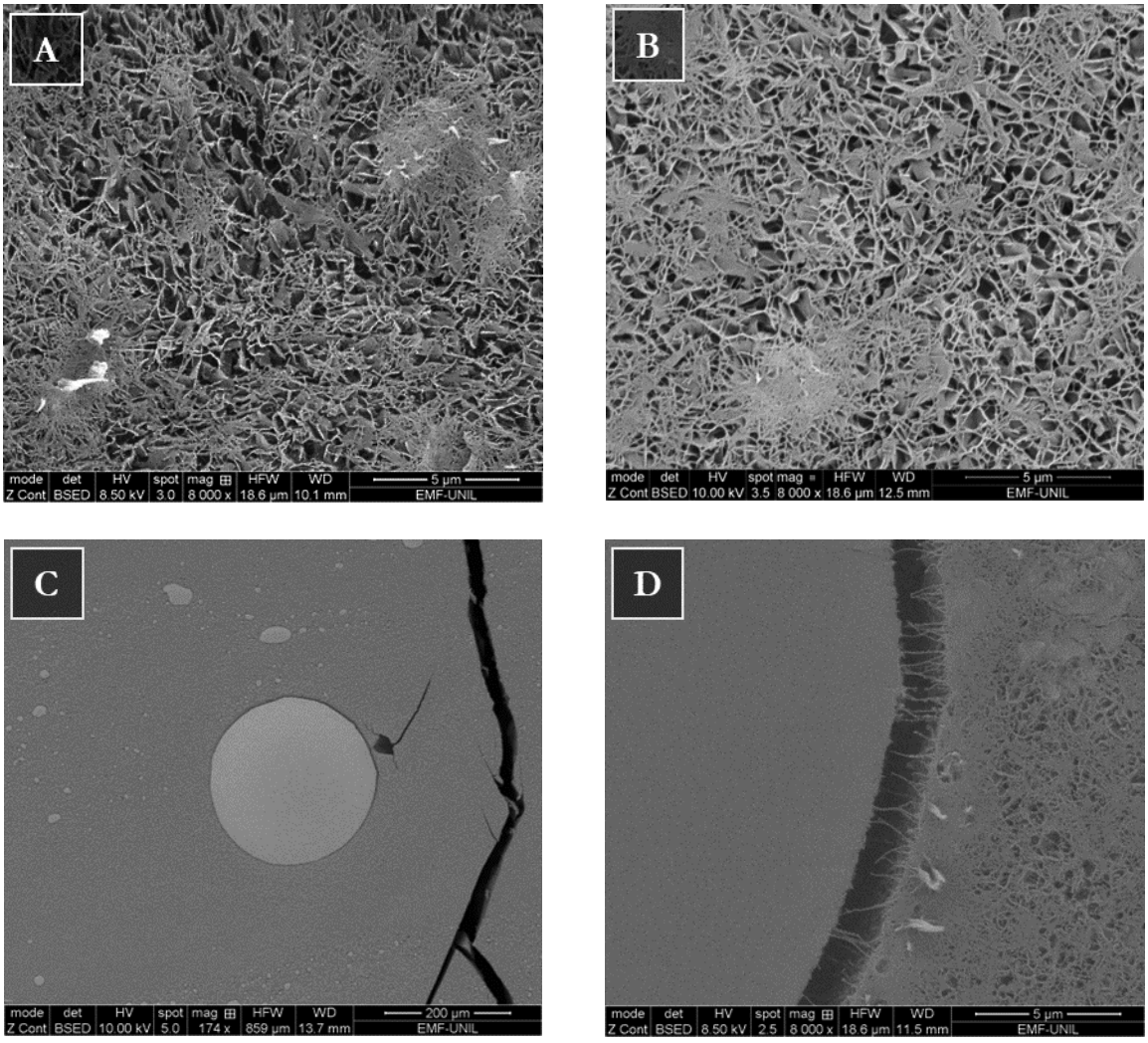

Figure 4.11 Cryo-SEM back-scattered electrons (BSE) images of PHB-EL-EDDS inner structure after sublimation etching and platinum coating. Inner porosities of the PHB-EL-EDDS gel (A) compared to the PHB-EL system (B). Broad aspect of the PHB-EL-EDDS gel showing differently sized EDDS droplets (C) and their interaction with the PHB-gel matrix (D). The scale bar indicates 5 μm in images A, B, and D, and 200 μm for image C.

4.3.3.3 Thermogravimetric analysis (TGA)

The PHB-EL-EDDS gel was analysed by thermogravimetric analysis (TGA) to evaluate the evaporation of the liquid phase retained compared to the unrestrained EDDS solution (i.e., 20% in deionised water) in

ethyl lactate (i.e., 1:5). The analysis was an isothermal run at 40 °C, hence the recorded weight loss could be ascribed entirely to the volatilization of the liquid phase present in the samples and not to the polyhydroxybutyrate matrix in the case of gelled specimens. Indeed, the bio-polymer will remain in a solid state at the temperature reached during the TGA run (McAdam *et al.*, 2020). On the other hand, it was expected that EDDS would remain in solution as long as water was present, therefore a priori also the weight related to Na_3EDDS salt was excluded from the calculations. Accordingly, results shown in Figure 4.12 were estimated as weight loss percentages considering exclusively samples' liquid fraction to correctly interpret the obtained data. Additionally, the calculated first derivative of the TGA isothermal curves are shown in SM-Figure 13 to help the comparison of mass loss trends (i.e., evaporation rates) over time for each sample.

Thermogravimetric analysis proved that the EL-EDDS solution (Figure 4.12, purple dashed line) was more susceptible to evaporation compared to when retained in the polyhydroxybutyrate system (PHB-EL-EDDS gel) (Figure 4.12, purple solid line) over the 60 minutes of analysis in the set conditions. More precisely, at the end of the isothermal run, the residual weight of the unstrained EL-EDDS solution was approximately 15% of its initial value; on the other hand, the same solution could still preserve about 33% of its starting weight, when restrained in the PHB-EL-EDDS gel. The test proved that the gelled formulation could hamper the unwanted loss of active solution in the atmosphere in the explored conditions.

The comparison of the TGA responses obtained from a plain PHB-EL gel (Figure 4.12, green solid line) to the version additionally loaded with EDDS (i.e., PHB-EL-EDDS, Figure 4.12, purple solid line) could highlight a different behaviour of the two systems when analysed in the same experimental conditions. Specifically, the two TGA curves intercept each other along the isothermal run. It was noticeable that before this crossover point, the PHB-EL-EDDS gel tended to lose weight faster than the PHB-EL gel, whereas trends changed after the crossover. This difference was possibly linked to the presence of EDDS-aqueous solution. Indeed, water has higher vapour pressure (i.e., 2.34 kPa at 20 °C) compared to ethyl lactate (i.e., 0.27 kPa at 20 °C), therefore would explain the greater initial rate of evaporation for the PHB-EL-EDDS system. However, in a second instance, water is also the solvent employed to solubilise the Na_3EDDS salt. Figure 4.12 (black dashed line) presents the TGA curve collected, in the same conditions, for an aliquot of 35% Na_3EDDS solution, considering only the liquid fraction for the weight loss calculation. It could be clearly evidenced that despite an initially rapid weight loss (approximately till 10 minutes), the analysis then registered lower %weight changes over time, justifying the behaviour of the PHB-EL-EDDS system.

Finally, when comparing the EL-EDDS solution (Figure 4.12, purple dashed line) to the sole ethyl lactate solvent (Figure 4.12, red dashed line), the trend of the two TGA curves were similar over time and in the same set conditions, if considering only the liquid fractions.

In general, as already mentioned, the analysis proved the ability of the gelled formulation to mitigate the undesired loss of active solution by evaporation in the explored conditions. Nonetheless, shown values cannot be considered quantitatively due to jeopardising factors such as the different geometry of the cut gels (i.e., thickness, surface) and possible partial evaporation of the loaded solutions during the preparation of different specimens (i.e., water and ethyl lactate fractions).

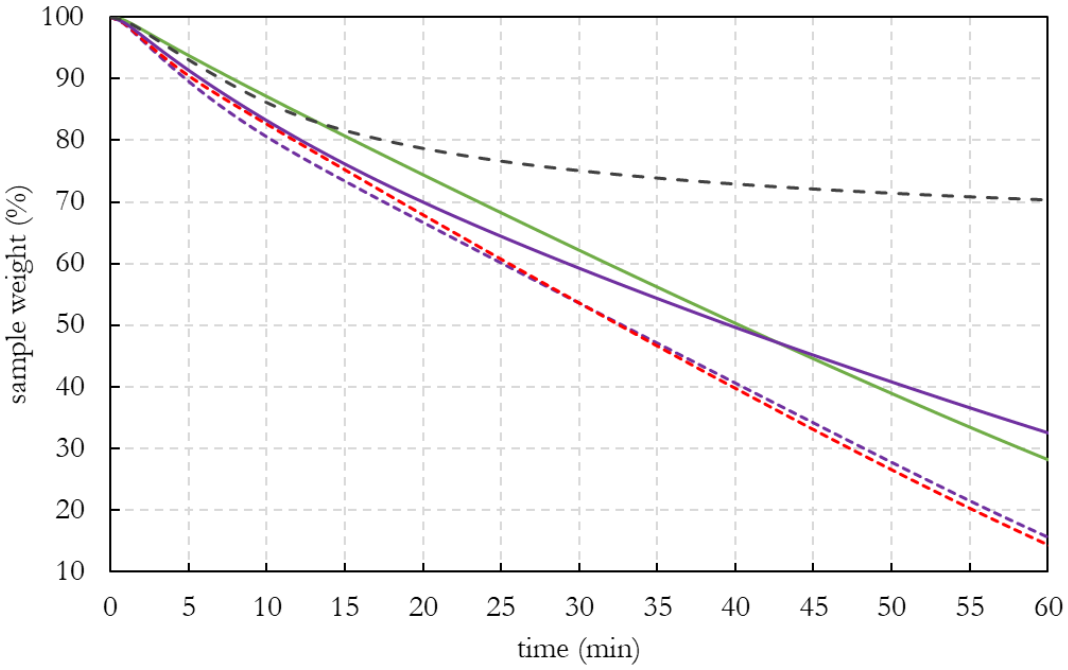

Figure 4.12 Isothermal TGA scan at 40 °C in nitrogen atmosphere comparing the weight loss of free EL-EDDS-water solution (purple, dashed) to the PHB-EL-EDDS gel (purple, solid). As a comparison, TGA curves for PHB-EL gel (green, solid), neat EL solvent (red, dashed), and 35% EDDS solution (black, dashed) acquired in the same experimental conditions are also reported. Data were processed considering samples' liquid fraction solely.

4.4 Cleaning assessment

4.4.1 Preliminary test

Before proceeding with the assessment of the cleaning system loaded with EDDS, some preliminary evaluations are pointed out in order to understand the outcomes displayed on mock-ups.

Firstly, it is relevant to remind the assay carried out to verify the reliability in the use of ethyl lactate on brass (i.e., Cu 66%, Zn 34%), already presented in Paragraph 2.3.1. The 90-minute immersion test in ethyl lactate (i.e., solvent present in the PHB-EL-EDDS system) did not show possible negative effects provoked by the interaction between brass and the organic solvent. No manifest surface alteration could be noticed on brass when inspected by optical microscopy (50× magnification), neither when comparing colorimetric data before and after immersion, fostering the exploitation of ethyl lactate in this study.

In the second instance, a 5 × 5 cm^2 brass coupon, tarnished following the method described in Paragraph 4.2, was employed to evaluate the potential contribution of the individual gel components in the process of tarnish removal. Namely, the liquid fraction was explored, therefore the same quantity (200 µL) of deionised water, ethyl lactate, and EDDS (35%) was applied in different areas of the mock-up, as described in Figure 4.13. In the case of ethyl lactate (EL) and deionised water, 30 minutes of application and afterwards dry cotton swabbing was employed to remove any residue and potentially detach tarnishing products for the metal sheet. No visual evidence of efficacy in cleaning could be observed for both methods. On the contrary, when testing EDDS with the same application time (i.e., 30 minutes), a clear removal of alteration was noticeable. Encouraged by the outcome, longer application times (i.e., 200 µL left for one and two hours) were essayed on the same coupon for comparison, demonstrating the ability of the compound to further chelate the corrosion products present with prolonged applications (Figure 4.13).

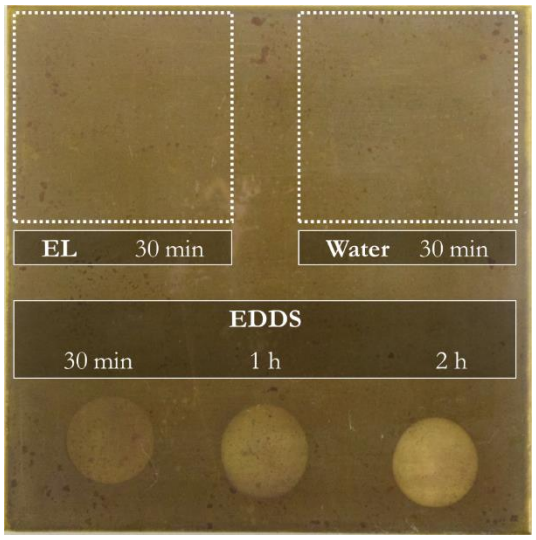

Figure 4.13 Chemically tarnished brass coupon (5 × 5 cm^2) treated with ethyl lactate (EL) and deionised water for 30 minutes (related areas outlined in white), and with EDDS (35% in water) for 30 minutes, 1 hour, and 2 hours, as graphically reported. The photography shows the final outcomes after dry cotton swabbing for EL- and water-treated areas, whereas wet (i.e., deionised water) cotton swabbing was used in the areas treated by EDDS solution.

It is crucial to report that when testing EDDS, a final clearance of the metal by cotton buds soaked in deionised water was required to remove the metal-EDDS complexes formed. Indeed, preliminary attempts demonstrated the residual presence of EDDS and possibly related complexes, when closing the cleaning protocol solely by dry cotton swabbing, identifiable by optical microscopy as little droplets on the metallic sheet (Figure 4.14, a). The use of a water-based clearance solution appeared necessary to solubilise and remove EDDS-related species present on the metal coupon. As illustrated in Figure 4.14, b, no traces of EDDS compounds are found when clearing the same mock-up with ethanol 70% v/v by cotton-swabbing. Ethanol 70% v/v was selected as clearance solution because it is normally used by CRs to clear treated surfaces with a volatile solution that would be less prone to persist on brass substrates.

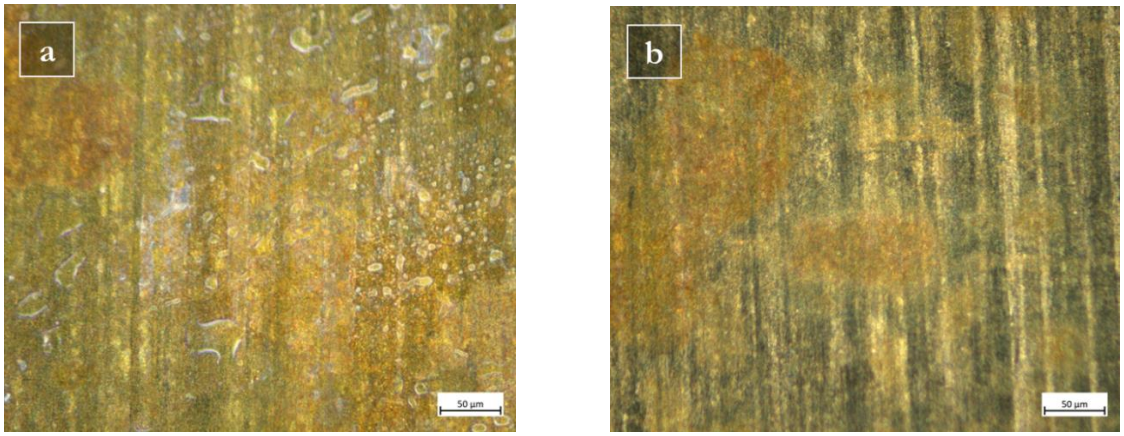

Figure 4.14 Optical microscope images, acquired in dark-field illumination, of chemically tarnished brass after 30-minute EDDS (35%) application. Metal surface after dry cotton swabbing still showing EDDS solution droplets (a) and after clearing with ethanol 70% v/v solution by cotton-swabbing (b). The scale bar indicates 50 µm.

Colorimetry was also applied in order to corroborate the visual appearance of the brass coupon after cleaning. The variation of CIELab coordinates collected on the chemically tarnished brass coupon before and after each cleaning assay (i.e., ethyl lactate, deionised water, and EDDS solution 35%) is reported in Table 4.3. No relevant variations occurred in areas cleaned for 30 minutes with deionised water and ethyl lactate. On the contrary, a gradual enhancement of the metal brightness (i.e., ΔL^*) was registered during the

treatment by EDDS solution with the prolongation of contact time (i.e., 30 minutes, 1 hour, and 2 hours). Additionally, the cleaning by EDDS drop for all explored timings yielded higher Δb* values, which suggested a gain in the yellow component in line with the original colouration of brass sheets before the patination process (Figure 4.4).

Table 4.3 Variation of CIELab coordinates of chemically tarnished brass coupon before and after different cleaning tests. ΔL*, Δa* and Δb* SCE values measured on the coupon areas treated for 30 minutes with deionised water and ethyl lactate, and by EDDS (35% w/w solution in deionised water) for 30 minutes, 1 hour, and 2 hours. Data are reported along with their standard deviation into brackets.

Method	Contact time	ΔL*	Δa*	Δb*
Deionised water	30 minutes	-0.06 (±0.56)	0.22 (±0.36)	-0.65 (±0.51)
Ethyl lactate	30 minutes	-0.14 (±0.59)	0.51 (±0.05)	0.12 (±0.13)
EDDS 35% w/w solution	30 minutes	4.42 (±1.32)	0.68 (±0.03)	4.28 (±0.51)
	60 minutes (1 hour)	9.16 (±1.07)	0.67 (±0.04)	3.35 (±0.34)
	120 minutes (2 hours)	16.12 (±0.27)	1.32 (±0.04)	5.44 (±0.45)

Finally, elemental analysis by X-ray fluorescence (XRF) spectroscopy was carried out on the EDDS solution (35%) applied for 30 minutes on the coupon. Indeed, before cleaning by cotton swabbing, the EDDS drop was re-collected by micropipette and stored in a glass vial (Figure 4.15). XRF analysis was repeated on non-used EDDS samples in order to verify the origin of the blue colour then acquired by EDDS during the application on the tarnished brass coupon.

Figure 4.15 EDDS solution (35%) collected from a chemically tarnished brass coupon after 30 minutes of application.

The technique revealed the presence of copper and zinc only after EDDS was applied on the tarnished brass mock-up for 30 minutes (Figure 4.16). Specifically, the XRF peaks detected at approximately 8.0 and 8.9 keV correspond to the Kα and Kβ lines characteristic for copper, whereas zinc was distinguished by the signal at about 8.6 (Kα lines) and possibly the weak XRF peak at 9.5 keV (Kβ lines Zn). The presence of copper and zinc was evidently attributable to brass alloy and proved the ability of the EDDS solution to create complexes with the metallic ions coming from the tarnished layer. Additionally, the signals detected around 11.9 and 13.3 keV pointed out the unexpected presence of bromine. This element was registered in EDDS samples both before and after application, making assumable that a contamination was present in the material. Several tests were conducted to identify bromine source (e.g., EDDS, tools, glassware) and exclusively in the case of EDDS the presence of Br could be detected clearly, also when checking multiple

bottles of the product, despite not being reported in its specifications by the supplier (Merck, 2024b). The presence of bromine could be hypothetically linked to one of the most common ways of manufacturing EDDS in industry through the reaction between L-aspartic acid and ethylene dibromide (Neal and Rose, 1968). Nevertheless, this scenario would evidently question the bio-origin of the chemical and possibly make unsafe its use, being ethylene dibromide a toxic and carcinogenic compound (European Chemicals Agency (ECHA), 2024). Finally, for all samples, signals recorded in the spectral region above 16 keV were linked to the instrument X-ray tube anode in molybdenum (Figure 4.16).

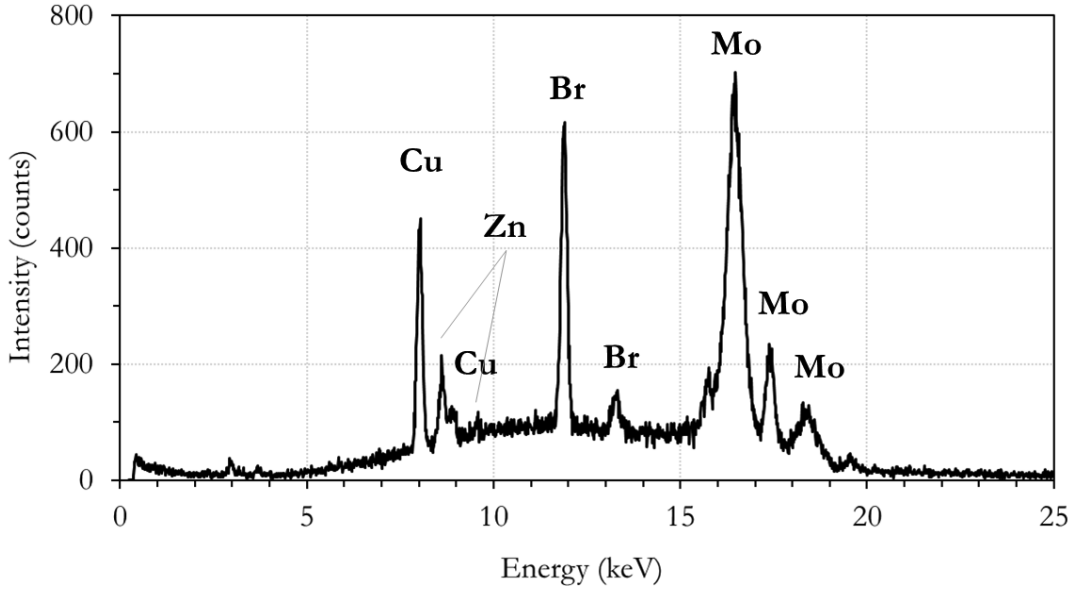

Figure 4.16 XRF spectrum of 35% w/w EDDS solution after a 30-minute application on a chemically tarnished brass coupon.

4.4.2 Cleaning protocol

The cleaning performance of the PHB-EL-EDDS gel was assessed modulating the application time and number of renewals on brass mock-up triplicates presenting both tarnish and coating, namely Zaponlack (Paragraph 4.2).

When preliminary tested on tarnished brass sheets, the gel was creating a staining effect on the metallic surface while cleaning (Figure 4.17), possibly because of the non-uniform distribution of the EDDS solution as verified by cryo-SEM images (Figure 4.11). To prevent this unwanted outcome, Japanese paper was additionally interposed between gel and coupon when operating for cleaning, in order to homogenise the contact between substrate and EDDS aqueous solution that was more evenly spread thanks to Japanese paper hydrophilicity and capillarity.

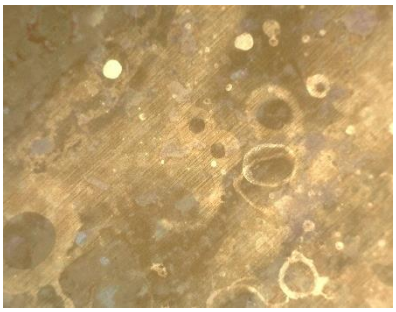

Figure 4.17 Chemically tarnished brass after a 10-minute application with PHB-EL-EDDS formulation without the use of Japanese paper. Optical microscope, 5× magnification.

Therefore, when tested on the double target mock-ups, firstly, Japanese paper (6 g/m^2, CTS) was cut into 5-cm-diameter circle-quarters and placed on the mock-up in the defined sectors described in Figure 4.18. After cutting the PHB-EL-EDDS gel in a 5-cm-diameter circle-quarter shape with a metallic spatula, the system was laid onto the pre-formed Japanese paper piece, and gently pressed with the metallic spatula to ensure the contact with the mock-up surface. The organogel was assayed on triplicate mock-ups by intervals of 10, 20, and 30 minutes, and by three consecutive applications, renewing both gel and Japanese paper each time. On each mock-up triplicate, a remaining area was kept untreated as a control (Figure 4.18).

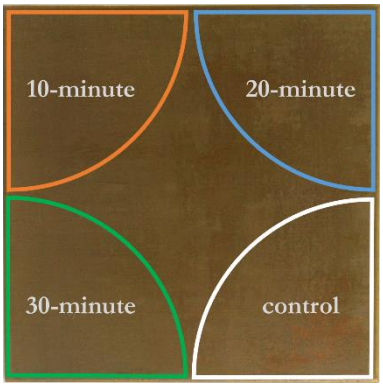

Figure 4.18 Graphical representation of the four equal areas (5-cm-diameter circle-quarters) defined on brass mock-ups (50 × 50 × 1 mm^3) for PHB-EL-EDDS cleaning assessment. Three areas were cleaned by intervals of 10 (top left corner, orange outline), 20 (top right corner, blue outline), and 30 minutes (bottom left corner, green outline), and a remaining area (bottom right corner, white outline) was kept untreated as a control.

After application, gels and Japanese paper were detached in one move by a metallic spatula. Eventually, the mock-up surface was cleared with ethanol 70% v/v by cotton-swabbing to remove possible gel residues, swollen Zaponlack, and EDDS-complexes formed during the application (Paragraph 4.4.1).

The described cleaning protocol was developed by varying only the gel application time (10, 20, or 30 minutes), while keeping constant factors such as chelating agent quantity ($4.8 \cdot 10^{-2}$ M) provided at each gel renewal, treated mock-up area dimensions (5-cm-diameter circle-quarter), and post-cleaning cotton-swabbing and clearance solution.

4.4.3 Multi-analytical protocol for the assessment of PHB-EL-EDDS gel cleaning

4.4.3.1 Visual appearance

Throughout the cleaning protocol, the action of the PHB-EL-EDDS formulation was visually manifest and increasing with the number of gel renewals for all different application times (i.e., 10, 20, and 30 minutes), leading to a final appearance after three reiterations as shown in Figure 4.19, a. In general, all cleaned sectors acquired a coloration closer to unaltered brass after cleaning. Moreover, the 30-minute cleaning yielded a more uniform removal and finishing with the naked eye. The cleaning process was stopped after 3

applications, since in the sector treated with the 30-minute protocol, the result was satisfactory by visual inspection (SM-Figure 12).

The effective double-target (i.e., corrosion layer and nitrocellulose lacquer) removal could be verified already when adopting a short-time protocol (i.e., 10 minutes). Indeed, already after one gel application, the system acquired a blue coloration that certified the ability of the gel to bypass the coating layer and tackle the corrosion products present underneath. Due to the poor translucence of the PHB-EL-EDDS gel, it was complex to monitor the chelating action over time. However, this could be clearly appreciated when removing gel and Japanese paper employed during the cleaning process. Compared to non-used gel and Japanese paper, the two materials acquired a blue colour, more vivid and homogeneously spread for longer application timings (Figure 4.19, b-c). The change in colour was linked to the formation of metal-EDDS complexes, as already observed when testing the EDDS solution directly on chemically tarnished brass (Figure 4.15).

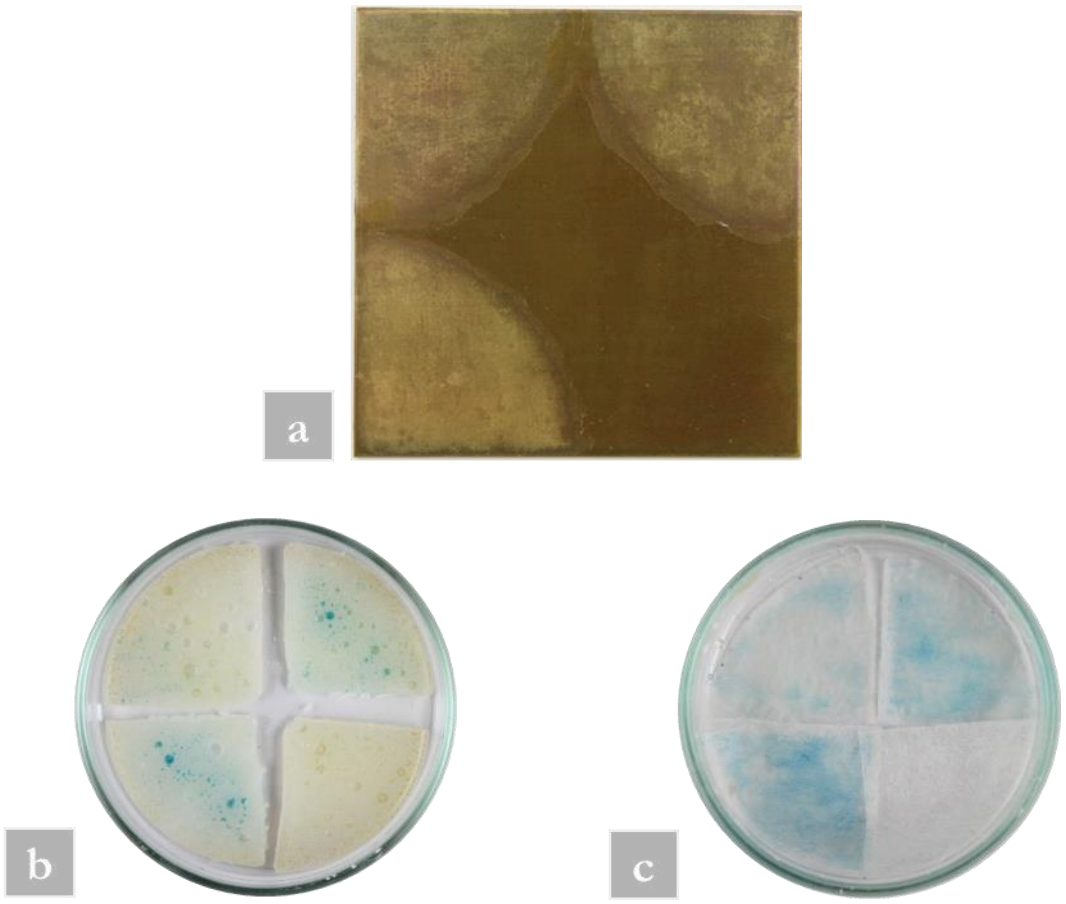

Figure 4.19 a) Brass mock-up (50 × 50 × 1 mm^3), chemically tarnished and coated with Zaponlack, treated by PHB-EL-EDDS gel. Cleaning outcomes after three gel applications of 10 (top left corner), 20 (top right corner), and 30 (bottom left corner) minutes, respectively. Bottom-right sector left untreated as a control. b) PHB-EL-EDDS gels removed from the mock-up after 10 (top-left sector), 20 (top-right sector), and 30 (bottom-left sector) minutes, and PHB-EL-EDDS gel not applied (bottom-right sector) as a control. c) Japanese paper pieces, employed together with the PHB-EL-EDDS gels, detached from the mock-up after 10 (top-left sector), 20 (top-right sector), and 30 (bottom-left sector) minutes, and Japanese paper not applied (bottom-right sector) as a comparison.

4.4.3.2 Optical microscopy

Optical microscopy could easily emphasise the mock-up surface features, in accordance with the broad observations obtained by simple naked eye inspection.

The treatment of 30 minutes with three PHB-EL-EDDS gel applications yielded a more homogeneous and efficient cleaning (Figure 4.20, c) compared to shorter timings of 10 and 20 minutes (Figure 4.20, a and b, respectively) despite adopting the same number of gel reiterations. Mock-up zones cleaned with the 30-minute protocol showed less dark-coloured patina compared to other application times, while gaining a more metallic yellow appearance, in agreement with the original appearance of brass coupons (Figure 4.4). Remarkably, no marked traces of gel residues could be observed in all treated areas.

When inspecting the same mock-up spots under UV light (SM-Figure 14), the technique could not reveal any characteristic fluorescence linked to an undesired residual presence of Zaponlack, which would appear blue when spread on the metallic surface, as observed on brass coupons previously (Figure 2.24). The outcome would verify the absence of nitrocellulose remains after treatment, however further investigation was carried out by vibration spectroscopy, as presented at page 182.

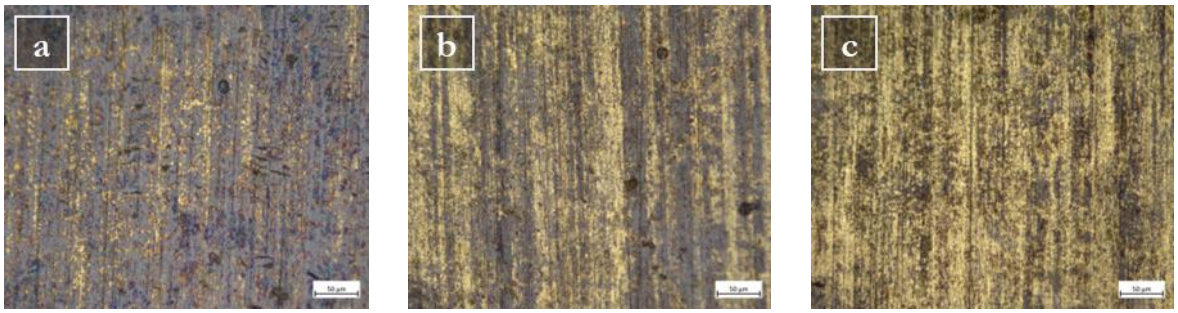

Figure 4.20 Optical microscope images in bright field of chemically tarnished brass coated with Zaponlack after three gel applications of 10 (a), 20 (b), and 30 (c) minutes, respectively. The scale bar indicates 50 μm.

4.4.3.3 Colorimetry

In the reference literature, often it is not specified whether SCI (i.e., Specular Component Included) or SCE (i.e., Specular Component Excluded) method was considered for the colour evaluation of brass substrates (Albano *et al.*, 2020; Truffa Giachet, Schröter and Brambilla, 2021; Molina *et al.*, 2023). Therefore, colorimetric data collected in both SCE and SCI modes are provided and discussed in this manuscript (raw data available in SM-Table 5). The measurements were performed on mock-up triplicates, before and after each PHB-EL-EDDS gel application, and were consistent with the observations provided by visual inspection and optical microscopy.

Comparing the CIELab coordinates of chemically tarnished brass coated with Zaponlack before and after cleaning, treated areas gained in brightness, as expressed by the positive ΔL^* values in both SCE and SCI modes, which are increasing consistently with gel renewals for all tested timings (Table 4.4). On the contrary, the progressive reduction in the red component, as stated by the mostly regular decrease in a^* values for all cleaning times explored (i.e., 10-, 20-, and 30-minute) (Table 4.4 for both SCE and SCI data), might indicate probably the removal of red tarnish phases such as cuprite and zincite, initially recognised on brass mock-ups by Raman spectroscopy (Paragraph 4.2). On the other hand, Δb^*, calculated between original metal surface and after cleaning, was higher in value for each gel reiteration and employing all times explored, as displayed in Table 4.4. This evidence would suggest a progressive reduction of the blue shades present on the surface of the mock-ups, probably related to the removal of covellite and possible residual copper nitrate

used for the chemical patination of the metallic sheets, in favour of yellow shades that are more linked to bare brass appearance (Paragraph 4.2).

When relating the cleaned mock-ups to non-tarnished and non-coated (i.e., without Zaponlack) brass coupons, the colour difference was still noticeable with the naked eye for cleaning protocols of 10- and 20-minute because of the residual presence of sporadic tarnish, whereas less difference was perceptible for areas treated with the 30-min cleaning. Visual perception was confirmed by colorimetry measurements that allowed to verify that the colour difference (ΔE*) between treated areas and bare brass decreased progressively with the number of gel renewals and for longer application times, as shown in Table 4.5 for both SCE and SCI methods. In particular, considering the SCE outcomes after three successive PHB-EL-EDDS applications, the ΔE* was calculated equal to 10.20 (± 0.26), 8.53 (± 0.21), and 4.11 (± 0.41) for mock-up areas cleaned with 10-, 20- and 30-minute process, respectively. It is relevant to highlight that only when adopting long application time (i.e., 30 minutes protocol), brass sheets reacquired a colour appearance considered acceptable as below the value of 5, which is generally considered a threshold for clear perception of colour difference by human eye – and therefore acceptability in art conservation (Kim, Kim and Park, 2011). However, when observing the same data in SCI mode, the colour difference between cleaned and bare brass was still relevant also in the case of a triple application of PHB-EL-EDDS gel for 30 minutes, being calculated equal to 27.25 (±0.05) (Table 4.5).

Statistical analysis was finally applied to colorimetric data to validate the significance of differences detected as visual appearance for mock-up sectors cleaned by the various times and reiterations tested by application of PHB-EL-EDDS gels (Lo Monaco *et al.*, 2011). In particular, Tukey's HSD test demonstrated that the combination of time and reiteration was crucial for the distinction of colorimetric outcomes in SCE mode. The method proved that the difference in terms of a* and b* values between cleaned mock-up sectors and bare brass was considered significant ($p < 0.01$) for all timings and gel renewals explored during the cleaning protocol, except for the case of the triple 30-minute application ($p > 0.05$). This outcome would possibly confirm what discussed previously, hence that the altered mock-ups cleaned by this protocol (i.e., 30 minute × 3 applications) could recover a colour appearance typical of brass substrates by the effective removal of reddish-blue shades related to the presence of the tarnish compounds.

On the contrary, when applying the statistical test to colorimetric data in SCI mode, a relevant difference was determined when comparing L*, a*, and b* values related bare brass coupons (i.e., references) to all cleaned mock-ups ($p > 0.05$), without demonstrating the 30-minute as better performing for the recovery of the unaltered brass appearance. However, the colorimetric outcome provided by this cleaning protocol (i.e., 30 minute × 3 applications) was recognised as significantly different compared to all other timings and gel renewals explored, when evaluating L* (i.e., brightness) and b* (i.e., yellow component) variables.

Table 4.4 Variation of CIELab coordinates of the tarnished and coated (i.e., Zaponlack) brass mock-up sectors after each cleaning step by PHB-EL-EDDS gel compared to their initial condition. ΔL*, Δa*, Δb* and related ΔE* SCE and SCI values are reported along with their standard deviation into brackets.

	Cleaning time	Number of gels	ΔL*	Δa*	Δb*	ΔE*
SCE	10 minutes	1	4.18 (±0.18)	-1.25 (±0.45)	-6.57 (±0.18)	8.42 (±0.19)
		2	6.14 (±0.84)	-1.85 (±0.62)	-6.93 (±0.25)	9.93 (±0.59)
		3	8.72 (±0.11)	-2.37 (±0.11)	-4.93 (±0.57)	10.67 (±0.29)
	20 minutes	1	3.41 (±0.21)	-0.79 (±0.16)	-7.80 (±0.47)	8.06 (±0.44)
		2	6.94 (±2.02)	-1.71 (±0.57)	-6.96 (±0.85)	9.36 (±1.53)
		3	10.75 (±0.20)	-2.22 (±0.06)	-4.50 (±0.34)	11.22 (±0.22)
	30 minutes	1	6.98 (±1.00)	-1.62 (±0.04)	-7.12 (±0.47)	10.10 (±0.77)
		2	10.27 (±0.71)	-2.32 (±0.13)	-4.52 (±0.16)	11.46 (±0.64)
		3	14.62 (±0.74)	-2.18 (±0.12)	-1.49 (±0.03)	14.86 (±0.73)
SCI	10 minutes	1	7.68 (±1.60)	-0.19 (±0.30)	-5.09 (±0.68)	9.01 (±1.38)
		2	12.38 (±3.55)	-0.64 (±0.10)	-4.45 (±1.74)	13.01 (±3.39)
		3	13.85 (±2.12)	-0.89 (±0.16)	-1.77 (±0.56)	13.88 (±2.10)
	20 minutes	1	5.75 (±2.15)	-0.53 (±0.14)	-6.86 (±1.24)	8.65 (±1.68)
		2	11.98 (±2.49)	-0.47 (±0.28)	-5.09 (±2.63)	12.74 (±2.51)
		3	13.43 (±0.55)	-0.16 (±0.12)	-0.50 (±0.77)	13.22 (±0.55)
	30 minutes	1	10.64 (±1.37)	-0.40 (±0.08)	-4.69 (±0.63)	11.64 (±1.28)
		2	15.32 (±1.15)	-0.61 (±0.15)	0.09 (±1.22)	15.34 (±1.15)
		3	19.93 (±0.25)	-0.69 (±0.17)	5.07 (±0.90)	20.58 (±0.33)

Table 4.5 Variation of CIELab coordinates of the tarnished and coated (i.e., Zaponlack) brass mock-up sectors after each cleaning step by PHB-EL-EDDS gel compared to bare unaltered brass sheets, used as control. ΔL*, Δa*, Δb* and related ΔE* SCE and SCI values are reported along with their standard deviation into brackets.

	Cleaning time	Number of gels	ΔL*	Δa*	Δb*	ΔE*
SCE	10 minutes	1	-12.77 (±0.08)	4.19 (±0.53)	-6.76 (±0.37)	15.05 (±0.23)
		2	-10.81 (±0.74)	3.59 (±0.70)	-7.12 (±0.44)	13.43 (±0.67)
		3	-8.23 (±0.20)	3.06 (±0.19)	-5.13 (±0.38)	10.17 (±0.26)
	20 minutes	1	-14.26 (±0.11)	4.60 (±0.23)	-7.14 (±0.56)	16.60 (±0.27)
		2	-10.73 (±1.92)	3.68 (±0.65)	-6.30 (±0.76)	12.98 (±1.64)
		3	-6.93 (±0.11)	3.17 (±0.01)	-3.84 (±0.42)	8.53 (±0.21)
	30 minutes	1	-10.14 (±0.87)	3.63 (±0.32)	-6.75 (±0.61)	12.71 (±0.77)
		2	-6.84 (±0.58)	2.93 (±0.23)	-4.15 (±0.01)	8.53 (±0.47)
		3	-2.49 (±0.61)	3.07 (±0.24)	-1.12 (±0.11)	4.11 (±0.41)
SCI	10 minutes	1	-34.41 (±1.82)	2.40 (±0.43)	-25.80 (±0.73)	43.07 (±1.04)
		2	-29.70 (±3.13)	1.95 (±0.02)	-25.16 (±1.78)	38.97 (±2.65)
		3	-28.23 (±1.70)	1.70 (±0.03)	-22.48 (±0.60)	36.13 (±1.38)
	20 minutes	1	-36.49 (±1.82)	1.37 (±0.04)	-27.53 (±0.80)	45.73 (±1.53)
		2	-30.26 (±2.15)	1.44 (±0.45)	-25.77 (±2.19)	39.77 (±2.17)
		3	-28.80 (±0.21)	1.75 (±0.06)	-21.17 (±0.33)	35.79 (±0.26)
	30 minutes	1	-31.36 (±1.07)	2.03 (±0.15)	-25.65 (±0.22)	40.56 (±0.84)
		2	-26.68 (±0.85)	1.82 (±0.08)	-20.87 (±0.37)	33.92 (±0.71)
		3	-22.07 (±0.05)	1.74 (±0.06)	-15.89 (±0.05)	27.25 (±0.05)

4.4.3.4 Eddy current measurements

Eddy current data could clearly verify the massive removal of Zaponlack already after one application for all explored timings (i.e., 10, 20, and 30 minutes) (Table 4.6). Specifically, the device registered an initial average thickness of the corrosion-Zaponlack layer present on mock-ups equal to 3.70 (± 0.64) μm that decreased down to 0.03 (± 0.42) μm for areas cleaned by one gel application of 10 minutes, -0.03 (± 0.30) μm for one application of 20-min, and finally -0.14 (± 0.37) μm after one gel application of 30 minutes. In general, average values, correlated with their standard deviations, were all falling in the instrumental sensitivity error of ±0.7 μm + 1% of value, justifying the occasional negative values registered by the device. However, no relevant difference could be appreciated within the several steps of application of each cleaning timing, as shown in Table 4.6 and further confirmed by Tukey's HSD test (i.e., p value greater than 0.05).

To understand this not informative outcome, it was necessary to refer to mock-ups before being coated with the nitrocellulose lacquer. Indeed, Eddy current measurements collected from chemically tarnished brass coupons prior to coating showed an average thickness equal to 0.18 (± 0.43) μm (Table 4.6). It could be deduced that the alteration thickness present on the tarnished brass coupons was out of the sensitivity range of the device employed in this study. Therefore, the system could not be exploited to discriminate among the different application times when referring to the removal of the tarnish layer, which on the contrary could be followed by visual inspection, optical microscopy, and partially by colorimetry in SCE mode.

Table 4.6 Average alteration (i.e., tarnish and organic coating) layer thickness (μm) measured by Eddy current for chemically tarnished and chemically tarnished and coated (i.e., Zaponlack) brass coupons before and after each interval of PHB-EL-EDDS gel cleaning. Values are reported along with their standard deviation.

Mock-up initial condition	Cleaning time	Number of gels	Alteration thickness (μm)
Tarnished	0 minutes	0	0.18 (±0.43)
Tarnished and coated	10 minutes	0	3.28 (±0.62)
		1	0.03 (±0.19)
		2	-0.14 (±0.34)
		3	0.15 (±0.16)
	20 minutes	0	3.78 (±0.40)
		1	-0.03 (±0.30)
		2	0.05 (±0.33)
		3	0.05 (±0.37)
	30 minutes	0	4.05 (±0.64)
		1	-0.14 (±0.37)
		2	-0.10 (±0.33)
		3	-0.05 (±0.30)

4.4.3.5 X-Ray Fluorescence (XRF) spectroscopy

Elemental analysis by X-ray fluorescence (XRF) spectroscopy was carried out on PHB-EL-EDDS gels and Japanese paper employed for a 10-minute cleaning on brass mock-ups tarnished and coated with Zaponlack. The analysis was repeated before and after the cleaning application in order to verify both the cleaning efficiency of the gel already with a short-time application (10 minutes) and the origin of the blue colour acquired during the cleaning treatment by the two types of samples. Equally, cotton buds, used for the clearance step on mock-ups, were analysed to investigate the blue coloration acquired.

The technique revealed the presence of copper and zinc only after the PHB-EL-EDDS gel was applied on the tarnished brass mock-up coated with Zaponlack. Specifically, the XRF peaks detected at approximately 8.0 and 8.9 keV correspond to the Kα and Kβ lines characteristic for copper, whereas zinc was detected by the signals at about 8.6 (Kα lines) and 9.5 keV (Kβ lines) (Figure 4.21). The presence of copper and zinc was evidently attributable to brass and proved the ability of the gel system to tackle the tarnished layer present and adsorb the metal-EDDS complexes formed. Additionally, the signal detected around 11.9 keV could be linked to an unexpected presence of bromine, as already found when analysing neat EDDS applied for 30 minutes on chemically tarnished brass (Figure 4.16), which was considered as a contamination of the commercial product (Sigma Aldrich).

Similarly, Japanese paper employed in support of the PHB-EL-EDDS system and cotton buds employed to clear treated mock-up areas were analysed and showed the presence of Cu and Zn after the cleaning protocol, as reported in Figure 4.22.

Finally, for all samples, the triplet of signals recorded in the spectral region above 16 keV were linked to the instrument X-ray tube anode in molybdenum (Figure 4.21 and Figure 4.22).

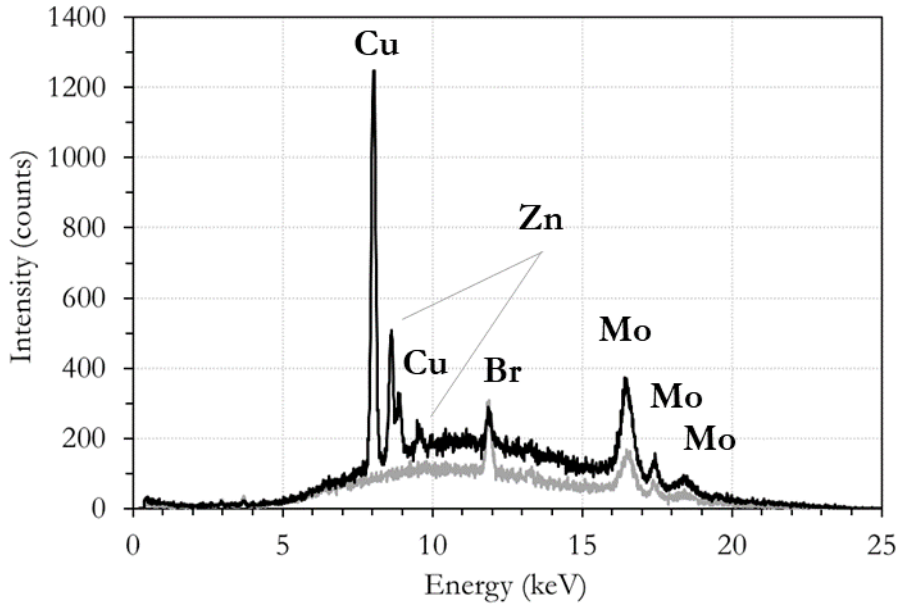

Figure 4.21 XRF spectra of PHB-EL-EDDS gel before (grey) and after (black) one application of 10 minutes on a tarnished brass mock-up coated with Zaponlack. Signals interpretation is reported in the figure.

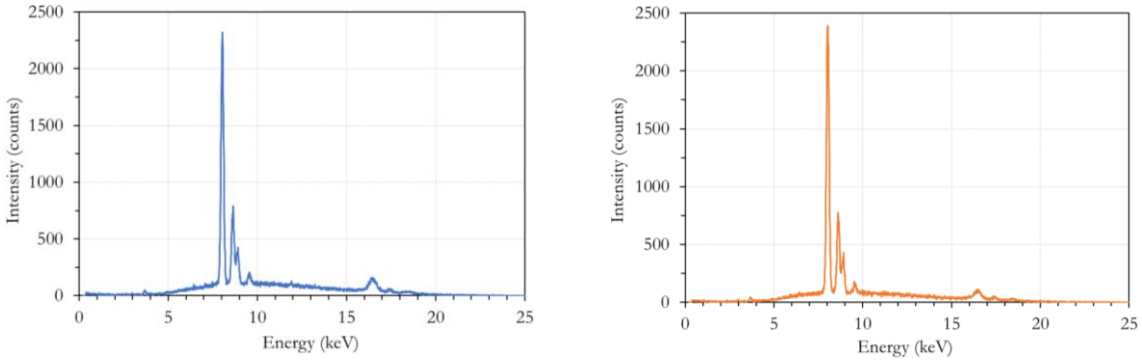

Figure 4.22 XRF spectra of Japanese paper (blue) and cotton swab (orange) employed during the 10-minute cleaning protocol on tarnished brass mock-ups coated with Zaponlack.

4.4.3.6 Fourier-transform infrared (FTIR) spectroscopy – Gel characterisation

Reference FTIR spectra of 35% w/w EDDS solution before and after 30-minute application on chemically tarnished brass were collected in macro-ATR mode to investigate the chelating action of the ligand and characterise EDDS and related complexes (Figure 4.23).

Previous studies, focusing on the identification of EDDS and its complexes by Fourier-transform infrared spectroscopy, discussed mainly FTIR bands detected in the spectral region 1700-1300 cm^{-1}, being more significant for the detection of metal-EDDS complexes (Lanigan and Pidsosny, 2007; Tsang *et al.*, 2013). A similar approach was adopted for the interpretation of collected FTIR spectra, and a satisfying correlation between acquired data and literature could be achieved (Table 4.7). The most diagnostic features for the detection of metal-EDDS complexes were recognised in the stretching vibrations of carboxyl groups (Lanigan and Pidsosny, 2007). More in detail, the formation of complexes with metal ions tends to shift the intense band present in EDDS spectrum at 1621 cm^{-1} towards lower wavenumbers, and the couple of bands at about 1564 and 1386 cm^{-1} seemed diagnostic for Me-EDDS complexes, being poorly intense or fully absent in EDDS FTIR spectrum (Figure 4.23).

Little bands shifts are reported in the literature for EDDS species formed in association to zinc and copper ions (Lanigan and Pidsosny, 2007). In this study, the analysis could not reveal such distinction on EDDS after application on brass (Figure 4.23, b). The collected spectra were characterised by strong but quite broad bands, which might be symptomatic of the co-presence of Cu- and Zn-complexes.

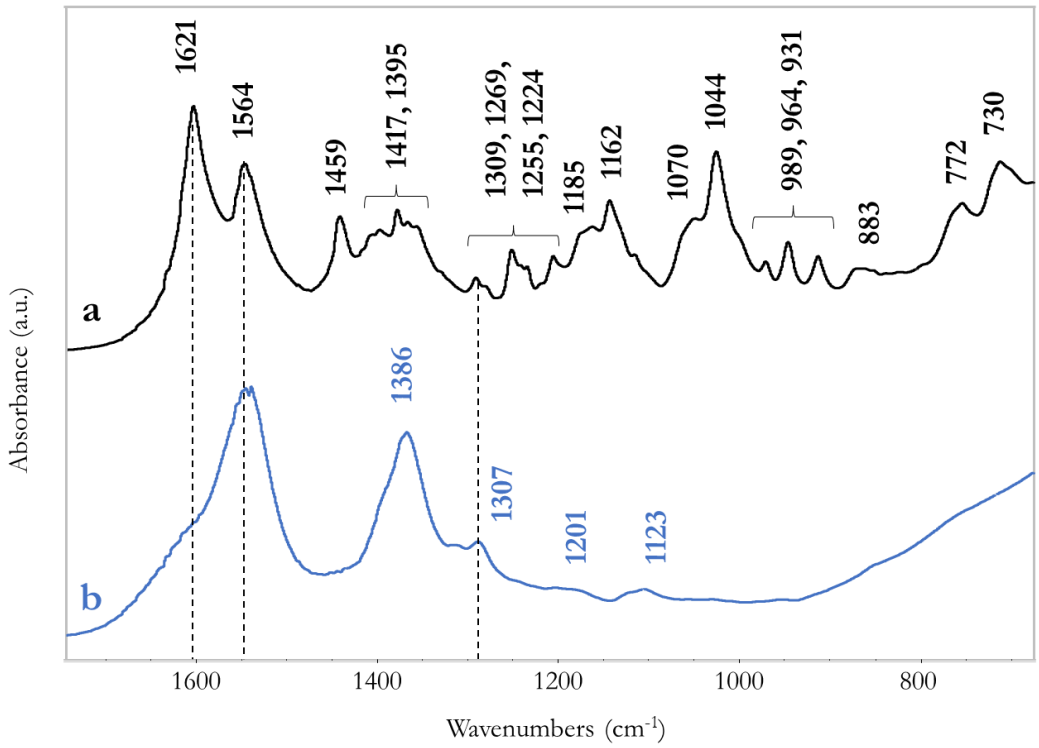

Figure 4.23 ATR-FTIR spectra of EDDS solution (35% w/w) before (a) and after being applied on chemically tarnished brass (b). FTIR signals in common between spectra are highlighted by dashed lines. The FTIR wavenumbers diagnostic for the two samples are reported in the figure above the respective spectra.

Table 4.7 Characteristic FTIR signals detected for EDDS before (a) and after 30-minute application on chemically tarnished brass (b) (Lanigan and Pidsosny, 2007).

EDDS (a)		EDDS on brass (b)		Assignment
1621	s			$\nu(CO_2^-)$
1564	s	1564	vs	$\nu(CO_2^-)$
1459	m			$\delta(CH_2)$
1417	w			$\nu(CO_2^-)$
1395	w			ν(C-N)
		1386	vs	ν(C-N)
1309	w	1307	m	-COO$^-$
		1123	w	ν(C-N)

vs = very strong, s = strong, m = medium, w = weak, vw= very weak signal; ν = stretching, δ= bending. All values are expressed in cm^{-1}.

No clear distinction could be enhanced by comparison of FTIR spectra collected on PHB-EL-EDDS gels before and after application on chemically tarnished brass coated with Zaponlack for 30 minutes. Neither

metal-EDDS complexes nor Zaponlack removed from the mock-up surface could be identified on the gel side in contact with mock-ups during the cleaning, because of the predominant FTIR signals related to the PHB matrix.

In contrast, FTIR spectrum collected from the Japanese paper employed for the cleaning process, together with PHB-EL-EDDS gel, could verify the double presence of EDDS complexes and Zaponlack on the tissue surface in contact with the brass mock-up (Figure 4.24, a). Intense signals at 1567 and 1386 cm^{-1} could ascertain the presence of Me-EDDS species, whereas Zaponlack detached from the mock-up would be present on the Japanese paper as suggested by the weak signals recorded at 1725 and 1280 cm^{-1}, which cannot be assigned to EDDS species (Figure 4.24, c) or to Japanese paper (Figure 4.24, d).

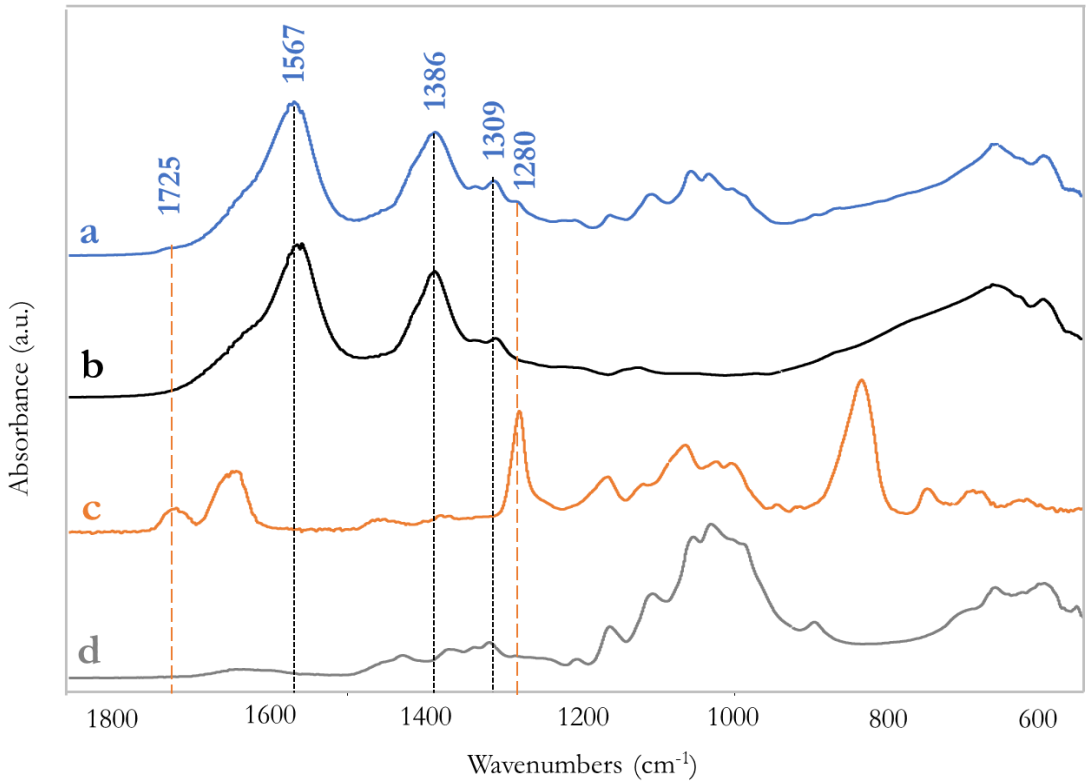

Figure 4.24 ATR-FTIR spectra of Japanese paper, used together with PHB-EL-EDDS gel, after 10-minute application on chemically tarnished brass coated with Zaponlack (a), EDDS solution (35% w/w) applied for 30 minutes on a chemically tarnished brass sheet (b), Zaponlack (c), and non-used Japanese paper (d). For spectrum a, FTIR signals in common with spectrum b and c are highlighted by black dotted and orange dashed lines, respectively.

4.4.3.7 Raman spectroscopy – Gel characterisation

Similarly, reference spectra of both EDDS (35% w/w solution) and EDDS after 30-minute application on chemically tarnished brass were collected by micro-Raman spectroscopy to verify the chelating action of the ligand, and successively ascertain the effectiveness directly on PHB-EL-EDDS gels (Figure 4.25).

To the best of author's knowledge, no previous characterisation of EDDS and EDDS complexes with Cu and Zn (i.e., brass alloy) is reported in literature by means of Raman spectroscopy. However, a recent study exploited Raman spectroscopy in both resonance and non-resonance mode with a 532-nm laser to characterise EDDS complexes with Al(III) and Co(III) (Yang *et al.*, 2023). Despite expecting different Raman shifts due to the different metal cations (i.e., Cu and Zn), the publication was employed as a compass

for a tentative interpretation of signals detected in this research (Table 4.8). In particular, reference publications associate to both Al-EDDS and Co-EDDS species diagnostic Raman signals in the spectral region 1000-1200 cm^{-1}, linked to bending and torsion vibrations of metallic cations bonded to amino groups in the EDDS molecule (Yang *et al.*, 2023). In the same spectral region, similar vibrations were absent for EDDS, but could be detected in the case of EDDS after being in contact with tarnished brass (Figure 4.25). Specifically, Raman signals at about 573, 1004, 1075, and 1108 cm^{-1} would possibly indicate the formation of Cu- and/or Zn-EDDS complexes.

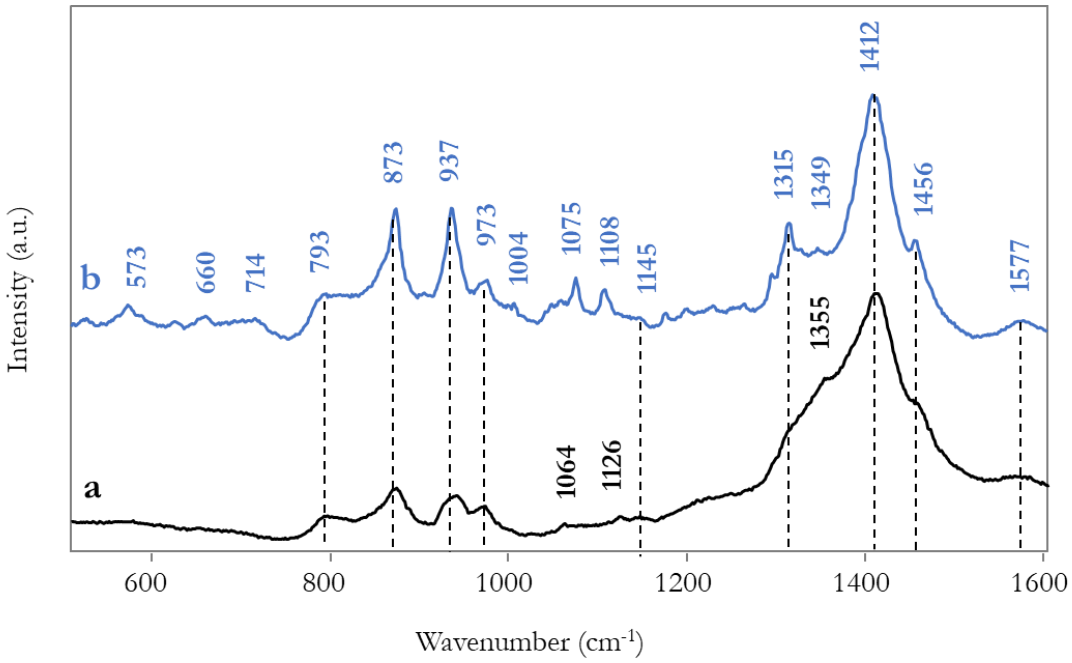

Figure 4.25 Raman spectra of EDDS solution (35% w/w) before (a) and after being applied on chemically tarnished brass (b). Raman bands in common between the spectra are highlighted by dashed lines. The wavenumbers of Raman peaks diagnostic for the two samples are reported in the figure above the respective spectra.

Table 4.8 Characteristic Raman signals detected for EDDS (a) and EDDS after 30-minute application on chemically tarnished brass (b). Hypothetical band interpretation based on Yang *et al.*, 2023.

EDDS (a)		EDDS on brass (b)		Assignment
		573	w	τ(C-C), ν(Me-N)
793	m	793	m	missing
873	m	873	s	τ(C-N), τ(C-C)
937	m	937	s	τ(C-N)
		1004	vw	δ(H-N-Me)
1064	vw			ν(C-C)
		1075	m	δ(H-N-Me), τ(N-Me)
		1108	m	τ(N-Me)
1126	vw			missing
1145	vw	1145	vw	missing
1315	sh	1315	s	δ(H-C-C)
1355	s	1349	m	δ(H-C-N)
1412	vs	1412	vs	δ(H-C-C)
1456	sh	1456	m	δ(H-C-N), δ(H-C-H)
1577	w	1577	m	missing

Me = metallic cation(s); vs = very strong, s = strong, m = medium, w = weak, vw= very weak, sh = shoulder signal; ν = stretching, δ= bending, τ = torsion. All values are expressed in cm^{-1}.

When researching similar spectral features in the PHB-EL-EDDS gel after application on tarnished brass coated with Zaponlack and on the Japanese paper sheet employed together with the gel, no clear distinction could be recognised between before and after application for both samples despite the blue coloration that was visibly present after application. Indeed, the spectral region, where Me-EDDS complexes could be recognised in the previous case, was showing characteristic bands for PHB (SM-Figure 15) and interference from fluorescence in the case of Japanese paper, respectively. Equally, no Raman peaks could be ascribed to the nitrocellulose lacquer on the gel-Japanese paper system after cleaning application.

4.4.3.8 Fourier-transform infrared (FTIR) spectroscopy – Mock-up cleaning

FTIR spectroscopy in reflectance mode was performed on mock-up replicates to monitor the effect of the several application times and gel reiterations tested on the cleaning achieved. Due to the wavenumber cut-off of the MCT detector couple to the FTIR spectrometer, the maximum spectral range of the technique employed was 4000-675 cm^{-1}, therefore no signals related to brass tarnish could be detected, since for copper sulphides Cu-S stretching vibrations are expected around 615 cm^{-1} (Kadam *et al.*, 2020), for zinc oxide the Zn-O stretching mode is at about 570 cm^{-1}, and in the case of cuprite IR vibrations are normally registered around 660 cm^{-1} (Hosseinpour and Johnson, 2017). Therefore, the technique was used to examine the presence of the organic coating (i.e., Zaponlack) on the mock-ups throughout the cleaning process.

Due to the large number of spectra to be compared (raw data are displayed in SM-Figure 16), a better readability was achieved processing FTIR data by Principal Component Analysis (PCA) in order to enhance differences related to the several applications and cleaning timings explored. Moreover, FTIR spectra collected from bare brass coupons were considered in the analysis as references. Finally, the spectral range was reduced to 1900-1250 cm^{-1} to focus the attention on the region of interest for the presence of Zaponlack (page 99).

Figure 4.26 proposes the resulting score (a) and loading (b) plots obtained by PCA when considering PC1 versus PC2. When referring to the loading plot for PC1, a separation along this axis was given especially by wavenumbers in the range 1440-1400 cm^{-1} and 1350-1280 cm^{-1}, which were read as a negative contribution of these variables on the loadings plot. These two sets of wavenumbers could be ascribed to C-H bending

and NO_2 stretching vibrations which are linked to the presence of Zaponlack in this study (Fernández de la Ossa *et al.*, 2011; Brock *et al.*, 2018). The result would suggest that relevant residual presence of the coating was detected only when applying the PHB-EL-EDDS system for 10 and 20 minutes without reiteration (Figure 4.26, black and yellow, respectively). In all the other cases the spectral features obtained by FTIR spectroscopy were resulting similar to those of bare brass.

This consideration would be corroborated by the observation of PC2 axis. In general, it was possible to visualise that the majority of spectra collected from cleaned mock-up sectors, together with bare brass references, were grouping around 0-value. PC2 was mainly characterised by a set of wavenumbers between 1670 and 1500 cm^{-1} that negatively affected the related loadings. In this spectral region, the FTIR signals for water bending vibrations are detected. Despite all collected spectra were pre-treated for the removal of atmospheric background noise (i.e., H_2O and CO_2), it could not be excluded an influence on the loading plot for PC2 linked to the presence of water vapour. This assumption would also explain why, for instance, the data collected for bare brass coupons were located also at PC2 negative values in the score plot.

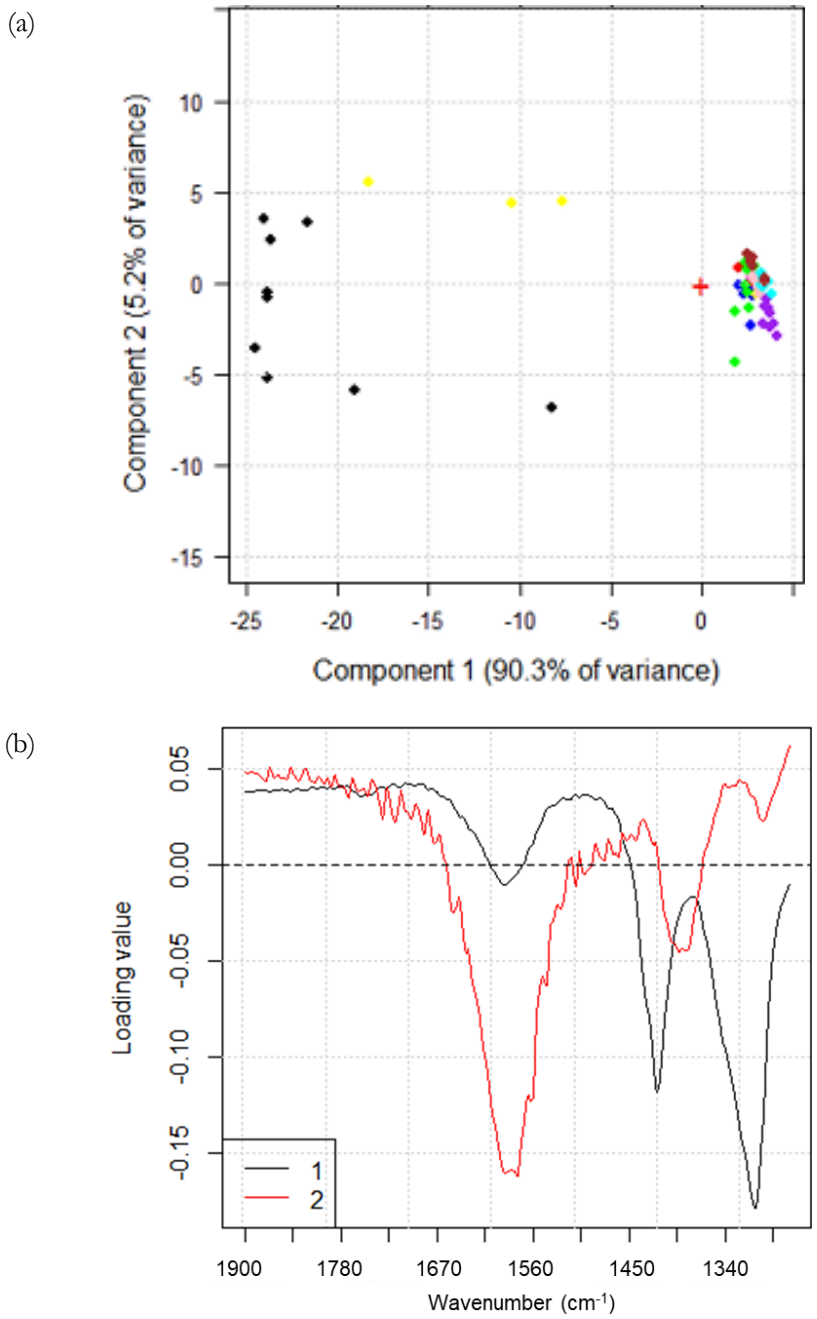

Figure 4.26 Score (a) and loading (b) plots obtained from PCA applied to FTIR spectra recorded on chemically tarnished brass mock-ups, coated with Zaponlack, after cleaning by one 10-minute (black), two 10-minute (red), three 10-minute (green), one 20-minute (yellow), two 20-minute (magenta), three 20-minute (turquoise), one 30-minute (blue), two 30-minute (pink), and three 30-minute (brown) PHB-EL-EDDS gel applications, and untreated bare brass coupons (purple). (b) Related PC1 (black) and PC2 (red) loading plot.

4.4.3.9 Raman spectroscopy – Mock-up cleaning

Micro-Raman spectroscopy was exploited to verify the removal of tarnish phases originally present on the surface of chemically aged brass coated with the nitrocellulose lacquer. The analysis was performed on the mock-ups before and after cleaning by PHB-EL-EDDS gel and on unaltered bare brass sheets as reference to verify the cleaning outcome. The resulting spectra (raw data are displayed in SM-Figure 17) were elaborated by Principal Component Analysis (PCA) to ease the readability of the information collected and,

in particular, evidence potential differences related to the cleaning timings explored. Consequently, the spectral range was circumscribed between 180-800 cm^{-1}, being of interest for the detection of Raman shifts diagnostic for the tarnish phases present on the brass mock-ups, as already observed (Figure 4.3). The resulting PC1 versus PC2 scatter plot is presented in Figure 4.27 (a), correlated with the loading plot for PC1 vs PC2 (b) that displays the spectral variables (i.e., wavenumbers) more involved in the data discrimination (i.e., clusters position along the PC axes).

A separation along PC1 axis in the loading plot was evident for wavenumbers in the range 200-230 cm^{-1} and 610-650 cm^{-1}, which were read as a positive contribution of these variables on the loadings plot (Figure 4.27, b). These two sets of wavenumbers could be ascribed to Raman shifts around 216 and 634 cm^{-1}, which could be linked to the presence of cuprite (Cu_2O) in this work (Bouchard and Smith, 2003; Cakir, 2017). The additional presence of variables between 550 and 590 cm^{-1} in the loading plot for PC1/PC2 was linked to the Raman-active vibration around 576 cm^{-1} diagnostic for amorphous zincite (ZnO) in this study (Qiu and Leygraf, 2011). In particular, this range of wavenumbers was read on the loading plot as a negative contribution along PC1 and a positive contribution for PC2 (Figure 4.27, b). This outcome allowed to discriminate mostly along PC1 cleaned mock-up areas (i.e., 10-, 20-, and 30-minute protocols) from the cluster of bare brass coupons, which would suggest a poor recovery of the unaltered condition after cleaning (Figure 4.27, a). In particular, bare brass sheets were presenting amorphous zincite, whereas cleaned mock-ups were characterised by both zincite and cuprite on the treated surface. No significant difference could be highlighted among the three cleaning timings, being tarnish still present after treatment. As already discussed in Chapter 3 when commenting Raman data collected on altered (i.e., corrosion and acrylic coating) steel mock-ups after cleaning by PHB-EL-DFO gels (page 142), the residual presence of brass tarnish products could not be read from a quantitative perspective to compare neither different cleaning times, nor before and after cleaning conditions. Indeed, even though the intensity of a Raman peak is proportional to the analyte concentration, factors such as matrix absorption, surface inhomogeneity and laser beam focusing jeopardises the quantitative interpretation of Raman data (Vandenabeele, 2013).

The presence of residual tarnish phases could be considered a positive outcome when cleaning historical metal artefacts, being desired the preservation of a naturally aged appearance according to CRs criteria (Cuvillier *et al.*, 2022; Guilminot, 2023). Additionally, no important wavenumber shifts or new Raman bands were observed on mock-up areas after cleaning, suggesting the absence of surface phase modifications derived from the interaction between brass and PHB-EL-EDDS systems.

Finally, observing the spectral range 800-1200 cm^{-1}, where EDDS complexes showed the most diagnostic Raman peaks (page 180), no evident vibrational bands related to these species were detected for any application time (i.e., 10, 20, and 30 minutes), thus suggesting the absence of eventual cleaning residues.

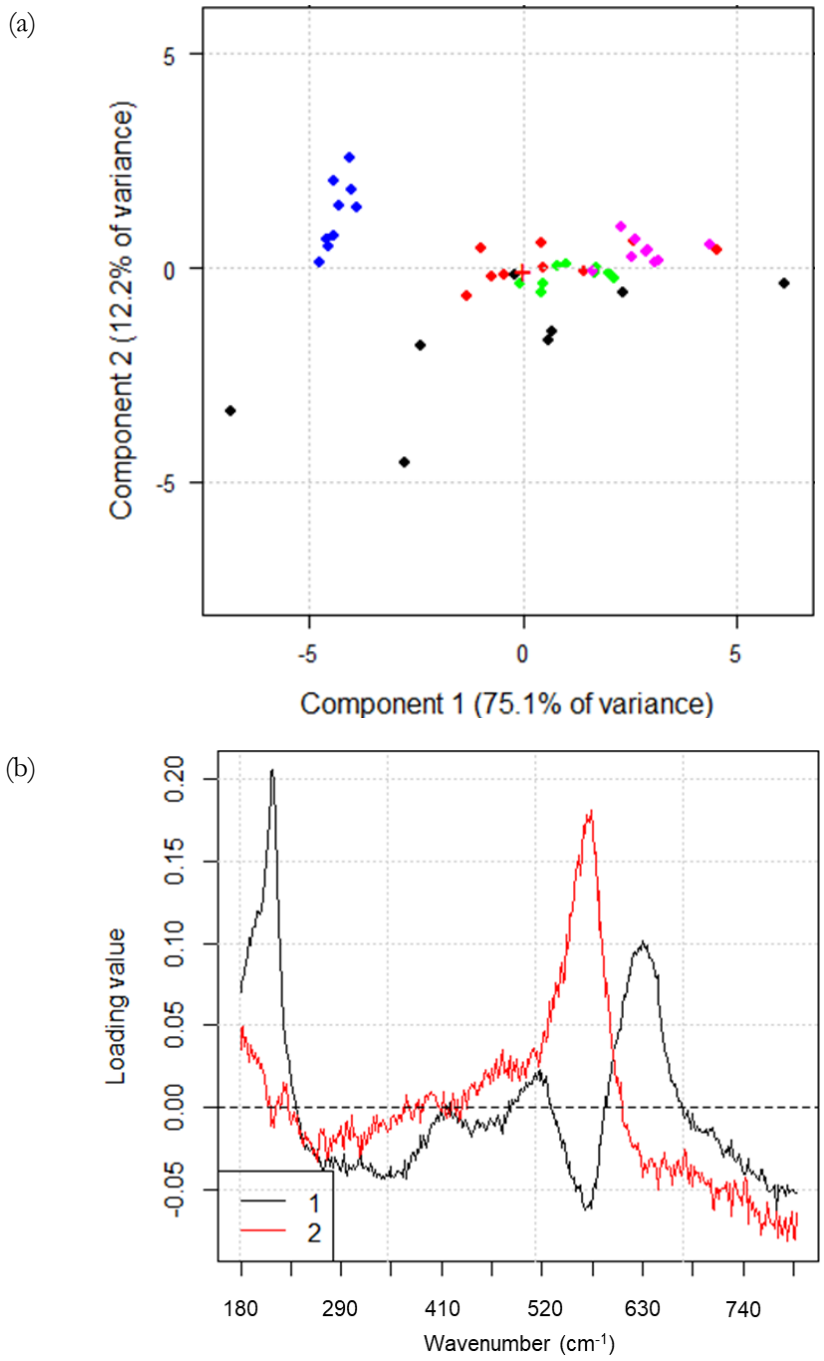

Figure 4.27 Score (a) and loading (b) plots obtained from PCA applied to Raman spectra recorded on chemically tarnished brass mock-ups, coated with Zaponlack, before (purple) and after cleaning by three PHB-EL-EDDS gel applications of 10 (black), 20 (red), and 30 (green) minutes, and untreated bare brass coupons (blue) as control. (b) Related PC1 (black) and PC2 (red) loading plot.

4.4.3.10 Electrochemistry

Electrochemistry was run to evaluate the resistance of brass mock-ups (50 × 50 × 1 mm^3) against corrosion by measuring the polarisation resistance (*R*p). Measurements were performed in triplicates on the metal presenting different conditions (Figure 4.28), specifically:

a. Bare brass;
b. Bare brass after 3-month ageing in climatic chamber;
c. Chemically tarnished brass coated with Zaponlack, eventually cleaned by triple PHB-EL-EDDS gel application of 30 minutes;
d. Chemically tarnished brass coated with Zaponlack, eventually cleaned by triple PHB-EL-EDDS gel application of 30 minutes, after 3-month ageing in climatic chamber.

The average Rp values, correlated by standard deviation, are reported in Table 4.9. Electrochemical data were not evaluated by statistical analysis (e.g., ANOVA) due to the scarce number of measurements available (i.e., three per each series of mock-ups). The interpretation was therefore qualitative, based on the comparison of values' magnitudes and changes among the different series.

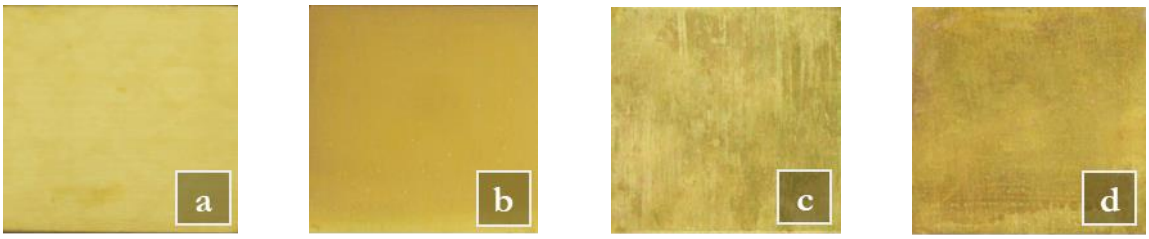

Figure 4.28 Photographs of bare brass coupons (50 × 50 × 1 mm^3) before (a) and after 3-month ageing in a climatic chamber (b) and chemically tarnished brass coupons cleaned by three 30-minute applications of a PHB-EL-EDDS gel before (c) and after 3-month ageing in a climatic chamber (d).

A first observation focuses on the lowest *R*p value, which was calculated for chemically tarnished brass coupons coated with Zaponlack after being cleaned by PHB-EL-EDDS gels (Table 4.9). The recording of low *R*p values right after a cleaning treatment was expected, since the removal of tarnished layer (and organic coating) would lead the metal substrate to be newly exposed to caustic agents present in the surrounding atmosphere and therefore "reactivated" towards corrosion processes (Petiti *et al.*, 2020). The successive reformation of tarnish patina on cleaned brass mock-ups, when exposed to artificial ageing in a climatic chamber, was then justifying the increase of the calculated polarisation resistance on the metallic surface (Table 4.9).

Electrochemical measurement could highlight a different behaviour between bare brass coupons and chemically altered (and coated) brass mock-ups, when comparing the two series before and after artificial ageing in a climatic chamber. In the first case, indeed, the brass coupons resulted in being more prone to corrosion after three months of ageing in a climatic chamber if comparing the collected electrochemical data. On the contrary, as discussed in the previous paragraph, cleaned brass mock-ups proved to be more resistant to corrosion after exposure in the same ageing conditions (Table 4.9). This consideration was estimated by the decreasing (i.e., -27.9 ±12.3 kΩ cm^2) and increasing (i.e., +14.1 ±17.5 kΩ cm^2) of polarisation resistance values for bare brass and cleaned brass mock-ups, respectively, when comparing before after ageing results.

To elucidate this outcome, micro-Raman spectroscopy was performed on mock-up surfaces to verify the presence of different corrosion species that would explain the different electrochemical response. The technique would suggest the presence of dissimilar phases when comparing the two series of samples before

and after 3-month ageing in climatic chamber. In particular, Raman peaks related to covellite (CuS) and zincite (ZnO) were mainly detected for aged bare brass pieces (SM-Figure 18, a). On the other hand, in the case of aged mock-ups after cleaning, the additional presence of cuprite (Cu_2O) was revealed (SM-Figure 18, b), implying the formation of a more passivating and uniform layer, as stated by the previous literature (Qiu and Leygraf, 2011).

Finally, as a general consideration, the data registered for both coupon series (i.e., bare and cleaned) after 3-month ageing in a climatic chamber were comparable, as reported in Table 4.9. Analogous polarisation resistance values were calculated for bare brass (i.e., 69.7 ±16.3 kΩ cm^2) and cleaned brass after artificial ageing (i.e., 61.3 ±20.1 kΩ cm^2), which was considered a positive result concerning the long-term impact of the PHB-EL-EDDS formulation when employed for the cleaning of altered brass surfaces.

Table 4.9 Average values of polarisation resistance (*R*p) measured for bare brass and chemically tarnished and coated (i.e., Zaponlack) brass after cleaning by PHB-EL-EDDS gel (i.e., 30-min × 3 applications). Data collected before and after ageing in a climatic chamber are reported. All values are expressed in kΩ cm^2.

	Before ageing	*After ageing*
Bare brass	97.6 (±4.0)	69.7 (±16.3)
Cleaned brass mock-ups	47.2 (±2.6)	61.3 (±20.1)

4.5 Conclusions

A novel green gel system could be designed for the cleaning of altered brass collections. In particular, the research was focused on the simultaneous removal of two features frequently present indoors on this class of metals: a nitrocellulose-based coating (i.e., Zaponlack) and corrosion, mainly constituted of copper and zinc oxides and sulphides.

The formulation was developed employing green "building-blocks", namely, the bio-sourced and biodegradable polymer poly-3-hydroxybutyrate (PHB), the bio-solvent ethyl lactate (EL), and the biodegradable and potentially bio-derived ligand ethylenediamine-N,N'-disuccinic acid (EDDS), which is proven to form complexes with copper and zinc ions (Orama *et al.*, 2002). Several factors were taken into account, such as the hydrophobicity of the polymer, the conditional stability constants for EDDS-complexes, the final concentration of the complexing agent.

The cleaning efficiency of the resulting formulation was assessed on brass mock-ups chemically altered and coated with Zaponlack in order to present the desired features. X-ray fluorescence, Raman, and Fourier-transform infrared spectroscopies could provide evidence for the complexing action occurring between EDDS and copper and zinc ions when analysing the gelled systems after the intervention. The outcome was considered remarkable since a frequent limiting factor, when using rigid gelled systems as the PHB-EL-EDDS, can be an uneven contact between gel and metal, leading to a poor cleaning action. Additionally, first evidence of Cu- and Zn-EDDS complexes could be detected by Raman spectroscopy.

In parallel, colorimetry and statistical analysis proved that the original yellow aspect of bare brass was recovered after three applications of 30 minutes by PHB-EL-EDDS gel, when working on data in SCE mode. The same data in SCI did not verify a satisfactory recovery of inherent brass brilliance. However, both colorimetric data demonstrated a reliable and positive action of the gel for the cleaning of brass substrates, when operating by long and repeated applications. FTIR spectroscopy verified the effective removal of the organic coating from the coupons, whereas Raman spectroscopy did not yield a clear evidence of tarnish removal from the treated brass sheets, because not providing a quantitative outcome. Finally, analogous polarisation resistance values were calculated for bare and cleaned brass coupons after

artificial ageing, possibly indicating a non-deleterious impact of the PHB-EL-EDDS formulation on treated brass surfaces in the long-term.

Bibliography

Albano, M. et al. (2020) 'A Preliminary Spectroscopic Approach to Evaluate the Effectiveness of Water- and Silicone-Based Cleaning Methods on Historical Varnished Brass', Applied Sciences, 10(11), p. 3982. Available at: https://doi.org/10.3390/app10113982.

Angelini, E. and Argyropoulos, V. (2008) 'PROMET state-of-the-art approach for protecting, preserving, and interpreting metals from museums in the Mediterranean basin', in V. Argyropoulos (ed.) Metals and Museums in the Mediterranean. Protecting, Preserving and Interpreting. TEI (Athens), pp. 23–37.

Artesani, A. et al. (2020) 'Recent Advances in Protective Coatings for Cultural Heritage–An Overview', Coatings, 10(3), p. 217. Available at: https://doi.org/10.3390/coatings10030217.

Bouchard, M. and Smith, D.C. (2003) 'Catalogue of 45 reference Raman spectra of minerals concerning research in art history or archaeology, especially on corroded metals and coloured glass', Spectrochimica Acta Part A: Molecular and Biomolecular Spectroscopy, 59(10), pp. 2247–2266. Available at: https://doi.org/10.1016/S1386-1425(03)00069-6.

Brock, F. et al. (2018) 'Testing the Effectiveness of Protocols for Removal of Common Conservation Treatments for Radiocarbon Dating', Radiocarbon, 60(1), pp. 35–50. Available at: https://doi.org/10.1017/RDC.2017.68.

Cagnini, A., Gennai, S. and Mazzoni, M.D. (2012) 'La Banderuola di Palazzo Vecchio: storia, vicende conservative, restauro', OPD restauro, pp. 13–32. Available at: https://opificiodellepietredure.cultura.gov.it/pubblicazioni/opd-restauro-n-24-2012/.

Cakir, D. (2017) Enhanced Raman signatures on copper based-materials. Université Montpellier. Available at: https://theses.hal.science/tel-01944233/.

Chauhan, G., Pant, K.K. and Nigam, K.D.P. (2012) 'Extraction of nickel from spent catalyst using biodegradable chelating agent EDDS', Industrial and Engineering Chemistry Research, 51(31), pp. 10354–10363. Available at: https://doi.org/10.1021/ie300580v.

Chen, L. et al. (2019) 'Effect of biodegradable chelators on induced phytoextraction of uranium- and cadmium- contaminated soil by Zebrina pendula Schnizl', Scientific Reports, 9(1), p. 19817. Available at: https://doi.org/10.1038/s41598-019-56262-9.

Cuvillier, L. et al. (2022) 'Exploiting Biologically Synthetized Chelators in Conservation: Gel-based Bio-cleaning of Corroded Iron Heritage Objects', in P. Mardikian, L. Näsänen, and A. Arponen (eds) Metal 2022, proceedings of the interim meeting of the ICOM-CC metals working group. Helsinki, Finland.

Dzhagan, V. et al. (2022) 'Copper-Content Dependent Structural and Electrical Properties of CZTS Films Formed by "Green" Colloidal Nanocrystals', Electronic Materials, 3(1), pp. 136–153. Available at: https://doi.org/10.3390/electronicmat3010013.

Eggert, G. et al. (2019) 'Metal conservation, cellulose nitrate and the Oddy test', in C. Chemello, L. Brambilla, and E. Joseph (eds) Metal 2019 Proceedings of the Interim Meeting of the ICOM-CC Metals Working Group. International Councils of Museums - Committee for Conservation, p. 473.

European Chemicals Agency (ECHA) (2024) Dibromomethane. Available at: https://echa.europa.eu/brief-profile/-/briefprofile/100.000.750 (Accessed: 26 February 2024).

Farkas, E., Enyedy, É.A. and Csóka, H. (1999) 'A comparison between the chelating properties of some dihydroxamic acids, desferrioxamine B and acetohydroxamic acid', Polyhedron, 18(18), pp. 2391–2398. Available at: https://doi.org/10.1016/S0277-5387(99)00144-8.

Fernández de la Ossa, M.Á. et al. (2011) 'Analytical techniques in the study of highly-nitrated nitrocellulose', TrAC Trends in Analytical Chemistry, 30(11), pp. 1740–1755. Available at: https://doi.org/10.1016/j.trac.2011.06.014.

Giraud, T. et al. (2021) 'Use of gels for the cleaning of archaeological metals. Case study of silver-plated copper alloy coins', Journal of Cultural Heritage, 52, pp. 73–83. Available at: https://doi.org/10.1016/j.culher.2021.08.014.

Grattoni, C.A. et al. (2001) 'Rheology and Permeability of Crosslinked Polyacrylamide Gel', Journal of Colloid and Interface Science, 240(2), pp. 601–607. Available at: https://doi.org/10.1006/jcis.2001.7633.

Guilminot, E. (2023) 'The Use of Hydrogels in the Treatment of Metal Cultural Heritage Objects', Gels, 9(3), p. 191. Available at: https://doi.org/10.3390/gels9030191.

Guo, H. et al. (2010) 'Ethyl lactate enhances ethylenediaminedisuccinic acid solution removal of copper from contaminated soils', Journal of Hazardous Materials, 174(1–3), pp. 59–63. Available at: https://doi.org/10.1016/j.jhazmat.2009.09.016.

Heginbotham, A. et al. (2014) 'An evaluation of protective coatings for brass in indoor environments, with an emphasis on Boulle marquetry', in Furniture finishes: past, present and future of transparent wood coatings. Proceedings of 12th International Symposium on wood and furniture conservation: Stichting Ebenist, Amsterdam, pp. 14–15.

Hosseinpour, S. and Johnson, M. (2017) 'Vibrational Spectroscopy in Studies of Atmospheric Corrosion', Materials, 10(4), p. 413. Available at: https://doi.org/10.3390/ma10040413.

Hughes, R. and Rowe, M. (1983) The colouring, bronzing, and patination of metals : a manual for the fine metalworker and sculptor. Edited by Thames and Hudson. New York, N.Y.: Watson-Guptill Publications. Available at: https://lccn.loc.gov/90049860.

Jaeger, T. (2008) 'Short Communication Removal of Paraffin Wax in the Re-treatment of Archaeological Iron', Journal of the American Institute for Conservation, 47(3), pp. 217–223. Available at: https://doi.org/10.1179/019713608804539619.

Kadam, S.L. et al. (2020) 'Electrochemical Synthesis of CuS Thin Film for Supercapacitor Application', Macromolecular Symposia, 392(1). Available at: https://doi.org/10.1002/masy.201900209.

Kim, A.-R., Kim, H.-S. and Park, S.-O. (2011) 'Measuring of the Perceptibility and Acceptability in Various Color Quality Measures', Journal of the Optical Society of Korea, 15(3), pp. 310–317. Available at: https://doi.org/10.3807/JOSK.2011.15.3.310.

Kołodyńska, D. (2011) 'Green complexing agent - EDDS in removal of heavy metal ions on strongly basic anion exchangers', Desalination, 280(1–3), pp. 44–57. Available at: https://doi.org/10.1016/j.desal.2011.06.060.

Lanigan, K.C. and Pidsosny, K. (2007) 'Reflectance FTIR spectroscopic analysis of metal complexation to EDTA and EDDS', Vibrational Spectroscopy, 45(1), pp. 2–9. Available at: https://doi.org/10.1016/j.vibspec.2007.03.003.

Luo, C., Shen, Z. and Li, X. (2005) 'Enhanced phytoextraction of Cu, Pb, Zn and Cd with EDTA and EDDS', Chemosphere, 59(1), pp. 1–11. Available at: https://doi.org/10.1016/j.chemosphere.2004.09.100.

Luxford, N. and Thickett, D. (2007) 'Preventing silver tarnish--lifetime determination of cellulose nitrate lacquer', Metal, 7, pp. 88–93.

Mari Yanagishita (2012) 'Il restauro della grande Croce del Pollaiolo: un intervento all'interno del cantiere organizzato per l'Altare di San Giovanni', in Mandragora (ed.) E l'informe si fa forma... : studi intorno a Santa Maria del Fiore in ricordo di Patrizio Osticresi. Florence, Italy, pp. 281–286.

Mattsson, E. (1958) 'Staining of copper and brass', Corrosion, 14(2), pp. 48–52.

McAdam, B. et al. (2020) 'Production of Polyhydroxybutyrate (PHB) and Factors Impacting Its Chemical and Mechanical Characteristics', Polymers, 12(12), p. 2908. Available at: https://doi.org/10.3390/polym12122908.

Merck (2024) Ethylenediamine-N,N'-disuccinic acid trisodium salt solution. Available at: https://www.sigmaaldrich.com/CH/en/product/aldrich/92698 (Accessed: 26 February 2024).

Mikula, R.. and Munoz, V.. (2000) 'Characterization of emulsions and suspensions in the petroleum industry using cryo-SEM and CLSM', Colloids and Surfaces A: Physicochemical and Engineering Aspects, 174(1–2), pp. 23–36. Available at: https://doi.org/10.1016/S0927-7757(00)00518-5.

Molina, M.T. et al. (2023) 'Protective Coatings for Metals in Scientific—Technical Heritage: The Collection of the Spanish National Museum of Science and Technology (MUNCYT)', Heritage, 6(3), pp. 2473–2488. Available at: https://doi.org/10.3390/heritage6030130.

Molina, M.T., Cano, E. and Ramírez-Barat, B. (2023) 'Protective coatings for metallic heritage conservation: A review', Journal of Cultural Heritage, 62, pp. 99–113. Available at: https://doi.org/10.1016/j.culher.2023.05.019.

Lo Monaco, A. et al. (2011) 'Colour measurements of surfaces to evaluate the restoration materials', in, p. 80840P. Available at: https://doi.org/10.1117/12.889147.

Neal, J.A. and Rose, N.J. (1968) 'Stereospecific ligands and their complexes. I. A cobalt(III) complex of ethylenediaminedisuccinic acid', Inorganic Chemistry, 7(11), pp. 2405–2412. Available at: https://doi.org/10.1021/ic50069a043.

Orama, M. et al. (2002) 'Complexation of [S,S] and mixed stereoisomers of N,N'-ethylenediaminedisuccinic acid (EDDS) with Fe(III), Cu(II), Zn(II) and Mn(II) ions in aqueous solution', J. Chem. Soc., Dalton Trans., (24), pp. 4644–4648. Available at: https://doi.org/10.1039/B207777A.

Pawlaczyk, M. and Schroeder, G. (2021) ' Deferoxamine-Modified Hybrid Materials for Direct Chelation of Fe(III) Ions from Aqueous Solutions and Indication of the Competitiveness of In Vitro Complexing toward a Biological System ', ACS Omega, 6(23), pp. 15168–15181. Available at: https://doi.org/10.1021/acsomega.1c01411.

Petiti, C. et al. (2020) 'Effects of cleaning procedures on the long-term corrosion behavior of bronze artifacts of the cultural heritage in outdoor environment', Environmental Science and Pollution Research, 27(12), pp. 13081–13094. Available at: https://doi.org/10.1007/s11356-020-07814-4.

Prosek, T. et al. (2013) 'Real-time monitoring of indoor air corrosivity in cultural heritage institutions with metallic electrical resistance sensors', Studies in Conservation, 58(2), pp. 117–128. Available at: https://doi.org/10.1179/2047058412Y.0000000080.

Qiu, P. and Leygraf, C. (2011) 'Initial oxidation of brass induced by humidified air', Applied Surface Science, 258(3), pp. 1235–1241. Available at: https://doi.org/10.1016/j.apsusc.2011.09.080.

Race, M. (2017) 'Applicability of alkaline precipitation for the recovery of EDDS spent solution', Journal of Environmental Management, 203, pp. 358–363. Available at: https://doi.org/10.1016/j.jenvman.2017.08.013.

Schmuecker, E., Lees, R. and Richardson, T. (2011) 'The Examination and Conservation of a 17th Century Indian Horse Armour', in P. Mardikian et al. (eds) Metal 2010: proceedings of the interim meeting of the ICOM-CC Metal Working Group, October 11-15, 2010, Charleston, South Carolina, USA. Clemson: Clemson University, pp. 120–126.

Scott, D.A. (2002) Copper and bronze in art: corrosion, colorants, conservation. Getty publications.

Takahashi, R. et al. (1999) 'Production of (S,S)-Ethylenediamine- N,N'-disuccinic Acid from Ethylenediamine and Fumaric Acid by Bacteria', Bioscience, Biotechnology, and Biochemistry, 63(7), pp. 1269–1273. Available at: https://doi.org/10.1271/bbb.63.1269.

Truffa Giachet, M., Schröter, J. and Brambilla, L. (2021) 'Characterization and Identification of Varnishes on Copper Alloys by Means of UV Imaging and FTIR', Coatings, 11(3), p. 298. Available at: https://doi.org/10.3390/coatings11030298.

Tsang, D.C.W. et al. (2013) 'Mechanisms of EDDS Adsorption on Goethite and Hematite Under Aqueous and Dehydrated Conditions', Environmental Engineering Science, 30(12), pp. 733–741. Available at: https://doi.org/10.1089/ees.2013.0211.

Tuck, C.D.S., Powell, C.A. and Nuttall, J. (2010) 'Corrosion of copper and its alloys Shreir's corrosion'. Elsevier Oxford.

Turner-Walker, G. (2008) A practical guide to the care and conservation of metals. Taichung City, Taiwan: Headquarters Administration of Cultural Heritage, Council for Cultural Affairs.

Vandenabeele, P. (2013) Practical Raman spectroscopy: an introduction. John Wiley & Sons.

Vandevivere, P.C. et al. (2001) 'Biodegradation of Metal−[S,S]-EDDS Complexes', Environmental Science & Technology, 35(9), pp. 1765–1770. Available at: https://doi.org/10.1021/es0001153.

Wang, Y. et al. (2022) 'Research progress on the biosynthesis and bioproduction of the biodegradable chelating agent (S,S)-EDDS', Process Biochemistry, 116, pp. 38–48. Available at: https://doi.org/10.1016/j.procbio.2022.02.025.

Watkinson, D. (2010) 'Preservation of Metallic Cultural Heritage', in Shreir's Corrosion. Elsevier, pp. 3307–3340. Available at: https://doi.org/10.1016/B978-044452787-5.00172-4.

Xiao, Q. et al. (2022) 'A novel Pickering emulsion stabilized solely by hydrophobic agar microgels', Carbohydrate Polymers, 297, p. 120035. Available at: https://doi.org/10.1016/j.carbpol.2022.120035.

Yang, Q. et al. (2023) 'Combination of Resonance and Non-Resonance Chiral Raman Scattering in a Cobalt(III) Complex', Angewandte Chemie International Edition, 62(45). Available at: https://doi.org/10.1002/anie.202312521.

Chapter 5

First attempts towards the bio-cleaning of silver heritage

This chapter is based on
Passaretti, A., Cuvillier, L., Sciutto, G., Cano, E., Ramírez Barat, B., von Reuss, S., & Joseph E., Assessment of greener solutions for the cleaning of historical metal heritage. Oral presentation at *InART2024 - 6th International Conference on Innovation in Art Research and Technology*. Oslo, Norway, June 4-7, 2024.

5.1 Silver-copper alloy indoor tarnishing

Silver is another metal extensively represented in historical collections exposed and stored indoors in the form of coins, jewellery, liturgical, and ornamental objects, being a precious material and thus a symbol of prestigious status in ancient times (Angelini and Argyropoulos, 2008; Palomar, Ramírez Barat, *et al.*, 2016; Artesani *et al.*, 2020). Frequently, silver artefacts are not made of pure silver yet constituted of an alloy. Especially, it is associated predominantly with copper in several ratios, among which the so-called "sterling silver" or Ag_{925} (i.e., 92.5% Ag and 7.5% Cu) is the most represented (Águas *et al.*, 2008; de Caro *et al.*, 2016; Tissot *et al.*, 2016).

It is well known that the key alteration process affecting silver and its alloys is related to tarnishing, which is caused by the exposure to environments rich in gaseous sulphur compounds and accelerated in the presence of humidity (Palomar, Ramírez Barat, *et al.*, 2016). The main actors in the tarnishing phenomenon are hydrogen sulphide (H_2S) and carbonyl sulphide (COS) (Table 5.1), which might be originated indoors by out-gassing materials (e.g., furniture, showcases) or outdoors from industrial emissions (Vassiliou and Gouda, 2013; Palomar, Ramírez Barat, *et al.*, 2016). For pure silver substrates, the tarnishing process consists of an initial formation of a thin layer of silver oxide (Ag_2O) on the metallic substrate (Table 5.1, I), then reacting with gaseous sulphur compounds present in the atmosphere, yielding the formation of silver sulphide (Ag_2S) (Table 5.1, II) (Costa, 2001; de Figueiredo Junior *et al.*, 2021; Basilissi *et al.*, 2022).

Table 5.1 Series of reactions occurring during the tarnishing process of silver in atmospheres rich in gaseous sulphur compounds (de Figueiredo Junior *et al.*, 2021).

I) $4Ag + O_2 \rightarrow 2Ag_2O$

II) $Ag_2O + H_2S \rightarrow Ag_2S + H_2O$

III) $COS + H_2O \rightarrow H_2S + CO_2$

Furthermore, in several cases silver chloride (AgCl) has been identified as a major component on the surface of silver-based tarnished collections. When referring to indoor heritage, possible sources of chlorine are attributable to airborne particles (e.g., combustion processes) or cleaning treatments residues (e.g., products containing hydrochloric acid) that can interact with silver through an aqueous phase, leading to the precipitation of AgCl (Costa, 2001; Vassiliou and Gouda, 2013).

When considering Ag-Cu alloys exposed to similar indoor environmental conditions, the additional formation of copper corrosion products, such as copper oxide (i.e., cuprite Cu_2O) and sulphides (Cu_xS), is proven (Águas *et al.*, 2008; Schalm *et al.*, 2016; Artesani *et al.*, 2020; Basilissi *et al.*, 2022). In the presence of copper, the corrosion rate of the silver-based alloy is higher than pure silver because copper is expected to oxidise preferentially compared to silver in light of their standard electrode potentials, namely $E° = +0.34$ V for Cu^{2+}/Cu, $E° = +0.52$ V for Cu^{+}/Cu, and $E° = +0.80$ V for Ag^{+}/Ag (Schalm *et al.*, 2016). Furthermore, the additional formation of Ag-Cu-S species is documented in the literature when observing the surface of tarnished sterling silver (Tissot *et al.*, 2016).

The resulting tarnish layer formed on silver-based substrates is characterised by a colouration that can vary due to interference phenomena related to the superimposition of thin alteration layers formed over time and/or the series of different compounds formed during the alteration process, as studied in the previous literature (Schalm *et al.*, 2016) (Figure 5.1). Generally, it is proven that the colour of altered sterling silver ranges from yellow to violet-blue, reaching a dark grey shade by increasing the thickness of the tarnish film present (Schalm *et al.*, 2016; Tissot *et al.*, 2016).

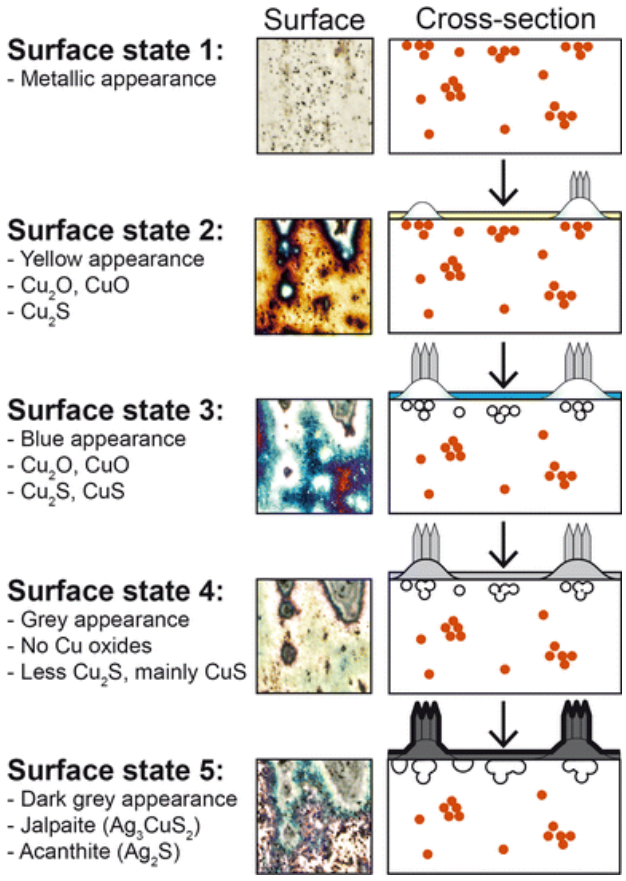

Figure 5.1 Evolution of the Ag_{925} surface during the corrosion process by consecutive immersions in Na_2S solution 0.1 M. The main surface states are visualised with microscopic images and schematic cross-sections. (Reproduced from Schalm *et al.*, 2016).

The alteration film has a significant impact on the aesthetic and readability of silver surface features despite the generally low thickness that can reach up to hundreds of nanometres (Schalm *et al.*, 2016; de Figueiredo Junior *et al.*, 2021). Currently, the methodologies employed by conservator-restorers (CRs) for the cleaning of tarnished silver artworks include mechanical (e.g., micro-abrasive solutions and pastes, erasers), chemical

(e.g., acids and chelating agents), and less conventional techniques such as electrochemical cleaning (i.e., reduction of ionic silver to the metallic state by immersion of the whole object in conductive solutions or by localised treatments according to the requirements) and laser ablation (Costa, 2001; Degrigny *et al.*, 2016; Palomar, Ramírez Barat, *et al.*, 2016; Basilissi *et al.*, 2022; Ricotta, Gagnini and Degrigny, 2022). Regarding the category of chemicals, commercial products (i.e., silver-dip) are well-rooted in the conventional work of CRs because of their immediate efficiency in removing the alteration layer present on silver-alloys. Generally, this outcome is achieved by complexing action towards copper present in the alloys thanks to acidified thiourea solutions present in the products (Contreras-Vargas, Ruvalcaba-Sil and Rodriguez-Gómez, 2013). Nonetheless, the demonstrated detrimental etching action of residual solutions after treatment and the well-known toxicity of thiourea define this cleaning method as not safe for art objects, operators, and, in a larger scale, for the nature (Contreras-Vargas, Ruvalcaba-Sil and Rodriguez-Gómez, 2013; Basilissi *et al.*, 2022).

Within this scenario, a preliminary exploration of the use of the bio-based PHB-EL-EDDS formulation, designed in the frame of this doctoral research project (Paragraph 4.3.2), was attempted as a greener chemical system to be potentially exploited for the localised cleaning of tarnished sterling silver. Indeed, the novel solution was previously demonstrated able to tackle copper-based corrosion products when employed on brass thanks to the complexing action of ethylenediamine-N,N'-disuccinic acid (EDDS) (Chapter 4), making this compound of interest also for the cleaning of sterling silver, being a Ag-Cu alloy. To the best of author's knowledge, no evidence in the literature reports a complexing affinity between EDDS and silver ions, therefore this potential feature will be investigated within this study.

5.2 Mock-up preparation

The potential cleaning action of PHB-EL-EDDS gels on tarnished sterling silver was evaluated on Ag_{925} (Ag 92.5%, Cu 7.5% by X-ray fluorescence analysis) sheets of 30 × 30 × 0.5 mm^3 purchased from Gyr Métaux Précieux SA (Switzerland). Following the literature, the coupons were preliminarily degreased by ethanol (96.0 – 97.2%) from Sigma Aldrich in an ultrasonic bath before proceeding with artificial ageing (Schalm *et al.*, 2016).

Generally, artificial tarnishing of silver can be achieved by K_2S or Na_2S solutions (Degrigny, 2008; Gouda *et al.*, 2009; Schalm *et al.*, 2016); in this study, a non-toxic protocol was preferred based on the use of an egg white powder (albumin) solution, which is equally able to release hydrogen sulphide (H_2S) vapours (Siatou *et al.*, 2022). The tarnishing protocol was performed in a closed container in polypropylene (PP), able to resist temperatures up to 100 °C. The sterling silver coupons were suspended and tied by a nylon thread to a central silver-coated rod set in the PP box, ensuring equal distance among the coupons (i.e., minimum 2 cm) and from the container sides and base in order to guarantee homogeneous airflow during the tarnishing process. The egg white powder (Prozis) was dissolved in deionised water at 20% w/v concentration and then placed in porcelain containers at the PP box's base. Finally, the container was closed with its lid and placed in a laboratory oven at 80 °C. The timing was selected after evaluating visually the tarnishing level achieved. A three-hour protocol at 80 °C yielded a satisfactory outcome with a dull and brownish surface appearance, generally with lighter shades in the central area of the metallic sheets and darker shades at the edges (Figure 5.2). On the contrary, shorter times were excluded because the created tarnish was easily removable by dry cotton swabbing, whereas longer ageing timings formed a dark grey homogenous finish that was not chosen for investigation in this research study, since it would normally present exclusively Ag_2S phases according to the previous literature (Schalm *et al.*, 2016).

During tarnishing and testing protocols, nitrile gloves were worn to handle sterling silver coupons in order not to contaminate the surface with fingerprints, while avoiding the use of latex gloves that are known for releasing sulphur-based compounds that would have jeopardised the evaluation after cleaning (Contreras-Vargas, Ruvalcaba-Sil and Rodriguez-Gómez, 2013). Analogous care was addressed for storing the coupons that were kept individually in sealed Corrosion Intercept® semi-transparent bags, including a Corrosion Intercept® strip to further prevent tarnishing.

Figure 5.2 Sterling silver mock-up (30 × 30 × 0.5 mm^3): initial aspect (left) and after chemical tarnishing protocol (right).

Micro-Raman spectroscopy was employed to examine the coupons and ascertain the reliability of the selected tarnishing protocol. Multiple single-point analysis was performed to characterise several spots (i.e., five per triplicate) on the visually heterogeneous surface of the altered mock-ups. Some representative Raman spectra are displayed in Figure 5.3. The interpretation of collected data was complex since broad bands were recorded rather than well-defined and narrow Raman signals. This was linked to the possible overlapping of Raman shifts related to formed silver and copper species, which were expected to be detected mainly in the spectral region 150 – 300 cm^{-1}, as reported by the literature (de Caro *et al.*, 2016). Nevertheless, data post-treatment (e.g., baseline correction, smoothing) was avoided since it is an approach that may jeopardise the correct interpretation of Raman spectra, especially when operating on low-intensity data highly affected by spectral noise, as the spectra shown in Figure 5.3 (Vandenabeele, 2013). In our case, a prominent presence of noise in the collected data was imputable to the use of low laser intensity (i.e., 0.5 mW with a 532-nm laser) and total exposure time to the beam (i.e., 3 seconds for 30 accumulations) that did not allow to acquire neat results. However, the selected experimental set-up was chosen in accordance with the literature in order to avoid decomposition and transformation of the phases present, since silver compounds are highly photo-sensitive (Martina *et al.*, 2012). Therefore, to better visualise the features present in the spectral region 150 – 300 cm^{-1}, the spectral ranges between 50-100 cm^{-1} (i.e., mainly lattice vibrations) and 1000-1600 cm^{-1} (i.e., characterised by broad bands approximately at 1361 and 1591 cm^{-1} associable to amorphous carbon compounds hence possibly linked to the albumin-based tarnishing method employed to prepare the sterling silver mock-ups) were excluded being predominant features on the y axis (i.e., intensity) yet not informative regarding the presence of tarnish species.

As said, several weak Raman bands were detected in the spectral region of interest (i.e., 150 – 300 cm^{-1}) that would suggest the presence of Ag_xCu_yS species by the Ag–S–Cu stretching modes registered around 257 and 275 cm^{-1} (de Caro *et al.*, 2016) (Figure 5.3, a and b, respectively) and achantite (Ag_2S) by Ag–S stretching and bending modes respectively at about 184 and 241 cm^{-1} (Martina *et al.*, 2012; de Caro *et al.*, 2016) (Figure 5.3, c). The additional presence of silver and copper oxides could not be excluded considering the broad band registered in the spectral region 200-300 cm^{-1} (Martina *et al.*, 2012; de Caro *et al.*, 2016). Given the uncertainty of the interpretation, a possible approach, which would be of interest for a future development of this research topic, could rely on the use of deconvolution functions applied to the collected Raman spectra. Supported by standards analysed by means of the same spectroscopic technique or others, such as X-ray diffraction (XRD) for crystalline compounds, the method would yield a greater data readability. Finally, Cu_xS species were recognised thanks to the weak peak sporadically detected around 464 cm^{-1} related to S–S stretching modes for amorphous copper sulphides (Cruz, Hernández and Coronel, 2012; de Caro *et al.*, 2016) (Figure 5.3, c). According to Schalm *et al.* (2016), the co-presence of both copper- and silver-based tarnishing products would indicate the formation of a nonuniform alteration layer on the sterling silver coupons, as also suggested by the uneven colour acquired by the metal sheets after the tarnishing process (Figure 5.2).

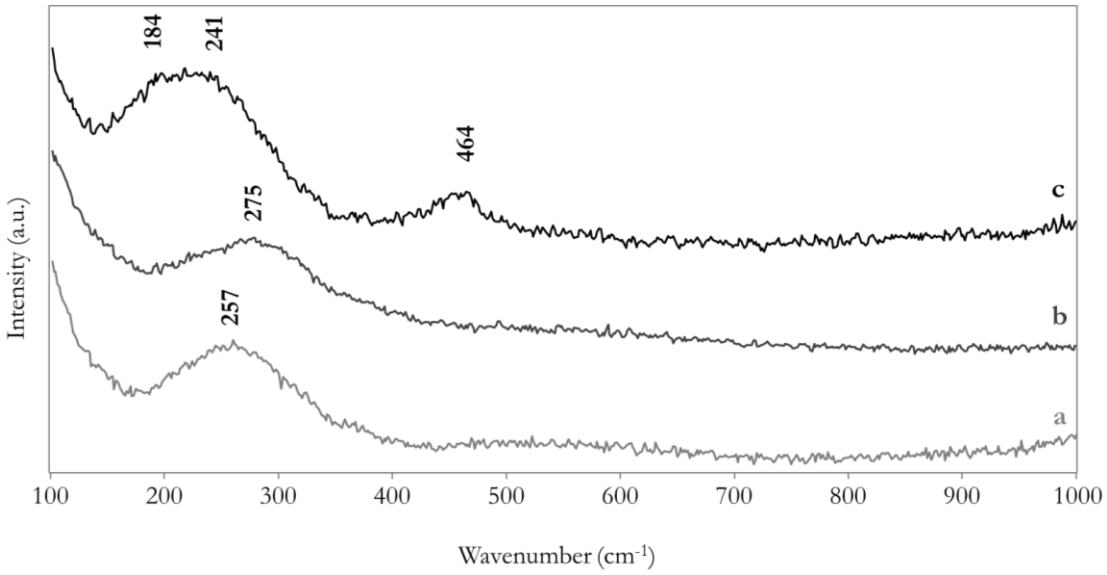

Figure 5.3 Representative Raman spectra of sterling silver coupons after tarnishing process.

5.3 Cleaning assessment

5.3.1 Preliminary test

In a preliminary phase, the potential action of ethyl lactate on tarnished sterling silver coupons was explored. Indeed, previous literature reports the use of organic solvents (e.g., alcohols and acetone) and weak acids (e.g., formic and citric acid) solely or together with thiourea in order to promote its chelating action for the cleaning of altered silver substrates (Palomar, Ramírez Barat, *et al.*, 2016; Selwyn and McKinnon, 2021). Indeed, under oxidising conditions and in the presence of acidic pH, silver sulphides can be slowly dissolved, yielding Ag^+ ions and sulphur species, thus favouring the formation of silver-thiourea complexes (Selwyn and McKinnon, 2021). Therefore, a possible effect of the acidic (i.e., pH 4, (Merck, 2024a)) organic solvent loaded in the PHB-EL-EDDS gel was foreseen and thus verified by prolonged exposure of the metal sheets to ethyl lactate.

At first, sterling silver coupons (30 × 30 × 0.5 mm^3, Gyr) were chemically tarnished, as described in paragraph 5.2. The sheets were then half-immersed into a crystallising dish containing ethyl lactate (≥98%, Sigma Aldrich) for several intervals: 10, 20, and 30 minutes, and 1, 2, and 4 hours (Figure 5.4). Each time, mock-up surfaces were quickly dried by gentle dry cotton swabbing and then their surface was monitored by a multi-modal approach, namely, photographic documentation, colorimetric and Eddy current measurements, and Raman spectroscopy. The test was performed in triplicates.

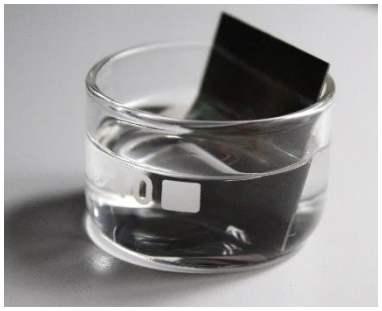

Figure 5.4 Chemically tarnished sterling silver coupon (30 × 30 × 0.5 mm^3) half-immersed into a crystallising dish containing ethyl lactate.

5.3.1.1 Visual appearance

Chemically tarnished sterling silver coupons showed a change in surface appearance already after a short-time (i.e., 10 minutes) immersion in ethyl lactate, as presented in the photographs shown in Figure 5.5. A clear distinction between the half-treated area and the one left as control could be observed. Over time, the yellow-brown alteration initially present on sterling silver coupons tended to fade, leaving a metallic silver-coloured appearance on the coupon area in contact with ethyl lactate. The regions characterised by a dark grey colour, visible especially on the edges of the coupons, exhibited a lighter appearance only after prolonged immersion in ethyl lactate, as visible when observing the outcome at 4-hour process compared to shorter immersion times (Figure 5.5). Finally, albeit using the cotton swabs gently to dry the coupons after each immersion interval, the sole impact of this intermediate step should be evaluated additionally for higher reliability of the obtained results.

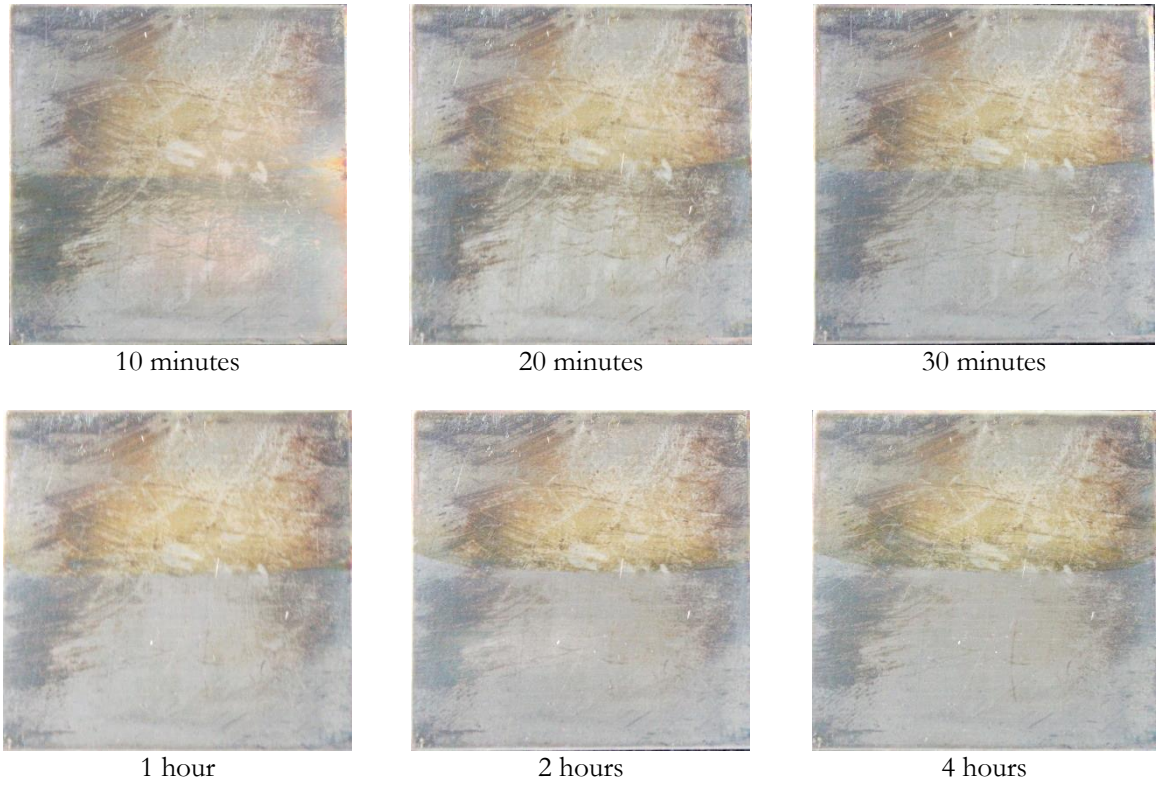

Figure 5.5 Chemically tarnished sterling silver coupon (30 × 30 × 0.5 mm^3) after being half-immersed into ethyl lactate for 10, 20, and 30 minutes, and 1, 2, and 4 hours, as indicated below the respective photographs.

5.3.1.2 Colorimetry

Colorimetric data were collected on tested sterling silver mock-ups at each immersion interval in ethyl lactate to monitor the appearance change due to the interaction with the organic solvent. The technique corroborated what was observed with the naked eye, hence a gradual reduction of brown-yellow shades initially present on the coupons, as demonstrated by the progressively lower values calculated for Δa^* (i.e., red component) and, mostly, Δb^* (i.e., yellow component) when comparing CIELab coordinates of tested coupons with bare sterling silver excluding the light specular component (i.e., SCE) (Table 5.2). Colorimetric measurements would therefore prove a gradual removal of typically yellow-brown tarnish phases initially present on altered sterling silver, confirming what observed by simple visual inspection (Palomar, Ramírez Barat, *et al.*, 2016; Schalm *et al.*, 2016).

Evaluating the colour appearance of the tested mock-ups in relation to bare sterling silver coupons, a colour difference was recognisable when calculating the ΔE* value at the end of each interval of immersion (Table 5.2). A gradually lower distinction between test mock-ups and bare silver coupons was achieved by prolonged interaction between altered metal sheets and ethyl lactate during the immersion time. In particular, calculated ΔE* was equal to 12.09 (±0.80) before immersion and finally 5.74 (±0.40) after 4 hours in ethyl lactate (Table 5.2).

Discussed data were further analysed by Tukey's HSD test to estimate if the difference observed for L*a*b* coordinates was statistically discriminant to monitor colour differences occurring on the tarnished coupons during the immersion in ethyl lactate. The test confirmed that in SCE mode the most discriminant variables were a* ($F = 6.294$) and b* ($F = 11.97$), whereas L* ($F = 0.9$) could not track differences that are considered statistically significant. In particular, both a* and b* coordinates resulted in providing information regarding a substantial difference to the initial mock-up colour condition after 30 minutes of immersion in ethyl lactate, having p values below the significance threshold of 0.05. Successively, when comparing timings in the range of 30 minutes – 4 hours, no particular discrimination could be achieved by Tukey's test ($p > 0.1$), not evidencing a statistically appreciable colour difference by evaluation of a* and b* coordinates in SCE mode. The outcome would suggest that the interaction of 30 minutes with ethyl lactate can be considered in this study as a threshold to start appreciating a colour difference on the chemically tarnished sterling silver. Moreover, longer exposure times to ethyl lactate would not yield to significant colour changes.

Table 5.2 Variation of CIELab coordinates of tarnished sterling silver coupons immersed in ethyl lactate to bare sterling silver. ΔL*, Δa*, Δb* and related ΔE* SCE values, collected for tarnished sterling silver coupons after each interval of immersion in ethyl lactate, are reported along with their standard deviation into brackets.

Immersion time	ΔL*	Δa*	Δb*	ΔE*
0 minutes	-3.66 (±1.55)	2.48 (±0.22)	11.25 (±0.70)	12.09 (±0.80)
10 minutes	-0.35 (±2.26)	2.42 (±1.31)	10.95 (±3.51)	11.22 (±3.44)
20 minutes	-1.47 (±2.27)	1.42 (±0.45)	8.36 (±0.53)	8.61 (±0.65)
30 minutes	-1.26 (±2.08)	1.02 (±0.60)	6.53 (±0.93)	6.73 (±0.99)
60 minutes (1 hour)	-0.78 (±2.13)	1.10 (±0.43)	6.56 (±1.01)	6.70 (±1.03)
120 minutes (2 hours)	-1.10 (±1.14)	0.75 (±0.40)	6.26 (±0.72)	6.40 (±0.73)
240 minutes (4 hours)	-1.24 (±1.15)	0.69 (±0.23)	5.56 (±0.33)	5.74 (±0.40)

In the reference literature, often it is not specified whether SCI (i.e., Specular Component Included) or SCE (i.e., Specular Component Excluded) method was considered for the tarnish evaluation of silver substrates. Nonetheless, the focus was addressed towards the discussion of both L* and b* values, considered as indicators of the tarnishing level present on both pure and sterling silver (Palomar, Ramírez Barat, *et al.*, 2016; Schalm *et al.*, 2016; Thickett and Hallett, 2021; Basilissi *et al.*, 2022). In this doctoral research, in particular, the evaluation of solely b* values in SCE mode was not considered sufficient when examining sterling silver coupons. Indeed, as already discussed in Paragraph 5.1 and schematically reported in Figure 5.1, sterling silver substrates normally go through different stages of alteration, hence tarnish compounds that determine several shades of colourations ranging from yellow (i.e., positive b*) to blue (i.e., negative b*) and dark grey (i.e., close-to-zero b*) (Schalm *et al.*, 2016). Willing to provide the most exhaustive result discussion in line with the criteria normally considered in the previous literature, SCI (i.e., specular component included) data were additionally examined.

The same colorimetric measurements reported in Table 5.2 in SCE mode were then evaluated including the specular reflection component (i.e., SCI method) as presented in Table 5.3. The relevance of L* was evident when observing data in SCI mode (Table 5.3). The results demonstrated that the tarnished metallic sheets immersed in ethyl lactate had lower brightness and poorer specular reflection if compared to bare sterling silver due to the negative ΔL* values, ranging between a minimum of -36.14 (±4.02) after 20 minutes and a maximum registered of -31.78 (±4.36) after 2 hours in ethyl lactate. Interestingly, the values could be compared to other outcomes obtained by traditional chemical methods reported in the literature, such as EDTA solutions embedded in agar gels (5% w/w), Rochelle salts (15% w/w) in an agar matrix, and sodium hydrogen carbonate in agar (5% w/w), but also mechanical cleaning by sodium hydrogen carbonate (SM-Table 7) (Basilissi *et al.*, 2022). Regarding SCI a* and b* values, as presented in Table 5.3, it was recorded a decrease in reddish and yellow shades initially present on the test coupons, as already observed with data in SCE mode (Table 5.2). However, these coordinates did not show an impact on the calculated colour difference ΔE* when considered including the specular component, which was in line with what observed by the previous literature (Basilissi *et al.*, 2022). When considering the ΔE* calculated for the several immersion times explored, the analysis in SCI mode did not show a specific trend among the different timings (Table 5.3), contrary to the observations with SCE coordinates (Table 5.2). On the contrary, analysing the colorimetric data collected in SCI mode by Tukey's HSD test, a clear relevance of L* ($F = 3.248$) and b* ($F = 3.189$) coordinates could be registered for the distinction of mock-up surface shades along the immersion in ethyl lactate. In particular, the test evidenced a significant distinction between the initial condition of the tarnished sterling silver coupons and the condition after 30 minutes of immersion ($p < 0.05$), stating this timing as a threshold for significant colour difference, as already discussed in the case of SCE mode.

Overall, the preliminary evidence collected by colorimetric measurements would suggest a favourable action of the organic solvent ethyl lactate in removing the tarnish products present on altered sterling silver as indicated by both L* and b* registered values for a minimum immersion time of 30 minutes, as also corroborated by statistical method. The evaluation of data including the specular reflection component (i.e., SCI) allowed to take into account the brightness factor (i.e., L*), which is considered a crucial parameter for CRs when cleaning silver-based artefacts (Palomar, Ramírez Barat, *et al.*, 2016; Schalm *et al.*, 2016; Thickett and Hallett, 2021; Basilissi *et al.*, 2022).

Table 5.3 Variation of CIELab coordinates of tarnished sterling silver coupons immersed in ethyl lactate to bare sterling silver. ΔL*, Δa*, Δb* and related ΔE* SCI values, collected for tarnished sterling silver coupons after each interval of immersion in ethyl lactate, are reported along with their standard deviation into brackets.

Immersion time	ΔL*	Δa*	Δb*	ΔE*
0 minutes	-42.45 (±0.45)	2.18 (±3.03)	-2.75 (±1.17)	42.59 (±0.48)
10 minutes	-35.66 (±1.30)	2.32 (±3.20)	0.69 (±4.00)	35.74 (±1.32)
20 minutes	-36.14 (±4.02)	1.62 (±1.47)	-3.07 (±2.46)	36.30 (±4.01)
30 minutes	-35.35 (±4.31)	1.22 (±1.01)	-4.62 (±2.02)	35.67 (±4.28)
60 minutes (1 hour)	-32.97 (±5.44)	0.12 (±0.58)	-4.87 (±2.15)	33.32 (±5.39)
120 minutes (2 hours)	-31.78 (±4.36)	0.63 (±1.12)	-4.23 (±2.33)	32.07 (±4.33)
240 minutes (4 hours)	-33.22 (±4.64)	0.18 (±0.68)	-5.07 (±2.02)	33.60 (±4.59)

5.3.1.3 Eddy current measurements

Eddy current measurements were tentatively employed to monitor the removal of tarnish initially present on sterling silver coupons, and potentially evidence the undesired formation of additional tarnish (i.e., thickness increase) over the exposition time to ethyl lactate. Table 5.4 reports the average alteration thickness initially present on sterling silver mock-up triplicates together with data after the multiple immersion times in ethyl lactate. As already observed in the case of brass (Table 4.6), all measured thicknesses, including initial tarnish layer, were close to 0 μm and, considering their standard deviations, their values were all falling in the instrumental error of the device used (i.e., ±0.7 μm + 1% of value). It could be assumed that the tarnish layer on silver coupons was out of the sensitivity range of the device employed, consequently excluding the further use of this technique for the evaluation of sterling silver coupons in this study (Schalm *et al.*, 2016; de Figueiredo Junior *et al.*, 2021).

Table 5.4 Average alteration layer thickness (μm) measured by Eddy current for tarnished sterling silver coupons before and after each interval of immersion in ethyl lactate. Values are reported along with their standard deviation.

Immersion time	Alteration thickness (μm)
0 minutes	-0.01 (±0.19)
10 minutes	-0.20 (±0.17)
20 minutes	0.17 (±0.04)
30 minutes	0.12 (±0.13)
60 minutes (1 hour)	-0.19 (±0.02)
120 minutes (2 hours)	0.09 (±0.03)
240 minutes (4 hours)	0.05 (±0.04)

5.3.1.4 Raman spectroscopy

The analysis performed by micro-Raman spectroscopy on the tarnished sterling silver coupons before and within the intervals of immersion in ethyl lactate could not provide clear information linked to the interaction between metal sheet and organic solvent. No clear band intensity (i.e., corrosion phase removal) or position (i.e., phase alteration or new formation) variations could be recognised by direct comparison when interpretating the collected Raman spectra.

Therefore, Principal Component Analysis (PCA) was applied to the data with the purpose of enhancing the readability of tarnish phase modifications possibly occurring on the metal sheet surface within the immersion test in ethyl lactate. The analysed spectral range was restricted to 140-800 cm^{-1}, being the region of interest for the detection of Raman shifts diagnostic for tarnishing products found on indoor altered sterling silver, as already observed (Figure 5.3).

SM-Figure 19 displays the resulting score (left) and loading (right) plots obtained by PCA when considering principal components 1 and 2. At a first observation, bare unaltered sterling silver coupons were positioned differently than all altered mock-ups, as displayed in PC1 vs PC2 score plot. Focusing the attention on the loading plot for PC2, a separation along this axis was observed especially for wavenumbers within 140-170 cm^{-1} and 230-290 cm^{-1}, which were read as positive and negative contributions, respectively, of these variables on the loading plot. In this study, these two ranges of spectral variables could be attributed respectively to lattice vibrations of bare silver metal and to Ag–S–Cu stretching modes possibly associated to Ag_xCu_yS species (de Caro *et al.*, 2016). Additionally, variables in the range 500-650 cm^{-1} were affecting

negatively and positively the loadings related to PC1 and PC2, respectively. This set of wavenumbers includes the Raman-active vibrations at about 518 and 630 cm^{-1} that could be linked to amorphous cuprite (Cu_2O) in this study (Bouchard and Smith, 2003; Cakir, 2017). Consequently, bare sterling silver sheets appeared characterised by lattice vibrations and corrosion products related to the first stages of tarnishing (i.e., copper oxides), as described by the literature (Schalm *et al.*, 2016). On the other hand, chemically tarnished and treated (i.e., immersion in EL) mock-ups were presenting tarnishing products associated to both copper oxides and Ag_xCu_yS species (de Caro *et al.*, 2016).

Principal Component Analysis, applied to Raman spectroscopy data, did not yield a discrimination among the several times of immersion in ethyl lactate or detect any potential effects of the organic solvent on the tarnish layer. These data were indeed distributed in the PC1/PC2 score plot without being organised in clusters (SM-Figure 19). The outcome could be potentially linked to the heterogeneity of the tarnish layer present on chemically altered sterling silver mock-ups.

5.3.2 Cleaning protocol

The potential cleaning performance of the PHB-EL-EDDS gel employed on tarnished sterling silver coupons was assessed in light of the collected evidence.

A PHB-EL-EDDS system was synthesised as described in Paragraph 4.3.2. Namely, a PHB-EL gel was initially formed using the bio-polymer poly-3-hydroxybutyrate (PHB) from Biomer and the bio-solvent ethyl lactate (≥98%) (EL) from Sigma Aldrich in a mixture of 7% w/v heated and magnetically stirred at about 110 °C for a few minutes. Once the formulation gained in thickness, a 20% w/v aqueous solution of ethylenediamine-N,N'-disuccinic acid trisodium salt (Na_3EDDS 35% in water, Sigma Aldrich) was added out of the heat, rapidly stirred manually, and finally let cool down to room temperature (i.e., 23.8 ±2.4 °C) to form a rigid gel. The final EDDS concentration was calculated as $4.8 \cdot 10^{-2}$ M in the gelled system.

The application of the resulting PHB-EL-EDDS gel was preceded by the use of Japanese paper (6 g/m^2, CTS) cut in the size and shape (i.e., 3 × 3 cm^2 square) of the metallic coupon to treat. The interposition of Japanese paper between gel and coupon was meant to avoid the uneven distribution of EDDS solution in the formed gel that would yield a potential non-uniform surface cleaning, as already observed when operating on tarnished brass sheets (Figure 4.17). After cutting the PHB-EL-EDDS gel in a square of 3 × 3 cm^2 with a metallic spatula, the formulation was laid onto the pre-formed Japanese paper piece, and gently pressed to achieve good contact with the metallic substrate. As an exploratory trial, the organogel was assayed on triplicate mock-ups by one application of 30 minutes, in accordance with results yielded by colorimetric and statistical analysis by simple interaction with ethyl lactate. Moreover, this timing was also verified as effective for the complexation of copper ions when treating altered brass with the PHB-EL-EDDS formulation in Chapter 4. At the end of the application process, gel and Japanese paper were detached in one move by a metallic spatula. Finally, the mock-up surface was cleared with ethanol 70% v/v by cotton-swabbing to remove possible gel residues and EDDS-complexes formed during the application, in line with what was observed when treating brass coupons (Paragraph 4.4.1). The wet cotton buds were gently used on the metallic surface in order to prevent visible scratches that are typically provoked on the soft alloy when strong mechanical action is adopted for tarnish cleaning (Palomar, Ramírez Barat, *et al.*, 2016; Basilissi *et al.*, 2022).

5.3.3 Multi-analytical protocol for the assessment of PHB-EL-EDDS gel cleaning on sterling silver

5.3.2.1 Visual appearance

The cleaning action of the PHB-EL-EDDS system was evaluated first by a simple naked eye inspection. In the literature it is not uncommon to find references evaluating the cleaning action or detrimental impact of

intervention by simple naked eye inspection, considering that this is the first way for conservator-restorers to evaluate a cleaning outcome and for museum visitors to appreciate the readability and condition of historical silver artefacts (Contreras-Vargas, Ruvalcaba-Sil and Rodriguez-Gómez, 2013; Basilissi *et al.*, 2022).

One application of 30 minutes by means of the PHB-EL-EDDS formulation led to an evident change in the visual appearance of tarnished sterling silver mock-ups, as documented in Figure 5.6 (A and B). The cleaning organogel loaded with EDDS showed better results on the most yellow-brown areas of the mock-up surface, without having an impact on the darker-black zones mainly present at the edges of the metallic sheets.

As previously discussed (page 171), the poor translucence of the PHB-EL-EDDS gel did not allow for monitoring the chelating action of EDDS on sterling silver tarnish over time. However, conversely to what was observed when operating on tarnished brass sheets (Figure 4.19), neither the gel nor Japanese paper, utilised for the cleaning process, acquired a vivid colour due to the potential formation of metal-EDDS complexes during the cleaning treatment. Similarly, cotton buds employed for the clearance step showed no remarkable colour change. Therefore, the formation and removal of metal-EDDS complexes could not be ascertained by simple visual inspection but required spectroscopic techniques to verify the effective chelating action of EDDS when operating on sterling silver.

The appearance of treated mock-ups was newly examined after 3 months of ageing in a climatic chamber to evaluate the efficacy of the newly developed cleaning system in terms of re-tarnishing over time (Figure 5.6, c). Excluding the mock-up edges from the estimation, the silver substrate after ageing reacquired some diffuse yellowish hue together with several white staining marks that could be identified on the metallic surface already after cleaning (Figure 5.6, b) but got enhanced through the ageing process (Figure 5.6, c).

(a) Tarnished (b) Cleaned (c) Aged

Figure 5.6 Photographs of a chemically tarnished sterling silver mock-up (30 × 30 × 0.5 mm^3) before cleaning (a), after one application of 30 minutes with a PHB-EL-EDDS gel (b), and resulting mock-up after 3-month ageing in a climatic chamber (c), respectively.

5.3.2.2 Optical microscopy

Optical microscopy corroborated the observations achieved by simple naked-eye inspection.

Comparing chemically tarnished sterling silver before (Figure 5.7, a) and after a 30-minute application of PHB-EL-EDDS gel (Figure 5.7, b), the technique could easily emphasise the mock-up surface features when observed in bright field. In the first case, an inhomogeneous tarnish film was present and was recognisable by vivid blue, red, and orange shades that are typically derived from the interference of the several films constituting the tarnish present on silver-based substrates (Schalm *et al.*, 2016). After cleaning, the mock-up surface did not show anymore most of these coloured tones initially present, regaining a more silver-coloured appearance as the original non-altered bare substrate was presenting (Figure 5.2). Some marks

recognised on the mock-up surface might be derived from the use of cotton swabs for the closing clearance step, however, they may be rather ascribable to the initial finishing of silver coupons, not being mirror polished preliminarily. Further investigation should be carried out to ascertain the origin of possible unwanted scratches on the precious metallic surface. No visible traces of gel and cleaning residues could be observed in any of the replicates.

Finally, cleaned coupons were subjected to three months of artificial ageing in a climatic chamber. The resulting metallic sheets showed a similar aspect to the non-aged cleaned coupons, yet a more yellow-brown hue was overall identifiable on the sterling silver surface, suggesting the reformation of a thin layer of alteration (Figure 5.7, c). This event would be in line with the previous literature observations, since any cleaning treatments would leave the metallic substrate newly exposed to the environmental caustic agents, if not providing additional inhibiting or protective solutions (Palomar, Ramírez Barat, *et al.*, 2016; Schalm *et al.*, 2016; Thickett and Hallett, 2021; Basilissi *et al.*, 2022).

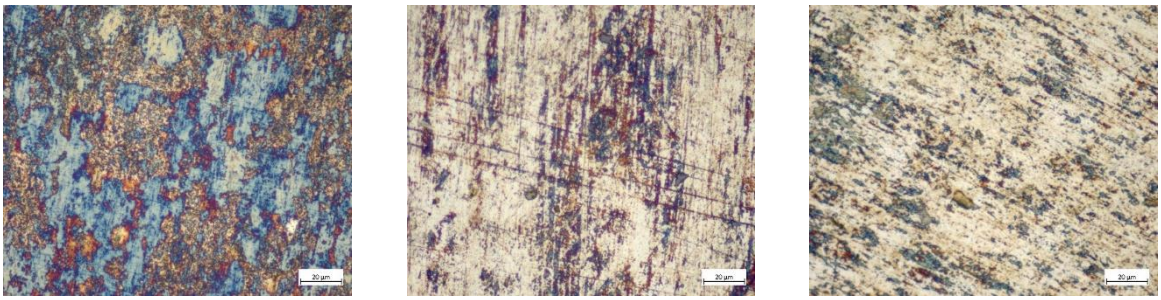

(a) Tarnished (b) Cleaned (c) Aged

Figure 5.7 Optical microscope images in bright field of chemically tarnished sterling silver mock-up before cleaning (a), after one application of 30 minutes with a PHB-EL-EDDS gel (b), and resulting mock-up after 3-month ageing in climatic chamber (c), respectively. The scale bar indicates 20 μm.

5.3.2.3 Colorimetry

The colour difference (i.e., ΔE*) between test coupons and bare sterling silver sheets are reported in Table 5.5 and SM-Table 8 for both SCI and SCE methods, respectively. Namely, the resuming tables present data related to chemically tarnished sterling silver left untread and cleaned by a 30-minute application with a PHB-EL-EDDS gel without and with subsequent ageing in a climatic chamber- The goal was to evaluate not only the cleaning performance of the PHB-EL-EDDS formulation on tarnished sterling silver, but also examine the re-tarnishing process on the cleaned substrates towards which they would tend over time (Palomar, Ramírez Barat, *et al.*, 2016).

As already highlighted in Paragraph 5.3.1, the chosen colorimetric method (i.e., SCI or SCE) appeared crucial also when evaluating the cleaning impact of the PHB-EL-EDDS gel on the silver-based mock-ups. Focusing the attention on ΔE* calculated after cleaning with the gel, great difference was registered between the values when considering SCI (i.e., 22.42 (±7.53)) and SCE (i.e., 4.16 (±2.73)) modes. In particular, the outcome obtained excluding the specular component of the light (i.e., SCE) would suggest a positive recovery of the bare metallic colour of unaltered sterling silver, if related to the threshold calculated as 5, which is often considered as a parameter of acceptability - and colour difference perception by human eye - in art conservation (Kim, Kim and Park, 2011). However, in order to allow a comparison with the literature, the SCI mode was preferred in light of the importance attributed to the bright appearance of silver substrates, and related raw data are available in SM-Table 6 (Palomar, Ramírez Barat, *et al.*, 2016; Schalm *et al.*, 2016; Thickett and Hallett, 2021; Basilissi *et al.*, 2022). Therefore, the colour difference 22.42 (±7.53), measured after cleaning, was compared to the previous literature reporting SCI colorimetric data for sterling

silver model samples cleaned by several traditional systems. Although the initial condition of the tarnished samples was expected to be different, due to the use of different ageing methods and surface finishing, the comparison was considered of interest for a preliminary evaluation of the final cleaning outcome (i.e., cleaned coupons versus bare sterling silver) excluding the relation to the initial condition of the artificially tarnished mock-ups. Therefore, referring to Basilissi, *et al.* (2022), the colorimetric outcomes yielded by PHB-EL-EDDS gel were similar to what reported for both chemical and laser cleaning methods, which were defined as unsatisfactory by the authors because of the poor recover in terms of original brightness (L*) compared to mechanical methods (SM-Table 7). Indeed, the same article reports that only few mechanical procedures yielded a colour difference lower than 10, which would indicate high similarity in appearance to bare sterling silver, in accordance with Palomar, *et al.* (2016). However, the authors also indicated that the mechanical ways left scratches on metals and new active surface that progressed rapidly to re-tarnishing more than the other methodologies, leading to an unsatisfactory intervention in the long-term (Palomar, Ramírez Barat, *et al.*, 2016; Schalm *et al.*, 2016).

In this research study, the global colour difference (i.e., ΔE*) was mainly attributed to the low brightness value (i.e., L*) registered for mock-ups cleaned by PHB-EL-EDDS gel, as reported in Table 5.5. The outcome is conventionally considered an indicator of the presence of residual tarnish on silver-based substrates after cleaning intervention (Palomar, Ramírez Barat, *et al.*, 2016). Furthermore, the ΔL* value calculated for cleaned mock-ups (i.e., -22.35 (±7.55)) resulted greatly different from the value obtained for bare sterling silver coupons after 3-month ageing in a climatic chamber (i.e., -9.28 (±0.42)), which were used as additional references for the evaluation of the cleaning outcome.

The re-tarnishing process of cleaned mock-ups was investigated by colorimetry after a simple wet-dry protocol in a climatic chamber (page 229). Collected data showed a lowering of brightness (i.e., ΔL*) and an enhancement of yellow component (i.e., Δb*) in the colour appearance after ageing, indicating the reformation of tarnish on the cleaned coupons (Table 5.5). Clearly, this determined higher colour difference (i.e., ΔE*) between aged mock-ups and bare sterling silver used as reference. The ΔE* value of cleaned and successively aged mock-ups reached a value equal to 26.92 (±6.87) (Table 5.5), which was still in the range of outcomes reported by Basilissi, *et al.* (2022) mainly for chemical cleaning methods (SM-Table 7).

In line with previous observations, L* ($F = 71.46$) and b* ($F = 12.31$) coordinates were estimated statistically significant for the discrimination of mock-ups conditions by Tukey's HSD test. Statistical analysis proved meaningful distinction ($p < 0.05$) related to both L* and b* coordinates when considering cleaned mock-ups before and after ageing in a climatic chamber. Equal estimation was obtained when comparing bare sterling silver coupons before and after being subjected to the same artificial ageing protocol. This evidence was linked to the spontaneous process of tarnishing towards which both series of coupons tended to. Remarkably, the test did not highlight a significant difference between cleaned mock-ups and bare sterling silver coupons when considering the b* value ($p > 0.05$), demonstrating a satisfactory removal of the yellow component, linked to tarnish, from the surface of treated mock-ups. However, relevant difference was recognised in terms of brightness (i.e., L*) when comparing the same conditions, which can be considered as a drawback according to CRs aestheticism standards (Palomar, Ramírez Barat, *et al.*, 2016; Schalm *et al.*, 2016; Thickett and Hallett, 2021; Basilissi *et al.*, 2022).

Table 5.5 Variation of CIELab coordinates of different sterling silver mock-ups compared to bare unaltered sterling silver, used as control. ΔL*, Δa*, Δb* and related ΔE* SCI values are reported along with their standard deviation into brackets.

Sterling silver mock-up		ΔL*	Δa*	Δb*	ΔE*
Bare	Aged	-9.28 (±0.42)	2.02 (±0.38)	7.10 (±1.58)	11.85 (±1.01)
Tarnished	Initial condition	-38.49 (±0.87)	1.19 (±3.03)	-2.55 (±4.57)	38.59 (±0.92)
	After cleaning	-22.35 (±7.55)	1.16 (±3.35)	-1.29 (±4.69)	22.42 (±7.53)
	Cleaned and aged	-26.33 (±7.01)	3.22 (±0.98)	4.59 (±2.53)	26.92 (±6.87)

5.3.2.4 X-Ray Fluorescence (XRF) spectroscopy

Elemental analysis was performed by means of X-ray fluorescence (XRF) spectroscopy on PHB-EL-EDDS gels and Japanese paper applied for 30 minutes on chemically tarnished sterling silver mock-ups to ascertain the cleaning action of the gelled solution.

As displayed in Figure 5.8, the technique detected the presence of copper in all samples thanks to the characteristic XRF peak detected at about 8.04 keV (Cu Kα line) correlated with a signal of minor intensity at 8.9 keV (Cu Kβ line), which was recognisable exclusively in the spectrum acquired for the cotton swab used for clearance. The presence of copper was particularly evident on the cotton sample, confirming the importance of the crucial step of clearance in order to remove the Cu-EDDS complexes formed during the gel application. On the other hand, no evidence of possible Ag-EDDS complexes formed was hinted by XRF spectroscopy due to the absence of silver-related peaks (i.e., around 22 and 25 keV for Kα and Kβ lines, respectively) in the spectra acquired for gel, Japanese paper, and cotton swab after cleaning application on chemically tarnished mock-ups. This outcome would suggest the absence of complexation affinity for ethylenediamine-N,N'-disuccinic acid towards silver ions that is also not documented in the scientific literature.

The XRF spectra of PHB-EL-EDDS gel (black, Figure 5.8) and Japanese paper (blue, Figure 5.8) were characterised by the additional presence of a signal around 11.9 keV that could be linked to bromine, which was considered as a contamination of the commercial product ethylenediamine-N,N'-disuccinic acid trisodium salt solution (Na_3EDDS 35% in water, Sigma Aldrich) as already discussed in Chapter 4 (Figure 4.16).

Finally, for all samples, the triplet of signals documented in the spectral region above 16 keV was associated to the X-ray tube anode in molybdenum present in the instrument employed (Figure 5.8).

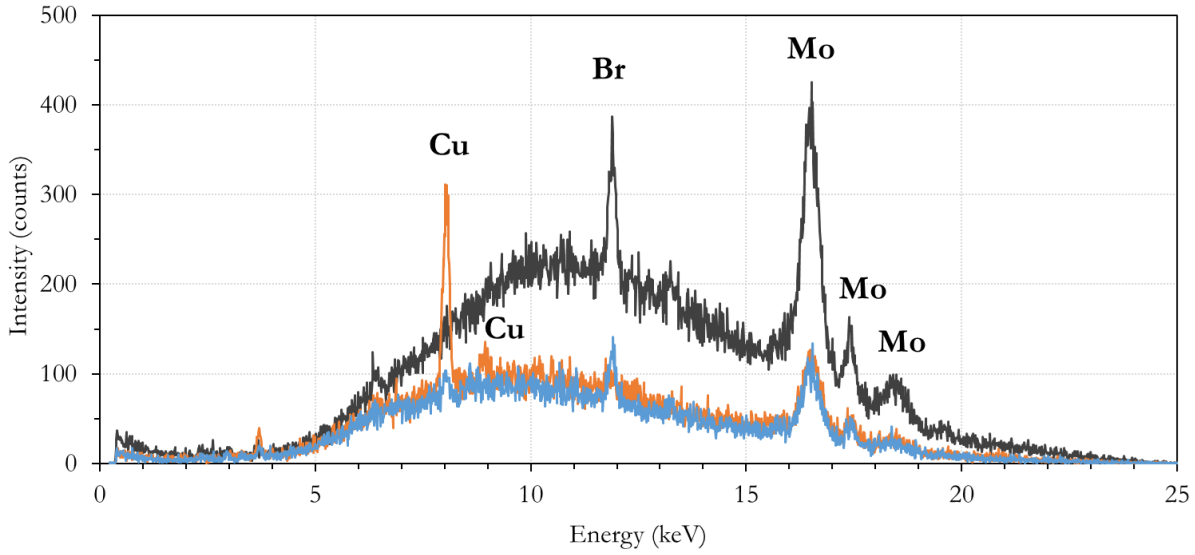

Figure 5.8 XRF spectra of PHB-EL-EDDS gel (black) and Japanese paper (blue) employed for an application of 30 minutes on tarnished sterling silver mock-ups, and XRF spectrum of cotton swab (orange) utilised for the post-treatment clearance. Signals interpretation is reported in the figure.

5.3.2.5 Fourier-transform infrared (FTIR) spectroscopy

Further investigation on PHB-EL-EDDS gels and Japanese paper employed for the cleaning application on tarnished sterling silver was carried out by ATR-FTIR spectroscopy. In particular, the analysis was performed on dried samples to avoid signals related to the presence of ethyl lactate that was not the target of this evaluation and, on the contrary, could have limited the readability of collected data because of possible FTIR band overlapping. Additionally, cotton swabs used in the clearance phase were analysed to check the presence of metal-EDDS complexes (i.e., possibly related to both Ag and Cu ions) and further justify the use of such solution to adequately remove possible treatment residues from target mock-ups.

In the case of gel samples, the predominant spectral features of the PHB matrix did not allow to recognise the presence of EDDS complexes. On the contrary, evident FTIR broad bands were registered at about 1572-1568 cm^{-1} and 1385-1379 cm^{-1} for Japanese paper and cotton specimens only after being used for the cleaning or clearance of tarnished sterling silver coupons, as displayed in Figure 5.9. As already discussed in Chapter 4, previous studies focusing on the identification of EDDS and its complexes by FTIR spectroscopy, demonstrated this couple of bands as diagnostic for stretching vibrations of carboxyl groups present in metal-EDDS complexes (Lanigan and Pidsosny, 2007; Tsang *et al.*, 2013). The other spectral features collected were characteristic for cellulose, lignin, and hemicellulose present in cotton and Japanese paper materials (Portella *et al.*, 2016), as exemplified by the proposed reference spectrum for Japanese paper (Figure 5.9, a).

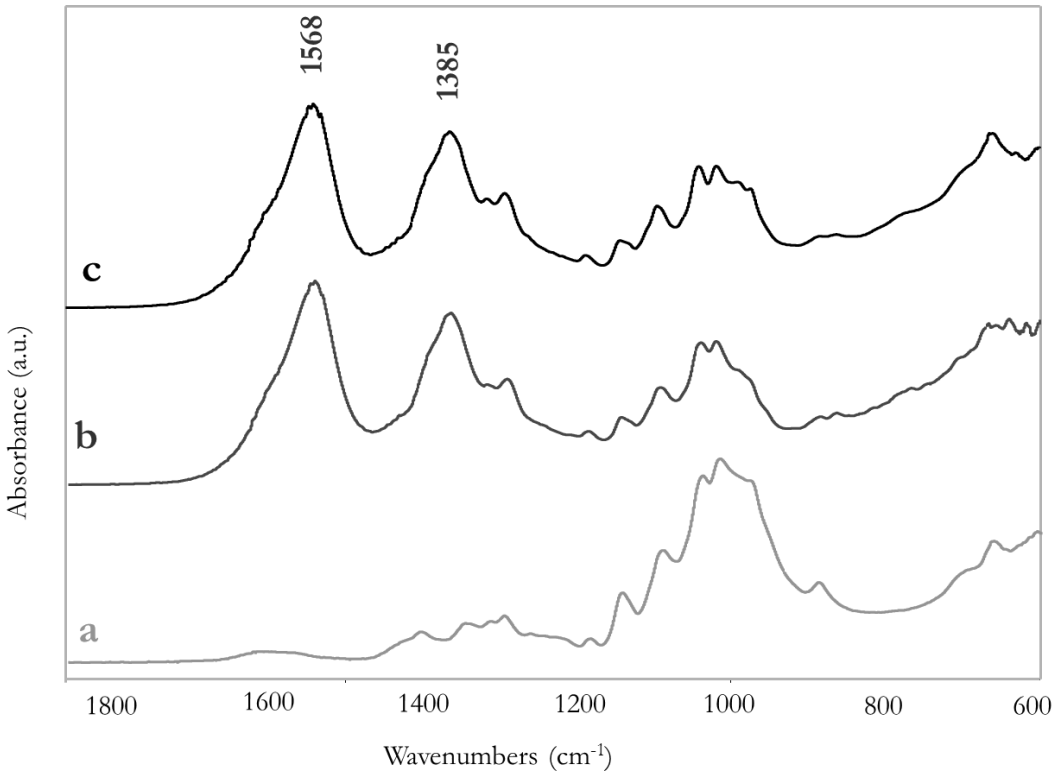

Figure 5.9 ATR-FTIR spectra of non-used Japanese paper (a), and Japanese paper (b) and cotton (c) used together with PHB-EL-EDDS gel for a 30-minute application on chemically tarnished sterling silver.

5.3.2.6 Raman spectroscopy

The analysis of PHB-EL-EDDS gels, both swollen and once dry, Japanese paper, and cotton swabs employed for the cleaning test on tarnished sterling silver did not provide any relevant information regarding the presence of metal-EDDS complexes formed during the cleaning. Similar result was obtained when attempting to extract the complexes by deionised water. indeed, for all samples a high fluorescence interference was recorded by the instrument, whether operating by means of 532 and 785 nm lasers. This unwanted spectral feature hid the diagnostic signals related to the compounds of interest (i.e., EDDS and related complexes) when comparing gels, Japanese paper, and cotton before and after cleaning on sterling silver (Yang *et al.*, 2023). Only in the case of dry used gels, a lower fluorescence interference was detected yet exclusively Raman shifts linked to the polyhydroxybutyrate matrix were recognisable (SM-Figure 20).

Regarding the analysis carried out on the coupons, exclusively lattice vibrations related to metallic silver could be detected sporadically in the spectra acquired after cleaning protocol. Mainly, the residual presence of the original tarnish layer could be identified if compared to the untreated initial surface condition, in line with the results achieved by optical microscopy and colorimetry (Figure 5.10, a and b). A broad band maximum could be recognised around 282 cm^{-1} possibly linked to Ag–S–Cu stretching modes (de Caro *et al.*, 2016), together with weak Raman bands at about 145 and 240 cm^{-1}, respectively related to Ag lattice vibrations and Ag–S bending vibrations (Martina *et al.*, 2012; de Caro *et al.*, 2016) (Figure 5.10, b). The result would indicate no significant variation of the tarnish phases present on the coupons after cleaning by the PHB-EL-EDDS gel. Nonetheless, no significant quantitative analysis could be addressed to evaluate the tarnish removal yield by Raman spectroscopy without the employment of reference standards, since the quantitative interpretation of these data is generally jeopardised by multiple factors (e.g., matrix absorption, surface inhomogeneity, laser beam focus) (Vandenabeele, 2013).

Concerning an evaluation of the cleaning effect in the long-term perspective, cleaned mock-ups were then subjected to artificial ageing in a climatic chamber for three months (page 229). Raman data collected from

the surface of the resulting mock-ups did not highlight evident spectral differences compared to both tarnished and cleaned sterling silver sheets (Figure 5.10, c). As a further comparison, the analysis was finally performed on bare sterling silver coupons artificially aged in the same conditions in a climatic chamber. A representative Raman spectrum is shown in Figure 5.10 (d) and displays clear differences compared to the spectrum acquired on chemically tarnished coupons (a) and cleaned samples before (b) and after 3-month accelerated ageing. Indeed, bare sterling silver sheets subjected to artificial ageing did not present any evident Raman peaks around 280 cm^{-1}, normally assigned to Ag-S-Cu vibrations in this study (de Caro *et al.*, 2016). On the contrary, additional broad signals at about 216, 518, and 630 cm^{-1} would indicated the presence of both crystalline and amorphous cuprite (Cu_2O) that could not be identified on the surface of the chemically tarnished mock-ups (Bouchard and Smith, 2003; Cakir, 2017). The presence of such phases was in accordance with the information provided by PCA applied to Raman spectra collected during the preliminary test by immersion in ethyl lactate (page 201) and are in line with the previous literature discussing the early tarnishing stages affecting sterling silver substrates indoors (Schalm *et al.*, 2016).

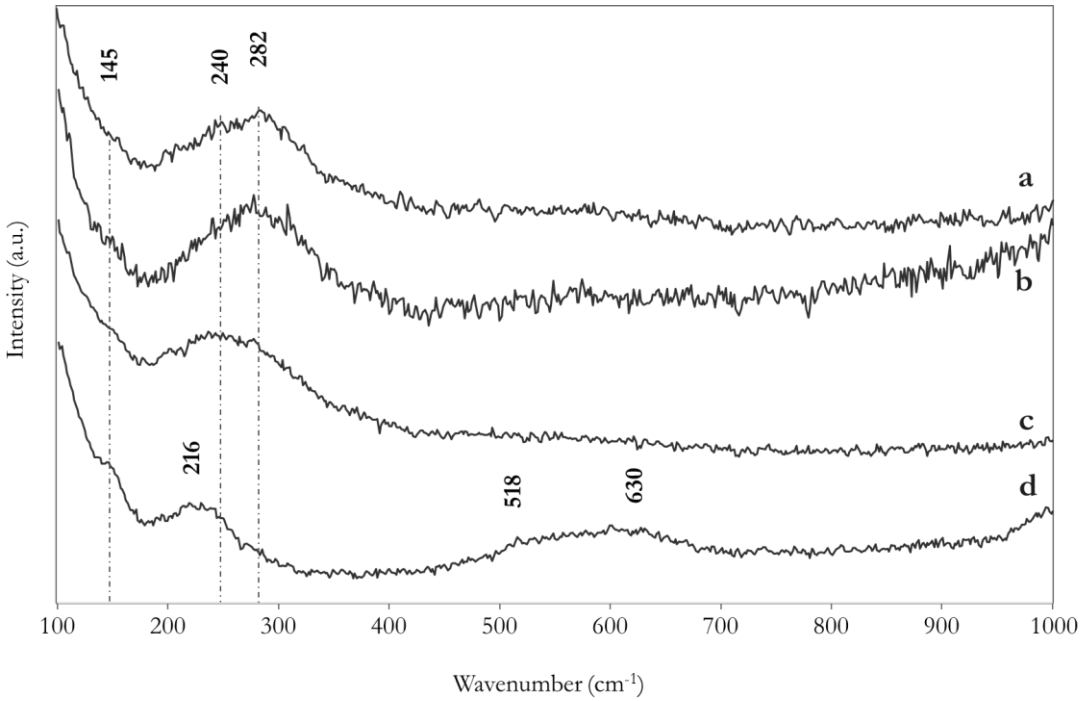

Figure 5.10 Representative Raman spectra collected from chemically tarnished sterling silver (a), cleaned by a 30-minute application with a PHB-EL-EDDS gel (b), and successively aged in a climatic chamber for 3 months (c), and bare sterling silver aged in a climatic chamber for 3 months (d), respectively. Raman shifts are reported in the figure correlated by dashed lines to emphasise similarities and differences within the spectra.

5.3.2.7 Electrochemistry

Electrochemistry was employed to assess the resistance of sterling silver mock-ups against the natural process of re-corrosion by measuring the polarisation resistance (*R*p). Measurements were run in triplicates on the surface of coupons (30 × 30 × 0.5 mm^3) presenting different conditions (Figure 5.11), namely:

a. Bare sterling silver coupons;
b. Bare sterling silver coupons after 3-month ageing in a climatic chamber;
c. Chemically tarnished sterling silver coupons after cleaning by one 30-minute application of a PHB-EL-EDDS gel;

d. Initially chemically tarnished sterling silver coupons cleaned by one 30-minute application of a PHB-EL-EDDS gel, after 3-month ageing in a climatic chamber.

Figure 5.11 Photographs of bare sterling silver coupons (30 × 30 × 0.5 mm^3) before (a) and after 3-month ageing in a climatic chamber (b) and chemically tarnished sterling silver coupons cleaned by a 30-minute application of a PHB-EL-EDDS gel before (c) and after 3-month ageing in a climatic chamber (d).

Calculated average *R*p values, correlated by their standard deviations, are presented in Table 5.6. it has to be remarked that collected electrochemical data were not validated by statistical analysis (e.g., ANOVA) due to the poor amount of measurements available (i.e., three per each series of samples). The interpretation here proposed is thus qualitative and rather based on the comparison of values' magnitudes to evidence possible differences among the multiple series of mock-ups.

The average polarisation resistance measured on the surface of bare sterling silver sheets was evidently different from all other analysed mock-up series, being about one order of magnitude higher than the others, as displayed in Table 5.6. It is known that silver is a quite stable metal (i.e., high polarisation resistance) and, in particular, it is quite resistant to organic acids as verified by the standard electrode potential ($E° = +0.80$ V for Ag^+/Ag), which would justify the high *R*p value registered for bare sterling silver coupons (140.0 (±29.5) kΩ cm^2) (de Figueiredo, Asevedo and Barbosa, 2014). Also tarnishing products formed indoor on silver-based substrates are generally stable yet less in the presence of acidic environments (de Figueiredo, Asevedo and Barbosa, 2014; Selwyn and McKinnon, 2021). This situation would correspond to the experimental conditions used in this study, since an acetic acid solution was employed as electrolyte for the measurements (page 229). This consideration would justify the lower *R*p values collected on all altered samples, presenting tarnish, in contrast to bare sterling silver coupons (Table 5.6). In order to verify this hypothesis, it may be suggested a control test employing a neutral solution as electrolyte (i.e., agarose gel loaded solely with deionised water) to investigate the behaviour of the different mock-up series.

Interestingly, the polarisation resistance measured on the surface of chemically tarnished sterling silver coupons had an average value of 33.6 (±2.61) kΩ cm^2, which was approximately equal to the value registered for bare sterling silver coupons after 3-month ageing in a climatic chamber (i.e., 32.6 (±9.5) kΩ cm^2) (Table 5.6). Unexpectedly, the calculated polarisation resistances were comparable despite the evident difference in the appearance, as observed by optical microscope inspection (SM-Figure 21), and the presence of different tarnish phases, as suggested by Raman spectroscopy (page 208). Possibly, Scanning Electron Microscopy (SEM) analysis may evidence surface features for both series of samples that would better clarify the electrochemical results obtained in this study.

After cleaning by PHB-EL-EDDS gel, the average *R*p value registered on the surface of the coupons dropped from 33.6 (±2.61) kΩ cm^2 to 19.1 (±9.39) kΩ cm^2 (Table 5.6). This outcome is typically proven when removing protective tarnish patina from metallic surfaces or when lowering their thickness (Petiti *et al.*, 2020). At the end of the 3-month ageing protocol in a climatic chamber, the average *R*p value for cleaned mock-ups changed only slightly (22.5 (±12.4) kΩ cm^2), demonstrating a reasonably stable and protective tarnish layer still present on the treated metallic sheets.

Table 5.6 Average values of polarisation resistance (*R*p) measured for bare sterling silver and chemically tarnished sterling silver cleaned by PHB-EL-EDDS gel (i.e., 30-min protocol). Data collected before and after accelerated ageing in a climatic chamber are reported and expressed in kΩ cm^2.

	Before ageing	*After ageing*
Bare sterling silver	140.0 (±29.5)	32.6 (±9.5)
Cleaned sterling silver	19.1 (±9.4)	22.5 (±12.4)

5.4 Conclusions

First attempts for the exploitation of a polyhydroxybutyrate-based (PHB) organogel loaded with ethyl lactate (EL) and ethylenediamine-N,N'-disuccinic acid (EDDS) were here presented for the potential cleaning of tarnished sterling silver substrates. The method was chosen with the goal to provide a greener option in the framework of chemical cleaning methods, which include toxic and pollutant substances such as ethylenediaminetetraacetic acid (EDTA) and thiourea solutions (i.e., silver-dips) (Contreras-Vargas, Ruvalcaba-Sil and Rodriguez-Gómez, 2013; Basilissi *et al.*, 2022). In particular, the complexing agent EDDS was considered an appealing candidate being considered a greener alternative to EDTA, and potentially effective on sterling silver tarnish due to its proven complexing affinity towards Cu ions (Orama *et al.*, 2002). On the contrary, no evidence regarding an affinity for Ag ions is reported in the previous literature.

The assessment was carried out on sterling silver coupons aged chemically with a protocol that was considered more sustainable than traditional K_2S or Na_2S solution, since it employs albumin solutions as source of H_2S vapours (Siatou *et al.*, 2022). The resulting mock-up surface was dull and yellow-brown with darker edges mimicking the normal features of tarnished silver-based artworks.

In a first phase, altered mock-ups were immersed in ethyl lactate, which is the organic solvent included in the gel formulation, to ascertain the impact of its acidic pH (i.e., 4) on the tarnish film. Being the aim of tarnish removal rather oriented towards the preservation of the original metallic finishing typical of silver-based substrates, colorimetry was considered a crucial method to be employed for the evaluation of the visual appearance of test mock-ups. Colorimetric data analysed by statistical approach (i.e., Tukey's HSD test) could provide information about a significant change in the aspect of the altered coupon after 30 minutes of immersion in ethyl lactate, which was considered as a timing for further assay by PHB-EL-EDDS formulation. On the contrary, Raman spectroscopy analysis could not provide a reliable monitoring regarding possible changes in the corrosion present on sterling silver mock-ups throughout the immersion test, even when supported by Principal Component Analysis. Possibly, the spectroscopic analysis would provide meaningful information if supported by standards for a quantitative evaluation of EL impact on the tarnish layer.

Assaying the PHB-EL-EDDS system on the altered sterling silver mock-ups with one application of 30 minutes, colorimetric data, supported by statistical analysis, demonstrated a significant reduction in b* (i.e., yellow shade) values after cleaning on the mock-up surfaces. The difference between cleaned mock-ups and bare sterling silver coupons was evaluate statistically non-significant for b* coordinate, thus demonstrating a positive cleaning action of the PHB-EL-EDDS gel towards tarnish phases. On the contrary, when considering the brightness factor (i.e., L*), a significant difference was observed between the same coupons (i.e., cleaned vs bare), stating a non-optimal recovery of the metallic brightness typical of silver substrates and sought by CRs when intervening on similar collections. Nonetheless, colorimetric values obtained were in line with data reported in the previous literature especially for chemical cleaning approaches on sterling silver (Basilissi *et al.*, 2022). Therefore, the proposed PHB-EL-EDDS system should be considered as an interesting cleaning method for further research towards greener chemical alternatives in metal care. Raman spectroscopy did not highlight relevant differences comparing chemically tarnished coupons before and after cleaning by PHB-EL-EDDS gel, which is encouraging evidence since it would verify the absence of

phases transformation on the treated substrates due to the interaction with the proposed formulation. In parallel, electrochemical measurements demonstrated a reasonably stable and protective tarnish layer still present on the cleaned mock-ups over time. On the other side, the lack of a quantitative explanation of the collected Raman spectra did not allow to assess the cleaning yield on tarnish phases, despite the clear visual and colorimetric outcomes. Finally, X-ray fluorescence analysis could prove the presence of copper on used gelled systems after cleaning, but no signals could indicate the presence of silver. This result might suggest the absence of affinity towards the formation of Ag-EDDS complexes, which is also not reported in the current literature, however more sensible analyses (e.g., ICP-MS) would be of interest to further ascertain this consideration.

Bibliography

Águas, H. et al. (2008) 'Study of environmental degradation of silver surface', physica status solidi c, 5(5), pp. 1215–1218. Available at: https://doi.org/10.1002/pssc.200777842.

Angelini, E. and Argyropoulos, V. (2008) 'PROMET state-of-the-art approach for protecting, preserving, and interpreting metals from museums in the Mediterranean basin', in V. Argyropoulos (ed.) Metals and Museums in the Mediterranean. Protecting, Preserving and Interpreting. TEI (Athens), pp. 23–37.

Artesani, A. et al. (2020) 'Recent Advances in Protective Coatings for Cultural Heritage–An Overview', Coatings, 10(3), p. 217. Available at: https://doi.org/10.3390/coatings10030217.

Basilissi, G. et al. (2022) 'Evaluation of a dry method using erasers for silver--copper alloy tarnish cleaning and comparison with traditional methods', Journal of the American Institute for Conservation, 61(2), pp. 112–128.

Bouchard, M. and Smith, D.C. (2003) 'Catalogue of 45 reference Raman spectra of minerals concerning research in art history or archaeology, especially on corroded metals and coloured glass', Spectrochimica Acta Part A: Molecular and Biomolecular Spectroscopy, 59(10), pp. 2247–2266. Available at: https://doi.org/10.1016/S1386-1425(03)00069-6.

Cakir, D. (2017) Enhanced Raman signatures on copper based-materials. Université Montpellier. Available at: https://theses.hal.science/tel-01944233/.

de Caro, T. et al. (2016) 'Micro-Raman innovative methodology to identify Ag–Cu mixed sulphides as tarnishing corrosion products', Journal of Raman Spectroscopy, 47(7), pp. 852–859. Available at: https://doi.org/10.1002/jrs.4900.

Contreras-Vargas, J., Ruvalcaba-Sil, J.L. and Rodriguez-Gómez, F.J. (2013) 'Effects of the cleaning of silver with acidified thiourea solutions', in Conference proceedings of Metal, pp. 223–228.

Costa, V. (2001) 'The deterioration of silver alloys and some aspects of their conservation', Studies in Conservation, 46(sup1), pp. 18–34. Available at: https://doi.org/10.1179/sic.2001.46.Supplement-1.18.

Cruz, J.S., Hernández, S.M. and Coronel, J. (2012) 'Characterization of CuxS thin films obtained by CBD technique at differents annealing temperatures', Chalcogenide Letters, 9(2), pp. 85–91.

Degrigny, C. (2008) 'The search for new and safe materials for protecting metal objects', in V. Argyropoulos (ed.) Metals and Museums in the Mediterranean. Protecting, Preserving and Interpreting. TEI (Athens), pp. 179–235.

Degrigny, C. et al. (2016) 'A new electrolytic pencil for the local cleaning of silver tarnish', Studies in Conservation, 61(3), pp. 162–173. Available at: https://doi.org/10.1179/2047058415Y.0000000015.

de Figueiredo, J.C.D., Asevedo, S.S. and Barbosa, J.H.R. (2014) 'Removal of brownish-black tarnish on silver–copper alloy objects with sodium glycinate', Applied Surface Science, 317, pp. 67–72. Available at: https://doi.org/10.1016/j.apsusc.2014.08.096.

de Figueiredo Junior, J.C.D. et al. (2021) 'The Cleaning of Silver Objects With a Basic Solution of Sodium Glycinate: A Study on Artificially and Naturally Tarnished Silver', Studies in Conservation, 66(7), pp. 375–383. Available at: https://doi.org/10.1080/00393630.2020.1859876.

Gouda, V. et al. (2009) '3 Silver artifacts protection by anticorrosive coatings', Egyptian Journal of Chemistry, 52(Special issue), pp. 29–45.

Kim, A.-R., Kim, H.-S. and Park, S.-O. (2011) 'Measuring of the Perceptibility and Acceptability in Various Color Quality Measures', Journal of the Optical Society of Korea, 15(3), pp. 310–317. Available at: https://doi.org/10.3807/JOSK.2011.15.3.310.

Lanigan, K.C. and Pidsosny, K. (2007) 'Reflectance FTIR spectroscopic analysis of metal complexation to EDTA and EDDS', Vibrational Spectroscopy, 45(1), pp. 2–9. Available at: https://doi.org/10.1016/j.vibspec.2007.03.003.

Martina, I. et al. (2012) 'Micro-Raman characterisation of silver corrosion products: instrumental set up and reference database', E-Preserv Sci, 9, pp. 1–8.

Merck (2024) (-)-Ethyl L-lactate, properties. Available at: https://www.sigmaaldrich.com/CH/en/product/aldrich/e34102 (Accessed: 13 February 2024).

Orama, M. et al. (2002) 'Complexation of [S,S] and mixed stereoisomers of N,N'-ethylenediaminedisuccinic acid (EDDS) with Fe(III), Cu(II), Zn(II) and Mn(II) ions in aqueous solution', J. Chem. Soc., Dalton Trans., (24), pp. 4644–4648. Available at: https://doi.org/10.1039/B207777A.

Palomar, T. et al. (2016) 'A comparative study of cleaning methods for tarnished silver', Journal of Cultural Heritage, 17, pp. 20–26. Available at: https://doi.org/10.1016/j.culher.2015.07.012.

Petiti, C. et al. (2020) 'Effects of cleaning procedures on the long-term corrosion behavior of bronze artifacts of the cultural heritage in outdoor environment', Environmental Science and Pollution Research, 27(12), pp. 13081–13094. Available at: https://doi.org/10.1007/s11356-020-07814-4.

Portella, E.H. et al. (2016) 'Influence of Stacking Sequence on the Mechanical and Dynamic Mechanical Properties of Cotton/Glass Fiber Reinforced Polyester Composites', Materials Research, 19(3), pp. 542–547. Available at: https://doi.org/10.1590/1980-5373-MR-2016-0058.

Ricotta, N., Gagnini, A. and Degrigny, C. (2022) 'Analysis of heterogeneous tarnish on silver-based alloys using the Pleco for local, controlled electrolytic cleaning', in Metal 2022, proceedings of the interim meeting of the ICOM-CC metals working group.

Schalm, O. et al. (2016) 'The corrosion process of sterling silver exposed to a Na2S solution: monitoring and characterizing the complex surface evolution using a multi-analytical approach', Applied Physics A, 122(10), p. 903. Available at: https://doi.org/10.1007/s00339-016-0436-6.

Selwyn, L. and McKinnon, W.R. (2021) 'Silver and Acid-thiourea Silver Dips: Rinsing and Aging Monitored by Electrochemistry', Studies in Conservation, 66(2), pp. 98–112. Available at: https://doi.org/10.1080/00393630.2020.1773056.

Siatou, A. et al. (2022) 'A Methodological Approach for Multi-Temporal Tracking of Silver Tarnishing', in Proceedings of the 4th ACM International workshop on Structuring and Understanding of Multimedia heritAge Contents. New York, NY, USA: ACM, pp. 5–13. Available at: https://doi.org/10.1145/3552464.3555686.

Thickett, D. and Hallett, K. (2021) 'Managing silver tarnish', in Transcending Boundaries: Integrated Approaches to Conservation. In Proceedings of the ICOM-CC 19th Triennial Conference Preprints, Beijing, China, pp. 17–21.

Tissot, I. et al. (2016) 'Corrosion of silver alloys in sulphide environments: a multianalytical approach for surface characterisation', RSC Advances, 6(57), pp. 51856–51863. Available at: https://doi.org/10.1039/C6RA05845K.

Tsang, D.C.W. et al. (2013) 'Mechanisms of EDDS Adsorption on Goethite and Hematite Under Aqueous and Dehydrated Conditions', Environmental Engineering Science, 30(12), pp. 733–741. Available at: https://doi.org/10.1089/ees.2013.0211.

Vandenabeele, P. (2013) Practical Raman spectroscopy: an introduction. John Wiley & Sons.

Vassiliou, P. and Gouda, V. (2013) 'Ancient silver artefacts: corrosion processes and preservation strategies', in Corrosion and Conservation of Cultural Heritage Metallic Artefacts. Elsevier, pp. 213–235. Available at: https://doi.org/10.1533/9781782421573.3.213.

Yang, Q. et al. (2023) 'Combination of Resonance and Non-Resonance Chiral Raman Scattering in a Cobalt(III) Complex', Angewandte Chemie International Edition, 62(45). Available at: https://doi.org/10.1002/anie.202312521.

Chapter 6

Conclusions and future perspectives

"Si poteva fare di più e meglio?
Probabilmente sì, come sempre.
Ma non va ignorato neppure quanto di positivo è stato realizzato"

Extract from the End-of-Year Address of the President of the Republic Sergio Mattarella,
December 31, 2020

The research study presented in this dissertation started with the exploitation of several commercially available bio-sourced and biodegradable compounds for the design of gelled formulations aimed to remove undesired protective coatings from the surface of historical metal collections. In line with the responses gathered through a worldwide survey conducted in 2020 within the framework of the HELIX project, the coatings selected for the cleaning assessment were acrylic varnishes (i.e., Paraloid® B72) and nitrocellulose lacquers (i.e., Zaponlack), being among the most traditional solutions for indoor metal care. Three formulations were designed loaded with the bio-solvent ethyl lactate (EL) in order to provide potentially new methods for the bio-cleaning of altered historical metals. Poly-3-hydroxybutyrate (PHB), agar, and polylactic acid (PLA) were employed as thickening agents to design PHB-EL, agar-water/EL, and PLA-EL cleaning systems, respectively. The formulations showed different features by multi-modal analysis. In particular, rheology verified PHB-EL and agar-water/EL systems as stiff gels, whereas PLA-EL was classified as a viscous liquid. The different nature of the formulations determined also different ways of application and clearing approaches. Triplicate cleaning tests were performed on mild steel and brass mock-ups coated with Paraloid® B72 and Zaponlack, respectively, operating through one or two applications of 5 or 10 minutes for each proposed formulation. A clear alteration of mild steel coupons treated by agar-water/EL gel was noticed by the naked eye, by optical microscopy, and corroborated by colorimetry that measured an increment in yellow-reddish shades typical of iron corrosion species. In parallel, X-ray fluorescence spectroscopy verified the presence of iron for the used gel, corroborating the hypothesis of a corrosive effect occurring between gel and substrate, possibly related to water and/or the unexpected presence of alginic acid in the commercial product. Colorimetry measurements, supported by statistical analysis (i.e., Tukey's HSD test) did not provide meaningful information to discern outcomes obtained by PHB-EL and PLA-EL systems along the several timings and applications explored. Only for the PHB-EL system applied on mild steel mock-ups coated with PB72, the analysis suggested a cleaning performance linked to gel renewal rather than application time. Fourier-transform infrared spectroscopy demonstrated the ability of the PHB-EL gel to retain both swollen Paraloid® B72 and Zaponlack, detaching them already after one short-time application (i.e., 5 minutes). Similarly, Zaponlack could be identified on used PLA-EL systems. In contrast, used agar-water/EL gels, analysed by FTIR spectroscopy, did not show any ability to entrap the swollen coatings in the gelled matrix, possibly due to the hydrophobicity of the materials to be removed. Finally, the same spectroscopic technique, supported by Principal Component Analysis (PCA) for the interpretation of collected data, could provide useful information about the achieved cleaning and the potential presence of systems' residues on the differently treated mock-ups.

In light of the results obtained, a new green organogel based on the polymer poly-3-hydroxybutyrate was designed with the innovative perspective to simultaneously tackle different targets present on historical metal collections. Steel was the first protagonist of this innovative research, and specifically the concurrent

removal of an acrylic coating (i.e., Paraloid® B72) and the underlying iron corrosion (i.e., iron oxyhydroxides) that can be found on altered artworks. Poly-3-hydroxybutyrate (PHB), ethyl lactate (EL), and deferoxamine B (DFO) were employed as thickening agent, organic solvent, and complexing agent, respectively, for the design of the innovative double-action formulation. Remarkably, all components respected the green principles of biodegradability, renewability of the source of production, and were inherently low or non-toxic. The cleaning efficiency of the resulting system was tested on mild steel mock-ups chemically corroded and coated by Paraloid® B72. Colorimetric measurements on the surface of treated mock-ups ascertained that a significant difference in appearance was present between bare steel references and mock-ups after cleaning for all tested times and repetitions. Nevertheless, a complete recovery of a metallic aspect is also an unsought outcome when working on historical iron artworks. Therefore, the PHB-EL-DFO gel was considered a reliable tool for moderate, well-localised, and adjustable cleaning on altered iron-based substrates. Statistical analysis verified that gel renewal (and possibly consecutive clearance step) was a more relevant variable compared to application time for the final cleaning of the mock-ups. This was considered a relevant conclusion for the exploitation of the formulation on real cases. Indeed, in order to better control the level of cleaning achieved, CRs may rely on a short-time protocol with multiple gel reiteration to ascertain at each step the outcome on the metal artwork. Finally, the siderophore was proven effective towards the chelation of iron ions by multi-modal analysis despite being loaded in a rigid gel matrix. This is a relevant aspect since poor contact, hence interaction between cleaning system and altered metallic surfaces, is often remarked when employing rigid and stiff systems (e.g., agar pre-formed gels) (Cuvillier *et al.*, 2023). The capability of the PHB-EL-DFO gel to tackle simultaneously the two undesired materials (i.e., corrosion products and organic lacquer) was demonstrated by Principal Component analysis applied to FTIR spectra collected from the treated mock-ups along the cleaning assessment. In parallel, electrochemical measurements would suggest that residual corrosion products present on the surface of cleaned mock-ups were possibly a protective "barrier" against the spontaneous process of re-corrosion.

Moving to another family of metals often present in indoor historical collections, the cleaning of altered brass was addressed. In particular, the research focused on the simultaneous removal of a nitrocellulose-based coating (i.e., Zaponlack) and corrosion, mainly constituted of copper and zinc oxides and sulphides, which can be found on altered brass objects. A polyhydroxybutyrate-based (PHB) organogel loaded with ethyl lactate (EL) and ethylenediamine-N,N'-disuccinic acid (EDDS) was designed for the groundbreaking exploitation of EDDS as a greener alternative in metal heritage cleaning (Orama *et al.*, 2002). The assessment of the novel system on brass mock-ups, chemically altered and coated with Zaponlack, achieved encouraging outcomes for the exploitation of the cleaning system on real artworks. In particular, X-ray fluorescence, Raman, and Fourier-transform infrared spectroscopies confirmed the complexing action of EDDS towards copper and zinc ions when embedded in the PHB-system. The evidence was considered remarkable since frequently a limiting factor, when using rigid gelled systems, as the PHB-EL-EDDS, can be a lack of even contact between gel and metal, leading to a poor cleaning action. Additionally, first evidence of Cu- and Zn-EDDS complexes could be detected by Raman spectroscopy. A positive regain of yellow-coloured aspect typical of bare brass was measured by colorimetry after cleaning on the mock-ups treated by multiple (i.e., three applications) and prolonged (i.e., 30 minutes) gel applications. However, the colour difference, compared to bare brass sheets, was still relevant when working with SCI data. Despite having a slow cleaning action on test mock-ups, the outcome also showed that the PHB-EL-EDDS system can provide an easily tuneable and moderate action that would guarantee the avoidance of undesired overcleaning on altered brass objects. Finally, FTIR spectroscopy could verify the effective removal action of the PHB-EL-EDDS gel towards Zaponlack lacquer. On the other hand, Raman spectroscopy could not provide a clear monitoring of the progressive removal of brass tarnish, which on the contrary was evident by colorimetric data. The absence of data interpretation in a quantitative perspective resulted in being a limiting factor when performing Raman analysis. Finally, analogous polarisation resistance values were calculated for bare and cleaned brass coupons after artificial ageing, possibly indicating a non-deleterious impact of the PHB-EL-EDDS formulation on treated brass surfaces in the long-term.

The same functionalised organogel (i.e., PHB-EL-EDDS) was assayed for the cleaning of tarnished sterling silver substrates. The goal was to test a greener alternative for localised cleaning in order to replace toxic

and pollutant substances, such as ethylenediaminetetraacetic acid (EDTA) and thiourea solutions (i.e., silver-dips), frequently used on silver (Contreras-Vargas, Ruvalcaba-Sil and Rodriguez-Gómez, 2013; Basilissi *et al.*, 2022). In particular, the complexing agent EDDS was considered a good candidate due to its proven complexing affinity towards Cu ions (Orama *et al.*, 2002). The research was carried out on chemically tarnished sterling silver coupons. A significant cleaning impact caused by ethyl lactate was ascertained by statistical method applied to colorimetric data collected after 30 minutes of interaction between the organic solvent and the metal sheet. Consequently, the same timing was used for a single application of PHB-EL-EDDS gel to investigate the possible cleaning action on tarnished mock-ups. Again, colorimetric measurements screened by statistical analysis (i.e., Tukey's HSD test) evidenced a positive loss of the yellow shade, typically related to tarnish products, after gel application; yet no significant recover of metallic brightness could be noticed. However, the results were in line with reference literature reporting data acquired for traditional chemical methods employed for the cleaning of silver collections (Palomar, Ramírez Barat, *et al.*, 2016). Additionally, electrochemical measurements would demonstrate a reasonably stable tarnish layer still present on the cleaned mock-ups over time. Therefore, the proposed PHB-EL-EDDS gelled system should be considered as an interesting cleaning method for further research.

In parallel to the laboratory activity, the formulations designed within the framework of the HELIX project and this doctorate were presented to and tested with metal conservators during workshops. The events were useful for the evaluation of the proposed solutions on real cases. Furthermore, they provided the opportunity to receive feedback from the potential future end-users.

For instance, during a workshop carried out at Arc'Antique in Nantes (France) with conservators and restorers, a silver-based plate coated with Paraloid® B72 (i.e., information provided by the restorer working on the object) was cleaned by PHB-EL gel (Figure 6.1). In particular, the system was applied once and twice for 5 minutes. In the case of reiteration (i.e., 5-min twice), both sides of the rigid gel were used alternatively. The double-side cleaning (Figure 6.1, white arrow) performed well, leaving no visible residues of swollen Paraloid® B72 in the treated area, on the contrary to one single application (Figure 6.1, yellow arrow) and comparison cleaning by cotton swabs soaked in ethyl lactate (Figure 6.1, red arrow). Within the same atelier, the potential of the PHB-EL gel were exploited also on curved objects. In the case of an iron-based key, for example, the goal was to remove the acrylic-based inventory number and coating present on its curved surface. The gel was applied gently pressing by fingers to adapt the formulation to the object shape (Figure 6.2, left). One application of 10 minutes resulted effective for the complete removal of both materials, as evidenced also by portable UV lamp (Figure 6.2, right). Gentle dry cotton swabbing was employed to remove residual swollen material present on the object after gel application.

Figure 6.1 Silver plate coated with Paraloid® B72 treated by two 5-minute applications of PHB-EL gel (white arrow), one 5-minute application of PHB-EL gel (yellow arrow), and cotton swabs soaked in ethyl lactate (red arrow).

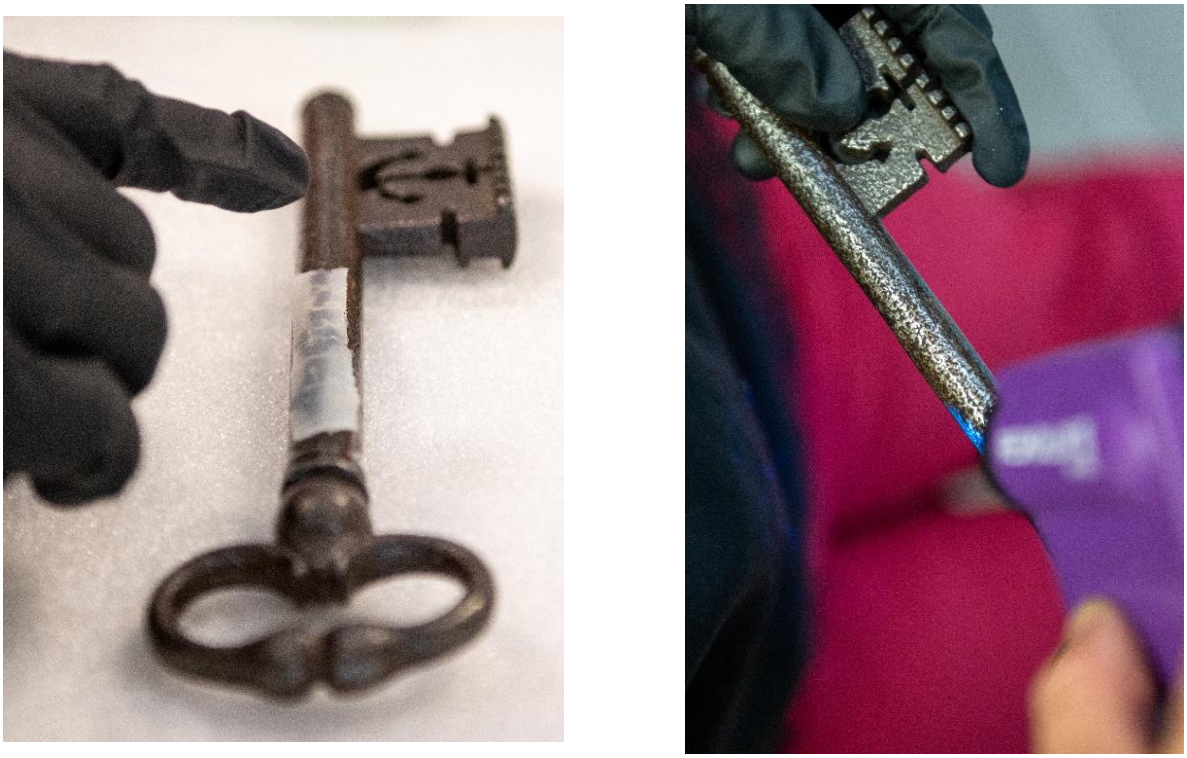

Figure 6.2 Iron-based key presenting acrylic-based inventory number and coating. PHB-EL gel applied for 10 minutes on the artefact (left) and final result inspected under UV lamp (right).

During another HELIX workshop organised at the Haute Ecole Arc in Neuchâtel (Switzerland), an object made of brass – verified by means of XRF spectroscopy – was the target of the double-cleaning provided by the PHB-EL-EDDS gel (Figure 6.3). The small artefact (approximately 4 × 4 cm^2) was characterised by the presence of a nitrocellulose protective coating, as verified by FTIR spectroscopy (Figure 6.4) (Brock *et al.*, 2018), and visible dark corrosion stains, which could not be analysed by Raman spectroscopy prior to cleaning because of the high interference recorded in the collected spectra (i.e., fluorescence). The object was treated by triple 20-minute application by PHB-EL-EDDS gel that led to the successful removal of brown stains initially present on the object, while reacquiring the typical colour of metallic brass substrates. Only the left side of the object was treated, therefore it is possible to appreciate the different appearance achieved also in the post-cleaning photography (Figure 6.3). Finally, FTIR spectroscopy could verify the effective removal of the nitrocellulose lacquer, as presented in Figure 6.4.

Figure 6.3 Photography of brass object before (left) and after cleaning treatment by three 20-minute applications of PHB-EL-EDDS gel (right).

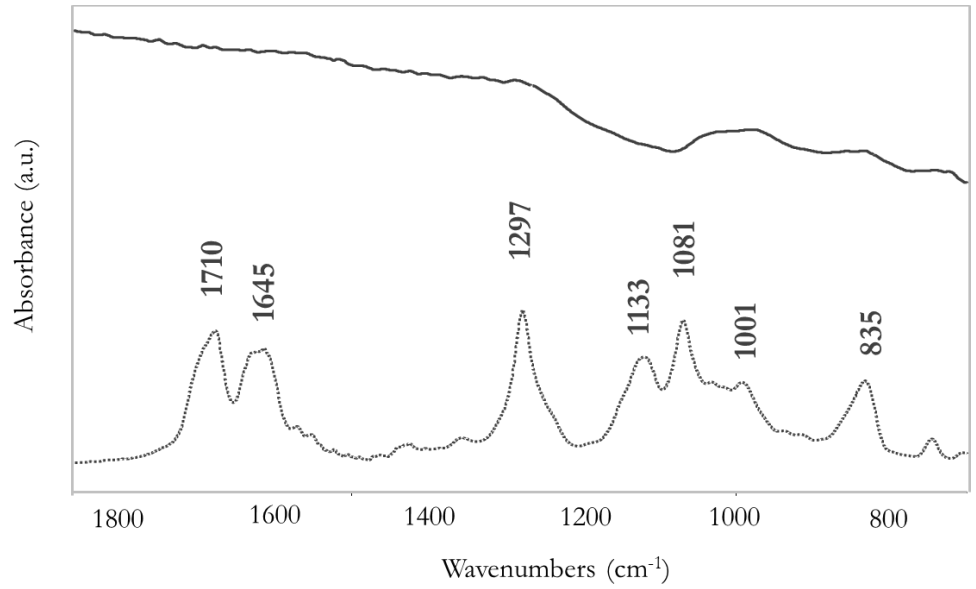

Figure 6.4 FTIR spectra collected in reflectance mode from the surface of the brass object before (dotted line) and after cleaning treatment by three 20-minute applications of PHB-EL-EDDS gel (solid line).

Similarly, the PHB-EL-DFO gel was tested on corroded steel scissors, belonging to the collection of the Musée Historique in Lausanne (Switzerland) (Figure 6.5). In particular, the object was presenting an inventory number made of an acrylic-based material – verified by FTIR spectroscopy on other objects of the same collection because of geometrical limitations to perform the analysis directly on the scissors. The purpose of the intervention was to remove the written number while "lightening" the corrosion present on the scissors. Cleaning intervention by PHB-EL-DFO gel was thus performed by short-time (i.e., 15 minutes) repeated (up to six times) applications to monitor the cleaning achieved. Resulting visual appearance outcome obtained was considered satisfactory by CRs and it is displayed in Figure 6.5.

Figure 6.5 Photographic close-ups of steel scissors (Musée Historique in Lausanne, Switzerland) before (left) and after (right) cleaning by six applications of 15 minutes with PHB-EL-DFO gels.

In conclusion, the formulations, explored during the doctoral activity, open to an innovative way of cleaning altered historical metals respecting several aspects listed in the Green Chemistry principles, such as potential sources renewability, biodegradability, and limited or low toxicity of the materials employed. In particular, the simultaneous action for the removal of polar organic substances (i.e., Paraloid® B72 and Zaponlack) and inorganic compounds (i.e., corrosion products normally present on indoor iron-based, brass, and sterling silver historical collections) was explored with the purpose of possibly condensing working time and amount of materials usually employed by metal conservators for the individual treatment of similar cases. The use of gelled systems demonstrated well-defined and localised action on the treated mock-up samples. Additionally, the moderate cleaning action of the proposed formulations would guarantee a sought adaptability of the treatment, by modulation of application time and gel reiteration, according to specific object condition and conservation purposes.

From a more audacious perspective, the doctoral research was aimed to promote the exploration of innovative methods and materials in the activity of metal conservators, while fostering the industrial research towards more sustainable approaches for the production of bio-sourced materials (e.g., EDDS manufacturing without the use of ethylene bromide) because of their potentials.

The discussed research provided preliminary evidence for a reliable implementation of innovative greener systems in metal care. In particular, further investigation should be carried out to compare the proposed gel formulations to traditional cleaning methods (e.g., mechanical and chemical) to obtain a clear evaluation of pros and cons related to their use by multi-modal analysis (Basilissi *et al.*, 2022). The assessment should not only evaluate the cleaning outcomes, but also verify the potential presence of post-treatment residues. This was a collateral point addressed within this doctoral project when characterising mock-up surfaces by vibrational spectroscopies (i.e., FTIR and Raman spectroscopy) for the evaluation of gels' cleaning performance. However, deeper research should be carried out, employing also other methodologies such as

fluorescent markers in the gels to be tracked post-cleaning under UV light or Scanning Electron Microscopy (SEM) (Guilminot, 2023). The latter technique (i.e., SEM) should also be used to observe the morphology of cleaned metal sheets, which would help to interpret certain analytical data (e.g., polarisation resistance values) and thus verify the reliability of the designed gelled systems (Schalm *et al.*, 2018). Finally, the use of inductively coupled plasma - optical emission spectroscopy (ICP-OES) could be of interest to investigate the potential ability of EDDS solutions to complex Ag ions that is not reported in the previous literature and could not be ascertained within the research.

A limiting factor for the design of the gels was the unavoidable presence of water for the dissolution of the complexing agents employed. Similarly, water was a requirement for the removal of formed metal-ligand complexes from the treated metal substrates. It would be of interest to assess if the use of gelled systems (e.g., agar retaining the clearance solution made of ethanol and water) could be a valid option to reduce the quantity of free solvents to be employed while ensuring a satisfactory post-treatment clearance (Jia *et al.*, 2021).

In general, the formulations were designed respecting conventional concentrations reported in the literature and facing the problem linked to the hydrophobicity of the polymer employed (i.e., poly-3-hydroxybutyrate). From a green perspective, however, it would be of interest to evaluate at the "atom economy" level if lower concentrations would yield comparable cleaning outcomes (Anastas and Warner, 1998). This research would require the use of test solutions at different concentrations of target species (e.g., iron corrosion compounds) and complexing agents (e.g., DFO), and then include used gels loaded with the selected concentrations of complexing solution and/or solvents. Raman spectroscopy and inductively coupled plasma-mass spectroscopy (ICP-MS), supported by statistical analysis (i.e., Principal Component Analysis and ANOVA), may be proposed for the qualitative and quantitative assessment of the study.

Considering the global environmental impact of the proposed formulations, the Life Cycle Assessment (LCA) should be carried out on the components employed (Anastas and Eghbali, 2010; Prat, Hayler and Wells, 2014; Calvo-Flores *et al.*, 2018). Despite the willing, several problems were encountered during the doctoral period to perform this evaluation. Indeed, LCA works on a wide range of parameters, including transportation, process and cost of production, that could not be provided univocally or are confidential.

From a wider perspective, the use of other bio-based solvents should be explored. Within the proposed research, ethyl lactate was chosen in light of its proven greenness and ability in dissolving the organic coatings of interest (Pereira, Silva and Rodrigues, 2011). Moreover, the solvent was miscible in water, which, as already mentioned, was a limiting factor for the design of the gels. Attention should be addressed for the removal of non-polar coatings and materials (e.g., wax, grease), which are substances normally found on metal heritage (e.g., scientific and technical objects) (Molina *et al.*, 2023). A possible research line might be defined by the use of selected essential oils that would be effective on the targets due to their non-polarity and that proved encouraging and positive protective effects on steel and copper-based materials (Wei *et al.*, 2020; Dhouibi *et al.*, 2021).

Bibliography

Anastas, P. and Eghbali, N. (2010) 'Green Chemistry: Principles and Practice', Chem. Soc. Rev., 39(1), pp. 301–312. Available at: https://doi.org/10.1039/B918763B.

Anastas, P.T. and Warner, J.C. (1998) 'Green chemistry', Frontiers, 640(1998), p. 850.

Basilissi, G. et al. (2022) 'Evaluation of a dry method using erasers for silver--copper alloy tarnish cleaning and comparison with traditional methods', Journal of the American Institute for Conservation, 61(2), pp. 112–128.

Brock, F. et al. (2018) 'Testing the Effectiveness of Protocols for Removal of Common Conservation Treatments for Radiocarbon Dating', Radiocarbon, 60(1), pp. 35–50. Available at: https://doi.org/10.1017/RDC.2017.68.

Calvo-Flores, F.G. et al. (2018) 'Green and Bio-Based Solvents', Topics in Current Chemistry, 376(3), p. 18. Available at: https://doi.org/10.1007/s41061-018-0191-6.

Contreras-Vargas, J., Ruvalcaba-Sil, J.L. and Rodriguez-Gómez, F.J. (2013) 'Effects of the cleaning of silver with acidified thiourea solutions', in Conference proceedings of Metal, pp. 223–228.

Cuvillier, L. et al. (2023) 'Testing of the siderophore deferoxamine amended in hydrogels for the cleaning of iron corrosion', The European Physical Journal Plus, 138(6), p. 569. Available at: https://doi.org/10.1140/epjp/s13360-023-04159-y.

Dhouibi, I. et al. (2021) 'A study of the anti-corrosive effects of essential oils of rosemary and myrtle for copper corrosion in chloride media', Arabian Journal of Chemistry, 14(2), p. 102961. Available at: https://doi.org/10.1016/j.arabjc.2020.102961.

Guilminot, E. (2023) 'The Use of Hydrogels in the Treatment of Metal Cultural Heritage Objects', Gels, 9(3), p. 191. Available at: https://doi.org/10.3390/gels9030191.

Jia, Y. et al. (2021) 'Deep eutectic solvent and agar: a new green gel to remove proteinaceous-based varnishes from paintings', Journal of Cultural Heritage, 51, pp. 138–144. Available at: https://doi.org/10.1016/j.culher.2021.08.001.

Molina, M.T. et al. (2023) 'Protective Coatings for Metals in Scientific—Technical Heritage: The Collection of the Spanish National Museum of Science and Technology (MUNCYT)', Heritage, 6(3), pp. 2473–2488. Available at: https://doi.org/10.3390/heritage6030130.

Orama, M. et al. (2002) 'Complexation of [S,S] and mixed stereoisomers of N,N'-ethylenediaminedisuccinic acid (EDDS) with Fe(III), Cu(II), Zn(II) and Mn(II) ions in aqueous solution', J. Chem. Soc., Dalton Trans., (24), pp. 4644–4648. Available at: https://doi.org/10.1039/B207777A.

Palomar, T. et al. (2016) 'A comparative study of cleaning methods for tarnished silver', Journal of Cultural Heritage, 17, pp. 20–26. Available at: https://doi.org/10.1016/j.culher.2015.07.012.

Pereira, C.S.M., Silva, V.M.T.M. and Rodrigues, A.E. (2011) 'Ethyl lactate as a solvent: Properties, applications and production processes – a review', Green Chemistry, 13(10), p. 2658. Available at: https://doi.org/10.1039/c1gc15523g.

Prat, D., Hayler, J. and Wells, A. (2014) 'A survey of solvent selection guides', Green Chem., 16(10), pp. 4546–4551. Available at: https://doi.org/10.1039/C4GC01149J.

Schalm, O. et al. (2018) 'How effective are reducing plasma afterglows at atmospheric pressure in removing sulphide layers: Application on tarnished silver, sterling silver and copper', Surface and Interface Analysis, 50(1), pp. 32–42. Available at: https://doi.org/10.1002/sia.6329.

Wei, H. et al. (2020) 'Green inhibitors for steel corrosion in acidic environment: state of art', Materials Today Sustainability, 10, p. 100044. Available at: https://doi.org/10.1016/j.mtsust.2020.100044.

Acknowledgements

"i thank the universe
for taking away
everything it has taken
and giving me
everything it is giving"

balance - Rupi Kaur, *milk and honey*

In a few lines, I would like to warmly thank all people who accompanied me along this four-year journey. Here just a few names to remind me, and everyone reading this manuscript, their relevance during this period.

The jury members: prof. Edith Joseph, prof. Giorgia Sciutto, prof. Stephan von Reuss, prof. Giuseppe Lazzara, and Dr. David Thickett.

Thesis directors and co-supervisors within the framework of the HELIX project (Investigating metal bioremediation for the preservation of historical metal artworks; funded by the Swiss National Science Foundation (SNSF), grant number 205121_188755, 2020-2024, P.I. Edith Joseph): prof. Edith Joseph, prof. Giorgia Sciutto, prof. Stephan von Reuss.

My colleagues at the Haute Ecole ARC in Neuchâtel: Régis Bertholon, Agnès Gelbert-Miermon, Isabelle Rerat, Laura Brambilla, Luana Cuvillier, Silvia Russo, Amalia Siatou, Elodie Granget, Ocson Reginald Cocen, Miriam Truffa Giachet, Alexandra Lefebvre, Patrycja Janina Petrasz, and Qing Wu.

My former colleagues at the University of Neuchâtel: Sarah James and Mathilde Monachon.

My colleagues at the University of Bologna (Ravenna), in particular Lucrezia Gatti and Emilio Catelli, without forgetting the kind doorkeepers.

Other key people: Luisa Hammond, Emilio Cano, Blanca Ramírez-Barat, Elodie Guilminot, Antonio Mucciolo, Samuel Untherofer, Guillaume Rapp, Claude-Alain Künzi, Federica Megaro, Laurence, Riccardo Tagliapietra, and the CROSTH students in Conservation-Restauration at the HE-Arc.

My lovely friends spread across the world: Alessio, Alex, Javi, Elena, Jan, Silvia, Amalia, and Agnese.

My caring housemates in Neuchâtel: Cathy, Shannon, Ayhsé, and Hip Hop.

My beloved Stefano and my family.

All people who I forgot to mention here but make me smile when I think of.

Supplementary materials

Cleaning formulations

A summary of all developed cleaning formulations is reported here to ease the reader for a future exploitation of the proposed systems.

PHB-EL gel

For the synthesis of the PHB-EL formulation poly-3-hydroxybutyrate (PHB, CAS Number: 29435-48-1, Biomer) and ethyl lactate (≥98%) (EL, CAS Number: 97-64-3, Sigma Aldrich) were employed in a mixture 7% w/v, as reported in the reference literature (Volpi, 2017; Prati *et al.*, 2019). The mixture was stirred in a covered glass petri dish at about 110 °C for a few minutes until the PHB powder got dissolved and the mixture gained in thickness. The resulting mixture was cooled down to room temperature before application (i.e., 23.8 ±2.4 °C, laboratory conditions in this study). The resulting rigid gel could be cut by a metallic spatula and applied directly on the target surface. The post-application clearing consisted of dry cotton swabbing.

Agar-water/EL gel

Firstly, an agar (AgarArt, CTS) hydrogel was prepared with deionised water at a concentration of 4% w/v. The mixture was stirred in a covered glass petri dish at about 90-100 °C until gelation occurred. Once removed the petri dish from the hot plate, and while the mixture was still above the sol-gel transition temperature of around 40 °C (Medina-Esquivel *et al.*, 2008), ethyl lactate (≥98%, CAS Number: 97-64-3, Sigma Aldrich) was added in a volume ratio of 1:3 in regard to the deionised water already present in the agar gel. The resulting mixture was manually stirred by a metallic spatula for a few seconds, and finally let cool down to room temperature before application (i.e., 23.8 ±2.4 °C, laboratory conditions in this study). The resulting rigid gel could be cut by a metallic spatula and applied directly on the target surface. The post-application clearing consisted of dry cotton swabbing.

PLA-EL formulation

Polylactide acid (PLA) Resomer® R 207 S from Merck (CAS Number: 26680-10-4) was mixed with ethyl lactate (≥98%) (EL, CAS Number: 97-64-3) from Sigma Aldrich in a concentration 30% w/v. Few seconds of manual stirring with a metallic spatula at room temperature (i.e., 23.8 ±2.4 °C, laboratory conditions in this study) were sufficient to homogenise the mixture. The resulting viscous liquid formulation could be spread on Japanese paper applied to the target substrate. The post-application clearing protocol consisted of alternate dry and wet (i.e., deionised water) cotton swabbing.

PHB-EL-DFO gel

A 20% w/v solution of deferoxamine B mesylate salt (Desferal®) (DFO, CAS Number: 138-14-7) from Novartis was dissolved in deionised water and then added to ethyl lactate (≥98%) (EL, CAS Number: 97-64-3) from Sigma Aldrich in a volume ratio of 1:6. The bio-polymer poly-3-hydroxybutyrate (PHB, CAS Number: 29435-48-1), purchased from Biomer, was subsequently added at 7% w/v concentration. The final concentration of the DFO solution was $4 \cdot 10^{-2}$ M. The mixture was stirred in a covered glass petri dish at about 110 °C until the gel was formed and let cool down to room temperature before application (i.e., 23.8

±2.4 °C, laboratory conditions in this study). The resulting rigid gel could be cut by a metallic spatula and applied directly on the target surface. The post-application clearing protocol consisted of wet cotton swabbing with an ethanol 70% v/v solution.

PHB-EL-EDDS gel

A PHB-EL gel was initially prepared employing poly-3-hydroxybutyrate (PHB, CAS Number: 29435-48-1, Biomer) and ethyl lactate (≥98%) (EL, CAS Number: 97-64-3, Sigma Aldrich) in a mixture 7% w/v. The mixture was magnetically stirred in a covered glass petri dish at about 110 °C for a few minutes until the PHB powder got dissolved and the mixture gained in thickness. In parallel, a solution of ethylenediamine-N,N'-disuccinic acid trisodium salt (Na_3EDDS 35% in water, Sigma Aldrich, PubChem Substance ID: 57653485) was diluted in deionised water to reach a final concentration of 20% v/v. Out of heating, the EDDS solution was added in the glass petri dish while the PHB-EL gel was not rigid yet, quickly stirred manually, and finally let cool down to room temperature before application (i.e., 23.8 ±2.4 °C, laboratory conditions in this study). The aqueous EDDS solution was added in a volume ratio of 1:5 compared to the ethyl lactate loaded in the PHB system and the final EDDS concentration was calculated as $4.8 \cdot 10^{-2}$ M. The resulting rigid gel could be cut by a metallic spatula and applied on Japanese paper for the cleaning of the target surface. After application, gels and Japanese paper were detached in one move by a metallic spatula. Eventually, the mock-up surface was cleared with ethanol 70% v/v by cotton-swabbing.

Analytical techniques

Rheology

The mechanical features of the formulations were investigated by amplitude sweep test with an Anton Paar rheometer MCR 102. The analysis configuration included a parallel-plate (25 mm) measuring system, temperature at 25 °C, pre-set force for the detection of the sample surface and to avoid sample slipping was set at 1N, angular frequency (ω) of 5 s^{-1}, 25 data points, and shear strain amplitude (γ) range of 0.001 – 100%. Only in the case of agar-water/EL gels and plain agar hydrogels (4% w/v), a profiled plate was necessary to overcome the sliding effect when subjecting the sample to the shear strain.

The analysis is a conventional method to collect information about the formulation nature (i.e., gel-structured or liquid) and its mechanical features (i.e., rigidity, malleability, tendency to crack) as already stated by the previous literature (Carretti *et al.*, 2008; Prati *et al.*, 2019; Yiming *et al.*, 2019).

Cryo-Scanning Electron Microscopy (Cryo-SEM)

Cryo-Scanning Electron Microscopy (Cryo-SEM) was performed with a Quanta FEG-250 SEM (Thermo Fisher Scientific Inc.) instrument coupled with a cryo-chamber Quorum PP3010 Cryo-Unit. The technique allowed to observe at high resolution the inner structure of the formulations. Still-moist rigid gels were placed on an aluminium stub, frozen by liquid nitrogen slush, and transferred into the cryo-vacuum chamber precooled to −140 °C. The samples were then fractured and sublimated at -60 °C to remove ice contamination. In the case of PLA-EL, due to the liquid consistence, a double layered system was employed as sample-holder in order to obtain the cut of the specimen by detachment of one of the two sides. Several intervals of 25 minutes each were tested to reach an ideal sublimation level without altering the features of the examined formulations by over-etching effect. The final sublimation time adopted for the formulations presented in this manuscript was 75 minutes. Finally, the samples were coated by sputtering with platinum (between 15 - 60 seconds coating at 10 mA current according to the proximity of samples to the sputtering

system) in an argon atmosphere at −140 °C. SEM secondary electrons (SE) and backscattered electrons (BSE) images of samples fractures were captured with a voltage between 6-10 kV and a working distance of approximately 10-13 mm.

Thermogravimetric analysis (TGA)

Thermogravimetric analysis (TGA) was performed to investigate the capacity of the designed systems to retain the solvents and active solutions by comparison of the evaporation rates obtained for neat liquids and gelled formulations. A Perkin–Elmer TGA 7 thermogravimeter was employed and the Pyris™ software (Perkin-Elmer) was used for data acquisition. About 20 mg of samples were used for both gel and liquid specimens and placed in open aluminium pans. The analysis consisted of an isothermal run at 40 °C for 60 minutes and performed under nitrogen flow. The temperature of 40 °C was reached by a programming heating rate of 40°C/min starting from the default system temperature of 25 °C. The experimental temperature of 40 °C was selected because the lowest condition within the operational limits of the TGA instrument employed and in accordance with the previous literature as the most representative of CRs working conditions (Parisi *et al.*, 2018; Prati *et al.*, 2019).

Optical microscope

A ZEISS Axioscop 2 MAT optical microscope equipped with an Axiocam 305 color camera was employed to observe and monitor the surface of mock-ups and test objects beforehand and along the cleaning protocol. EDF (Extended Depth of Focus) images were collected by manual focus drive using the ZEISS software ZEN core 3.2. The examination was done under reflected light in brightfield mode and under UV light with a fluorescence filter at 365 – 420 nm, employing 20× and 50× magnification objectives (ZEISS Epiplan). The parameters for exposure time and white balance were set automatically by the software.

Colorimetry

Two portable spectrophotometers were used to collect colorimetric data on the mock-ups beforehand and after each gel application in order to evaluate the potential chemical alterations caused by the gel in a preliminary phase, and to ascertain the impact of application time on cleaning efficiency. Collected data were correlated to colorimetric measurements acquired on non-corroded and non-coated bare metal coupons (i.e., mild steel, brass, sterling silver) as controls.

Specifically, a X-rite Ci62 device and a Konica-Minolta CM26d instrument were employed when the research was carried out at the Haute Ecole Arc (Neuchâtel, Switzerland) or during the research periods abroad at the University of Bologna (Italy), respectively. In order to ensure a right comparison among data, each device was employed consistently for each series of mock-ups analysed and presented in this dissertation. Specifically, data presented in Chapters 2, 4, and 5 were acquired with the X-rite Ci62 system, whereas measurements reported in Chapter 3 were collected by means of the Konica-Minolta CM26d instrument.

The colorimetric data were recorded using the CIELab colour space with standard illuminant D65, d/8° geometry, 10° standard observer, and instrument window size of 6.5 mm (X-rite Ci62) or 3 mm (Konica-Minolta CM26d) according to the instrument used. For each investigated mock-up area, three different spots were examined, and then both Specular Component Excluded (SCE) and Included (SCI) data were averaged and elaborated. Colour changes are reported and discussed as L*, a*, b* coordinates and ΔE* value, which was calculated, according to EN 15886:2010, as $\Delta E^* = \sqrt{(L_2^* - L_1^*)^2 + (a_2^* - a_1^*)^2 + (b_2^* - b_1^*)^2}$, where L_1^*, a_1^*, b_1^* are the CIELab values of the first measurement, and L_2^*, a_2^*, b_2^* those of the second one. Additionally, data were statistically analysed by analysis of variance (ANOVA) and Tuckey's HSD test to evaluate their relevance.

Eddy current measurement

Eddy current measurements were used to quantify the thickness of the coatings applied (i.e., Paraloid® B72 and Zaponlack) and/or corrosion layer formed on test mock-ups (i.e., mild steel, brass, sterling silver). Data were acquired with a PHYNIX Surfix® S instrument and FN combination probe. The instrument was calibrated before each use using the bare coupons as the zero standard. For coating calibration, a PHYNIX precision standard 8-μm sheet was placed on top of the bare coupon for an additional calibration of the instrument. Three measurements were taken for each cleaning triplicate, as well as, for the control. Data were statistically analysed by Tuckey's HSD test to evaluate their relevance.

X-Ray Fluorescence (XRF)

X-Ray Fluorescence (XRF) analysis was carried out by means of a Bruker ARTAX portable XRF spectrometer. The device is provided with a low-power metal-ceramic-type X-ray tube with Mo anode and a Peltier-cooled silicon drift detector (SDD). The X-ray beam was focused on the samples thanks to a CCD camera and a motor-driven XYZ stage. The analysis was set with potential at 30 kV, current intensity at 700 μA, life-time of 50 s, and spot of analysis lower than 1 mm^2.

Micro-Fourier-transform infrared spectroscopy (FTIR)

Micro-Fourier-transform infrared spectroscopy (FTIR) was performed with a Thermo Nicolet™ iN10 MX infrared imaging microscope, equipped with a mercury-cadmium-telluride (MCT) detector cooled by liquid nitrogen. Mock-ups and samples were analysed by single-point analysis in reflectance mode in the spectral range 4000-675 cm^{-1}, with an optical aperture of 400×400 μm, a spectral resolution of 4 cm^{-1} and 64 scans. Additional mapping analysis was run on metal coupons with the same parameters but lowering the number of scans to 16. Maps were acquired employing a set-up of 200×200 μm step-size and 10×10 steps. Data were collected with the dedicated software OMNIC Picta™ and elaborated with OMNIC™ (Thermo Fisher Scientific). Principal Component Analysis (PCA) was employed using nine single-point FTIR spectra recorded on bare metals (i.e., mild steel, brass, and sterling silver) as references and three spectra per replicate (for a total of nine spectra per each cleaning treatment) to evaluate the cleaning performance according to the application time and reiterations. When applying PCA, FTIR spectra were pre-treated by standard normal variate (SNV) transform and by column centring before applying PCA by the CAT (Chemometric Agile Tool) software, an open-source software based on the R platform.

Additionally, spectra of dry samples (i.e., gels, extraction residues, reference for polymers and coatings) were acquired using Thermo Fisher Scientific Nicolet™ iS 5 FTIR spectrometer with a diamond attenuated total reflectance (ATR) crystal plate (iD5 ATR accessory). Data were collected in the spectral range 4000-650 cm^{-1}, by 64 scans at a resolution of 4 cm^{-1}. OMNIC™ (Thermo Fisher Scientific) software was used for data acquisition and processing (i.e., suppression of the atmospheric contribution linked to H_2O and CO_2).

Micro-Raman spectroscopy

A Renishaw Virsa™ Raman Analyser was employed for single-point analysis with 3-4 cm^{-1} spectral resolution, using both a 532 nm frequency-doubled Nd:YAG and a 785 nm diode excitation lasers and a 50× Nikon objective. The analysis set-up was adapted according to the target nature and sensitivity to the beam radiation, as resumed by manuscript chapter and target in SM-Table 1. Data elaboration was performed on Thermo Grams/AI 8.0™ suite software (Thermo Fischer Scientific).

SM-Table 1 Parameters employed for the analysis by Raman spectroscopy.

Chapter	Target	Laser (nm)	Intensity (mW)	Exposure time (s)	Accumulations
3	Mock-ups	785	3	3	100
	Others	785	30	1	10
4	Mock-ups	532	2	4	60
	Others	785	10	5	300
5	Mock-ups	532	0.5	4	60
	Others	785	10	5	200
6	Brass object	785	1	2	100
	Iron scissors	785	3	1	30

Electrochemistry

Electrochemical measurements were performed in collaboration with the Centro Nacional de Investigaciones Metalúrgicas (CENIM) in Madrid (Spain). The electrolyte system was prepared by gelling a liquid electrolyte with agarose powder (Panreac). As liquid electrolyte a 10-ppm solution of acetic acid in deionised water was employed in order to reproduce a corrosive environment that might be present indoors. To prepare the electrolyte, agarose powder was added to the electrolyte in a concentration 2% w/v inside a beaker, then gently heated in a microwave oven at low power, regularly stirring the mixture with a spatula, until dissolution. The resulting mixture was poured into a mould of 3.14 cm^2 aperture that corresponded to the mock-ups are exposed to the analysis. The mixture was left to cool at room temperature before employment (i.e., 23.8 ±2.4 °C, laboratory conditions in this study). A stainless-steel wire (AISI 316 L) was used as pseudo-reference electrode and a spiral made of the same material as counter electrode (CE). Measurements were acquired by means of a Gamry 600 Potentiostat, using a frequency swept from 100 kHz to 10 mHz, 10 mV RMS amplitude (at the open circuit potential, OCP) and 10 points/ decade. Data analysis was made using the ZView software. The system was left to stabilise at OCP for 30 minutes before measuring polarisation resistance.

Climatic chamber

A Memmert™ Climate Chamber ICH110 was employed within this research study to artificially age test mock-ups. The machine provides working conditions for temperature in the range +10 °C - +60 °C (± 0.1 °C) and relative humidity (RH) between 10 and 80% (± 1%). Different protocols were employed, as described here below:

Chapter 2 Accelerated ageing of the organic coatings tested in this research (i.e., Paraloid® B72 and Zaponlack) was achieved following the protocol described by Degrigny (2008). The ageing conditions set in the climatic chamber consisted of a cyclic program of a wet phase (38 °C at 80% RH) for 16 hours followed by a dry phase (23 °C at 55% RH) of 8 hours, repeated daily for three months.

Chapters 3, 4, and 5 The long-term behaviour of mock-ups was verified thanks to a three-month accelerated ageing, following the protocol ISO 16701:2015 Cycle B. In order to bypass the instrumental limit for relative humidity (i.e., maximum 80%), the protocol was adapted while keeping the same dew point temperature T_d required by the standard. The value was calculated through the formula $T_d = T - [(100 - RH)/5]$, where T_d is the dew point temperature (in °C), T is the set temperature (in °C), and RH is the relative humidity. Consequently, the mock-ups ageing was set and performed by the following steps: (1) exposure at 38 °C and 80% RH (i.e., T_d = 34 °C) for 4 hours; (2) exposure at 35 °C while reducing relative humidity from 80% to 50% over 2 hours; (3) exposure at 35 °C and 50% RH for 4 hours; (4) exposure at 35 °C to linear increase of relative humidity from 50% to 80% over 2 hours. The ageing cycle was repeated

twice a day over a period of three months. All triplicates and mock-ups for each series of metal (i.e., steel, brass, and sterling silver) were placed on the same level of the climatic chamber, as required by the ISO standard.

Supplementary figures and tables

Chapter 2 - Bio-formulations for the removal of synthetic organic coatings from historical metals

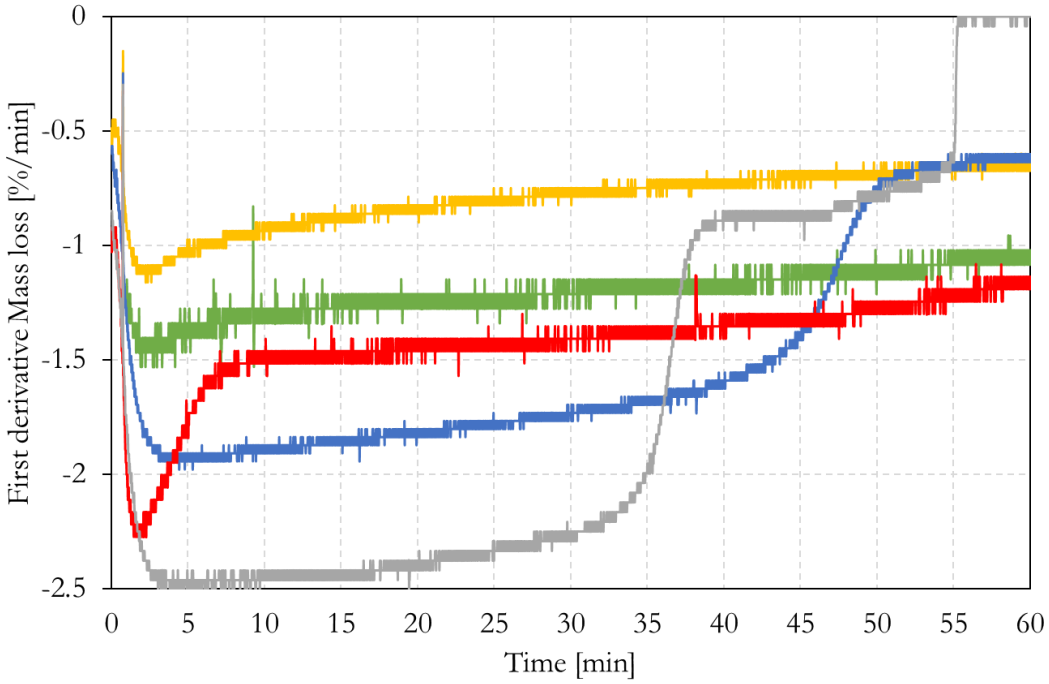

SM-Figure 1 First derivative of the isothermal curves, collected by TGA scan at 40 °C, in function of time. Relative mass loss of neat EL (red) and water/EL (3:1) solution (grey) and the liquid fraction of PHB-EL (green), PLA-EL (yellow), and agar-water/EL (blue) formulations.

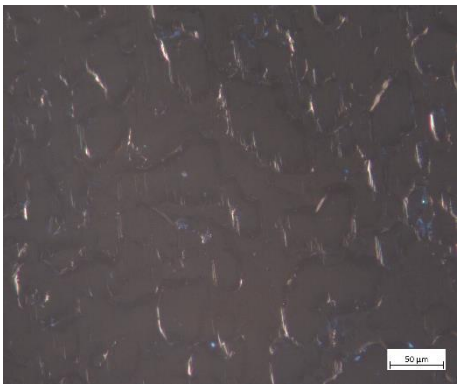

SM-Figure 2 Optical microscope image acquired under UV light of a bare mild steel sheet. Blue traces are visible despite the absence of any organic coatings on the substrate. The scale bar indicates 50 µm.

SM-Table 2 CIELab coordinates of mild steel mock-ups coated with Paraloid® B72 before and after cleaning. L*, a* and b* SCI values are reported along with their standard deviation into brackets.

	Cleaning time	Number of applications	L*	a*	b*
PHB-EL	-	0	71.90 (±0.24)	0.22 (±0.01)	1.37 (±0.10)
	5 min	1	73.66 (±0.48)	0.43 (±0.06)	2.20 (±0.21)
		2	77.49 (±0.72)	0.25 (±0.01)	2.08 (±0.20)
	10 min	1	72.72 (±0.90)	0.51 (±0.06)	2.61 (±0.16)
		2	78.64 (±0.72)	0.21 (±0.01)	2.02 (±0.08)
Agar-water/EL	-	0	70.56 (±0.48)	0.28 (±0.04)	0.98 (±0.09)
	5 min	1	78.74 (±0.67)	0.24 (±0.02)	1.81 (±0.09)
		2	67.45 (±1.98)	0.83 (±0.05)	6.61 (±0.32)
	10 min	1	78.28 (±0.87)	0.27 (±0.03)	1.97 (±0.10)
		2	70.26 (±1.05)	0.85 (±0.12)	6.05 (±0.73)
PLA-EL	-	0	69.42 (±0.15)	0.26 (±0.01)	0.89 (±0.02)
	5 min	1	73.13 (±2.07)	0.23 (±0.04)	1.18 (±0.36)
		2	78.41 (±0.66)	0.27 (±0.02)	1.95 (±0.18)
	10 min	1	75.63 (±0.87)	0.24 (±0.02)	1.40 (±0.08)
		2	76.64 (±0.75)	0.33 (±0.03)	2.35 (±0.16)

SM-Table 3 CIELab coordinates of brass mock-ups coated with Zaponlack before and after cleaning. L*, a* and b* SCI values are reported along with their standard deviation into brackets.

	Cleaning time	Number of applications	L*	a*	b*
PHB-EL	-	0	83.16 (±0.30)	0.65 (±0.06)	38.92 (±0.16)
	5 min	1	77.96 (±2.69)	1.91 (±0.26)	41.16 (±0.82)
		2	80.38 (±1.27)	2.25 (±0.26)	43.34 (±1.09)
	10 min	1	78.88 (±1.06)	2.82 (±0.19)	45.76 (±1.49)
		2	81.73 (±2.61)	1.97 (±0.17)	42.50 (±1.34)
Agar-water/EL	-	0	79.71 (±0.69)	1.02 (±0.04)	37.47 (±0.20)
	5 min	1	79.45 (±1.33)	1.06 (±0.11)	36.51 (±0.41)
		2	81.01 (±1.61)	1.58 (±0.68)	37.12 (±0.51)
	10 min	1	82.38 (±0.78)	0.79 (±0.09)	37.67 (±0.44)
		2	80.55 (±2.10)	1.86 (±0.47)	40.13 (±1.82)
PLA-EL	-	0	80.86 (±1.84)	0.79 (±0.12)	37.65 (±0.95)
	5 min	1	79.93 (±1.50)	1.70 (±0.27)	39.67 (±0.73)
		2	82.91 (±1.92)	1.75 (±0.34)	40.13 (±1.05)
	10 min	1	80.86 (±2.51)	2.23 (±0.41)	42.68 (±1.24)
		2	81.31 (±1.70)	1.92 (±0.37)	39.45 (±1.09)

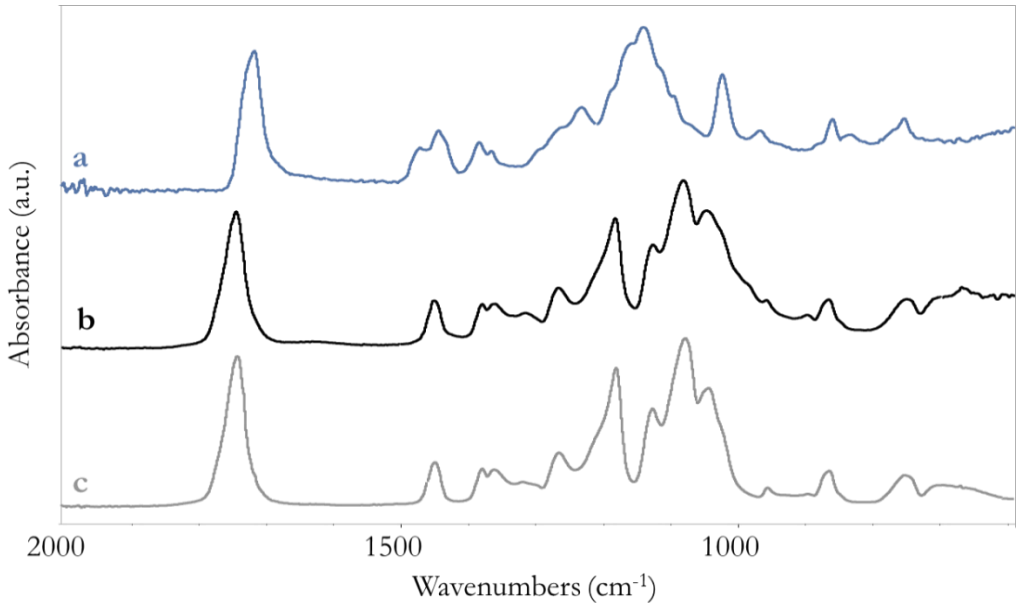

SM-Figure 3 ATR-FTIR spectra of Paraloid® B72 (a), PLA-EL system after one application of 10 minutes on a mild steel mock-up coated with Paraloid® B72 (b), and dry non-used PLA-EL system (c).

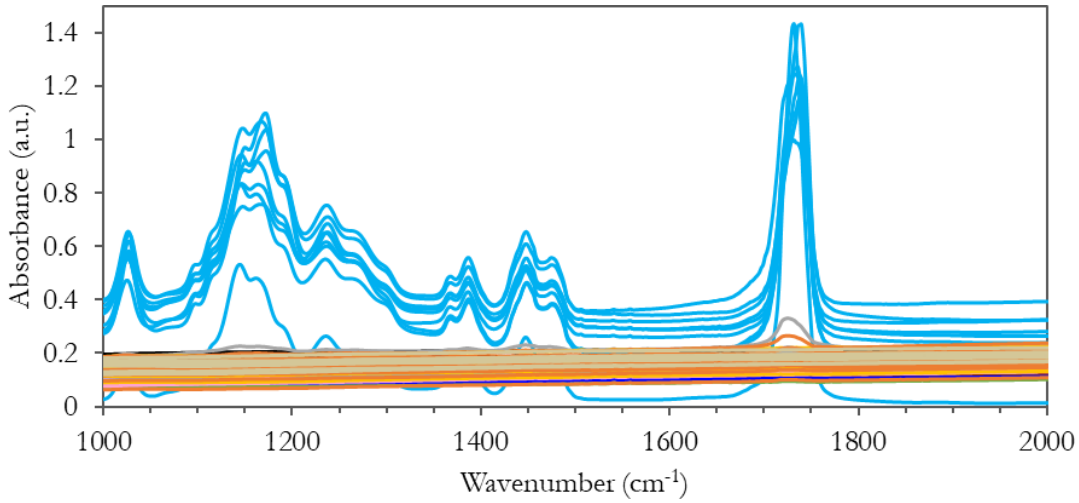

SM-Figure 4 Raw FTIR spectra collected for bare mild steel mock-ups and mild steel mock-ups, coated with Paraloid® B72, before and after cleaning with agar-water/EL, PHB-EL, and PLA-EL systems by one or two applications of 5 or 10 minutes each, as reported in the key above the score plot in Figure 2.34.

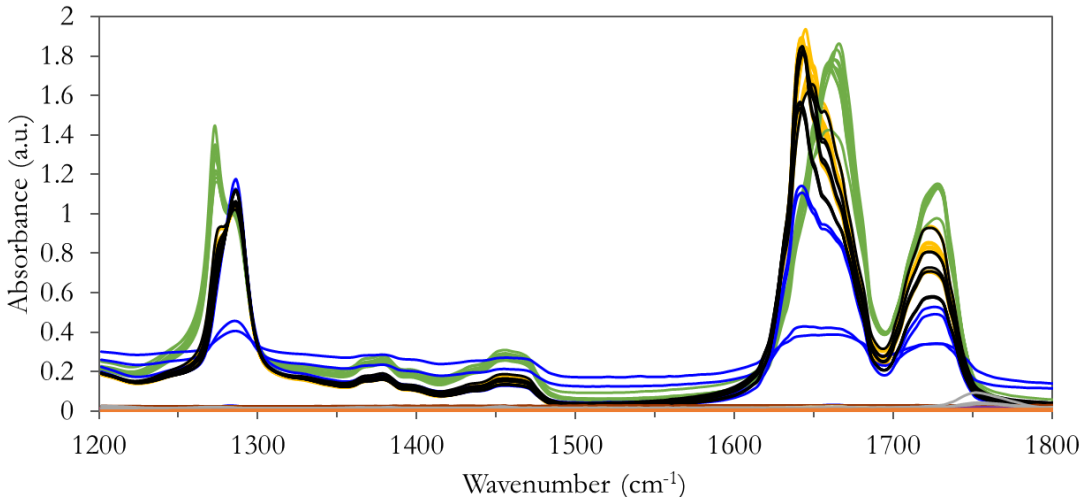

SM-Figure 5 Raw FTIR spectra collected for bare brass mock-ups and brass mock-ups, coated with Zaponlack, before and after cleaning with agar-water/EL, PHB-EL, and PLA-EL systems by one or two applications of 5 or 10 minutes each, as reported in the key above the score plot in Figure 2.35.

Chapter 3 - Multi-target cleaning gel: an innovative green approach in historical iron care

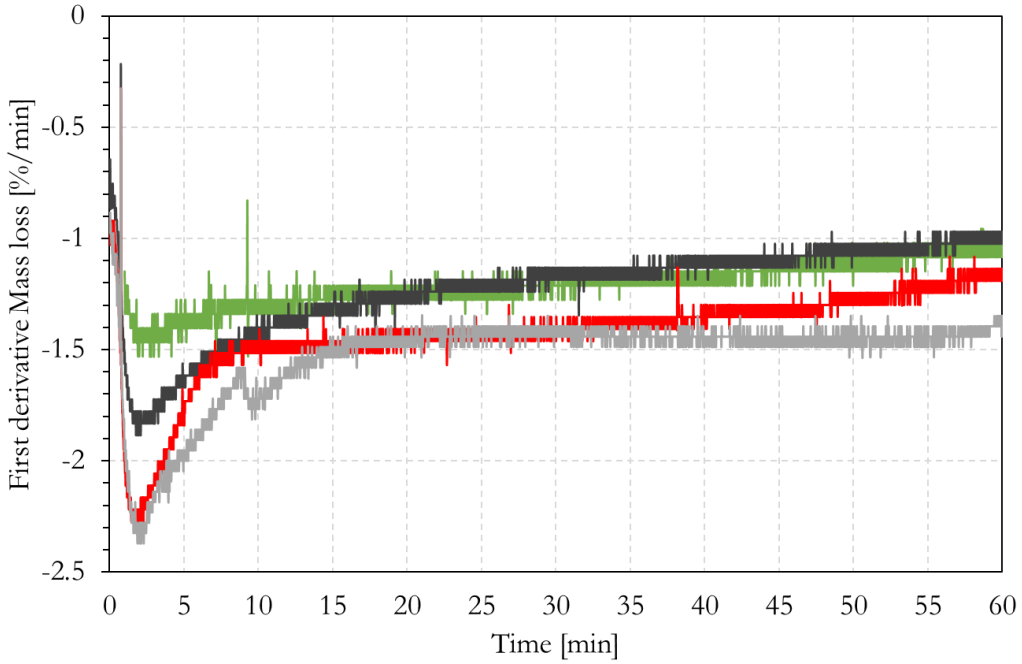

SM-Figure 6 First derivative of the isothermal curves, collected by TGA scan at 40 °C, in function of time. Relative mass loss of neat EL (red) and EL-DFO-water solution (grey) solutions and the liquid fraction of PHB-EL (green) and PHB-EL-DFO (black) formulations.

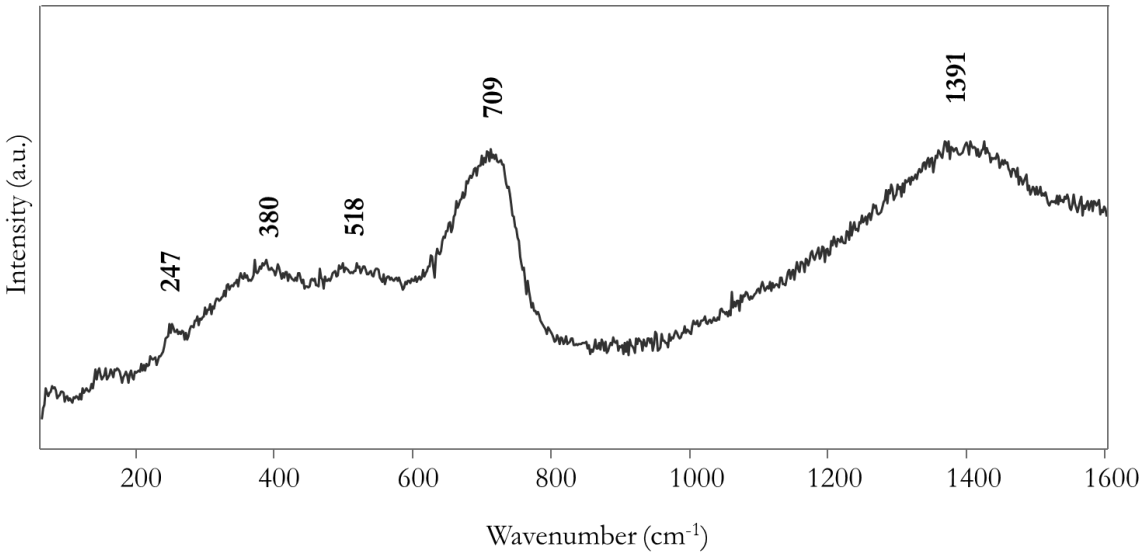

SM-Figure 7 Representative Raman spectrum collected by 532-nm laser on the surface of chemically corroded mild steel mock-ups prior to coating.

SM-Figure 8 FTIR spectra collected in reflectance mode from the surface of mild steel mock-ups, chemically corroded and coated with Paraloid® B72, after 10-minute PHB-EL-DFO gel application, with (a) and without (b) the use of clearance solution (i.e., ethanol 70% v/v) by cotton-swabbing. Diagnostic FTIR bands for lepidocrocite (1023 cm^{-1}) and DFO-related species (1045 cm^{-1}) are highlighted and reported in the figure.

(a) (b) (c)

SM-Figure 9 Mild steel mock-up (50 × 50 × 1 mm^3), chemically corroded and coated with Paraloid® B72, treated by PHB-EL-DFO gel. Initial appearance (a) and cleaning outcomes after one (b) and two gel applications of 10 (coupon top-left corner), 20 (coupon top-right corner), and 30 (coupon bottom-left corner) minutes, respectively. Bottom-right coupon sector left untreated as a control.

SM-Table 4 CIELab coordinates of the corroded and coated (i.e., Paraloid® B72) mild steel mock-up sectors before and after each cleaning step by PHB-EL-DFO. L*, a* and b* SCE values are reported along with their standard deviation into brackets.

Cleaning time	Number of gels	L*	a*	b*
10 minutes	0	37.20 (±2.11)	5.41 (±2.20)	15.27 (±2.39)
	1	43.14 (±3.59)	4.97 (±2.12)	14.92 (±2.26)
	2	49.68 (±3.52)	3.20 (±1.68)	10.79 (±2.33)
20 minutes	0	38.38 (±1.39)	2.76 (±0.35)	12.32 (±1.19)
	1	49.04 (±3.27)	1.65 (±0.36)	9.29 (±1.25)
	2	53.86 (±4.20)	1.09 (±0.24)	7.13 (±1.05)
30 minutes	0	37.46 (±1.08)	4.01 (±1.02)	14.18 (±2.26)
	1	47.89 (±3.45)	2.46 (±0.76)	10.35 (±1.89)
	2	54.56 (±3.14)	1.31 (±0.41)	7.14 (±1.42)

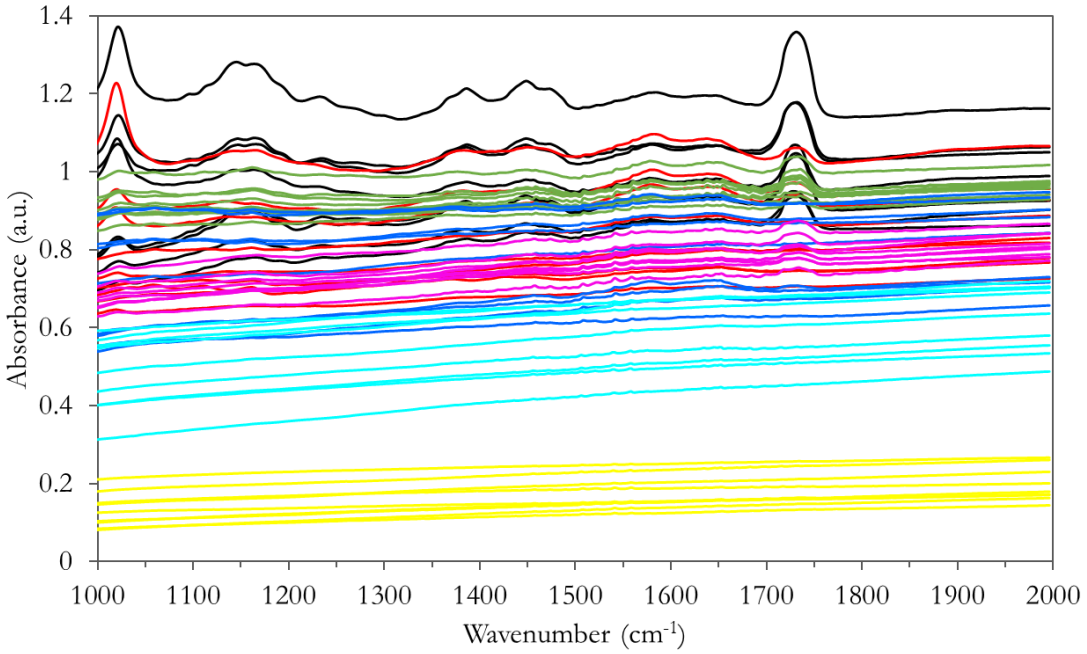

SM-Figure 10 Raw FTIR spectra collected for chemically aged mild steel mock-ups, coated with Paraloid® B72, cleaned by one 10-minute (black), two 10-minute (red), one 20-minute (green), two 20-minute (blue), one 30-minute (purple), and two 30-minute (turquoise) gel applications, and untreated bare mild steel coupons (yellow).

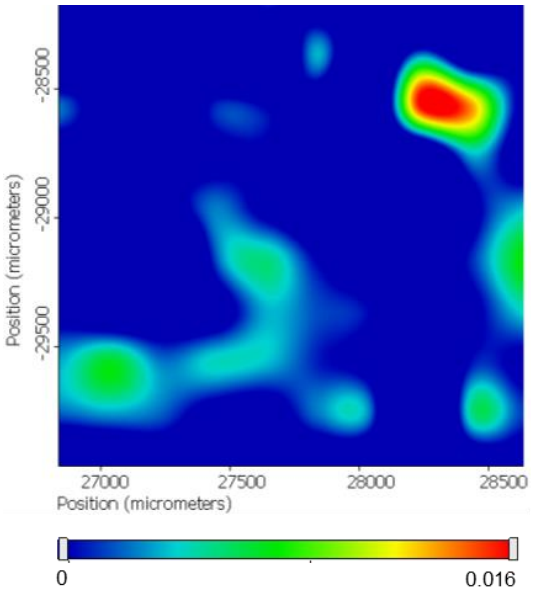

(a)

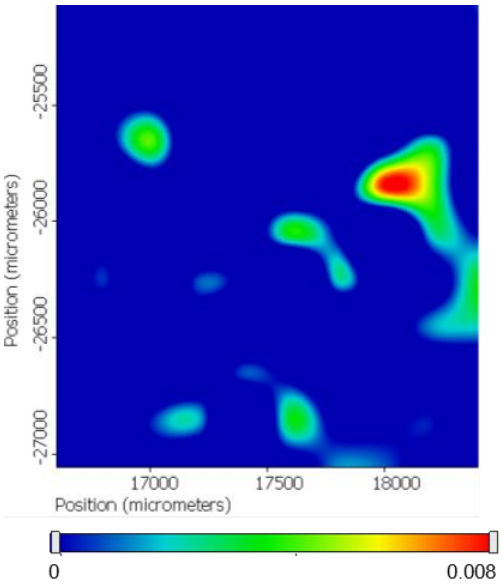

(b)

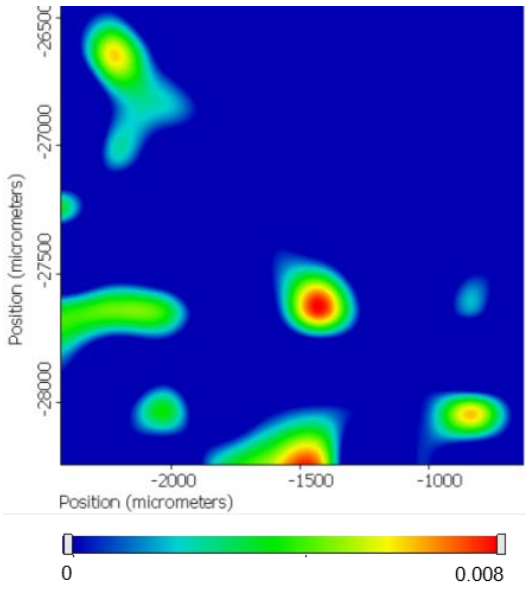

(c)

SM-Figure 11 FTIR chemigram maps collected in reflectance mode on the surface of mock-ups after 10- (a), 20- (b), and 30-minute (c) cleaning protocols. Resulting maps when considering the FTIR signal at 1045 cm^{-1} related to both DFO and iron-DFO complexes. Absorbance scale bar reports values from min (blue) to max (red).

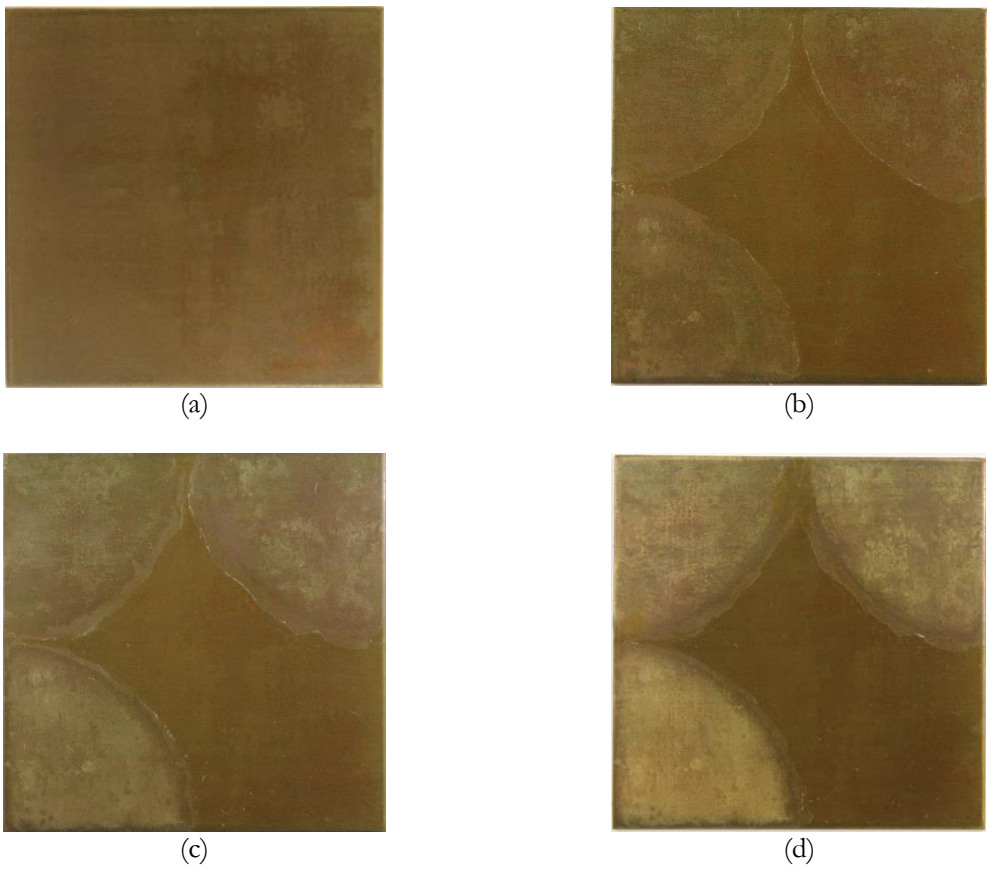

SM-Figure 12 Brass mock-up (50 × 50 × 1 mm^3), chemically tarnished and coated with Zaponlack, treated by PHB-EL-EDDS gel. Initial appearance (a) and cleaning outcomes after one (b), two (c), and three gel applications (d) of 10 (coupon top-left corner), 20 (coupon top-right corner), and 30 (coupon bottom-left corner) minutes, respectively. Bottom-right coupon sector left untreated as a control.

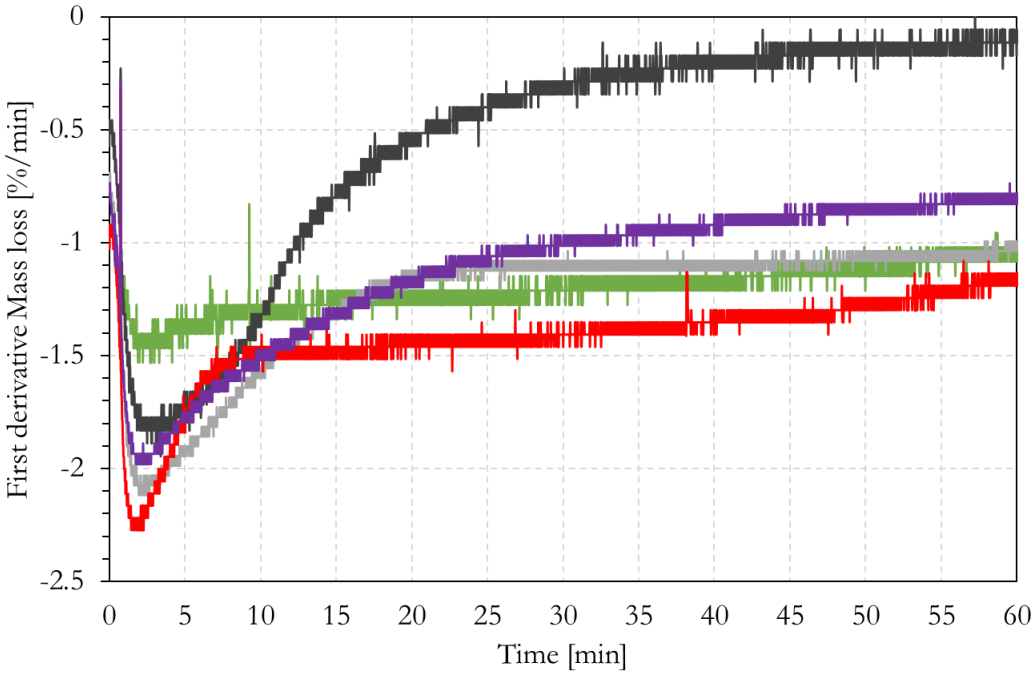

SM-Figure 13 First derivative of the isothermal curves, collected by TGA scan at 40 °C, in function of time. Relative mass loss of neat EL (red), EL-EDDS-water (grey), and EDDS (35%, black) solutions and the liquid fraction of PHB-EL (green) and PHB-EL-EDDS (purple) formulations.

SM-Figure 14 Optical microscope images under UV light of chemically tarnished brass coated with Zaponlack after three PHB-EL-EDDS gel applications of 10 (a), 20 (b), and 30 (c) minutes, respectively. The scale bar indicates 50 μm.

SM-Table 5 CIELab coordinates of the tarnished and coated (i.e., Zaponlack) brass mock-up sectors before and after each cleaning step by PHB-EL-EDDS gel. L*, a* and b* SCE and SCI values are reported along with their standard deviation into brackets.

	Cleaning time	Number of gels	L*	a*	b*
SCE	10 minutes	0	37.46 (±0.41)	3.99 (±0.16)	20.30 (±0.86)
		1	41.63 (±0.58)	2.74 (±0.60)	13.74 (±1.03)
		2	43.60 (±1.24)	2.14 (±0.77)	13.37 (±1.11)
		3	46.17 (±0.30)	1.62 (±0.27)	15.37 (±0.29)
	20 minutes	0	36.73 (±0.41)	3.95 (±0.15)	21.16 (±0.58)
		1	40.14 (±0.61)	3.15 (±0.31)	13.36 (±0.11)
		2	43.67 (±2.43)	2.24 (±0.72)	14.20 (±1.43)
		3	47.48 (±0.61)	1.73 (±0.09)	16.66 (±0.25)
	30 minutes	0	37.29 (±0.37)	3.81 (±0.44)	20.87 (±0.52)
		1	44.27 (±1.38)	2.18 (±0.40)	13.74 (±0.06)
		2	47.56 (±0.30)	1.62 (±0.27)	15.37 (±0.29)
		3	51.91 (±1.11)	1.63 (±0.32)	19.37 (±0.56)
SCI	10 minutes	0	45.64 (±0.46)	3.31 (±0.19)	13.70 (±0.97)
		1	53.32 (±2.06)	3.12 (±0.49)	8.61 (±1.64)
		2	58.02 (±4.01)	2.67 (±0.09)	9.26 (±2.70)
		3	59.49 (±2.58)	2.42 (±0.03)	11.93 (±1.52)
	20 minutes	0	45.49 (±0.54)	2.63 (±0.24)	13.74 (±0.48)
		1	51.24 (±2.70)	2.09 (±0.10)	6.88 (±1.72)
		2	57.47 (±3.04)	2.16 (±0.52)	8.65 (±3.11)
		3	58.92 (±1.09)	2.47 (±0.12)	13.24 (±1.25)
	30 minutes	0	45.72 (±0.58)	3.14 (±0.29)	13.46 (±0.07)
		1	56.36 (±1.95)	2.75 (±0.21)	8.77 (±0.70)
		2	61.04 (±1.73)	2.54 (±0.15)	13.54 (±1.29)
		3	65.65 (±0.83)	2.46 (±0.13)	18.53 (±0.97)

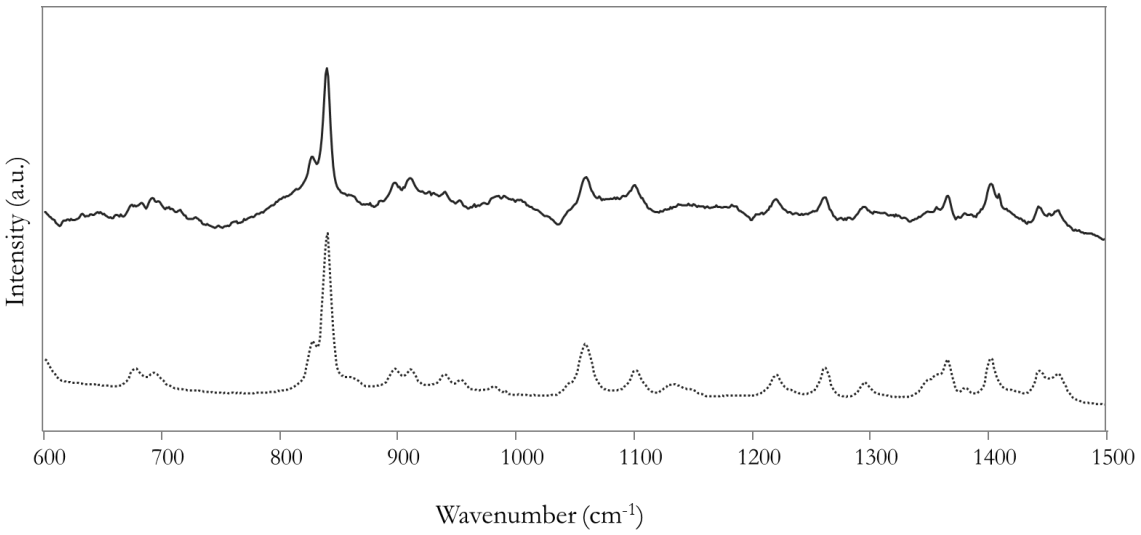

SM-Figure 15 Raman spectra of dry PHB-EL-EDDS gel after application on tarnished brass coated with Zaponlack (solid line) and PHB powder (dashed line).

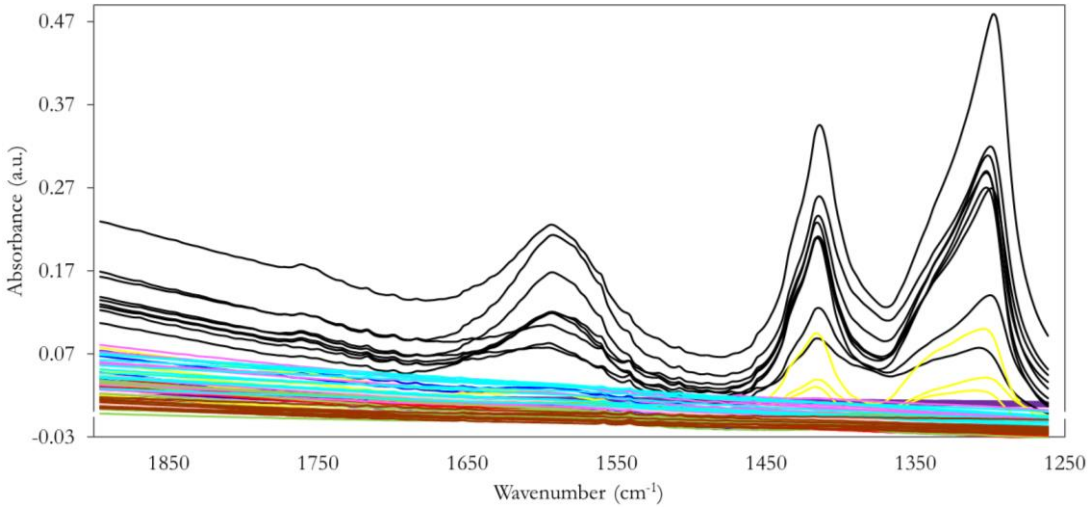

SM-Figure 16 Raw FTIR spectra collected for chemically tarnished brass mock-ups, coated with Zaponlack, after cleaning by one 10-minute (black), two 10-minute (red), three 10-minute (green), one 20-minute (yellow), two 20-minute (magenta), three 20-minute (turquoise), one 30-minute (blue), two 30-minute (pink), and three 30-minute (brown) PHB-EL-EDDS gel applications, and untreated bare brass coupons (purple).

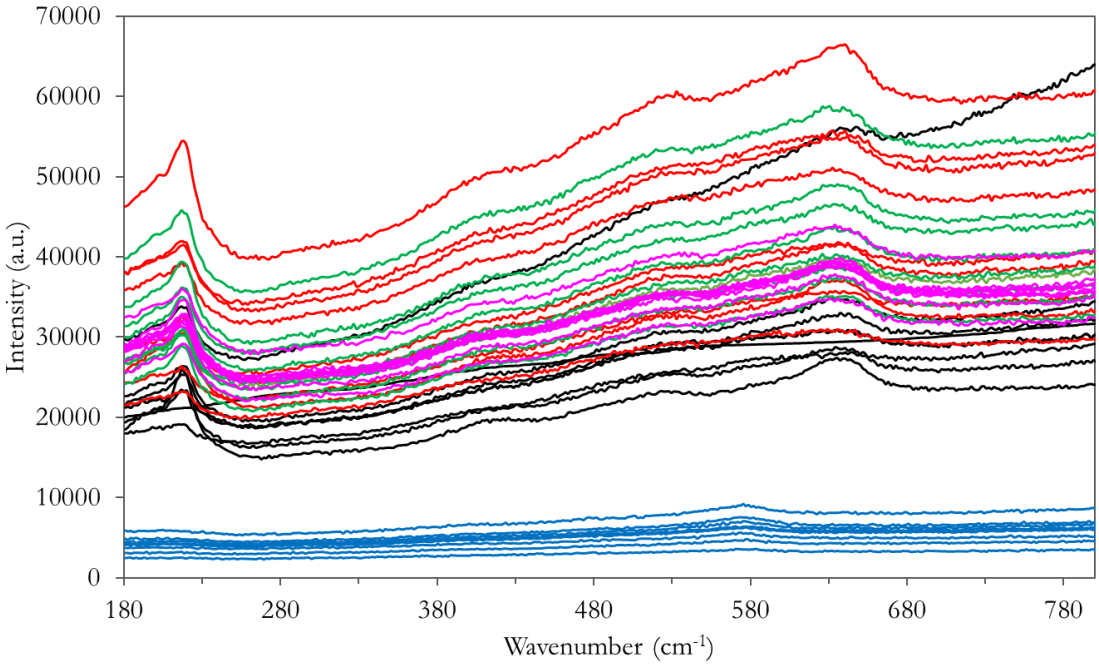

SM-Figure 17 Raw Raman spectra collected for chemically tarnished brass mock-ups, coated with Zaponlack, before (purple) and after cleaning by three PHB-EL-EDDS gel applications of 10 (black), 20 (red), and 30 (green) minutes, and untreated bare brass coupons (blue) as control.

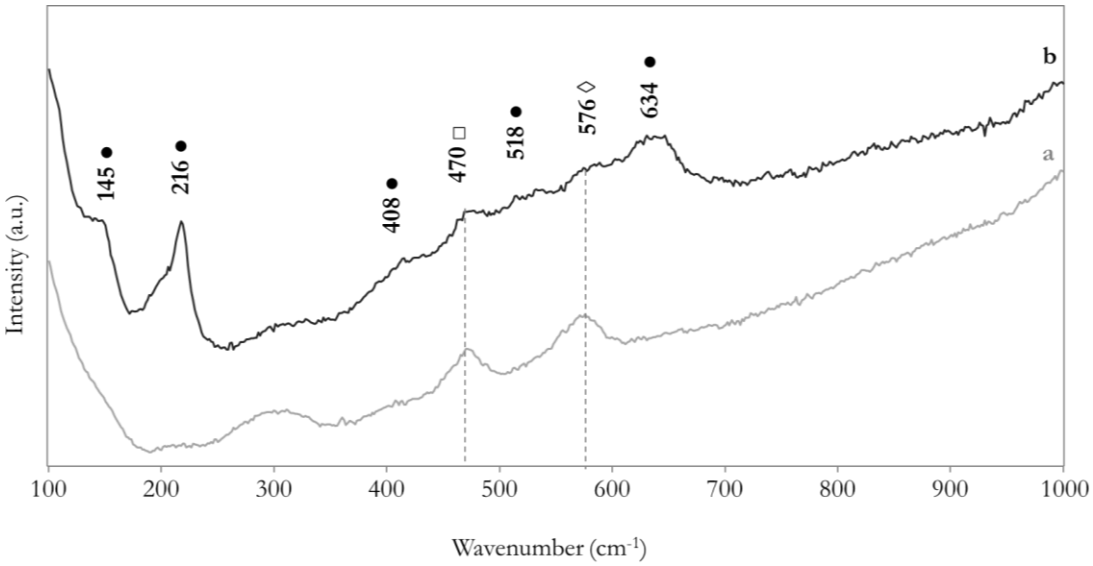

SM-Figure 18 Representative Raman spectra of brass aged for three months in a climatic chamber. Bare brass (a) and chemically tarnished brass coupons coated with Zaponlack and cleaned with three applications of 30 minutes by PHB-EL-EDDS gel (b). Signals attributed to cuprite (●), tenorite (*), zincite (◊), and covellite (□) are reported in the figure.

SM-Table 6 CIELab coordinates of different sterling silver mock-ups. L*, a*, and b* SCI values are reported along with their standard deviation into brackets.

Sterling silver mock-up		L*	a*	b*
Bare	Initial condition	96.03 (±0.95)	0.72 (±0.11)	7.01 (±0.34)
	Aged	86.75 (±1.37)	2.74 (±0.49)	14.10 (±1.92)
Tarnished	Initial condition	57.54 (±1.82)	1.91 (±3.14)	4.46 (±4.92)
	After cleaning	73.68 (±8.50)	1.88 (±3.46)	5.72 (±5.03)
	Cleaned and aged	69.69 (±7.96)	3.95 (±1.09)	11.60 (±2.87)

SM-Table 7 Variation of CIELab coordinates in SCI mode of tarnished sterling silver coupons after cleaning using different methods and procedures. Standard deviation value is reported into brackets. (Data published by Basilissi *et al.*, 2022)

Cleaning	Procedure	ΔL*	ΔE*
Chemical	Sodium hydrogen carbonate in agar (5% w/w)	-31.78 (±0.15)	32.6
Chemical	Immersion in a Rochelle salts solution (15% w/w)	-36.88 (±0.12)	37.3
Chemical	EDTA with agar (5% w/w)	-32.30 (±0.07)	32.6
Mechanical	Sodium hydrogen carbonate in water applied by swab	-30.68 (±0.23)	31.1
Laser	Energy 250 mJ, 2 J/cm², 2 mm spot	-17.17 (±0.36)	21.2

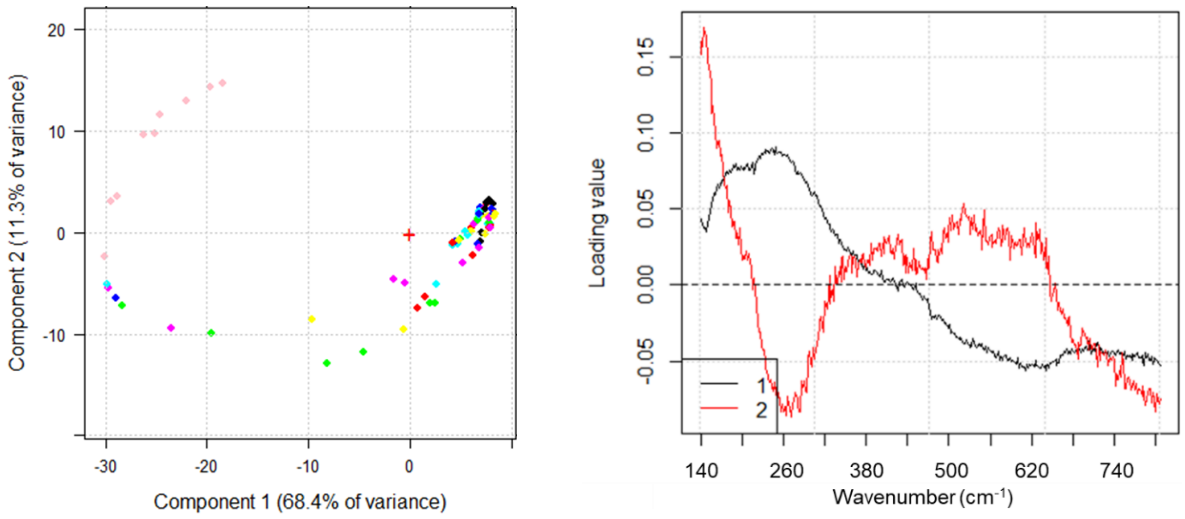

SM-Figure 19 Score (left) and loading (right) plots obtained from PCA applied to Raman spectra recorded on chemically tarnished sterling silver coupons, before (black) and after immersion in ethyl lactate for 10 (red), 20 (blue), and 30 (turquoise) minutes, for 1 (green), 2 (purple), and 4 (yellow) hours, and untreated bare sterling silver coupons (pink). (b) Related PC1 (black) and PC2 (red) loading plot.

SM-Table 8 Variation of CIELab coordinates of different sterling silver mock-ups compared to bare unaltered sterling silver, used as control. ΔL*, Δa*, Δb* and related ΔE* SCE values are reported along with their standard deviation into brackets.

Sterling silver mock-up		ΔL*	Δa*	Δb*	ΔE*
Bare	Aged	1.65 (±0.82)	0.68 (±0.14)	5.50 (±1.06)	5.79 (±1.04)
Tarnished	Initial condition	-3.64 (±1.83)	4.93 (±0.44)	15.07 (±3.61)	16.26 (±3.38)
	After cleaning	1.22 (±1.62)	1.07 (±0.93)	3.83 (2.91)	4.16 (±2.73)
	Cleaned and aged	3.42 (±1.34)	1.71 (±0.65)	9.39 (±3.41)	10.14 (±3.19)

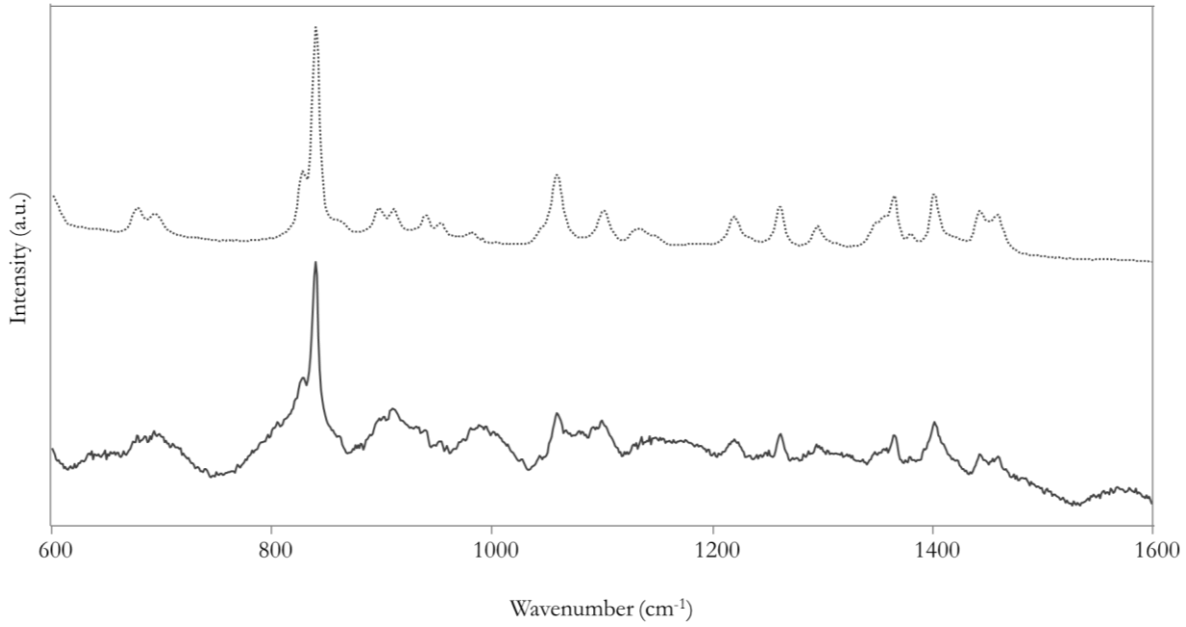

SM-Figure 20 Raman spectra of PHB powder (dashed line) and dry PHB-EL-EDDS gel after being applied for 30 minutes on chemically tarnished sterling silver mock-up (solid line).

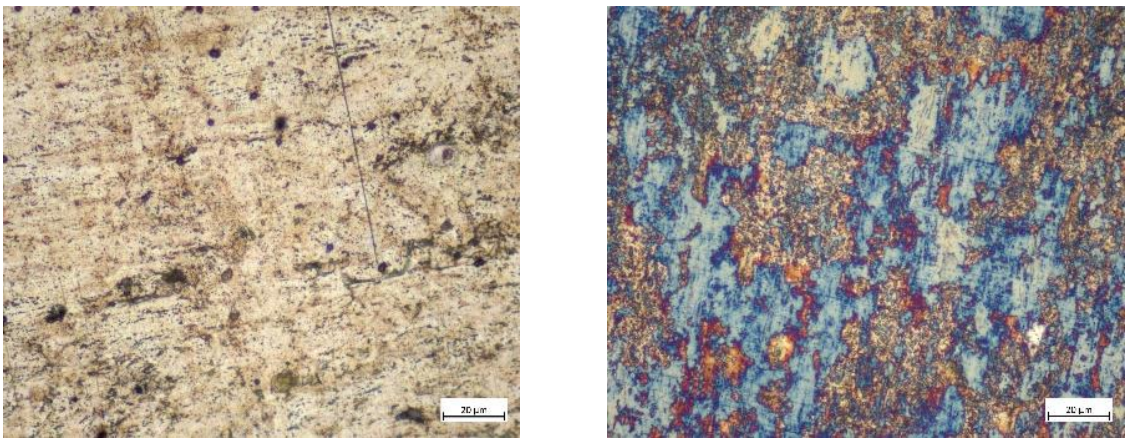

SM-Figure 21 Optical microscope images in bright field of bare sterling silver after 3-month ageing in climatic chamber (left) and chemically tarnished sterling silver (right) mock-ups. The scale bar indicates 20 μm.

Short curriculum vitae and Contributions

Arianna Passaretti obtained her Master's degree in Conservation Science from the University of Milano (Italy) in 2019. She joined research projects mainly related to the employment of non-invasive spectroscopic analyses for cultural heritage both at the Chemistry department in the University of Milano (Italy) and at the Raman Spectroscopy Research Group in the University of Ghent (Belgium). She is currently working on her PhD in Chemistry at the University of Neuchâtel (Switzerland), focusing on the design and the assessment of bio-derived organogels for the cleaning of altered historical metal artworks.

Dissemination within the framework of the doctorate project

Joseph, E., Albelda-Berenguer, M., Cornet, E., Cuvillier, L., James, S., Mathys, L., Monachon M., **Passaretti** A., & Russo, S. (2020). Innovative Approaches towards a Green and Sustainable Metal Conservation. *CHIMIA International Journal for Chemistry, 74*(7-8), 611-611.

Passaretti, A., Cuvillier, L., Sciutto, G., Guilminot, E., & Joseph, E. (2021). Biologically derived gels for the cleaning of historical and artistic metal heritage. *Applied Sciences, 11*(8), 3405.

Cuvillier, L., **Passaretti**, A., Guilminot, E., Sciutto, G., & Joseph, E. (2022). Bio-cleaning of historical iron artworks: innovative green gels amended with microbial derivatives. *Un patrimoine pour l'avenir, une science pour le patrimoine. Heritage for the Future. Science for Heritage*.

Passaretti, A., Cuvillier, L., Guilminot, E., Sciutto, G., & Joseph E., Sustainable cleaning of metal artworks using innovative biologically derived water- and solvent-gels. Oral presentation at 4th Green conservation of Cultural Heritage conference. Rome, Italy, February 3 4 2022.

Passaretti, A., Cuvillier, L., & Joseph E., Bio-cleaning of historical metal heritage. Poster presentation at *Première journée doctorale multidisciplinaire de la HES-SO et des HEP romandes*. Lausanne, Switzerland, May 20, 2022.

Passaretti, A., Cuvillier, L., Sciutto, G., von Reuss, S., & Joseph E., Innovative green gels for the biocleaning of historical metal heritage. Oral presentation at *CHEMCH 6th International Congress Chemistry for Cultural Heritage*. Ravenna, Italy, July 4-8, 2022.

Cuvillier, L., **Passaretti**, A., Raimon, A., Dupuy, V., Guilminot, E., & Joseph, E. (2022). Exploiting Biologically Synthetized Chelators in Conservation: Gel-based Bio-cleaning of Corroded Iron Heritage Objects. In *Metal 2022, proceedings of the interim meeting of the ICOM-CC metals working group*. ICOM-CC; The National Museum of Finland.

Passaretti, A., Cuvillier, L., Guilminot, E., Sciutto, G., & Joseph, E. Biopulitura di artefatti metallici in collezioni storiche. Workshop: Bioscienze nei beni culturali. Rome, Italy. April 5, 2023.

Cuvillier, L.; **Passaretti**, A.; Wu, Q.; Petrasz, P.; Brambilla, L.; Joseph, E. Green and bio-based remediation processes of metal corrosion. Swiss Corrosion Science Day 2023. Zurich, Switzerland. April 24, 2023.

Cuvillier, L., **Passaretti**, A., Guilminot, E., & Joseph, E. (2023). Testing of the siderophore deferoxamine amended in hydrogels for the cleaning of iron corrosion. *The European Physical Journal Plus, 138*(6), 569.

Passaretti, A., Cuvillier, L., Guilminot, E., Sciutto, G., & Joseph, E. (2023). Biocleaning of historical metal artworks: innovative green gels amended with microbial derivatives. *Frontiers in Materials, 10*, 1277972.

Passaretti, A., Cuvillier, L., Sciutto, G., & Joseph E., Innovative perspective for the cleaning of historical iron heritage: novel bio-organogel for the combined removal of undesired organic coatings and corrosion. *Heritage Science* [accepted for publication, pending minor revisions].

Cuvillier, L., **Passaretti**, A., Guilminot, E., & Joseph, E. (2023). Agar and chitosan hydrogels' design for metal uptaking treatments. *Gels, 10*(1), 55.

Cuvillier, L., Ganesan, S., James, S., Monachon, M., **Passaretti**, A., Albelda Berenguer, M., Mathys, L., & Joseph, E. (2023). Green corrosion mitigation and conservation strategies for metal heritage in *EFC series (Greenbook), Bridging the gap: corrosion science for heritage context*, Editor, D. Neff, Eds. Academic Press, ISBN 9780443186905 [under publication].

Passaretti, A., Cuvillier, L., Sciutto, G., Cano, E., Ramírez Barat, B., von Reuss, S., & Joseph E., Assessment of greener solutions for the cleaning of historical metal heritage. Oral presentation at *InART2024 - 6th International Conference on Innovation in Art Research and Technology*. Oslo, Norway, June 4-7, 2024. [accepted]

Supplementary collaborative works during the doctoral period

Galli, A., Gargano, M., Bonizzoni, L., Bruni, S., Interlenghi, M., Longoni, M., **Passaretti** A., Caccia M., Salvatore C., Castiglioni I., & Martini, M. (2021). Imaging and spectroscopic data combined to disclose the painting techniques and materials in the fifteenth century Leonardo atelier in Milan. *Dyes and Pigments, 187*, 109112.

Passaretti, A., Cuvillier, L., Künzi, C.-A., Brambilla, L., & Joseph, E. (2023). Multi-analytical characterisation of Art Déco dinanderie: single-point and map analysis of Jean Dunand's metal artworks. Oral presentation at *RAA2023-11th International Conference on the Application of Raman Spectroscopy in Art and Archaeology*. Athens, Greece, September 6-9, 2023.

Russo, S., **Passaretti**, A., Brambilla, L., Thomas, J. B., & Joseph, E., Metal soap detection on oil-coated copper and zinc model samples through vibrational spectroscopy. Poster presentation at *RAA2023-11th International Conference on the Application of Raman Spectroscopy in Art and Archaeology*. Athens, Greece, September 6-9, 2023.

Wu, Q., Zhou, H., Gubanov, K., **Passaretti**, A., Gonzalez Frutos, J., Degrigny, C., Bertrand, L., Stols-Witlox, M., Brambilla, L., Joseph E.; Development of silver test system with bio-based green aging methods and assessment with multi-analytical techniques. Poster presentation at *InART2024 - 6th International Conference on Innovation in Art Research and Technology*. Oslo, Norway, June 4-7, 2024. [accepted].

Passaretti, A., Cuvillier, L., Künzi, C.-A., Brambilla, L., & Joseph, E.; Multi-analytical characterisation of Art Déco dinanderie: single-point and map analysis of Jean Dunand's metal artworks. *Journal of Raman Spectroscopy* [accepted for publication, pending minor revisions].

Passaretti, A., Cuvillier, L., & Joseph E., Bio-cleaning of historical metal heritage. Poster presentation at *Première journée doctorale multidisciplinaire de la HES-SO et des HEP romandes*. Lausanne, Switzerland, May 20, 2022.

Bio-cleaning of historical metal heritage

Passaretti Arianna*, Cuvillier Luana*, Joseph Edith
Haute Ecole Arc Conservation-Restauration, HES-SO
Laboratoire des Technologies pour les Matériaux du Patrimoine, University of Neuchâtel

Context

In metal heritage preservation the core problem is the spontaneous process of corrosion, which alters original features or damages the integrity of artworks. As a result, it is common to remove corrosion when detrimental.
As alternative, the application of organic coatings is a favored method to prevent corrosion. However, these products are also sensitive to ageing factors through time. Therefore, there might arise the necessity of removing - and replacing - them once their protection purpose is compromised.

In the last decades, growing research attention towards safe and sustainable conservation practices has been carried out, in response to traditional cleaning methods potentially harmful for human health and the environment or artworks.

Previous studies have demonstrated the efficiency of particular microorganisms and their metabolites when exploited in conservation approaches. In addition, the employment of gels provides a controlled and adjustable cleaning action as well as a significant reduction of active agents quantity, appearing thus as an attractive delivery system for sustainable conservation treatments.

Methodology

Colour, morphology and chemical composition of gels and metal mock-ups are investigated before and after cleaning with complementary analytical techniques: colorimetry, optical microscopy, X-Ray Fluorescence, Raman and Fourier-transform Infrared spectroscopies, Scanning Electron Microscopy.

Furthermore, gels are also characterized by means of Atomic Absorption spectroscopy and rheology in order to define uptake rate and mechanical properties respectively.

Attention is given to the definition of an ad-hoc protocol, taking in account gel load concentration, duration and application repetition of the treatment.

Conclusion

HELIX green formulations show comparable outcomes with conventional cleaning methods on both corrosion and organic coatings.

Remarkably, it is possible to easily control the cleaning action adjusting the time and number of applications.

For an extensive use of bio-based gels in metal conservation, several points appear crucial:

- Close cooperation between scientists and stakeholders, to formulate reliable alternatives;
- Non-prohibitive cost of the proposed bio-gels;
- Easy set-up in workplaces or purchase by conservators.

Acknowledgments and contact

The HELIX project is funded by the Swiss National Science Foundation (SNSF); grant n°205121_188755, P.I. Edith Joseph.

Research Partners are the University of Neuchâtel, the University of Bologna (IT) and the conservation and research laboratory Arc'Antique (FR).
Authors thank E. Guilminot, G. Sciutto and S. von Reuss for the PhD co-supervisions.

contact@he-arc.ch: luana.cuvillier; arianna.passaretti

Research goal

The HELIX project seeks to develop eco-friendly, bio-based and easy-to-use gels for the cleaning of altered historical metal artworks, in particular on iron- and copper- based alloys. The ability of specific microbes to uptake metallic ions is exploited in parallel with the efficiency of specific bio-based solvents, in order to remove detrimental corrosion as well as altered or undesired organic protective coatings. Concurrently, high attention is addressed to the selection of bio-derived gelling agents to design green water- and solvent-gels.

Analysis and results

Metal corrosion removal

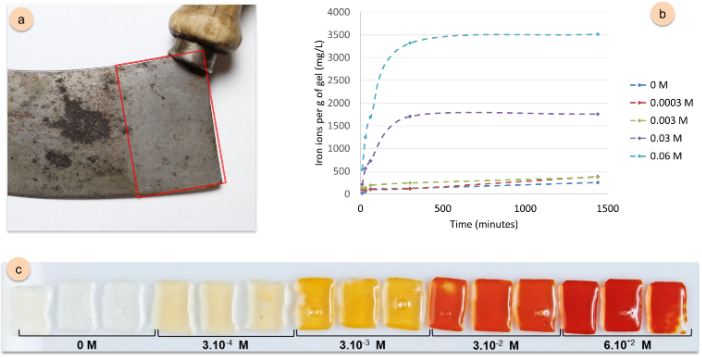

Figure 1. (a) Corroded iron-based mezzaluna knife after the application of a siderophore-amended 3% w/v agar gel during 20 minutes (red rectangle). (b) Quantity of Fe-ions absorbed by 3% w/v agar gels loaded with siderophores ($6 \cdot 10^{-2}$, $3 \cdot 10^{-2}$, $3 \cdot 10^{-3}$ and $3 \cdot 10^{-4}$ M) and applied during 10 and 30 minutes, 1, 5 and 24 hours on corroded iron. (c) Siderophore-amended 3% w/v agar gels (in triplicates) at different concentrations after a 10-minute application on corroded iron.

Organic coatings cleaning

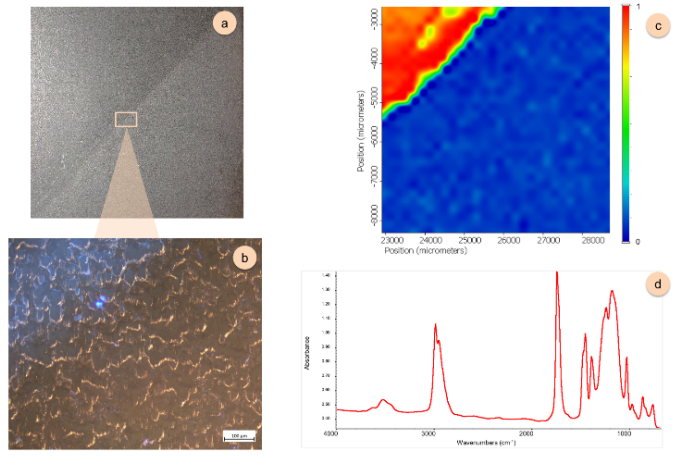

Figure 2. (a) Iron sample coated with an acrylic resin (paraloid B72) that has partly been removed using a Polyhydroxybutyrate-ethyl lactate gel. (b) Detail of the sample under UV illumination: evident difference between coated (left top half) and cleaned (right bottom half) regions. (c) FTIR correlation map collected in reflectance mode on coated (left top half) and cleaned (right bottom half) regions, using (d) a reference spectrum of paraloid B72. Correlation scale from min (blue) to max (red).

References

A. Passaretti, L. Cuvillier, G. Sciutto, E. Guilminot, and E. Joseph, "Biologically Derived Gels for the Cleaning of Historical and Artistic Metal Heritage," Appl. Sci., vol. 11, no. 8, p. 3405, Apr. 2021, doi: 10.3390/app11083405.
L. Cuvillier, A. Passaretti, A. Raimon, V. Dupuy, E. Guilminot, E.Joseph. Exploiting biologically synthetized chelators in art conservation: bio-cleaning gels for altered iron heritage. In Proceedings of the Metal 2022, 10th interim meeting of the ICOM-CC metals working group; Helsinki, Finland, 2022. [in press]
E. Joseph, M. Albelda-Berenguer, E. Cornet, L. Cuvillier, S. James, L. Mathys, M. Monachon, A. Passaretti and S. Russo. (2020). Innovative approaches towards a green and sustainable metal conservation. Chimia, 74, 611. https://doi.org/10.2533/chimia.2020.611
E. Joseph, P. Junier. (2020). Metabolic processes applied to endangered metal and wood heritage objects: Call a microbial plumber! New Biotechnology, 56, 21-26. https://doi.org/10.1016/j.nbt.2019.11.003

Russo, S., **Passaretti**, A., Brambilla, L., Thomas, J. B., & Joseph, E., Metal soap detection on oil-coated copper and zinc model samples through vibrational spectroscopy. Poster presentation at *RAA2023-11th International Conference on the Application of Raman Spectroscopy in Art and Archaeology*. Athens, Greece, September 6-9, 2023.

Metal soap detection on oil-coated copper and zinc model samples through vibrational spectroscopy

AUTHORS

Silvia Russo[1,2], **Arianna Passaretti**[1,2], Laura Brambilla[1], Jean Baptiste Thomas[3], and Edith Joseph[1,2]

[1]Haute Ecole Arc Conservation-Restauration, HES-SO University of Applied Sciences and Arts Western Switzerland, Neuchatel, Switzerland
[2]Laboratory of Technologies for Heritage Materials (LATHEMA), University of Neuchatel, Neuchatel, Switzerland,
[3]Norwegian University of Science and Technology, Gjøvik, Norway

KEYWORDS

metal soaps, metal carboxylates, painted metal artworks, metal degradation, vibrational spectroscopy, Raman microspectroscopy

ACKOWLEDGMENTS

The European Union's Horizon 2020 research and innovation programme under the Marie Skłodowska-Curie grant agreement No. 813789

S.R. and A.P. would like to thank Vi C.E. Kronberg for their support in the data processing and help with Matlab scripts

CONTACTS

SRU_ne@outlook.com

µ-Raman spectroscopy single-point analysis allowed identification of the **chain length** of the formed soaps.

Differences between copper and zinc were successfully highlighted.
Copper forms mostly **monounsaturated soaps (oleate, c18:1)**; **zinc** forms soaps with fatty acids having **saturated chains (palmitate, c16:0 and stearate, c18:0)**.

AIM: to explore the potential of FTIR and Raman micro-spectroscopies for the non-invasive investigation of the metal-oil interface and the monitoring of early-stage degradation of painted metal artworks.

METHOD: 6x6x0.1 cm³ copper and zinc sheets (Tartaix) coated with cold-pressed linseed oil (Kremer Pigmente) and aged first artificially in a laboratory oven for a month at 60°C and 80%RH, and then left in uncontrolled conditions.

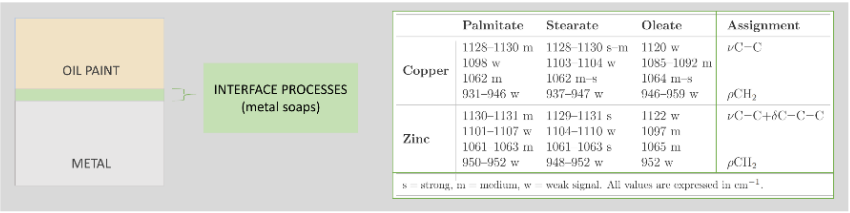

	Palmitate	Stearate	Oleate	Assignment
Copper	1128–1130 m 1098 w 1062 m 931–946 w	1128–1130 s–m 1103–1104 w 1062 m–s 937–947 w	1120 w 1085–1092 m 1064 m–s 946–959 w	νC–C ρCH₂
Zinc	1130–1131 m 1101–1107 w 1061–1063 m 950–952 w	1129–1131 s 1104–1110 w 1061–1063 s 948–952 w	1122 w 1097 m 1065 m 952 w	νC–C+δC–C–C ρCH₂

s = strong, m = medium, w = weak signal. All values are expressed in cm⁻¹.

COPPER

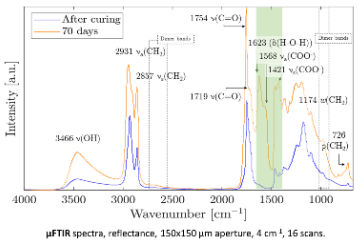

µFTIR spectra, reflectance, 150x150 µm aperture, 4 cm⁻¹, 16 scans.

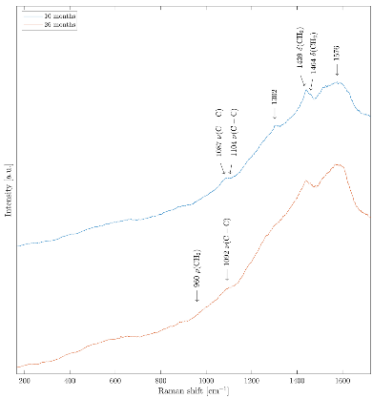

µRaman point analysis, 532 nm laser, spectral range 180 - 1650 cm⁻¹, 100x, 15 mW, 20 accumulations, 20s.

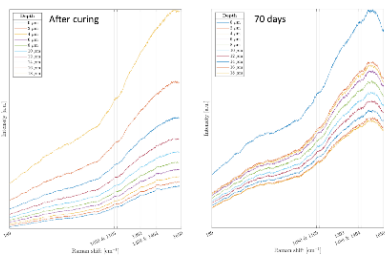

µRaman depth profiling, 532 nm laser, spectral range 180 - 1650 cm⁻¹, 50x LWD, 5 mW, 5 accumulations, 5s, 10 spectra consecutively collected at 2 µm incremental steps with respect to the surface of the oil.

ZINC

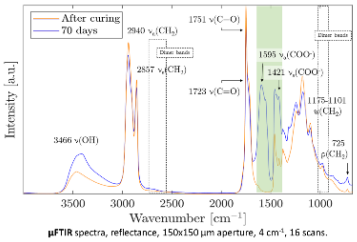

µFTIR spectra, reflectance, 150x150 µm aperture, 4 cm⁻¹, 16 scans.

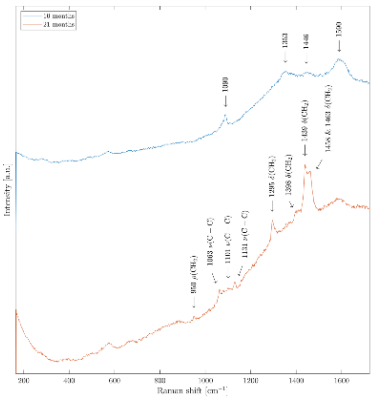

µRaman point analysis, 532 nm laser, spectral range 180 - 1650 cm⁻¹, 100x, 15 mW, 20 accumulations, 20s.

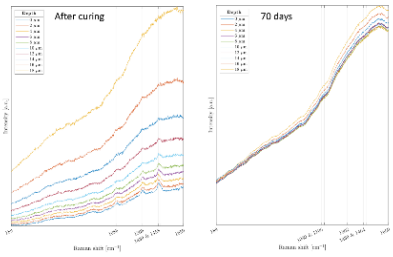

µRaman depth profiling, 532 nm laser, spectral range 180 - 1650 cm⁻¹, 50x LWD, 5 mW, 5 accumulations, 5s, 10 spectra consecutively collected at 2 µm incremental steps with respect to the surface of the oil.